STUDIES OF RARE EARTH ELEMENTS AND ASSOCIATED RADIOACTIVITY IN THE COASTAL SAND OF THE CENTRAL AND WESTERN REGIONS OF GHANA

THIS DISSERTATION IS SUBMITTED TO THE UNIVERSITY OF GHANA, LEGON IN PARTIAL FULFILMENT OF THE REQUIREMENTS FOR THE AWARD OF Ph.D. DEGREE IN NUCLEAR AND RADIOCHEMISTRY

BY

JOSHUA AYODEJI ABEY, (10444542)

B.Sc. (UNAD, Nigeria), 2009, M.Sc. (OAU, Nigeria), 2014

DEPARTMENT OF NUCLEAR SCIENCES AND APPLICATIONS

SCHOOL OF NUCLEAR AND ALLIED SCIENCES-ATOMIC

COLLEGE OF BASIC AND APPLIED SCIENCES

UNIVERSITY OF GHANA, LEGON

JULY, 2017

DECLARATION

This dissertation is the result of research work undertaken by JOSHUA AYODEJI ABEY in the Department of Nuclear Sciences and Applications, School of Nuclear and Allied Sciences, University of Ghana, Legon, under the supervision of Prof. Yaw Serfor-Armah, Prof. Samuel B. Dampare and Dr. Dennis K. Adotey.

Signature……

Joshua Ayodeji Abey

(Student)

Date ……

Signature…… Date ……

Prof. Yaw Serfor-Armah, Ph.D.

(Supervisor)

Signature……..… Date ……

Prof. Samuel B. Dampare, Ph.D.

(Co-Supervisor)

Signature…… Date ……

Dr. Dennis K. Adotey

(Co-Supervisor)

DEDICATION

This work is dedicated to the God of Science and Technology who is the Source of my Strength.

ACKNOWLEDGEMENT

My appreciation goes to God Almighty the source of my Existence and Inspiration. My thanks go to my parents, Mr. and Mrs. Abey, for their active role in the financing of my research project. I hereby wish to express my profound gratitude to my supervisor, Prof. Yaw-Serfor Armah, for his support, guidance and supervision of this work which has been able to widen my horizon. The moral support of the co-supervisor, Prof. S.B. Dampare cannot be overemphasized, as he provided critical information with respect to the geological perspective of this study. The contributions of Dr. D.K Adotey, who sacrificed his time during the drafting of the work-plan is highly appreciated.

The support of Dr. David Kpeglo in the studies of the naturally occurring radioactive materials (NORMs) is highly appreciated. I sincerely appreciate my brother, Mr. Solomon Abey and his wife, Nosarieme Abey for their moral and financial support during my research. Many thanks to my colleagues: Mrs. Irene Opoku-Ntim, Mrs. Jennifer Ofori, Mrs. Dzifa Banson, Ms. Delali Tulasi and Mr. Hyacinthe Ahimadjie. The relentless support of Messrs Patrick Bayowobie, Oswald Mkanda, Solomon Bello, Randy Davordzie, Philip Gasu, Ms. Afia Boatemaa and Ms. Florence Amoakohene during the course of the research is highly appreciated.

I appreciate the support of members of Mt. Sinai Methodist Church, Atomic, for their spiritual mentorship. I acknowledge the support of my beloved Temple Henry and my guardians Mr Alfred Fosu family, Aunty Doris and Mrs. Felicia Darko-Asare. The mentorship provided by Prof. F.O. Asubiojo, Prof. F.M Adebiyi and Prof. P.A Tchokossa of the Obafemi Awolowo University, Ile-Ife, Osun State, Nigeria, is highly appreciated.

I acknowledge the support of organizations such as the Ghana Atomic Energy Commission (GAEC); Ghana Standards Authority (GSA); Department of Physics, University of Ghana; Ghana Highway Authority; Separations Ltd. South Africa; Ore Research and Exploration Pty Ltd, Australia (OREAS); ALS Global Laboratory, Canada; African Mineral Standard (AMIS), South Africa; Eichrom Technologies U.S.A; and, TRISKEM International, France

ABSTRACT

Beach sands are known host of different heavy minerals, which occur mostly as placer deposits and are of great importance to the electronics, metallurgy, medical, defense, and automobile industries. Typical examples of such heavy minerals are the rare earth-associated minerals (e.g. monazite, bastnaesite, xenotime and euxenite). Some of these rare earth elements-containing ores are known to occur in association with naturally occurring radioactive uranium (U-238) and thorium (Th-232). Limited studies are available on identification of rare earth element fingerprints in the coastal sands of Ghana. Also, the relationship between the Naturally Occurring Radioactive Materials (NORMs) and the Rare Earth Elements (REEs) in Ghanaian coastal sands has not been well studied. The study developed an analytical procedure for mapping out the composition of rare earth elements in beach sands via the pathfinder role of naturally occurring radioactivity along the coast of the Central and Western regions of Ghana. This was achieved through: **(i)** assessment of naturally occurring radionuclides (^{238}Th, ^{232}Th and ^{40}K) using Gamma Spectrometry and ascertaining the presence of REEs-associated minerals using bromoform (density = 2.89 g/cm^3) prior to petrography of the heavy mineral concentrates; **(ii)** investigation of REEs in coarse, medium and fine fractions using Lithium Metaborate Fusion Method using Inductively Coupled Plasma Mass Spectrometry (ICP-MS); **(iii)** development of chemical method in the separation of selected REEs (Pr, Nd, Sm, Eu); and **(iv)** establishment of geospatial distribution pattern to aid exploration of REEs minerals. Beach sand samples were collected from 15 locations in the Central region (Gomoa Fetteh, Senya Beraku, Winneba, Mankwadze, Apam, Mumford, Dago, Akra, Ekumpoano, Edumafa, Anomabu, Cape Coast, Elmina, Dutch Komenda and Kafodzizi) and 10 locations in the Western region (Shama, Abuesi, Sekondi,

Takoradi, Cape Three Points, Egyembra, Axim, Esiama and Sanzule) along the coastline of Southwestern Ghana. The average concentrations of ^{238}U, ^{232}Th and ^{40}K in the beach sands of the Central and Western regions of Ghana were found to contain the United Nations Scientific Committee on Effects of Atomic Radiation (UNSCEAR) recommended permissible levels (35; 30; and 400 Bq/Kg respectively) for radionuclides; with mean activity concentrations (ranges) of 1.3 ± 0.47 to 31.50± 3.31 Bq/Kg (^{238}U); 0.7± 0.04 to 71.70± 4.55 Bq/Kg (^{232}Th); 73.9± 6.72 to 1775.5± 28.35 (^{40}K) for the Central region. In the Western region, the mean activity concentration ranged fom 1.0 ± 0.03 to 5.6± 0.24 Bq/Kg (^{238}U); 0.8± 0.04 to 3.8± 0.14 Bq/Kg (^{232}Th); and 18.6± 0.23 to 343.2± 18.35 (^{40}K). Beach sand dose rate in the Central region and Western region ranged from 4.13 to 132.39 (nGy/hr) and 1.78 to 19.32 (nGy/hr) respectively; with a total average across the two regions being 11.40 (nGy/hr). The annual effective dose in the Central region ranged from 0.0051 to 0.1624, while that for the Western region ranged from 0.002 to 0.024; total average for the two regions was 0.014 mSv/Yr. High radioactivity levels (Bq/Kg) (^{238}U; ^{232}Th; ^{40}K; Raeq) observed in the beach sands of Dago (31.5±3.31; 71.7±4.55; 1775.5±28.35; 258.21); Akra (4.1±1.13; 2.0±0.51; 81.6±6.39; 12.66); and Ekumpoano (27.2±5.8; 6.2±1.20; 69.7±8.12; 33.67) of the Central region exceeded the individual radioactivity levels of the Western region. Heavy minerals such as Zircon, Rutile and Amphibole were identified in the beach sands of the Central and Western regions. The minerals found are known to concentrate REEs and are indicative of shore-derived minerals. Rare earth elements were found in beach sands at both regions. Total Rare Earth Elements (TREEs) distribution in the beach sands of the Central region ranged as coarse fraction (6.33 to 13.30 ppm); medium fraction (8.56 to 53.15 ppm) and fine fraction (16.67 to 795.01 ppm). The sum of Light Rare

Earth Elements (LREEs); Heavy Rare Earths (HREEs); and ratio of light to heavy rare earth (LREE/HREE) distribution in the Central region were: coarse fraction (5.56 to 11.77 ppm; 0.64 to 1.53 ppm; 5.81to 9.89); medium fraction (7.72 to 48.13 pm; 0.84 to 5.02 ppm; 5.83 to 9.95); and fine fraction (14.98 to 727 ppm; 1.69 to 74.53 ppm; 4.43 to 10.79). The TREE distribution in the beach sands of the Western region varies as follows; coarse (5.69 to 29.78 ppm); medium (9.51 to 85.58 ppm) and fine fraction (24.3 to 86.28). The sum of light LREEs, HREEs and ratio of light to heavy rare earth (LREE/HREE) distribution in the Western beach sands were: coarse fraction (5.07 to 26.08 ppm; 0.62 to 3.70 ppm; 6.67 to 10.11); medium fraction (8.47 to 76.8ppm; 1.04 to 8.78 ppm; 3.97 to 9.56) and fine fraction (21.6 to 77.46 ppm; 2.7 to 17.63 ppm; 2.76 to 8.78). Despite the prominence of REE- fingerprints in the beach sands of Dago, Akra and Ekumpoano in the Central region, the corresponding increase in radioactivity concentrations at these locations (Dago, Akra and Ekumpoano) suggest strong influence of the geology of these areas. The sharp decrease in the concentration of total REEs in the beach sands of Akra shows an anomaly despite the fact that the sampling points are along the same trend. The geospatial observation of the coastline along the Central region showed that the sampling location at Dago and Ekumpoano are on probable geological faults and have differing geology. The study has also revealed that the radioactivity distribution in the beach sands serves as pathfinders to potential rare earth elements deposits in the Central region. Although heavy REEs were found in relatively higher concentrations in the beach sands of the Western region, the REEs in the fine fractions of the Central region exceeded that of the Western region. Consequently, the renewable energy target which relies on selected rare earth elements is achievable if more resources are committed towards potential sources of the REEs in-land.

TABLE OF CONTENTS

LIST OF FIGURES

LIST OF TABLES

LIST OF ACRONYMS

AED	Annual Effective Dose
CN	Coordination Number
CS	Coarse Sand
CMPO	Carbamoylmethyl-phosphine oxide
CREE	Critical Rare Earth Elements
DW	Dry Weight
FS	Fine Sand
HPGe	High Purity Germanium
HREE	Heavy Rare Earth Elements
ICP-MS	Inductively Coupled Plasma Mass Spectrometry
LN	Lanthanide
LREE	Light Rare Earth Elements
MCA	Multichannel Analyzer
MREE	Middle Rare Earth Elements
MS	Medium Sand
NORMs	Naturally Occurring Radioactive Materials
PTS	Petrographic Thin Section
RECl	Rare Earth Chloride
REE	Rare Earth Elements
REE-TM	Rare Earth Elements – Transition Metal
TBP	Tributylphosphate
TENORM	Technologically Enhanced Naturally Radioactive Materials
TRU	Trans-Uranium Resin
VCS	Very Coarse Sand
VFS	Very Fine Sand

CHAPTER ONE

GENERAL INTRODUCTION

1.1 Background

The demand for Rare Earth Elements (REEs) in critical areas of advanced technology such as renewable energy, electronic, nuclear, glass, petroleum, weapons, metals, magnets, chemical, and automobile industry has led to the increase in exploration and exploitation of known deposits of rare earth elements around the globe (ACC, 2014). It is widely known that the rare earth elements are a group of 15 elements Lanthanum (La) to Lutetium (Lu) that span across the atomic number 57 to 71. Scandium (^{21}Sc) and Yttrium (^{39}Y) share similar chemical properties with the rare earth elements, hence leading to their occurrence in similar geochemical environment. Promethium (^{61}Pm) which is a naturally radioactive element is no longer existent in the earth crust but can be prepared artificially in a cyclotron (Hu et al., 2006; Liao et al., 2005).

In the 21st Century, REEs are vital economic resource and considered as "Potential Energy of the Future". Globally, REEs are playing a critical role in the economics of emerging technologies with industrial value of about US$5.000 billion, which represents 5% of the worlds GDP (CEID, 2015). The market value for REEs is expected to hit about US$20 billion by 2024 (GMI, 2018).

The World's top 5 consumers of REEs are China, Japan, USA, France, and Korea respectively (He et al., 2014). China holds the world's largest REE reserves and it has been estimated to be about 48% of the world's total reserves as shown in Fig. 1.1. This makes China the leading producer of REEs in the world as shown in Fig. 1.2 (USGS, 2017a).

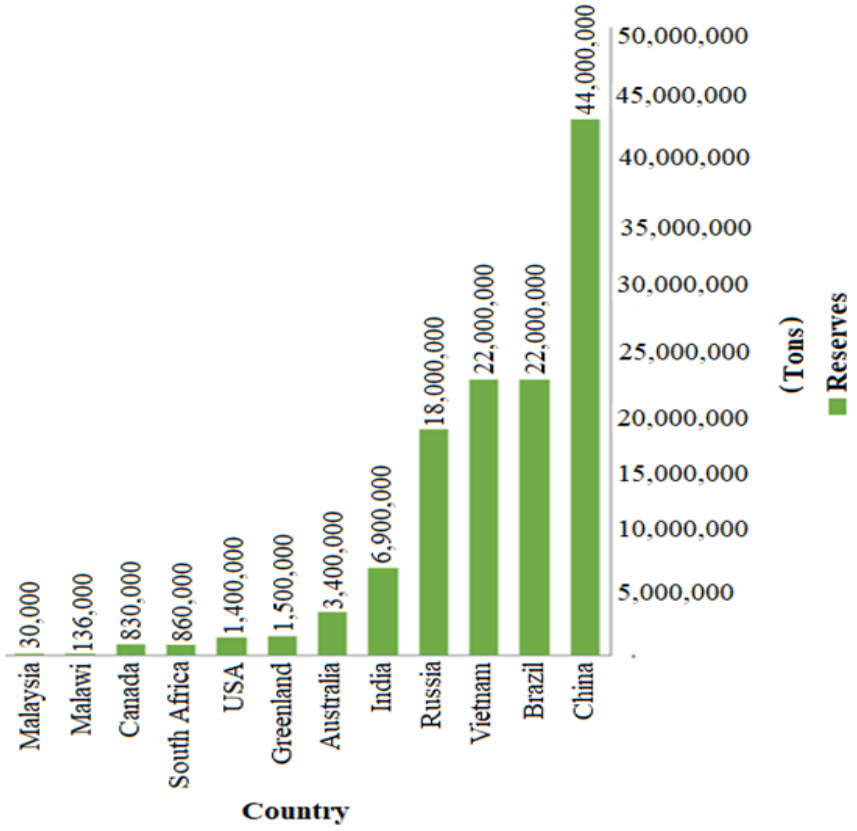

Fig. 1.1: Rare earth elements reserves in selected countries in the World

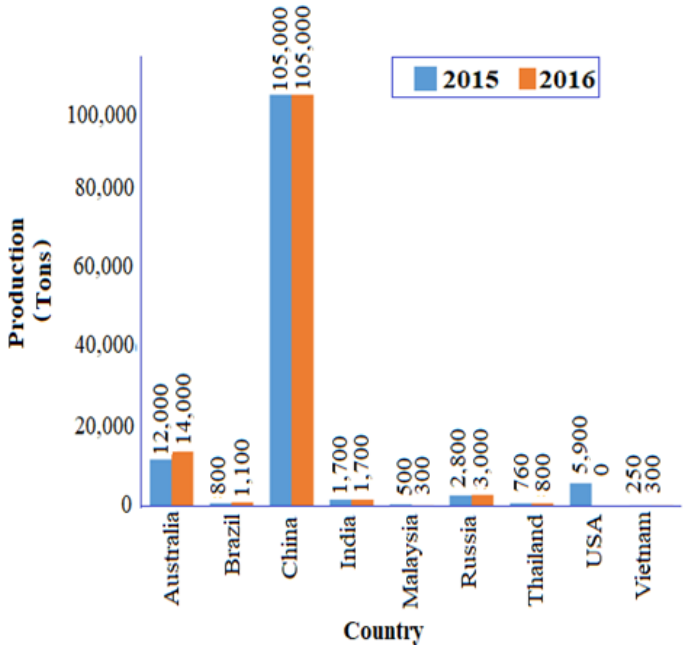

Fig. 1.2: Rare earth elements production in selected countries in the World between 2016 - 2017

Rare earth elements such as Yttrium and Lanthanum are used in $YLiFePO_4$ battery cell for electric vehicles and semiconductor transistors, while Cerium is useful in silicon microprocessor and glass surface polishing. Praseodymium and Neodymium are used as high strength metals in aircraft engines, magnets in consumer electronics such as mobile phones, and microphones. Artificially produced Promethium is used in heart pacemakers and fluorescent bulbs. Samarium, Europium, Terbium, and Yttrium are applied in energy efficient bulbs. Dysprosium, Neodymium, Praseodymium, Samarium and Terbium have found applications in wind turbines. Elements such as Gadolinium, Dysprosium, Holmium and Erbium have also been used as neutron absorbers in nuclear reactor. Ytterbium is used in stainless steel alloying while Lutetium is used as phosphors in Light Emitting Diodes (LED) and catalyst in petroleum refining (Esro et al., 2015; ACC, 2014; Krebs, 2006; Pisecny et al., 2004; Haoqing & Lijun, 2003).

Although REEs co-exist with over 200 minerals, they occur appreciably in ores such as monazite ($Th(Ln)PO_4.H_2O$), xenotime (Y, Dy, Yb, Er, Gd, PO_4), bastnaesite ((La, Y, Ce)CO_3F), and churchite $YPO_4.2(H_2O)$ (Xie et al., 2014; Jordens et al., 2013; Kanazawa & Kamitani, 2006). The REEs, based on similarity in their occurrence, physical and chemical properties, are broadly grouped into two groups which are Light Rare Earth (La, Ce, Pr, Nd, Pm, Sm, Eu) and Heavy Rare Earth (Gd, Tb, Dy, Ho, Er, Tm, Lu). Three-group classification has been observed based on the industrial processing of rare earth as Light-REEs (La, Ce, Pr, Nd); Medium-REEs (Sm, Eu, Gd,); and Heavy-REEs (Tb, Dy, Ho, Er, Tm, Yb, Lu) (Hu et al., 2006; Liang et al., 2013). The REEs have been exploited in countries such as China, Namibia, United States, Australia and in beach placers along the Indian coasts (Varnavas, 1990; Rajendran et al., 2008; Krishnamurthy & Gupta, 2004).

Selected beach sand along some coastal areas around the world are known to contain REE associated minerals which occur as placer deposits, due to the transport of mineral bearing fragments from source rocks under wave action (Krishnamurthy & Gupta, 2004). Although some of these REEs occur in addition to some radioactive elements like Thorium and Uranium-bearing ore (USGS, 2010), others are associated withnon-radioactive elements in their ore. Such non-radioactive associations are found in ores such as allanite, bastnaesite, and ion adsorbed clay minerals. REE studies have been conducted on different rocks in Ghana and some have proven to be potential sources of REEs (Hayford et al., 2013; Dampare et al., 2005; Schnetzler et al., 1967).

Some analytical methods used in the investigations of REEs include X-ray Fluorescence Spectrometry (XRF), Instrumental Neutron Activation Analysis (INAA), Inductively Coupled Plasma - Mass Spectrometry (ICP-MS), Inductively Coupled Plasma - Atomic Emission Spectrometry (ICP-AES), Atomic Absorption Spectrometry (AAS), and Spectrophotometric method (Liang et al., 2013).

The increased demand for REEs in renewable energy technology industries requires not just the identification of REEs in their natural geological matrix but also developing methods for identifying probable large deposit wherein they occur in association with radioactive elements via their fingerprints in coastal sands.

This study will focus on the identification of potential REE sources in selected beach sands in the Central and Western regions of Ghana.

Since the future of green energy technology rests on the application of rare earth metals, identification of REE distribution and investigating the associated

radioactivity will aid in the recognition of potential deposits of REEs and their pattern of distribution in the beach sands.

1.2 Problem Statement

The Paris agreement on climate change, of which Ghana is party to, was adopted on 12th December 2015 and signed by over 195 countries at the United Nations Headquarters on 22nd April 2016 in New York. The agreement is poised at sourcing funding and technology to mitigate climate change among supporting member nations; most especially in supporting the development of renewable energy sources towards mitigating climate change in Africa (Hart, 2013; Richard& Benedict, 2009).

Ghana is challenged with insufficient energy and high cost associated with power generation. The "*Africa 2030: Roadmap for a Renewable Energy Future*" report targets the need for the deployment of renewable energy technology towards facilitating industrial growth and a cleaner environment (IRENA, 2015). Rare earth elements magnets are key industrial component in offshore and onshore wind turbines. Existing report by the World Wind Association (WWA) at the end of 2017 showed that wind turbines accounts for about 539,291 Megawatt overall capacity of World's wind power, with China leading by 188 Gigawatt capacities, and Denmark sourced 43% of its power from wind turbine in the year 2017.

Ghana is well known for the exploration, mining, and export of minerals such as gold, diamond, bauxite, and manganese. Gold export accounts for over 90% of the country's total mineral revenue, with 46% increase export in 2016 compared to 2015 (GCM, 2017). Little or no emphasis is placed on the exploration of the rare earth elements minerals which are important to the green energy future of Ghana. Beach sands are known host of eroded rock materials from inland sources and continental

shelf. There is a tendency for beach sands to hold information about probable deposit of rare earth elements. Presence of Naturally Occurring Radioactive Materials (NORMs) in beach sands is indicative of radioactive minerals; these minerals (Monazite and zircon) are pointers to REEs (IAEA, 1989). It is therefore imperative to conduct an investigation on the presence of rare earth elements (REEs) fingerprints and extractability of selected REEs in the beach sands of the Western and Central regions along the coastline of Southern Ghana for future technological applications.

1.3 Objectives

The overall objective of this study is to develop an analytical procedure for mapping out rare earth element composition of beach sands via the naturally occurring radioactivity along the coast of Central and Western regions of Ghana.

The specific objectives of the study are to:

(a) assess the concentrations of naturally occurring radioactive nuclides (^{238}U, ^{232}Th and ^{40}K) in beach sands using γ- ray Spectrometry; and ascertain the presence of REE-associated minerals through Gravity Separation using bromoform and Petrographic Thin Section (after particle size distribution);

(b) investigate the lvels of REEs in coarse, medium and fine fractions of beach sands using Lithium metaborate fusion and ICP-MS; hence evaluate the % Y and REE : HREE as a measure of REE abundance;

(c) develop a chemical method for the separation of selected (*renewable energy Industry*) REEs (Pr, Nd, Sm, Eu) using extraction chromatographic technique; and

(d) establish the Geospatial distribution pattern of the REE- clusters in the coastal sands to aid exploration of REE minerals.

1.4 Justification for the Study

Layton (1958) described the economic geology of some radioactive minerals (monazite, xenotime, and zircon) and reported that relatively high radioactivity concentrations were observed in graphic granites and quartz veins observed during the construction of the Accra-Winneba road, as well as black sands in the Mankwadze, Abrekum and Apam, which are towns proximal to the coastal area of the Central region of Ghana.

In recent times, different authors have studied the naturally occurring radioactivity (^{238}U, ^{232}Th and ^{40}K) of sediments in selected areas of the coastal environment of Ghana, and admitted to the rhetoric of safe radiation level in the coastal area (Amekudzie et al., 2011; Botwe et al., 2017; Lawluvi, 2016).

While the study of Layton (1958) suggests the probable presence of monazite in some selected areas proximal to the coastal environment, this study will take a critical look at the distribution of naturally occurring radioactive elements in the coastal sands from a perspective of their probable association with rare earth elements (REEs).

Assessment of the REEs as they distribute within the coarse, medium and fine fractions of the beach sands will provide information about the prominence of either the light rare earth elements (LREE) or the heavy rare earth elements (HREEs). The rare earth distribution in the beach sands will eventually serve as a pointer to the geology of the environment and probable effect of long-range transport of the beach sands.

1.5 Extent of the Study

The study focuses on the collection of beach sand from twenty-five locations based on the geology of the Central and Western regions of Ghana. Acquisition of gamma spectrometry data of the beach sands will ascertain the levels of naturally occurring radioactivity of the beach sands along the Central and Western regions of Ghana. The collected sands will be sorted into different particle sizes and separated into three major fractions as coarse, medium and fine fractions. The three sand fractions from each location will be investigated for rare earth element contents and their trend in their distribution along the sampling location. Extraction chromatographic resins will be used in the separation of selected REEs. Petrographic details of the beach sands will provide information about the composition of minerals in the beach sands.

1.6 Arrangement of Chapters

This dissertation is divided into five chapters. Chapter one focuses on a brief introduction of the rare earth elements (REEs), background to the study and objectives of the studies of rare earth elements in beach sands. Chapter two discusses the literature available on the occurrence and coastal depositional environment of REEs and the associated radioactivity. Classification, industrial processing and separation methods of REEs are highlighted, while the instrumental methods for the determination of the REEs are not exempted. Chapter three focuses on the materials and methods involved in the experimental process of the grain size distribution of coastal sands, Gamma spectrometry of the coastal sands, analysis of the rare earth elements in the beach sands and the chemical separation of selected rare earth elements. Chapter four focuses on the discussion of results obtained from the experiments conducted in Chapter three while chapter five deals with conclusions of the study and recommendations for further studies.

CHAPTER TWO

LITERATURE REVIEW

2.1 Occurrence and Abundance of Rare Earth Elements

Rare earth elements traditionally occupy the f-block of the periodic table, having atomic number (Z) in the range 58-71(La - Lu), while the non-lanthanide rare earths are Yttrium and Scandium with Z= 39 and Z=21respectively. The lithophilic nature of rare earth implies that they are enriched in the earth crust (Hedrick et al., 2006). The varying concentration of the rare earth in the earth has been observed to follow a particular pattern whereby we have the light rare earth in higher concentration than the heavier rare earth. According to the Goldschmidt geochemical classification of elements within the earth crust, the elements are broadly divided into chalcophile, siderophile, lithophile and atmophile. Fig. 2.1 shows the Periodic Table representation of the Goldschmidt classification.

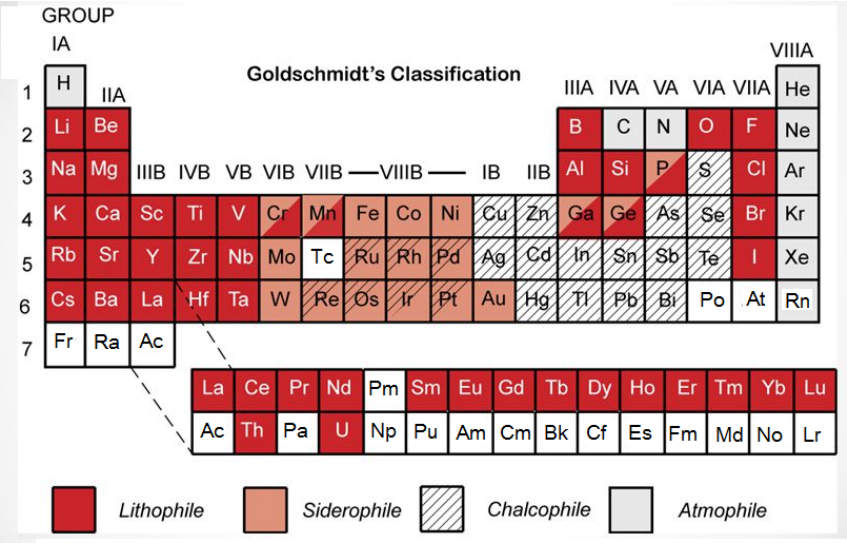

Fig. 2.1: Classification of elements in the Earth Crust ***(White, 2013)***

The lithophile elements (31-elements and REEs) are known to be closely associated with the earth surface, they bond with oxygen in silicates (tetrahedral sites, or octahedral sites, or decahedral sites) and oxides (Albarede, 2011). It is observed that the lithophile elements have closely filled outer electronic shells thereby forming ionic bonds. The trivalent (Ln^{3+}) nature of the rare earth is responsible for their availability in similar geochemical environments. Thus, it has been scientifically proven that in the list of the REEs, Ce and Eu occur mostly in nature as tetravalent (Ce^{4+}) and divalent elements (Eu^{2+}) due to varying oxidation states.

Marc (2010) alludes that there is moderate abundance of rare earth in the earth crust, and they are even more abundant than copper, lead, gold and platinum. About 150-220 mg/kg of REE are known to be found in the earth crust (Long et al., 2012). Table 2.1 shows a composition of estimated rare earth elements concentration in the lower, middle and upper continental crust. The commonly observed opinion about the REEs in the crust is that they share similar properties with those formed in CI Chondrite; this is reflected by similarity in the concentrations of Sm/Nd, $^{143}Nd/^{144}Nd$, $^{142}Nd/^{144}Nd$ (Huang et al., 2013a; Caro et al, 2008). However, recent trends suggest high concentration on Sm/Nd in the bulk silicate earth than the chondrite (Huang et al., 2013).

The concentration of Ce in the upper (63 ppm), middle (53 ppm) and lower crust (20 ppm) exceeds the concentration for the other REEs (Holland & Turekian, 2004). In other words, Ce is considered not only very reactive, but the most abundant of the REEs and the 25th most abundant element in the earth crust (Gschneidner et al., 2006; USGS, 2017b). Owing to the similarity in geochemical association, lanthanum through to europium are generally referred to as cerium-group (LREE), while gadolinium to lutetium are considered as yttrium-group (HREE) (Mortimer, 1979).

Table 2.1: Composition of rare earth elements in the Earths continental crust

Element	Crust			
	Upper	Middle	Lower	Bulk
Sc	14	19	31	21.9
Y	21	20	16	19
La	31	24	8	20
Ce	63	53	20	43
Pr	7.1	5.8	2.4	4.9
Nd	27	25	11	20
Sm	4.7	4.6	2.8	3.9
Eu	1	1.4	1.1	1.1
Gd	4	4.0	3.1	3.7
Tb	0.7	0.7	0.48	0.6
Dy	3.9	3.8	3.1	3.6
Ho	0.83	0.82	0.68	0.77
Er	2.3	2.3	1.9	2.1
Tm	0.3	0.32	0.24	0.28
Yb	2.0	2.2	1.5	1.9
Lu	0.31	0.4	0.25	0.3
Th	10.5	6.5	1.2	5.6
U	2.7	1.3	0.2	1.3

Source:(Holland & Turekian, 2004)

2.2 Ores of Rare Earth Elements

Rare earth elements are broadly grouped into the cerium group and yttrium group. The cerium group comprises lanthanum to europium while the yttrium group is mainly made up of gadolinium to lutetium (Mortimer, 1979b). This same classification explains the basis for the division of the rare earth elements into light rare earth (LREE) and heavy rare earth (HREE).

In a bid to further explain the REE broad classification in relation to their ore, it is important to look at the description of Guilbert et al. (2007) where the authors have discussed source, character, migration and deposit of ore bearing fluids in relation to their magmatic, metamorphic or sedimentary origin.

The largest deposits of rare earth ores in the world are associated with alkaline carbonate intrusive series (Kanazawa & Kamitani, 2006). During the formation of magma (a mobile rock originating from the earth), metallic elements have a tendency of association with the resulting magma which could be intrusive or extrusive (Fabian, 2013).

Rare earth elements (REEs) are considered as lithophile elements which are incompatible with the mantle (Sarbas & Töpper, 2013). The REEs are rather expunged during magmatic processes which occur during the partial melting of the mantle, thereby leading to their concentration in silicate phases in the crust (Wyllie, 1988).

The rare earth element contents in the primitive mantle, continental crust and upper crust have been estimated and reported (Workman & Hart, 2005; McDonough, 1995; Hart & Zindler, 1986) . Lanthanum has been described as the most incompatible of the rare earth elements, leading to its increased abundance in ores (monazite-La and bastnaesite-La) (McKenzie & O'Nions, 1991).

Data obtained from Taylor & McLennan (1985) for the upper continental crust shows a range of 0.32- 64 ppm with the highest concentration in cerium elements. Rare earth associated elements such as uranium and thorium are also enriched in the upper continental crust. Holland & Turekian (2004) and Rudnick & Gao (2003) discussed the enrichment of both uranium (2.7 ppm) and thorium (10.5 ppm) in the upper crust

and a gradual decline in their concentrations from the upper crust to the middle (U - 1.3 ppm; Th - 6.5 ppm) and lower crust (U-0.2 ppm; Th -1.2 ppm) (Hacker et al., 2015; Trindade et al., 2013) [Table 2.1].

Rare earth deposits generally are known to be of igneous, hydrothermal and sedimentary origin (Oliveira & Inverno, 2014). Dill (2010) reported a magmatic, structural and sedimentary rare earth deposits classification based on host rock and mineralogical content (Fan et al., 2016). A Recent review by Oliveira & Inverno, (2014) shows a documentation of the works of Weng & Co-workers (2013) in the recent classification of REE deposits which focuses on geological processes associated with the concentration of REEs and mineral formation.

2.2.1 Carbonatite Associated Rare Earth Deposits

Rare earth elements found in carbonatites accounts for about 80% of the world's supply of light rare earth elements (LREE) (Hayford et al., 2013; Hofstra et al., 2016; Wang et al., 2017). Available data obtained from airborne geophysical studies have shown that Africa hosts about 35% of the worlds' carbonatite deposits and about 35 % is found in Asia (Bell, 2009). Carbonatite is known to be associated with magmatic segregation of igneous origin (Jones et al., 2013). This implies that the igneous rock is rich in carbonates and related to alkali forming process, mantle degassing and magma evolution (Guilbert et al., 2007).

Carbonatite can be described as a type of intrusive or extrusive rock of igneous origin with varying degree of the Ca-Fe-Mg carbonate melt. Commonly associated minerals found in carbonatites include dolomite, calcite or siderites; others include pyrochlore, monazite, apatite, zircon and perovskite (Sinding-Larsen & Wellmer, 2010). While

some carbonatites are rich in REEs, others show increased affinity for the high magnetite-apatite content or high fluorine or barium content (Guilbert & Park, 1986).

Geochemical classifications of the carbonatite are mainly (i) Alkali (ii) Ferric iron (iii) Zirconium rich (iv) alkali poor (v) Fe-O-CaO-MgO rich and Zirconium-Poor Carbonatite (Guilbert & Park, 1986).

Hayford et al. (2013) in a study conducted on the igneous carbonatite complexes in Kpong area of Ghana, described it as a potential source of REEs having reported a concentration range of 540 – 705 mg/kg for the total REE observed. Table 2.2 shows selected locations in Africa where carbonatite complexes which host REEs are found. Although Africa owns large deposit of carbonatite, deposits found in Bayan Obo (Baotou) China and Mt. Pass (California) in the USA account for some of the largest in the world (Ali, 2014).

Studies conducted on the carbonatites of Zambia have shown carbonatites which are not in commercial quantity, but the bastnäsite-(Ce) carbonatite complex of the Nkombwa Hill shows potential for commercial exploitation (Mike, 2010; Sliwa, 1991). The carbonatite in the Songwe hill in Malawi is reported to be enriched in heavy rare earth elements due to the hydrothermal fluid apatite formation which accompanies the carbonatite complex (synchysite-Ce) (Broom-Fendley et al., 2017).

Table 2.2: Location of selected carbonatite deposits in Africa

Country	Location(s)	Deposit type
Angola	Monte Verde, Bonga, Virulundo, Bilundo, Tchivira.	Carbonatite
Congo Zaire	Bingo (Bingu)	Carbonatite with residual enrichment
Ghana	Kpong	Alkalic Igneous
Kenya	Buru, Mrima Hill	Carbonatite with residual enrichment
Malawi	Kangankunde, Kapiri Nsengwa, Tundulu, Songwe	Carbonatite with residual enrichment
Mali	Adiounedj, Anezrouf	Carbonatite
Morocco	Tamazert (OuedTamazert, Tamazeght, BouAgrao)	Carbonatite
Namibia	Lofdal-Bergville, Eureka, Okorusu Complex, Ondurukurme Complex	Carbonatite
Somalia	Dalkainle	Carbonatite
South Africa	Glenover, Goudini, Palabora (Phalaborwa), Sandkopsdrif (Zandkops Drift)	Carbonatite
	Pilanesberg Complex	Alkalic Igneous
Tanzania	Makonde Wigu Hill, Mbeya (Panda Hill)	Carbonatite with residual enrichment
Zambia	Kaluwe, Nkomba	Carbonatite with residual enrichment

Source:(USGS, 2014b; Orris & Grauch, 2002)

2.2.2 Alkaline Complexes and Alkaline Pegmatite REE Deposits

Alkaline intrusives are known for hosting rare earth and several intruding phases like that observed in the beryllium rare earth deposits found in Thor Lake which hosts minerals such as zircon, allanite-bastnaesite (Irving & Richardson, 1992). Characteristic minerals such as apatite, miserite, eudidymite and mosandrites have been found in the alkali igneous deposit of the Kipawa Lake of Ontario, Canada; in addition to zircon and uranium minerals, the host rocks contain peralkaline quartz syenite amphiboles schists (Woolley, 1987).

On the basis of the Henriech structural classification, it is known that not all carbonatites are associated with other mafic igneous rock (Traversa et al., 2001; Mitchell, 2005). Carbonatite types are as follows (i) Alkali Ring Complexes (ii) Alkali Non-ring Complexes (iii) Non-Alkalic Rock Association (iv) Pyroclastic Flows (Kinnaird & Bowden, 1991).

2.2.3 Rhyolite Associated REE Deposits

Rhyolites are classified as felsic extrusive igneous rocks, which have high silica content which forms lava domes. They are often extruded from the base of the upper crust and are composed of major minerals such as quartz, plagioclase, sanidine and minor minerals such as hornblende and biotite (Barry et al., 1988). Anderson (2007) discussed the crustal partial melting and the extrusion of rhyolitic magma from granitic magma origin. The round top mountain in Texas, U.S.A is considered as a typical rhyolite which has proven to be a reliable host of heavy REEs (HREE) (Pingitore et al., 2014). Miller (2015) described the HREE (Nd-Dy-Y-Tb) deposit

discovered in the Foxtrot area of Canada as being hosted by peralkaline volcanic rocks and a potential source of REEs.

2.2.4 Granitic Associated REE Deposits

Granites and granitic pegmatites are typical examples of REE hosts (Linnen et al., 2012) describes granitic pegmatites as poised sources of critical metals such as Ta, Nb and REEs which are accumulated alongside high flux elements (Li, B, P, F) which takes place during magmatic processes (Jahns & Burnham, 1969). Families of rare earth associated pegmatites include: LCT (Li-Cs-Ta) pegmatites, NYF (Nb-Y-F) pegmatites and a mixture of LCT- NYF pegmatites: with the NYF-pegmatites having a high tendency for accumulation of REEs and other elements such as Th, U, Be, Sc, Ti and Zr (Cerny & Ercit, 2005; Simmons, 2007).

Cerny & Ercit (2005) described NYF-pegmatites as derivatives of A-type granites and I-type granites which hold information about the REEs components in association with Th and U. Ghost lake batholiths found in Northwestern Ontario, Canada are a typical case of granite rare earth elemental pegmatite system. Although quartz and feldspars crystallize from granitic melts, REEs are known to be incompatible with these minerals. Linnen et al. (2012) argue that extreme fractionation originating from the extended crystallization of quartz and feldspar is responsible for increased concentration of REEs in residual melts.

Mckeough et al. (2013) explained rare earth enrichment in pegmatites as a result of pegmatite fractionation cum REE partitioning from pegmatite phase to the volatile phase in relation to their host rocks.

2.2.5 Hydrothermal Related REE Deposits

Rare earth elements associated with granites of hydrothermal origin mostly occur as veins emanating from heated magmatic water process under high temperature and pressure, resulting in the crystallization of rare earth associated minerals via pre-existing fissures within the host rock (Wenk & Bulakh, 2003).

Edwards & Atkinson (1986) described mineral deposits from hydrothermal sources to have emanated from the hot aqueous fluid of unspecified origin.

Conditions required for the mineral deposition from hydrothermal sources have been described to include the following; (i) Hot water (brine) for transportation of dissolved minerals, (ii) Available interconnected fissures for fluid passage (iii) Depositional sites availability and (iv) Favorable chemical reaction for deposition (Farooq, 2017).

Classification of vein-type hydrothermal deposits based on the various depths occurring at a temperature range of 50 – 500 ^{o}C is as follows: hypothermal (i.e. great depths and high temperature), mesothermal (intermediate depth and moderate temperatures), and epithermal (shallow depths and low temperatures). Rare earth minerals (Fe-oxide REE) elements associated with hydrothermal origin have been reported in the South of Australia (USGS, 2014a). Typical minerals associated with some hydrothermal deposits include monazite, bastnaesite, fluocerite, haematite, fluorite and uranite (Deb & Sarkar, 2017).

Einaudi & Oreskes (1983) described the Olympic dam granite hosts of REEs as a pink to yellowish-green coarse to medium grained equi-granular biotite granite. Uranium-

REEs have been associated with metamorphic-hydrothermal deposits (Oliver et al., 2010).

2.2.6 Skarn Deposit of REEs

Skarns basically are composed of the following types (i) Calcic Skarn and (ii) Magnesium Skarn (Ahankoub et al., 2015). The calcic skarn comprise mainly grossular-andradite series, diopside-hedenbergite series, wollastonite, vesuvianite, and scapolite in limestone or marble rocks.

The magnesian skarn contains forsterite, serpentine (altered forsterite), diopside, phlogopite, spinel, tremolite and humit in dolomite limestones.

Manganonan skarn contains Mn (Ca, Mg, Fe, Al), silicate minerals such as diopside, manganonan, hedenbergite, johansennite, tephrolite in relation to Pb-Zn (Ag) mineralization.

Alkaline skarns are subdivided into (i) Hydrothermal Metasomatic Alkaline Skarn (Carbonatite-related), (ii) Alkaline Skarn (alkaline granitoid-related) and (iii) Alkaline Skarn (syenite related) (Obolenskiy et al., 2007; Yiming et al., 2005).

The alkaline skarns formed in relation to dolomitic carbonatites are formed via the hydrothermal process. REE Nb-alkaline skarn related to alkali granitoid and carbonatites are found in the eastern Bayan Obo (Fe-Nb-REE) ore deposits; they are formed as a result of volcanic exhalative process (Fan et al., 2016).

2.2.7 Heavy Mineral Sands REE Deposits

Deposits of REEs have been found in secondary places such as in beach sands where they occur in association with other minerals. Commercial quantities of heavy minerals extending over a wide range of area are obtainable on different beaches around the world, thus making beach sands a potential source of industrial metals.

Rare earth elements associated minerals such as monazite, xenotime, apatite and other accessory minerals (zircon, ilmenite, rutile and leucoxene) are known to occur in beach sands (Cherniak, 2010). The sedimentary processes that lead to the formation of the heavy minerals in the coastal sands are due to the erosion of REE associated minerals from beach rocks (metamorphic, igneous and sedimentary) which are often located onshore. Rock materials weathered from inland sources are carried along by streams and rivers, thereby contributing to the sands and heavy minerals on beaches (Jones, 2009).

While attributing the concentration of heavy minerals on the beach sands along the coast to inland contributory sources, sediments from the sea floor are also being eroded and deposited on the shore as a result of the tidal wave (CISCAG, 2011).

Sorting of heavy minerals in the beach sands occur due to the reworking of the sands by waves, wind, longshore drifts and wind action, thereby leading to the formation of mineral layers based on particle size alignment in the beach sands (Gosen et al., 2014). Monazite sand of about 60 % and 4.68 Mt rare earth oxides have also been reported in the beach sands of New South Wales, Queensland, Australia (Williams, 2008). Although the associated radioactivity due to thorium poses a challenge to the production of REEs from monazite sands, the radioactive sands are major sources of light REEs.

2.2.8 Rare Earth Elements Ores in Placer Deposits

The etymology of the term “placer deposit” originates from the Spanish word *placea*, which explains the alluvial or glacial deposits of sand or gravel, while the term “alluvial” is derived from the Latin word *alluvius* which suggests sediments eroded over a long drift via agents of weathering and deposited in marine or non- marine environment (McColl, 2005). A well structured and lithified form of the alluvium is regarded as alluvial deposit.

The deposition of heavy minerals can occur in lake sediments which are regarded as lacustrine, river sediments (fluvial), glacial environments (glacial till) and beach sands (placers) (Suresh & Raja, 2014).

Granitic rocks are known to have a high content of REEs and could serve as a primary source which is subjected to weathering and the transported fragments serve as the basis for the existence of tertiary and quaternary placers in the marine environment. Monazite and xenotime minerals have been found as placers in beach sands of India, Brazil, U.S.A, Malaysia, Australia and Thailand (Sengupta, 2016).

2.3 Classification of Rare Earth Minerals

The rare earth minerals can be classified as carbonates, halides, borates, phosphates, sulphates, arsenates and silicates. The classification of REEs into cerium-group (La-Eu) and yttrium-group (Gd-Lu) is important while considering the association of REEs in minerals. Clark (1983) highlighted the arguments surrounding the role of the coordination number of REEs and how it influences their occurrence in minerals.

The Ce-group selective minerals have coordination number (CN) 10-12, minerals with CN 7-9 can inter-switch between the Ce or Y-group, whereas minerals with CN 6 have a selective preference for Y-group REES.

Most times, minerals in coastal environment are a product of the disintegrated rocks which host major minerals such as amphiboles, mica, schist and those that host minor minerals such as zircon, allanites, apatite, tourmaline (Mange & Maurer, 1992). Visual inspection of some beach sands shows dark-like color characteristics which suggest the accumulation of heavy minerals. Heavy minerals common to beach sands include garnet, ilmenite, monazite, rutile, sillimanite, zircon, leucoxene, magnetite, haematite, hornblende, augite and tourmaline (Gupta & Desa, 2001; Mange & Maurer, 1992).

The phosphate mineral, monazite is prominent among the heavy minerals in beach sands for the accumulation of REEs within its monoclinic crystal structure. The common structural derivative includes Ce-monazite, Nd-monazite, La-monazite; this is dependent on the dominant REE within the monazite crystal (Lima-de-Faria, 2001).

2.4 Rare Earths and Associated Radioactivity

Ramasamy and Co-workers (2014) in a study conducted on the level of radioactivity in the beach sands of Kerala in India, reported the radiation level as unsafe. The radiation levels from the beach sands were due to naturally occurring radioactive elements (uranium, thorium and potassium) which are formed in the heavy minerals. Thus we have minerals whose structural configuration supports their coordination with radioactive elements in addition to REEs. Typical rare earth elements found in radioactive minerals include; monazite [(Ce, La, Nd, Th)PO_4]; allanite [(Ca, Ce ,Y,

$La)_2$ $(Al,Fe)_3(SiO_4)_3(OH)]$; euxenite $[(Y,Ca,Er,La,Ce,U,Th)(Nb,Ta,Ti)_2O_6]$; micro-lite $[(Ca,Na)_2Ta_2O_6(O,OH,F)]$; pyrochlore $[(Ca,Na)_2Nb_2O_6(O,OH,F)]$; Samarskite-(Y) $[(Y,Ce,U,Fe)_3(Nb,Ta,Ti)_5O_{16}]$; and xenotime $[(YPO_4)]$. Fig. 2.2 shows selected radioactive minerals with a probability of hosting rare earth elements. Frondel & Fleischer (1958) documented a host of minerals which are radioactive in the document *"systematic mineralogy of uranium and thorium."*

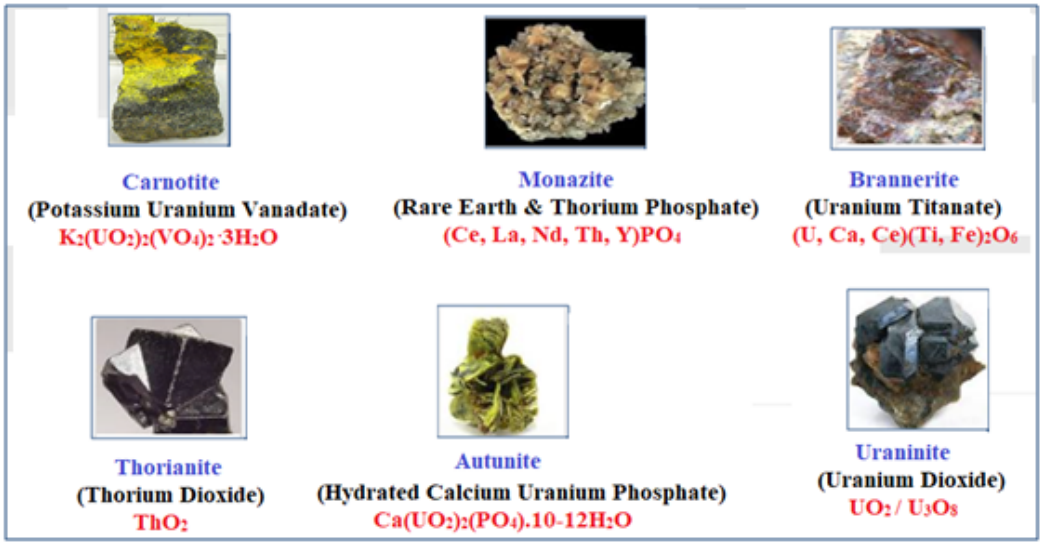

Fig. 2.2 Selected radioactive and rare earth associated minerals

2.5 Properties of Rare Earth Elements

2.5.1 Chemical Properties of Rare Earth Elements

Rare earth elements are known to have similar chemical properties. The coherence in chemical properties of REEs influences their occurrence and formation in the similar geological environment. The electronic configuration of REEs in their trivalent state is considered the most stable state as shown in Table 2.3. Ionic radii of the trivalent REEs decrease with increase in atomic number from La (III) to Lu (III).

The ground state configuration of REEs conforms to the expression $[Xe]4f^n6s^2$, with the exception of La, Ce and Gd which occurs as $[Xe]4f^{n-1}5d^16s^2$; where n=1-14 for the f-subshell (Huang & Bian, 2010). Lutetium has a completely filled f-orbital which suggests its stable ground configuration to be $[Xe]4f^{14}5d^16s^2$. The occurrence of

Table 2.3: Electronic configuration of rare earth elements and their corresponding ionic radius *(Huang & Bian, 2010)*

Element	Z	A	Configuration (Ln^{3+})	(r)
Lanthanum(La)	57	138.9	$[Xe]4f^0$	1.061
Cerium (Ce)	58	140.1	$[Xe]4f^1$	1.034
Praseodymium (Pr)	59	140.9	$[Xe]4f^2$	1.013
Neodymium (Nd)	60	144.2	$[Xe]4f^3$	0.995
Promethium (Pm)	61	-	$[Xe]4f^4$	0.979
Samarium (Sm)	62	150.4	$[Xe]4f^5$	0.964
Europium (Eu)	63	152.0	$[Xe]4f^6$	0.950
Gadolinium (Gd)	64	157.3	$[Xe]4f^7$	0.938
Terbium (Tb)	65	158.9	$[Xe]4f^8$	0.923
Dysprosium (Dy)	66	162.5	$[Xe]4f^9$	0.908
Holmium (Ho)	67	164.9	$[Xe]4f^{10}$	0.894
Erbium (Er)	68	167.3	$[Xe]4f^{11}$	0.881
Thulium (Tm)	69	168.9	$[Xe]4f^{12}$	0.869
Ytterbium (Yb)	70	173.0	$[Xe]4f^{13}$	0.858
Lutetium (Lu)	71	175.0	$[Xe]4f^{14}$	0.848
Yttrium (Y)	39	88.9	[Kr]	0.88

Z= Atomic Number**; A**= Mass Number**; [Xe]**=$1s^2\ 2s^2\ 2p^6\ 3s^2\ 3p^6\ 3d^{10}4s^24p^6\ 4d^{10}\ 5s^2\ 5p^6$**;** **[Kr]**= $1s^2\ 2s^2\ 2p^6\ 3s^2\ 3p^6\ 3d^{10}4s^24p^6$
r =ionic radius

Yttrium ($[Kr]4d^1 5s^2$) with REE ores and similarity in chemical and physical properties is responsible for its grouping with the REEs (Jack et al., 2016).

The configuration of the rare earth elements shows clearly that the 4f-orbital which is located within the 6s-orbital is shielded as it accepts electrons while the outer 6s-orbital is constantly filled throughout the lanthanide series. The lanthanide contractions observed in the defective electronic screening between the 4f-orbitals and the nuclear charge of the trivalent (Ln^{3+}) REEs is responsible for the decrease in ionic radii as the atomic number increases in-line with the effective attraction between the nucleus and the outer electron (Huang & Bian, 2010).

While REEs exist mainly in their tetravalent states, selected REEs such as Sm, Eu and Yb also form a stable divalent oxidation state, while Ce, Pr and Tb have the tendency to exist in a stable tetravalent state. REEs in their trivalent (Ln^{3+}) states form ionic salts and form complexes ($[Ln(H_2O)_9]^{3+}$) in aqueous solution. Compounds formed from the lanthanide trivalent state include LaF_3, $LaCl_3$, $LaBr_3$, La_2O_3, La_2O_2S,La_2S_3, while compounds such as SmI_2, YbI_2 and EuI_2 are typical examples of divalent REE salts (Dorenbos, 2000).

The typical stable tetravalent complex is formed by Ce in a nitrate complex $(NH4)_2$ $[Ce(NO_3)_6]$; other known solids include CeO_2, CeF_4, PrO_2, TbO_2 and TbF_4 (Alexander, 1975).

LREEs form oxides in their trivalent states due to oxidation. However, the LREE due to oxidation are air sensitive, hence they are mostly stored under inert condition. They form three basic crystal structures (A, B and C) under ambient condition due to the polymorphic nature of REE sesquioxides (Ln_2O_3). La to Nd forms hexagonal (A-type) structures; Sm to Gd monoclinic-(B-type); Tb to Lu cubic-(C-type) structures which

can be altered at high temperatures. Sesquioxides of Eu exhibit both B and C-type structure (Gschneidner & Eyring, 1978; Spitsyn et al., 1976). However, Samares (2013) reported A, B, C, X and H as five major crystal structure.

The reaction of REE oxides with water vapor forms alkaline hydroxides ($Ln(OH)_3$) which are sparingly soluble in water, with precipitation pH range of 6.82 to 7.62 (Lu to Ce) and have a progressively decreased basicity from Ce to Lu (Neikov et al., 2009). The reaction of REEs with hydrogen leads to the formation of hydrides (LnH_2) and at high-pressure forms (LnH_3). Trihydrides of Sm to Lu form air-sensitive hexagonal crystal structure. REEs reacts vigorously with acids leading to the production of hydrogen gas, except for the insoluble reaction with HF leading to REE-fluoride ($Ln(F)_3$) formation.

Other reactions of REEs with halides have shown that REEs of Cl, Br and I are less stable when compared to REE-fluorides. REEs react with elements such as Sulphur, hydrogen, carbon and nitrogen. Intermetallic compounds have been formed between REE-TM, REE-group IV and REE-group V, examples of such metals include (Ce-Gd)-Ni, Sm-Co and Nd-Fe-B alloys; Re-Ni-Co (Andrej & Janusz, 1994).

2.5.2 Physical Properties of Rare Earth Elements

Rare earth elements typically exist as metals with known silvery-white and silvery-gray colour characteristics, with an exception in the yellow color characteristics of Pr and Nd. Table 2.4 shows selected properties such as density, lattice structure, magnetic susceptibility, resistivity and neutron absorption cross section.

Table 2.4: Selected physical properties of rare earth *(Zhang & Zhao, 2016)*

REEs	Density (g/cm3)	Metal Lattice	Magnetic susceptibility $\chi_{mol}10^{-6}$ (cm^3/mol)	Resistivity ρ $\chi_{mol}/10^{-6}$ (cm^3/mol) (25°C)	Neutron absorption σ(barn)
Sc	2.985	HCP	+295.2(α)	66	24.0
Y	4.472	HCP	+187.7(α)	53	1.31
La	6.166	DHCP	+95.9	57	9.3
Ce	6.773	FCC	+2500(β)	75	0.73
Pr	6.475	DHCP	+5530(α)	68	11.6
Nd	7.003	DHCP	+5930(α)	64	46
Pm	7.260	DHCP			
Sm	7.536	**	+1278(α)	92	5600
Eu	5.245	BCC	+30900	81	4300
Gd	7.886	HCP	+185000	134	46000
Tb	8.253	HCP	+170000(α)	116	46
Dy	8.559	HCP	+98000	91	950
Ho	8.78	HCP	+72900	94	65
Er	9.054	HCP	+48000	86	173
Tm	9.318	HCP	+24700	90	127
Yb	6.972	FCC	+67(α)	28	37
Lu	9.84	HCP	+183	68	112

BCC: Body-Centred Cubic, **DHCP:** Double Hexagonal Closed-Packed, **FCC:** Face-Centred Cubic, **HCP:** Hexagonal Close-Packed, ****: (Rhombohedral** at ambient condition; **DHCP** at 300 °C / 40 Kbar; **HCP** at 731 °C**, BCC** at 922 °C)

Fig. 2.3 shows the temperature characteristics of REEs. The boiling point distribution in the LREEs decreases from Pr to Eu. The boiling point of Yb in the HREE is lower in relation to the HREE and the LREE. The lowering of the boiling point characteristics has been associated with hybridization. A similar occurrence is obtainable in the melting point of the REEs.

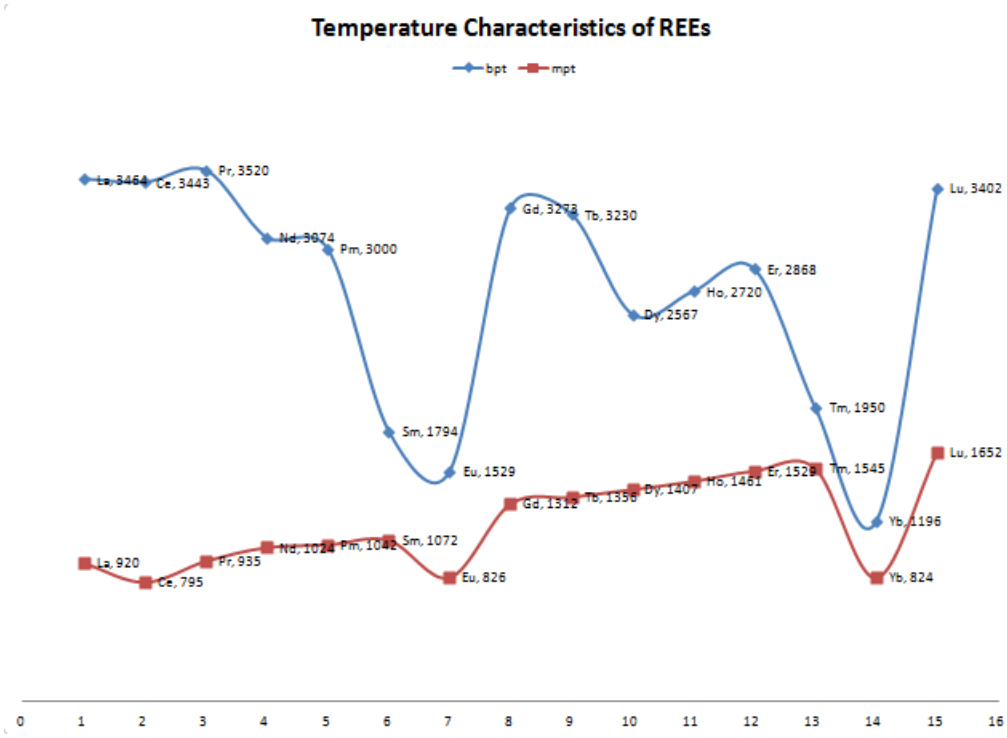

Fig. 2.3: Temperature characteristics of the rare earth elements

2.6 Industrial Processing of Rare Earth Ores

The major ores of rare earth are monazite, bastnaesite, churchite and xenotime. Table 2.5 shows a typical composition of monazite in the beach sands of Brazil and India (Habashi, 1997).

Table 2.5: Percentage composition of monazite in selected beach sands

Compound	ThO_2	U_3O_8	$(RE)_2O_3$	Ce_2O_3	P_2O_5	Fe_2O_3	TiO_2	SiO_2
India	8.88	0.35	59.37	28.46	27.03	0.32	0.36	1.00
Brazil	6.5	0.17	59.2	26.8	26.0	0.51	1.75	2.2

Source:(Habashi, 1997)

Monazite sands in coastal placer environments are usually found in addition with other heavy minerals such as ilmenite, xenotime, zircon, rutile, tantalite, epidote, tourmalime amongst others. The process required for the concentration of monazite from the beach sands is shown in Fig. 2.4. Important processes involved in the beneficiation processing of monazite and include the following; de-sliming, floatation, acid treatment, hypogravity separation and magnetic separation (Adam & Neil, 2014; Jack & Baodong, 2016; Misra et al., 2005).

The industrial mining process requires Dredge and Wedge Upgradation Plant (DWUP) which aids the upgrade of the accessory heavy minerals in the beach sands, leading to a higher percentage of heavy minerals and the discarding of quartz. The heavies obtained from the dredge and wedge up-gradation processes are further processed by the Heavy Upgrade Plant (HUP) which promotes the beneficiation of the minerals before the individual minerals separation. Venugopal et al. (2005) discusses

more on the mining processes involved in the beneficiation of heavy minerals from beach sands.

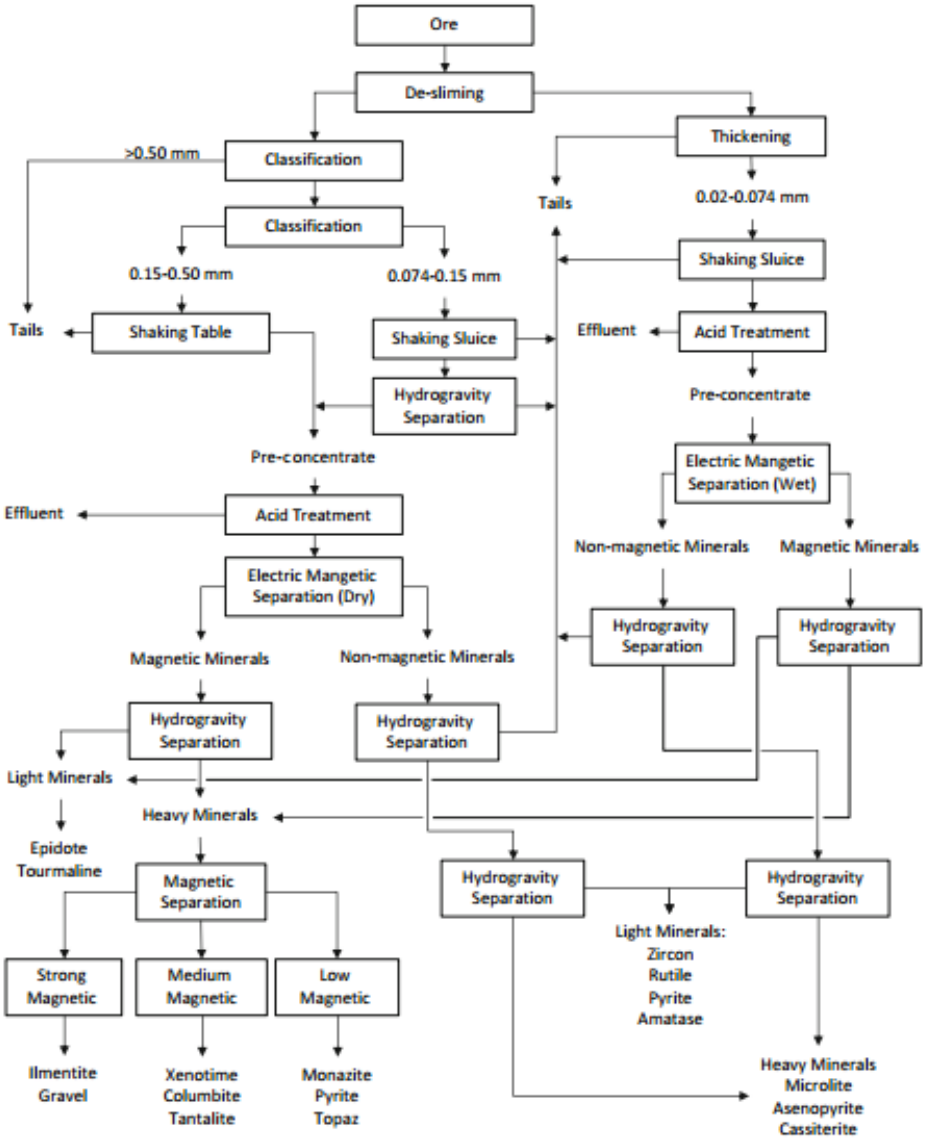

Fig. 2.4: Separation process for heavy minerals in beach sands *(Zhang & Zhao, 2016)*

2.6.1 Acid Digestion of Rare Earth Ores

Monazite sand which predominantly is associated with LREE is subjected to different physical separation processes such as crushing, screening, grinding, floatation (Zhang & Zhao, 2016). The concentrated monazite could be digested in acids such as H_2SO_4, HCl, HNO_3 at relatively high temperatures (~200-230 ^oC) to give rare earth phosphate ($REPO_4$), $RE_2(SO_4)_3$, $RECl_3$ and $RE(NO_3)_3$, Th. A two-stage digestion process described by Habashi (1997) demonstrates the use of 93% sulfuric acid (twice the mass of sand) in the digestion of monazite concentrate at the first stage and a second stage acid digestion which requires about 5 hrs fuming sulphuric acid digestion. The mixture is cooled while thorium and rare earth are dissolved in solution by addition of cold water. Thorium is precipitated using aqueous ammonia at a pH of 1.3 while REEs are precipitated at a pH of 2.3 (Habashi, 1997).

In a method developed by Lynascorp (2006), mixed oxides of rare earth are digested in H_2SO_4 and dissolved in water with the addition of MgO which aids in lowering of the pH control, thereby leading to the slight removal of residues (SiO_2, ThO_2, $ZrSiO_4$) via filtration. The monazite sulphate which contains $Ln_2(SO_4)_3$ in solution is further subjected to partial neutralization with ammonium hydroxide in a reaction tank at a pH of 1.05-1.1, this helps in the precipitation of thorium concentrate (ThO_2) which can be further processed to nuclear reactor grade (Abrao et al., 2001; Habashi, 1997). The precipitates of REEs are obtained at a pH of 2.0 at controlled pH using Na_2CO_3 and NH_4OH. The hydroxide REE-component is reacted with Na_2SO_4 for further precipitation of LREE and HREE. The filtrate is from the hydroxide precipitation is processed for the removal of uranium. Un-reacted REEs which is precipitated with the

thorium cake can be further removed during the thorium purification process. Fig. 2.5 shows the flow process for REE separation adopted by Peak Resources Ltd.

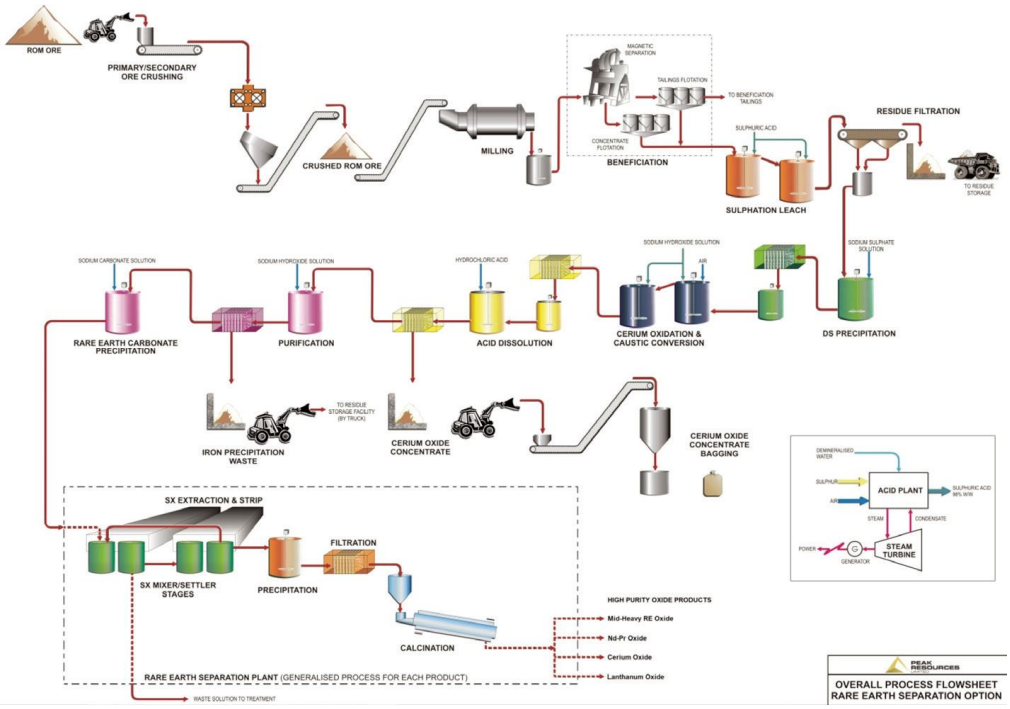

Fig. 2.5: Processes flow chart for rare earth separation *(Allen, 2016)*

Bastnaesite ores concentrated via floatation have been processed using acid digestion method under relatively similar conditions as monazite. The LREE-dominant concentrates can either be calcined at temperatures close to 600 ^{o}C prior to H_2SO_4 digestion or digested in concentrated H_2SO_4 at a temperature close to 200 ^{o}C, leading to the loss of CO_2, HF and SO_2. The resulting sulphates concentrate is leached with water to give REE sulphate [$RE_2(SO_4)_3$] and CeO_2 which is used in glass polishing (Kato et al., 2000).

2.6.2 Alkaline Digestion of Rare Earth Ores

The common ores digested on an industrial scale are monazite, bastnaesite, xenotime and ion-adsorbed clay. The conventional mode for alkaline digestion of monazite (<45 μm) requires the use of about 65% of NaOH for 3 hrs in a digester at about 140 ^{o}C. The residue obtained contains about $Th(OH)_4$, $Na_2U_2O_7$ and $RE(OH)_3$ residue while the $Na_3P0_4.10H_2O$ is filtered off from the digestate and cooled as crystals (Chayavadhanangkul et al., 2009; Habashi, 1997). Similar digestion method can be applied for bastnaesite; reaction takes place at about 200^{o}C in NaOH prior to acid digestion (IAEA, 1993).

The hydroxides obtained from the digestion phase are dissolved in concentrated HCl to give $ThCl_4$, $RECl_3$ and uranium chloride. The use of about 20% NaOH aids the precipitation of thorium and uranium at pH of 5.8 and the $RECl_3$ are precipitated at pH 3.5, radium is removed using barium sulphate solution. Solvent extraction is used in the separation of the individual components of the REEs (Kumar et al., 2014).

2.7 Separation of Rare Earth Metals

Separation of rare earth was considered a Herculean task in the early 50s due to the similarity in chemical properties of the REEs. This has led to the development of methods such as fractional crystallization, ion exchange, chelation ion exchange, solvent extraction, ionic liquid separation and molecular recognition separation.

2.7.1 Solvent Extraction in Rare Earth Processing

Critical to the separation of REEs is the idea of solvent extraction, which played a vital role in the selective distribution of rare earth between aqueous and organic phase. Solvent extraction has helped in the industrial separation of rare earth elements as a group and on an individual basis (Xie et al., 2014). Organophosphorus compounds are among the solvents which have found applications in the separation of REEs (Dulski, 1999). Commonly available solvents used in the separation process include the following; Di-(2-Ethylhexyl)phosphoric acid (D2EHPA), mono-(2-Ethylhexyl)phosphoricacid (HEHEHP), dibutyl-phosphoricacid, Versatic 10, tributylphosphate (TBP), Tributylphosphine oxide (TBPO), triphenylphosphine oxide, carbamoylmethyl phosphonate (CMP), carbamoylmethyl-phosphine oxide (CMPO), tetraoctyldiglycolamide and Aliquot 336 (Koshimoto et al., 2011; Sun & Waters, 2014).

Three classifications of organic extractants used in metal extraction are as follows; chelating, solvating and ion pair extractants.

The chelating extractants are reported to have weak acidic properties and form chelate complexes with metals in solution. They are often used in synergy with solvents in order to promote the easy recovery of metal analytes of interest. Examples of commonly available include organophosphoric acids, 2-thenoyltrifluoroacetone (HTTA), oximes and beta-diketones (Santhi et al., 1994; Petrova & Kurteva, 2011). Typical applications include the separate individual HREEs from solution into organic complexes. Rare earth producers follow similar principles and schemes when selecting specific solvent extraction routes.

Reddy et al. (1997) recorded success in the separation of selected lanthanides (Nd(III), Eu(III) and Lu(II)) using mixed ligand chelating organic extractant. Observed were the complex formation of $Ln(BFA)_3$ in benzene from a mixture of 4,4,4-trifluoro-1-phenyl-1,3- butanedione (HBFA) and neutral oxo-donors such as 2-Ethylhexylsulphoxide (B2EHSO) and triphenyl phosphine oxide (TPhPO).

Relatively similar studies were obtained in the works of Yamada & Freiser (1981) in the separation of Pr, Eu and Yb in a mixture of chloroform and 1,10-Phenanthroline or 7-dodecenyl-8-quinolinol. Inoue & Co-workers (1985) employed a similar method in the separation of Pr, Eu, and Yb, but a slight change in the extraction component using N-benzoyl-phenylhydroxylamine,N-m-tri-fluoromethyl-benzoylphenyl-hydroxylamine (HL) as stand-alone or in association with 1,10-Phenanthroline. This can be extended to include: La, Pr, Eu, Ho and Yb. Similar studies were found in the works of Atanassova & Dukov (2006) where 4-(2-pyridylazo)-resorcin was used in the separation of La, Nd, Eu, Ho and Lu.

Solvating extractants are employed in the removal of metal ions from the aqueous phase into the organic phase, thereby substituting for the hydrate water. Most solvating extractants can be used independently in extraction processes or combined in order to provide synergy in the REE separation process (Komorova & Tran, 1992). Typical solvating reagents applied in the separation of REEs and trans-uranium elements include phosphorus esters such astri-n-butyl-phosphate (TBP), dibutyl butyl phosphonate (DBBP); phosphine oxides as tri-n-octylphosphine oxide (TOPO, Cyanex 921), benzyldi-butylamine (BDBuN).

Ion pair extractants provide ligands which form metal-ligand pair interactions. The idea behind the interaction emanates from the reaction of the lanthanide metals with

acidic ligands which produce anions which form complex aqueous anionic system. On the other hand, ligands produce cations which form aqueous anionic metal complexes to form ionic pairs.

Typical ion pair extractant used as anion exchanger includes; primary amines-(Primene JMT, N1923); and quatenary amines (Aliquat® 336, Adogen® 464). Selected Cation exchanger extractants used in rare earth separation include phosphoric acids-(ethylhexylphosphoric acid (D2EHPA)),Phosphonic acids-(ethylhexylphosphonic acid mono-2-ethylhexyl ester (EHEHPA, HEHEHP, P507, PC88A), Phosphinic acids-(di-2-ethylhexylphosphinic acid (P229);, di-2,4,4-trimethylpentylphosphinic acid (Cyanex 272)), monothiophosphorous acids-(di-2,4,4-trimethylpentyl-monothiophosphinic acid (Cyanex 302)),dithiophosphorus acids-(di-2,4,4-trimethylpentyl-dithiophosphinic acid (Cyanex 301)) (Koshimoto et al., 2011; Williams, 2001; Xie et al., 2014; Yamada & Freiser, 1981).

Ionic liquid extractants in recent times have found application as a form of green solvent utilized in the separation of REEs. The ionic liquids are regarded as “green solvents” even though other scientists question the safety of ionic liquid (Robin & Kenneth, 2002; William, 2002).

In a bid to understand the functionality of ionic liquids, it is important to emphasize that RTILs comprise mostly of anionic and cationic group co-existing in a liquid state. Commonly synthesized ionic liquids have heteroatoms incorporated within their cations; such cations include pyridinium, imidazolium, ammonium, phosphonium, pyrrolidinium, isoquinolinium, sulphonium, imidazolium and cholinium cations (Zhang et al., 2006). Fig. 2.6a, and Fig. 2.6b show commonly used cation and anion ionic liquids. Although cations are mostly asymmetrical, they account for the low

melting point of RTILs, while anions are known to contribute to the overall distinctive properties of the ionic liquids.

Recent studies consider the development of Task-Specific Ionic Liquids (TSILs) in REE extraction. Nockemann & Co-workers (2006) are known to have studied the use of protonated betaine cation and bis-trifluorosulfonyl)imide anion [Hbet] [TF2N] in the selective dissolution of REE content in red phosphor [Y_2O_3: Eu] leaving other halophosphate in solution (Dupont & Binnemans, 2015). [Hbet] [TF2N] has also been reported in the selective recovery of Scandium(III) from aqueous solutions (Onghena & Binnemans, 2015). Araque et al. (2015) in their study tried to further elucidate ionic liquid structure in general and it's coupling to transport and dynamics.

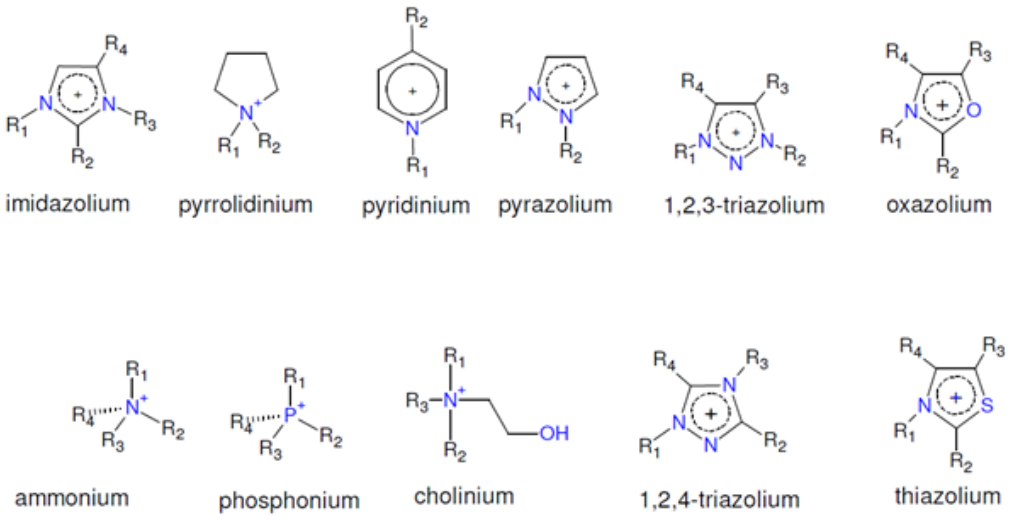

Fig. 2.6 (a): Typical cations of ionic liquid

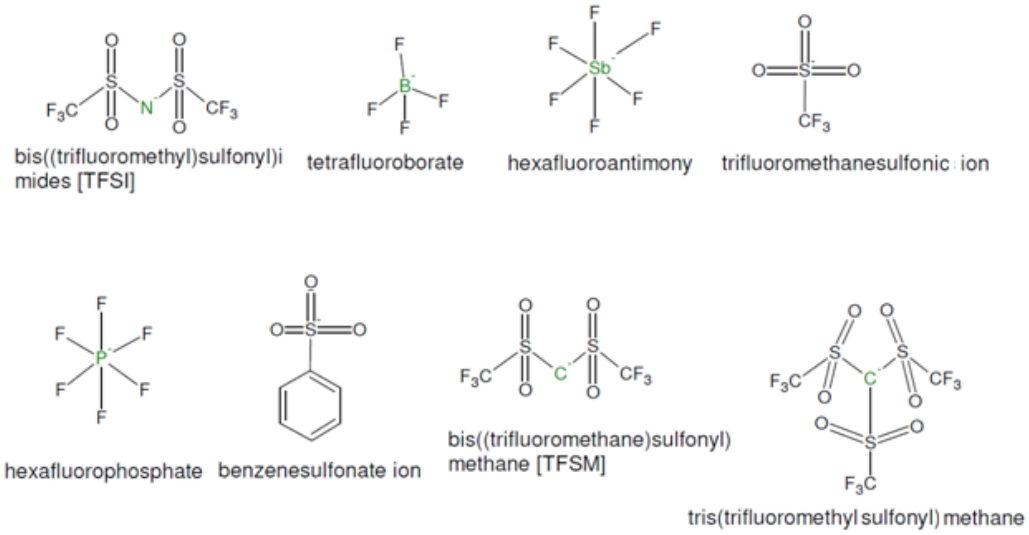

Fig. 2.6b: Typical anions of ionic liquid *(Olivier-Bourbigou et al., 2010; Zhang et al., 2006; Ye et al., 2013)*

2.7.2 Ion Exchange Resin Separation

The ion exchange chromatographic system has been established in the separation of REEs in the last five decades. The ion exchange system can be classified into cations(strong; moderate; weak), anion-(weak; strong), chelating, or bi-functional exchange system (Vértes, 2011). The development in ion exchange resin separation technique for REEs as reported in the works of Reddy et al., (1997), shows the separation of selected lanthanides (Nd(III), Eu(III) and Lu(II)) using mixed ligand chelating organic extractant. Observed were the complex formation of $Ln(BFA)_3$ in benzene from a mixture of 4,4,4-trifluoro-1-phenyl-1,3-butanedione (HBFA) and neutral oxo-donors such as 2-ethylhexylsulphoxide (B2EHSO) and triphenyl phosphine oxide (TPhPO).

The large volume solvent chromatography works of Gilbert (1980) shown in Fig. 2.7 utilized the Biorad AG1-XB anion exchange resin in the separation of REEs and LREEs from geological samples.

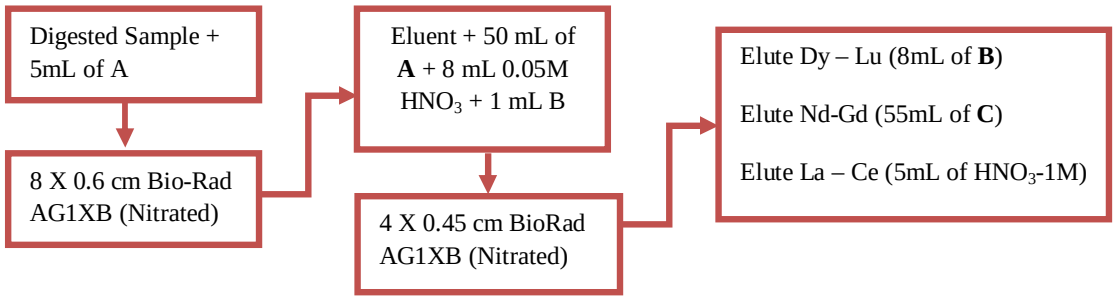

A: 90% glacial acetic acid + 10% 5M HNO_3
B: 90% methanol + 10% 15.4M HNO_3;
C: 90% methanol + 10% 0.05M HNO_3

Fig. 2.7: Anion exchange separation of rare earth element from rock (Gilbert, 1980)

2.7.3 Chromatographic Extraction Resin in REEs Separation

Eichrom technologies in the 1990's developed a solid-liquid system that allows the use of selective extraction chromatographic resins for the separation of lanthanides and actinides from acidic solution.

The resins combine the use of solvating extractants supported on a polymeric solid substrate for the sorption of lanthanides and actinides in different oxidation states from fission products (Horwitz et al., 2005 ; Alexandratos & Ripperger, 1998).

The commercially developed Eichrom resins utilized in the separation of lanthanides and actinides from geological matrix include; actinide ™, DGA ™ ,LN ™ , RE ™, TEVA ™ , TRU ™ and UTEVA ™ resin.

Horwitz et al. (2006) compared the use of solvent-extraction with chelating-extraction process in the recovery of metals. The use of large volumes of solvents and multiple solvent extraction stages was considered a disadvantage in the recovery of metals from solution (Horwitz et al., 2006; Ostapenko et al., 2015). On the other hand, extraction chromatographic system combines the solvent extraction capability and chromatographic properties, thereby reducing the turnaround time in the separation process.

The trans-uranium (TRU) chelation extraction resin developed by Eichrom Industries is applicable in actinide-lanthanide sorption and desorption. The chromatographic material is composed of 13% octyl(phenyl)-N,N-di isobutylcarbamoylmethylphosphine oxide (CMPO) dissolved in 27% n-tributyl phosphate (TBP) and supported on Amberchrom CG-71ms substrate (Pin & Zalduegui, 1997). The TRU resin has found application in the sorption and desorption of Fe, Th, Pa, U, Np, Pu, Am and Cm; and dating of the extraction process. TRU has been used in the separation of Eu in a mixture of radioactive waste and a recovery (> 80%) (Maischak & Fachinger, 2001). Fig. 2.8a and Fig. 2.8b shows a typical complex formed during the interaction between lanthanides, TBP and CMPO; A suggested TBP-CMPO and Lanthanide complex is suggested *(Appendix H)*. Pin & Gannoun (2017) reported the separation of Sm, Nd, Th, U and other LREEs using a coupled TRU and Ln resin system.

The LN resin is made up of di-(2-ethylhexyl)-phosphoric acid adsorbed Amberchrom CG-71ms substrate (Pin & Zalduegui, 1997). The separation of Nd and Sr for isotopic studies was achieved using a combination of Sr-resin, TRU-resin and LN-resin with a high rate of recovery (Míková & Denková, 2007). Ostapenko et al. (2015) in a study of the behavior of REEs on the extraction chromatographic resin (DGA, LN, TRU)

reported optimum conditions for the separation of Ce(III) and La(III) from nitric acid solution. The challenge associated with the interference of Fe in the separation of the LREEs was resolved via the reaction of digested rock samples with ascorbic acid (Míková & Denková, 2007).

The separation of the lanthanides using LN resin has recorded huge success with respect to the isotope determination of Nd/Sm in geological matrices (Saji et al., 2016). The impregnated di(2-ethylhexyl)orthophosphoric acid (HDEHP) extractant was used in the separation of LREE from basaltic rocks. The affinity of the LN resin in the extraction of REEs increases with increase in mass number (Lehto & Hou, 2011). Gharibyan et al. (2014) in a study compared the extraction of other derivatives of the LN, LN2, LN3 extraction resin.

Although DGA resin is mostly applied in the extraction of actinides, it has shown strong retention of Yttrium, while elution is achieved using nitric acid or hydrochloric acid (Horwitz et al., 2005). The DGA resin is impregnated on an inert substrate using straight chain or branched C8 groups of N,N,N',N'-tetra-n-octyldiglycolamide (DGA Resin, Normal) or N,N,N',N'-tetrakis-2-éthylhexyldiglycolamide extractant.

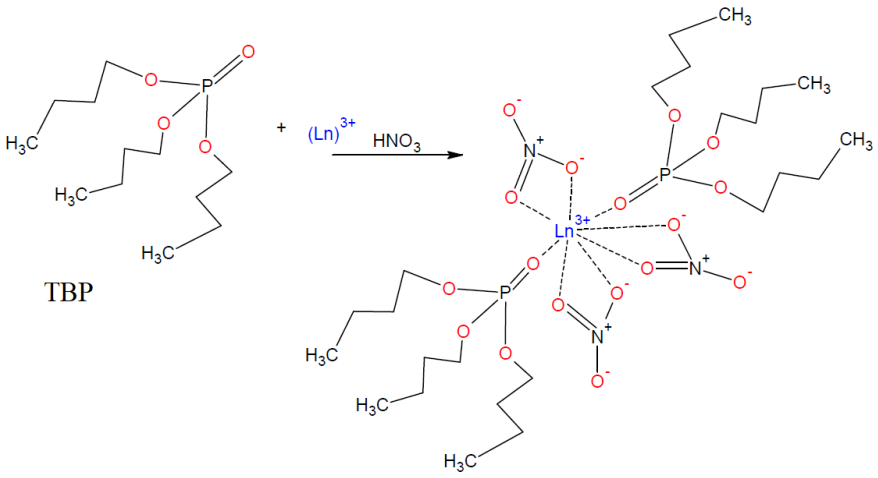

Fig. 2.8a: Structural complex of TBP interaction with Ln^{3+} in acidic solution. (Braatz et al., 2017)

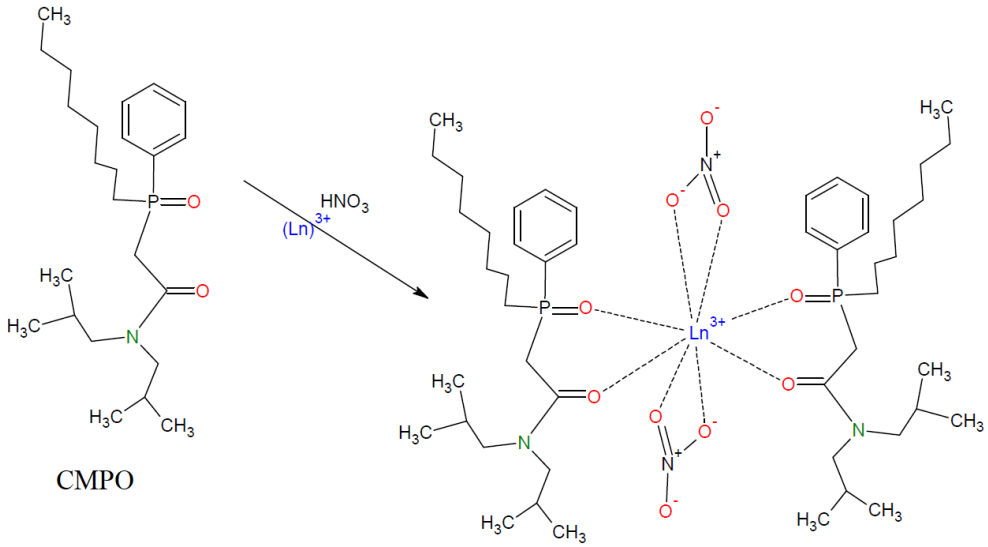

Fig. 2.8b: Inferred structural complex of CMPO interaction with Ln^{3+} in acidic solution

2.7.4 Molecular Recognition in the Separation of REEs

The recent search for environmentally friendly and selective separation mode for REEs led to the development of SuperLig® resins by the Ucore and IBC Advanced Technologies, Inc. The technology promised >99% recovery of REEs as a group or individual elements from pregnant leach solutions, faster flow rate when compared to ion exchange and solvent extraction system, minimal waste generation, minimal elution solvent and improved turn around in separation time (Littlejohn, 2007).

The SuperLig® relies on the development of a predesigned selective host ligand species bound chemically to a solid support and packed in a column. Pregnant leach solution of REE concentrates is passed through the column and eluted with dilute nitric acid solution. The question that arises is; how does this MRT technology differ from chelation extraction? What type of selective host ligands is used? The works of Izatt et al. (2016), shows that an organic metal selective ligand compound such as 18-crown-6 ether is attached to a solid silica gel support via a tether. Kruchten & Godfried (1998) in a patent described the solid support mostly used as silica, polystyrene and acrylates which can be covalently combined with immobilized crown ethers in a single step process. The methods of Horwitz et al. (2005) and the works of Izatt et al. (2016) used relatively similar method of chelating extraction procedures and column chromatographic system.

CHAPTER THREE

MATERIALS AND METHODS

This chapter of the study involves the description of the study area, geology, climate, vegetation and topology of the area. The sample preparation techniques and analysis methods are described. Rare earth elements determinations with respect to their particle size distribution are described. The description of the experimental procedure for the determination of activity concentration of the coastal sands is also reported.

3.1 Profile of the Study Area

3.1.1 Geographical Location

Ghana is located in the Western part of Africa. It has a total land area of 238,533 square kilometers with border countries such as Burkina Faso to the north, Ivory Coast to the west and the Atlantic Ocean (Gulf of Guinea) to the south (Norton, 2003). The total coastline of Ghana is about 550 kilometers and can be classified as intermediate to low tide terrace (McGlade et al., 2002).

Ghana has about ten regional capitals, of which three of these regional capitals form a border with the Atlantic Ocean (Gulf of Guinea). The three regions are Greater Accra, Central Region and Western Region. Figure 3.1 shows a map of Central and Western regions of Ghana.

The Central region is one of the administrative regions of Ghana with Cape Coast as its Capital and it occupies a land area of about 9,826 square kilometers (Conafric, 2000). The Central region forms border with the Western region on the West Ashanti,

and Eastern region to the North and Greater Accra to the East. The Southern part of the Central region forms border with the Atlantic Ocean (Gulf of Guinea) with a beach length of about 168 kilometer extending from Awutu (5°29'33.6"N 0°22'08.4"W) to Komenda (5°02'01.4"N;1°34'08.3"W) (NewsGhana, 2017).

The Western region of Ghana has a land area of approximately 2,3921 square kilometers. It forms a border with Ivory Coast (Côte d'Ivoire) at the west, Ashanti and Brong-Ahafo at the north and the Atlantic Ocean (Gulf of Guinea) to the south (Ghana Imigration, 2017). The coastal stretch for the Western region extends from Komenda (5°02'01.4"N; 1°34'08.3"W) to New Town (5°05'29.6"N; 3°06'31.3"W).

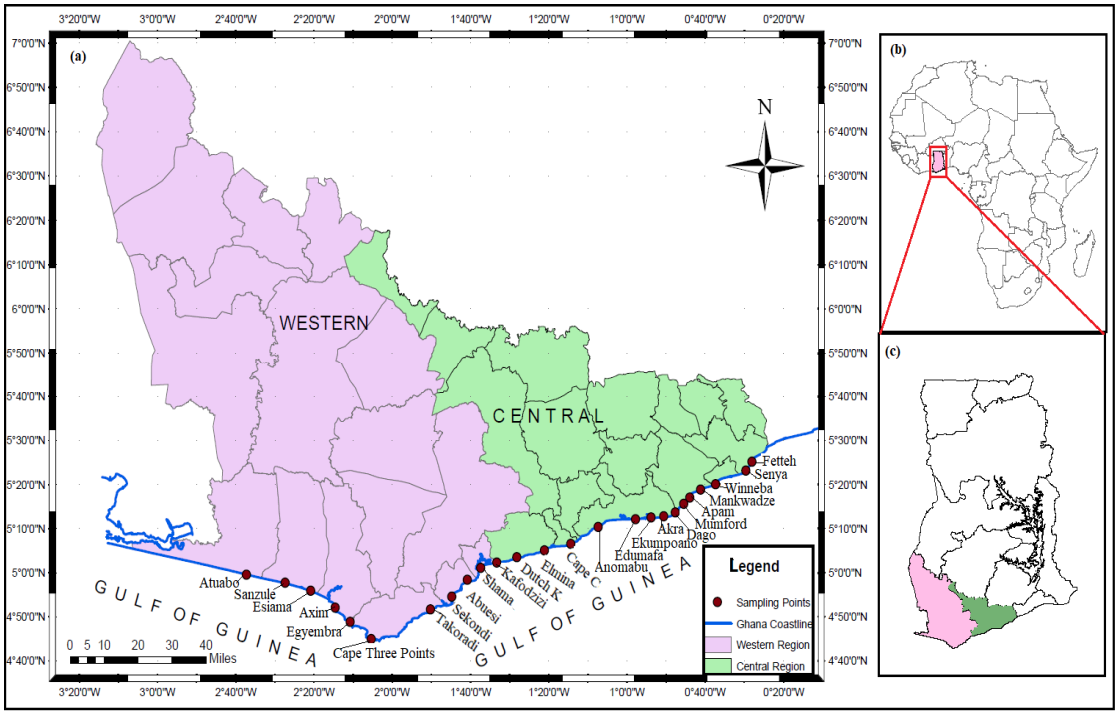

Fig. 3.1: (a) A map showing the Central and Western regions of Ghana, West Africa
(b) Inset showing Africa and a highlight of Ghana
(c) Inset showing Ghana and a highlight of Central and Western regions

3.1.2 Geology of the Coastal Area

The geology of the coastal area is considered as actively young and due to the lithostratigraphy, the basement rocks which comprise Sekondian, Accraian, Amisian and Apollonian group (IBP, 2008). The geology of Ghana is known to comprise of the Voltaian Basin, while the Birimian supergroup occupies a depth of 15000 km. The Birimian consist of sedimentary rocks containing basalts, sandstones and older shales whose origin can be associated with volcanoes of old origin (Yendaw, 2004). The isolated and spatially restricted coastal sedimentary basins of Ordovician to Cretaceous age are responsible for the opening of the Atlantic Ocean (Paul, 2003).

The basement rock of the coastline is known to have occurred as the lithostratigraphic opening of the Atlantic in which Dickson (1969) described the Birimian and Tarkwaian as series of economic importance to Ghana. The metavolcanic Paleoproterozoic rock from the Birimian supergroup and accounts for the major part of the Geology of Ghana. A Paleozoic and Cretaceous to Tertiary sediments are found along the coast (van, 2002).

There is an occurrence of a mix of conglomerates, volacnistic sediments, micaceous sandstones, mudstones, interbedded shales and granitoid which characterize the detrital sediments along the coast of Ghana (Yendaw, 2004). A list of the selected locations and coordinates in the Central and Western regions are shown in Table 3.1 and Table 3.2, while a description of the geology of the locations is shown in Table 3.3 and Table 3.4

3.2 Description of the Selection of Sampling Sites

Geological map provided by the Ghana Survey Department served as a pointer in the identification of the coastal geology. Geospatial pre-selection of 25 target locations were considered for sampling along the coast and the hand held GPS was used in locking the positions where the samples were collected. The target area for each sample was defined based on the geology of the coastal area.

Fifteen locations were selected in the Central region and ten locations were selected in the Western region. The sand samples were collected along the beach face at depths of 30 cm and 100 m by 100 m distance back shore using a composite sampling method. This was repeated for all the twenty-five locations selected along the Central and Western regions during the period of January to June 2016.

The samples were collected based on the geology of the coastal area as shown in Table 3.3 and Table 3.4. The common geology of the coastal environment includes deposits transported from the Dahomeyan, Birimian sediments, Birimian volcanics, Tarkwaian, Togo formation, Sekondian, Eocene & Cretaceous, Tertiary and recent sediments (GSD, 2009; Schluter, 2008).

Table 3.1: Selected sampling locations along the coast of the Central region of Ghana.

Site Code	Location	Coordinates
CR1	Gomoa Fetteh	5°25'03.97''N, 0°27'51.50"W
CR2	Senya Beraku	5°23'22.25''N, 0°29'20.93''W
CR3	Winneba	5°20'33.18''N, 0°37'02.80''W
CR4	Mankwadze	5°18'53.21''N, 0°41'04.56''W
CR5	Apam	5°16'55.86''N, 0°43'50.19''W
CR6	Mumford	5°16'02.15''N, 0°45'11.57''W
CR7	Dago	5°13'57.46''N, 0°47'23.86''W
CR8	Akra	5°12'26.45''N, 0°53'00.42''W
CR9	Ekumpoano	5°12'26.05''N, 0°53'23.28''W
CR10	Edumafa	5°12'10.97"N, 0°57'54.98''W
CR11	Anomabu	5°10'17.54''N, 1°07'38.49''W
CR12	Cape Coast	5°06'11.20''N, 1°40'36.45''W
CR13	Elmina	5°04'52.95''N, 1°21'06.62''W
CR14	Dutch Komenda	5°03'20.63''N, 1°28'26.50''W
CR15	Kafodzizi	5°02'10.68''N, 1°33'22.90''W

Table 3.2: Selected sampling locations along the coast of the Western region of Ghana.

Site Code	Site Name	Coordinates
WR1	Shama	5°00'58.30''N, 1°37'40.07''W
WR2	Abuesi	4°58'14.64''N, 1°39'12.03''W
WR3	Sekondi	4°55'59.14''N, 1°42'41.65''W
WR4	Takoradi	4°53'16.10''N, 1°44'52.11''W
WR5	Cape Three Point	4°45'01.41''N, 2°05'40.58''W
WR6	Egyembra	4°49'00.15''N, 2°10'56.53''W
WR7	Axim	4°53'27.33"N, 2°14'45.55"W
WR8	Esiama	4°55'43.52''N, 2°20'29.25''W
WR9	Sanzule	4°57'29.74''N, 2°27'00.49''W
WR10	Atuabo	5°00'39.92''N, 2°42'22.22"W

Table 3.3: Geology of selected sampling locations along the coast of the Western region of Ghana *(GSD, 2009)*

Site Code	Location	Characteristic Geology
WR1	Shama	- Biotite, (+/- Hornblende, +/- muscovite), granitoids, undifferentiated.
WR2	Abuesi	- Biotite, (+/- Hornblende, +/- muscovite), granitoids, undifferentiated.
WR3	Sekondi	- Sandstone (5-formations) and interbedded shale, (2-formations undifferentiated) <undifferentiated-Sekondian group>.
WR4	Takoradi	- Sandstone (5-formations) and interbedded shale, (2-formations undifferentiated) <undifferentiated-Sekondian group>.
WR5	Cape Three Points	- Hornblende-biotite granitoids, undifferentiated (strongly foliated) <syncovolcanic intrusive rocks> [embedded]-volcaniclastic sediment dominant.
WR6	Egyembra	- Hornblende-biotite tonalite <Volcano Plutonic Group-volcanic belts- synvolcanic intrusive rocks>
WR7	Axim	- Dacitic to rhyolitic flow/subvolcanic rock and minor interbeded volcaniclastics: [tab-trace] conglomerate, mature quartz pebble and quartzose sandstones.
WR8	Esiama	- Limestone, marl, mudstone with intercalated sandy beds (includes minor cenozoic sediments in the Tano basin area). <Timesozoic- Lower Cretaceous>; Argilitic/politic sediment dominan +/- kerogen (graphite)
WR9	Sanzule	- Limestone, marl, mudstone with intercalated sandy beds (includes minor cenozoic sediments in the Tano basin area). <Timesozoic- Lower Cretaceous>
WR10	Atuabo	- Limestone, marl, mudstone with intercalated sandy beds (includes minor cenozoic sediments in the Tano basin area). <Timesozoic- Lower Cretaceous>

Table 3.4: Geology of selected sampling locations along the coast of the Central region of Ghana *(GSD, 2009)*

Site Code	Location	Characteristic Geology
CR1	Fetteh	- Minor quartzite; bordered with, quartzite, minor mica schist <Togo Structural Unit>.
CR2	Senya	- Quartzite, minor mica schist; bordered with minor quartzite of <Togo Structural Unit>.
CR3	Winneba	- Biotite granite, with Archean continental signature), Winneba type <Erbunean Plutonic Suite>.
CR4	Mankwadze	- Amphibolites, partly of contact metamorphic origin
CR5	Apam	- Amphibolites, partly or contact metamorphic origin. Birimian protoliths affected by Eburnean tectono metamorphic overprint.
CR6	Mumford	- Detrital sediment, mainly sandstone and conglomerate, undifferentiated
CR7	Dago	- Wacke sediment dominant; bordered with detrital sediments, mainly sandstone and conglomerate, undifferentiated.
CR8	Akra	- Biotite, granitoids, with volacnistic sediments and undifferentiated mica schists.
CR9	Ekumpoano	- Wacke sediment dominant; bordered with detrital sediments, mainly sandstone and conglomerate, undifferentiated.
CR10	Edumafa	- Conglomerates, micaceous sandstones, arkose, mudstones.
CR11	Anomabu	- Sediment, volacnistic sediment, undifferentiated locally mica schists.
CR12	Cape Coast	- Biotite granitoids, undifferentiated; bordered with volacnistic sediments/ sediment, undifferentiated locally mica schists <Erbunean Plutonic Suite>.
CR13	Elmina	- Sandstones (5-formations) and interbeded shale (2-formations) undifferentiated.
CR14	Dutch Komenda	- Sandstones (5-formations) and interbeded shale (2-formations) undifferentiated.
CR15	Kafodzizi	- Sandstones (5-formations) and interbeded shale (2-formations) undifferentiated.

3.3 Collection of Beach Sand Samples

Ghana geological map was referred to the identification of the sample location along the coastal area. This was supported by the use of Google Earth Software (ver. 7.1.8.3036) freeware which provided a 2-dimensional detail of the coastal stretch. Most of the beaches are characterized by low lands and low tide.

A spatial pre-selection of 25 target locations were considered for sampling along the coast. Within 1-km^2 of each target area, sand samples were collected at the most representative setting. Visual inspection of the defined area was conducted in order to understand the setting of the beach.

The sand samples were collected along the beach face at depths of 30 cm and 100 m by 100 m distance back shore using a soil auger. Composite sampling was adopted during the sampling process, this was repeated for all the twenty five locations selected along the Central and Western regions during the period of January – June 2016. The target area for each sample was defined based on the geology of the coastal area. Fig. 3.1 shows a representation of the sampling points as defined on the map of Ghana. Coordinates were picked using hand-held GPS and details were recorded in the field logbook.

Geospatial identification of the sampling area was achieved using Shuttle Radar Topography Mission (SRTM) 1 Arc-Second Global data (USGS, 2015). The Environmental Systems Research Institute (ESRI) software package Ver. 10.2, which was licensed to the Remote Sensing Geospatial Information Services (RSGIS) Unit, University of Ghana, was used in the generation of 3-dimensional Imagery of the coastal stretch. The geospatial images for the Central and Western regions shown in

Fig. 3.2 and Fig. 3.3 were generated using ArcMap and ArcScene packages from ESRI.

The samples collected were transferred to a clean facility at the laboratories of the Ghana Atomic Energy Commission (GAEC) for air drying and oven drying in readiness for further processing.

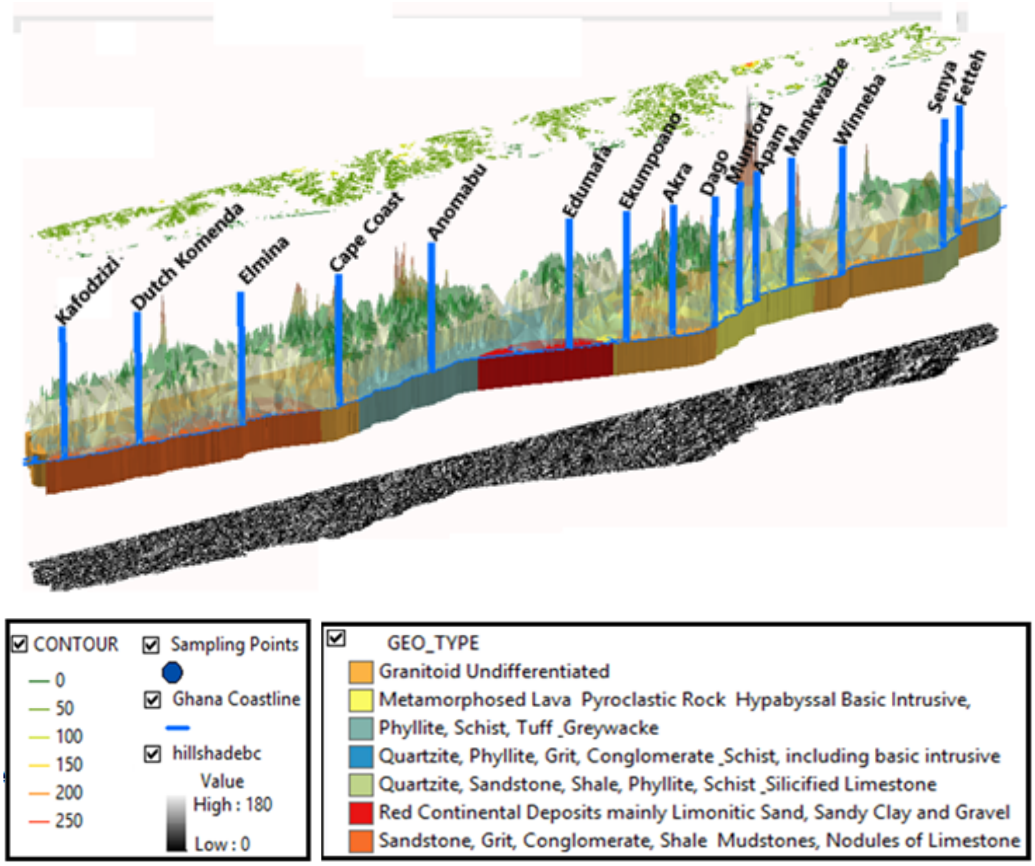

Fig. 3.2: GIS representation of the Central region coastline of Ghana

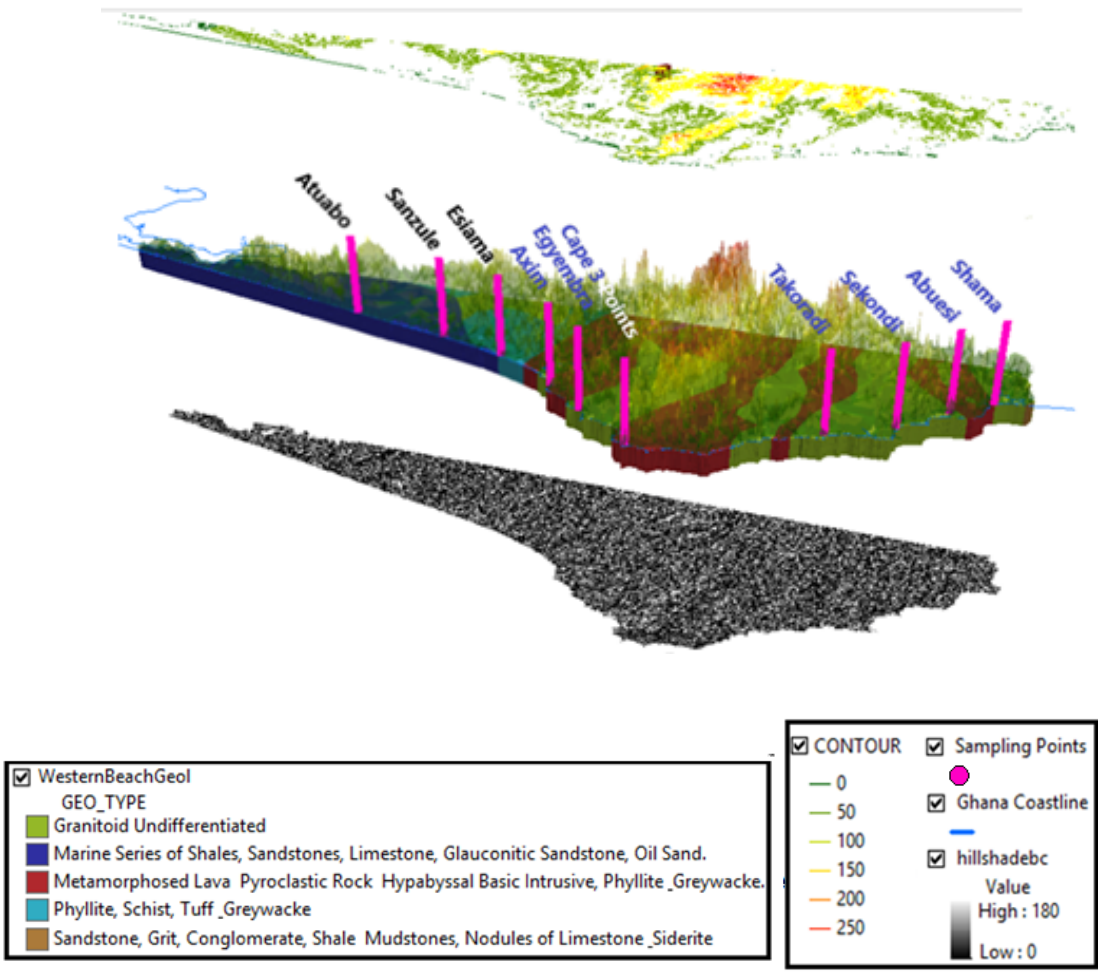

Fig. 3.3: GIS representation of the Western region coastline of Ghana

3.4 Preparation and Analysis of Samples

3.4.1 Flow Chart for General Scheme of Analysis

The experimental design for this study is illustrated by the flow chart for the scheme shown in Fig. 3.4a and Fig 3.4b.

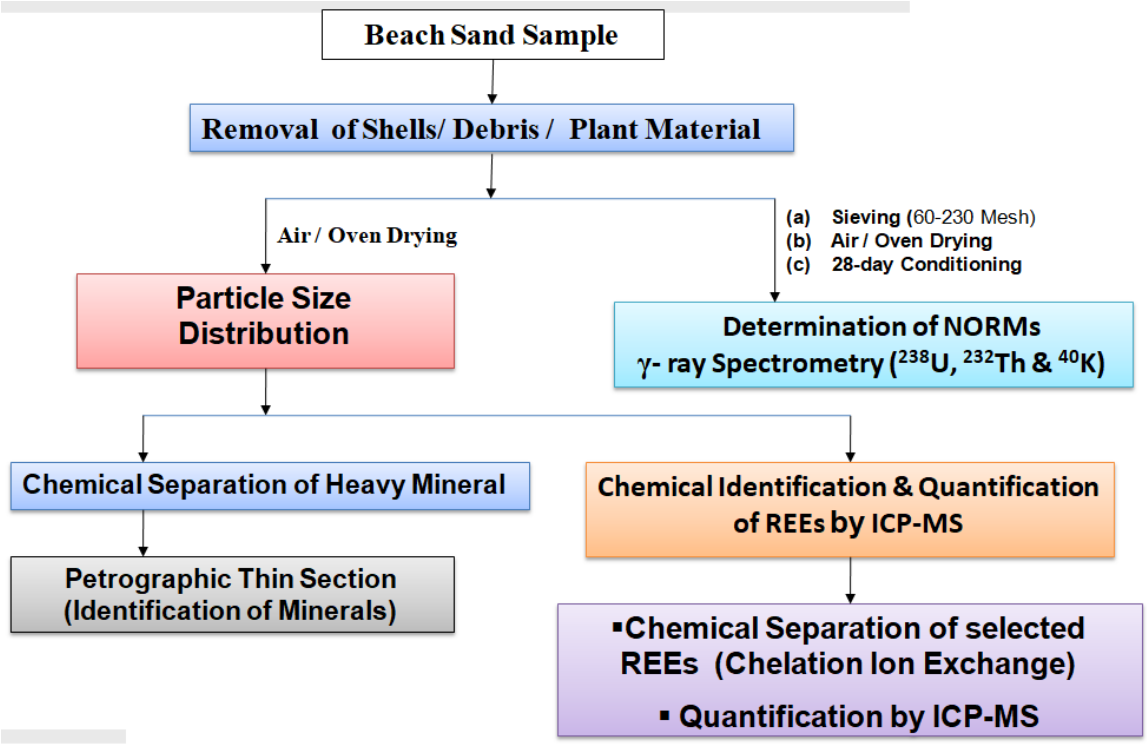

Fig. 3.4a: Flow chart for general experiment

Removal of shells, debris and plant materials as well as particle size distribution was done at the laboratories of the Ghana Research Reactor Centre (GRRC) of the Ghana Atomic Energy commission (GAEC). Determination of Naturally Occurring Radioactive Materials (NORMs) and Heavy Mineral Separation of the beach sands were performed at the γ-ray spectrometry laboratory of the Radiation Protection Institute (RPI) and the Nuclear Chemistry and Environmental Research Centre (NCERC), GAEC respectively. Chemical separation of selected REEs using

Extraction Chromatography was carried out at the Radiochemistry Laboratory of the Radiation Protection Institute (RPI).

Petrographic Thin Section was carried out at the laboratories of the Department of Earth Science, University of Ghana.

Chemical Identification and Quantification of REEs by Inductively Coupled Plasma Mass Spectrometer (ICP-MS) was done at the laboratories of ALS, Canada and the Metal Contaminant Laboratory of the Ghana Standards Authority.

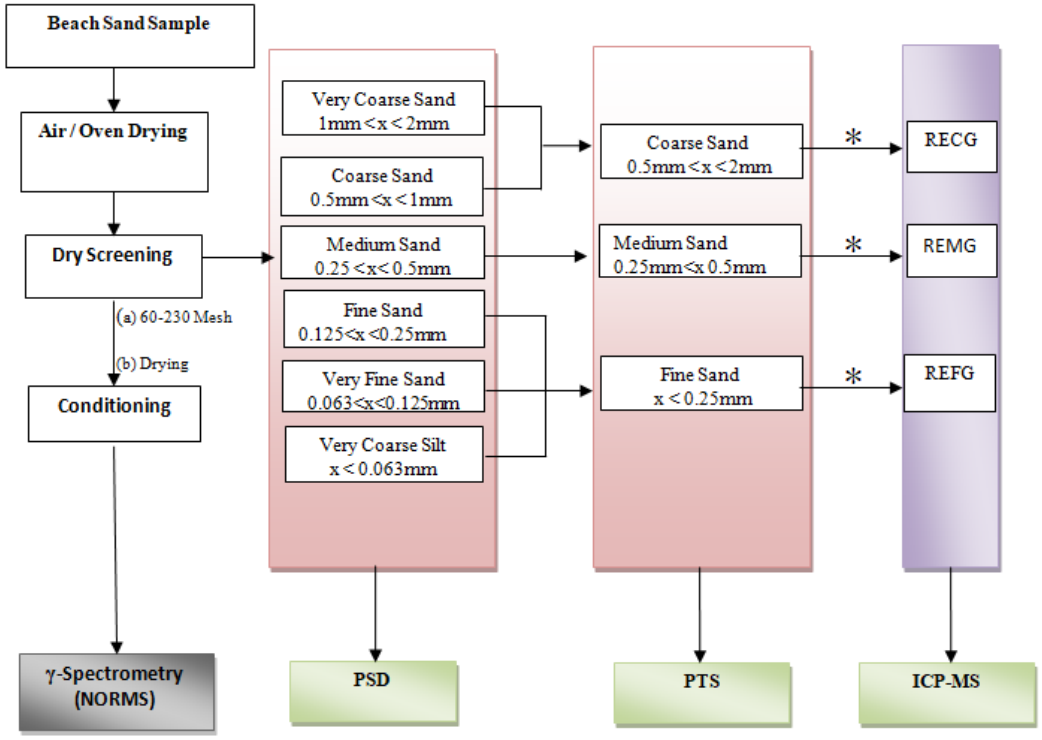

ICP-MS: Inductively Coupled Plasma Mass Spectrometer
NORMs: Naturally Occurring Radioactive Materials
PSD: Particle Size Distribution
PTS: Petrographic Thin Section
RECG: Rare Earth Coarse Grain
REFG: Rare Earth Fine Grain
REMG: Rare Earth Medium Grain
***** Pulverisation (<75 µm)

Fig. 3.4b: Flow chart of general experimental framework

3.5 Grain Size Distribution of Coastal Sands

3.5.1 Instrumentation for Grain Size Analysis

ASTM sieve (63, 125, 250, 500, 1000 and 2000 µm), Retsch© vibratory sieve shaker AS 200, Ohaus CS2000 weighing balance, Newtronic oven, Stainless steel weighing tray, 4 inch brush with natural soft bristle, boar bristle brush, HP computer with Microsoft Excel spreadsheet program and GRADISTAT ver. 4.0 software. Fig. 3.5 shows the chart used in grouping of the beach sands into three groups needed for the analysis

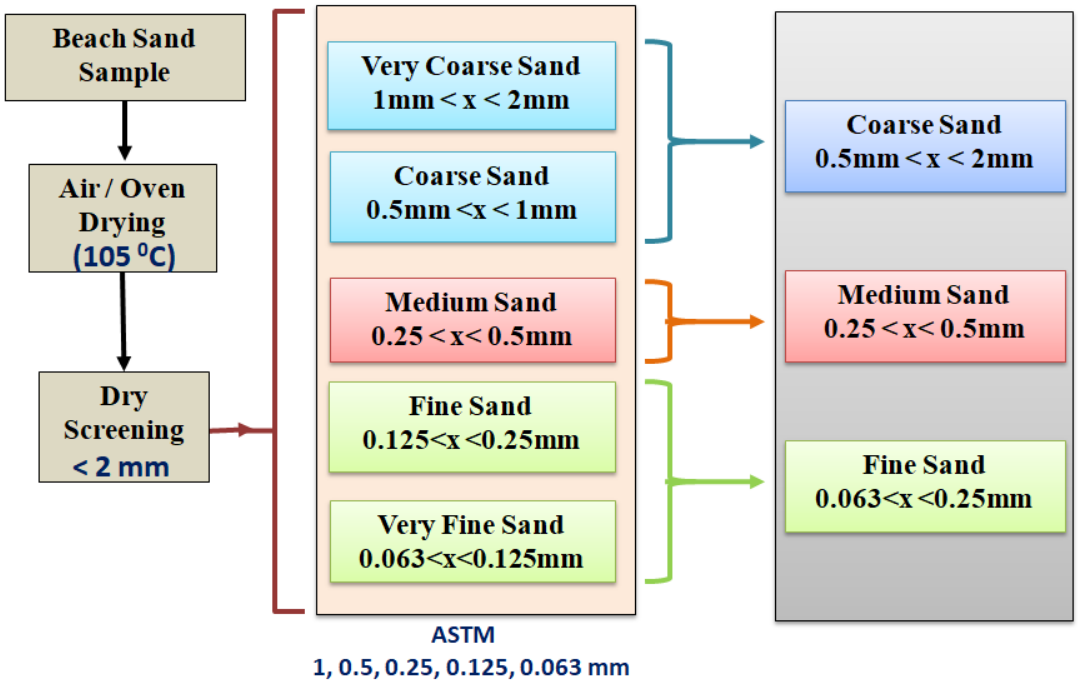

Fig. 3.5: Scheme for particle size distribution

3.5.2 Experimental Procedure for Particle Size Distribution

In a bid to characterize the coastal sands collected along the Central and Western regions of Ghana, a representative sample per target area is collected, stored in a grip sealed low density polyethylene plastic bag and tagged with an identifier. The samples were oven dried at about 100 °C for 24 hours. Cooling was achieved in a desiccator and about 500 g of the sample was run through a set of sieves (63, 125, 250, 500, 1000 and 2000 µm) with the largest pore size at the top and the smallest at the base.

The loaded sieves were clamped on the Retsch Vibratory Sieve Shaker AS-200 and agitated intermittently at 5 minutes and a total time of approximately 15 minutes. The sand retained on each sieve was weighed, recorded in the data book and transferred into a labelled grip sealed low density polyethylene plastic bag. The statistical data acquired during the course of the experiments were calculated using particle size-based statistical software Gradistat Ver. 4.0.

Statistical details were arrived at using the Folk & Ward (1957) method of grain size analysis. The statistical data obtained aids in the comparison of the different sediments and their distribution along the coast.

Information on the mean, mode(s), sorting (standard deviation), skewness, kurtosis, and cumulative percentiles can be acquired as a result of the use of Gradistat. Fig. 3.6 shows a flow process of the acquisition of the statistical data.

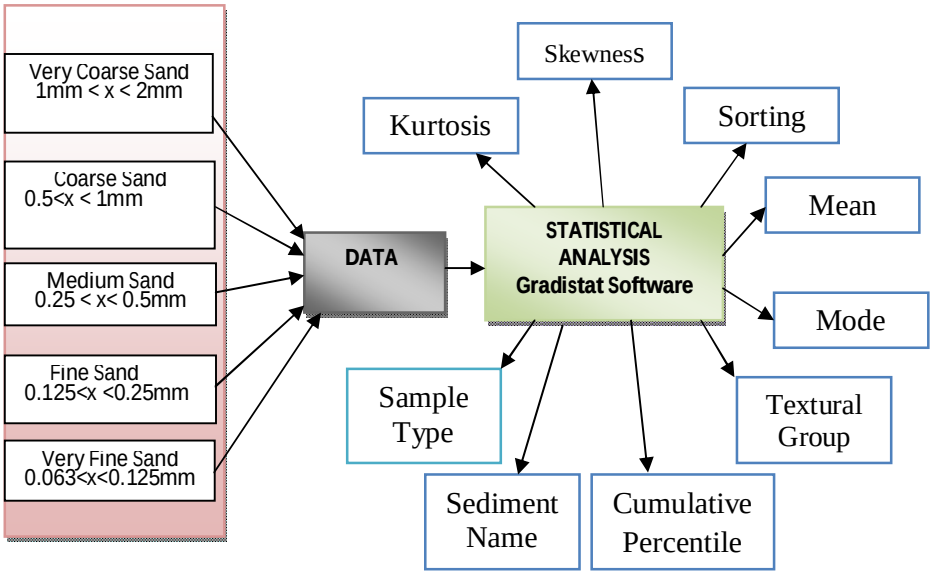

Fig. 3.6: Statistical analysis scheme for beach sands from the study area

The use of Folk and Ward method of moments was employed in deriving the statistics. Arithmetic mean was derived from the formulae given in Table 3.5 to 3.9 below:

Table 3.5: Arithmetic method of moment statistics

Mean	Standard deviation	Skewness	Kurtosis
$\bar{x}_a = \frac{\Sigma f m_m}{100}$	$\sigma_a = \sqrt{\frac{\Sigma f (m_m - \bar{x}_a)^2}{100}}$	$Sk_a = \frac{\Sigma f (m_m - \bar{x}_a)^3}{100\sigma_a{}^3}$	$K_a = \frac{\Sigma f (m_m - \bar{x}_a)^4}{100\sigma_a{}^4}$

Source: Blott and Pye (2001)

Table 3.6: Geometric method of moments

Mean	Standard deviation	Skewness	Kurtosis
$\bar{x}_g = \exp \frac{\Sigma f \ln m_m}{100}$	$\sigma_g = \exp \sqrt{\frac{\Sigma f (\ln m_m - \ln \bar{x}_g)^2}{100}}$	$Sk_g = \frac{\Sigma f (\ln m_m - \ln \bar{x}_g)^3}{100 \ln \sigma_g{}^3}$	$K_g = \frac{\Sigma f (\ln m_m - \ln \bar{x}_g)^4}{100 \ln \sigma_g{}^4}$

Source: Blott and Pye (2001)

Table 3.7: Logarithmic method of moments

Mean	Standard deviation	Skewness	Kurtosis
$\bar{x}_\phi = \frac{\Sigma f m_\phi}{100}$	$\sigma_\phi = \sqrt{\frac{\Sigma f (m_\phi - \bar{x}_\phi)^2}{100}}$	$Sk_\phi = \frac{\Sigma f (m_\phi - \bar{x}_\phi)^3}{100\sigma_\phi^3}$	$K_\phi = \frac{\Sigma f (m_\phi - \bar{x}_\phi)^4}{100\sigma_\phi^4}$

Source: Blott and Pye (2001)

Table 3.8: Original logarithmic graphical measures

Mean	Standard deviation	Skewness	Kurtosis
$M_Z = \frac{\phi_{16} + \phi_{50} + \phi_{84}}{3}$	$\sigma_I = \frac{\phi_{84} - \phi_{16}}{4} + \frac{\phi_{95} - \phi_5}{6{\cdot}6}$	$Sk_I = \frac{\phi_{16} + \phi_{84} - 2\phi_{50}}{2(\phi_{84} - \phi_{16})} + \frac{\phi_5 + \phi_{95} - 2\phi_{50}}{2(\phi_{95} - \phi_5)}$	$K_G = \frac{\phi_{95} - \phi_5}{2{\cdot}44(\phi_{75} - \phi_{25})}$

Source: Blott and Pye (2001)

Table 3.9: Modified geometric graphical measures

Mean	Standard deviation
$M_G = \exp\frac{\ln P_{16} + \ln P_{50} + \ln P_{84}}{3}$	$\sigma_G = \exp\left(\frac{\ln P_{16} - \ln P_{84}}{4} + \frac{\ln P_5 - \ln P_{95}}{6{\cdot}6}\right)$
Skewness	**Kurtosis**
$Sk_G = \frac{\ln P_{16} + \ln P_{84} - 2(\ln P_{50})}{2(\ln P_{84} - \ln P_{16})} + \frac{\ln P_5 + \ln P_{95} - 2(\ln P_{50})}{2(\ln P_{25} - \ln P_5)}$	$K_G = \frac{\ln P_5 - \ln P_{95}}{2{\cdot}44(\ln P_{25} - \ln P_{75})}$

Source: Blott and Pye (2001)

3.6 Mineral Identification in Coastal Sand Experiment (Petrography)

3.6.1 Materials for Petrographic Studies

Grinding wheel, Microscope Glass Slide, Leica DM 750P Petrographic Microscope coupled with Leica ICC 50 High Definition(HD) Complementary Metal Oxide Semiconductor (CMOS) digital camera (Leica, Germany), Fritsch Mortar Grinder Pulverisette 2 (Fritsch GmbH, Germany), Fritsch Jaw Crusher Pulverisette 2 (Fritsch GmbH, Germany), Rock-breaking hammer, Standard metal sample press.

Chemicals used include; Araldite® 506 epoxy resins (used in compaction of heavy mineral); Canada balsam (a mounting medium for microscopy) obtained from, Sigma Aldrich, Germany.

3.6.2 Sample Preparation for Mineral Identification

The beach sand samples retrieved from the particle size fractions are; coarse fraction (0.5 mm < x < 2 mm), medium fraction (0.25 mm <x <0.5 mm) and fine fraction (x < 0.25 mm).

About 25 grams of beach sand sample from the coarse, medium and fine sieved fractions were each passed through a gravity separation system. About 100 mL of bromoform was transferred into a 250 mL separatory funnel. The weighed beach sand was introduced into the separatory funnel while the mixture was stirred periodically in order to prevent bubble accumulation and promote easy sorting of the heavier minerals. The mixture was allowed to stand for 3 hrs in order to ensure complete separation of the heavier minerals from the lighter ones as shown in Fig. 3.7.

The heavier fragment which settled at the bottom of the separatory funnel was released into the filter paper while the bromoform was allowed to drain. The heavy-mineral collected on filter paper was transferred and rinsed into a Petri dish with acetone (Fig. 3.7 (iv)). This was followed by the decantation of the spent solvent (Fig. 3.7 (v)) and weighing of the dry mass. The heavy mineral was compacted with the aid of epoxy resin and Canada balsam in readiness for mineral examination under a Petrographic microscope. Prior to microscopic examination, the compacted heavy mineral was sanded on the grinding wheel to a 30 μm thickness on slide.

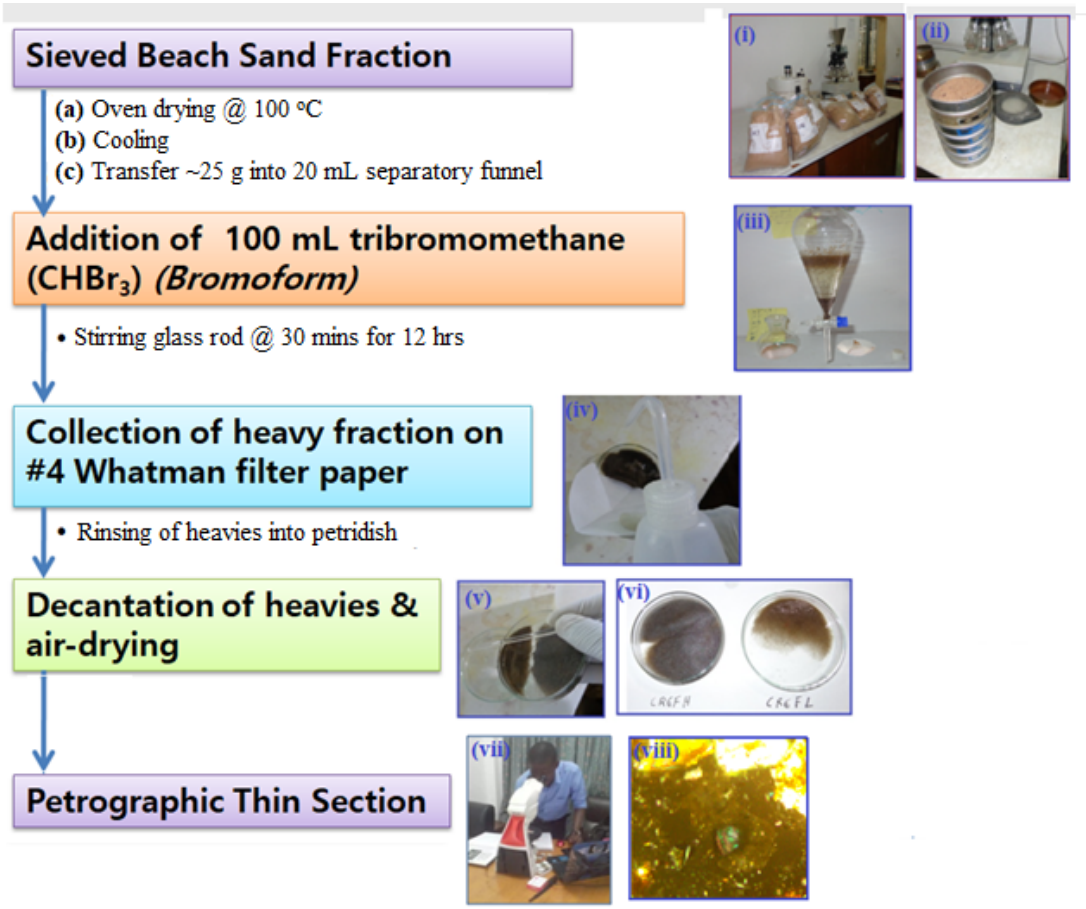

(i) *Dried Sample in zip lock bags* ***(ii)*** *Sieve Sorting* ***(iii)*** *Separation of sand in heavy liquid*
(iv) *Rinsing collected heavy mineral with acetone* ***(v)*** *Decanting of acetone from heavy mineral*
(vi) *Heavies and light mineral sand in petri-dish* ***(vii)*** *Microscope observation of slide*
(viii) *Typical photomicrograph*

Fig. 3.7: Mineral separation from beach sand fractions

The prepared slide was placed on the Leica Petrographic microscope for examination. A variation in colour characterization of the minerals is a function of their varying optical properties. The colour characteristics were comparatively indentified using the Michel- Lévy Interference Colour Chart. When the slide was placed between two polarizing filters set at right angles to each other, the optical properties of the minerals in the thin section altered the colour and intensity of the light (as seen by the viewer).

3.7 Determination of Naturally Occurring Radioactive Minerals (NORMs)

3.7.1 Instrumentation for Gamma-ray Spectrometry

The gamma spectrometry system comprises the N-type hyper pure germanium (HPGe) detector, computer system, multi-channel analyzer (MCA), lead shield (5 cm thickness). The listed components are coupled as illustrated in Fig. 3.8a-b. The multi-channel analyser (MCA) and a computer system are coupled for data analysis and interpretation. The nitrogen cooled HPGe detector system has an efficiency of 25% and an energy resolution of 1.8 KeV at gamma ray energy of 1332 KeV of Co-60. The qualitative and quantitative analysis of the radionuclides of interest was identified based on their gamma ray energies.

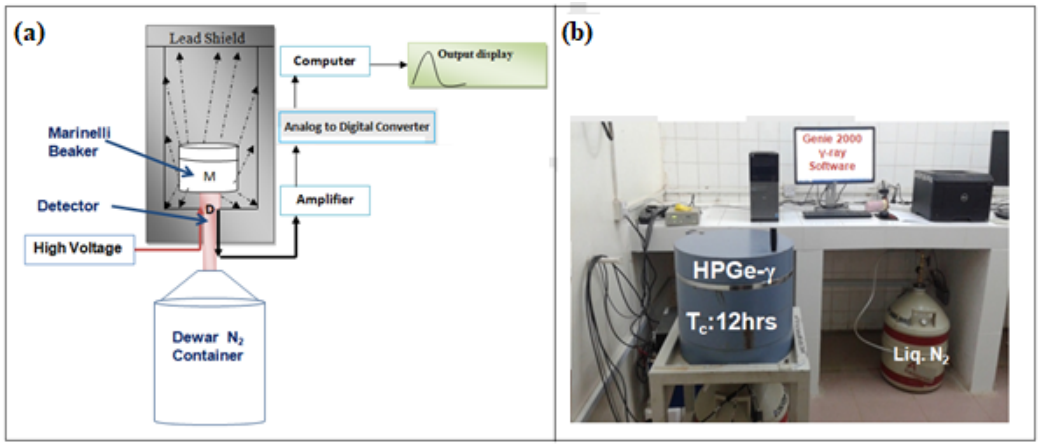

Fig. 3.8: (a) Block diagram for γ ray spectrometry experiment **(b)** Laboratory setup

3.7.2 Calibration of γ-ray Detector

In the determination of naturally occurring radioactive materials (NORMs), a comparison of an unknown source and a calibrated source is required. Initial calibration of the detector system was carried out using certified reference material (CRM). RGU-1(U-ore), RGTh-1 (Th-ore) and RGK-1 (K-ore) reference materials

obtained from the International Atomic Energy Agency were used in the energy and efficiency calibration of the detector. The standard was placed in a 1L Marinelli beaker of similar geometry with the sample and counted for about 36000 seconds.

Energy calibration was achieved by checking out the gamma energies of the radionuclides of interest and comparing the gamma rays spectrum with corresponding channel number of the standard. Calibration standard used have energies that span between 60 KeV and 2000 KeV.

Genie 2000 software installed on a Windows 7 SP1 x64 (64-bit) was used in the evaluation of the peaks. Microsoft Excel Program was used in the calculation of the data obtained from the Genie 2000 spectra. Fig. 3.9 shows a typical graphical user interface (GUI) of the Genie 2000.

The expression for the comparison of the energy and channel number in equation 1below shows the direct proportionality of the Energy to the channel number of a given radionuclide of interest. The energy is plotted against the channel number. (*Appendix A*)

$$E = A_0 + A_1 \cdot CN \quad \text{---------- (eq 1)}$$

Where

E= Energy (KeV), A_0 and A_1= Geometry calibration constants, CN= Channel number

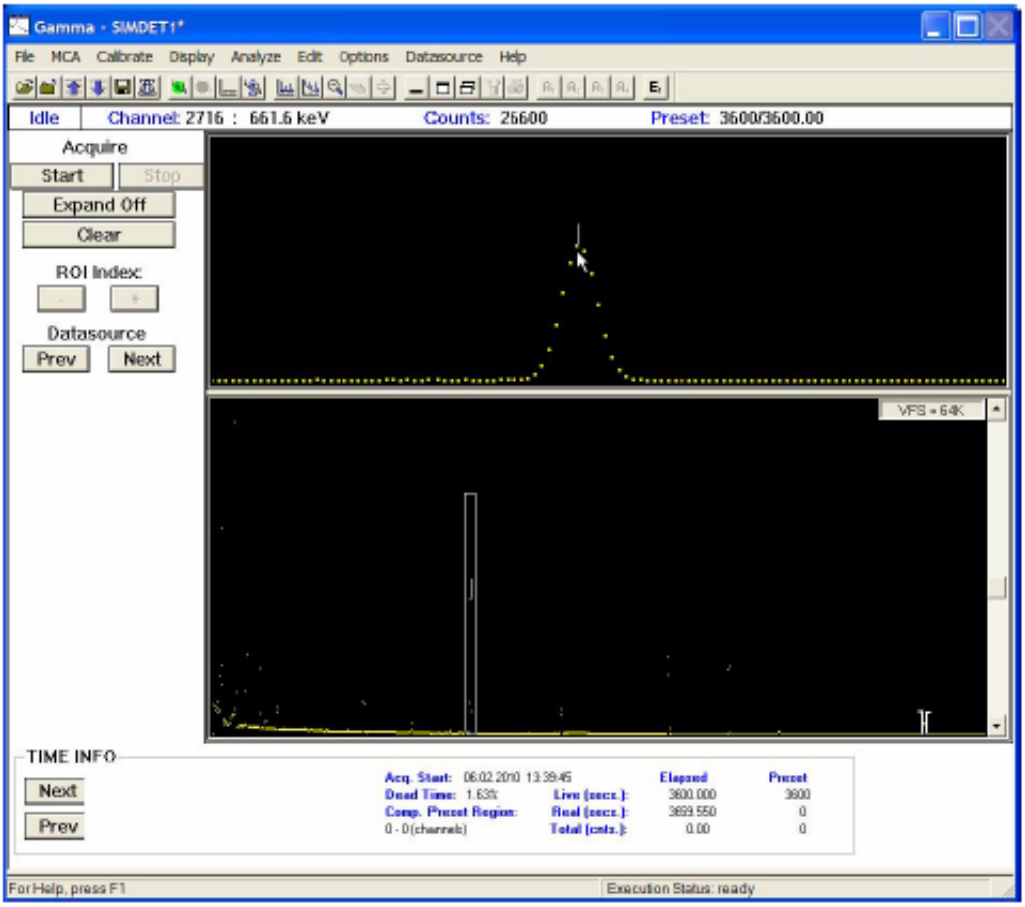

Fig. 3.9: Graphical user interface of a typical spectrum using Genie 2000 software

The expression required for the calculation of the detector efficiency is given in equation 2. The equation is obtainable when a mixed standard is used during the course of calibration

$$\eta(E) = \frac{N}{P\gamma \times Tc \times A} \text{ ---------- (eq 2)}$$

$$\mathbf{N} = N_T - N_B \text{----------(eq3)}$$

Where: $\boldsymbol{\eta}$ = Detector efficiency; **N**=Corrected count under a photopeak; $\mathbf{P}_\gamma$= Gamma emission probability for energy; $\mathbf{T}_c$= Counting time (s); **A** = Activity concentration of

specific radionuclide (Bq); N_T = Total count under a photopeak; N_B = Background count

This implies that radionuclides of interest with their specific energies are involved in the net count rate which is used in the calculation of the efficiency at the time of standard measurement.

The efficiency is related to the energy by the expression.

$$ln(E) = a_0 + a_1 ln E_1 + a_2 ln E_2 \text{----------} \textbf{(eq4)}$$

Where; a_0, a_1 and a_2 are calibration constants for a given geometry. The efficiency calibration curve is reported (*Appendix A*).

The first order polynomial expression of the calibration curve given in the equation 5 below:

$$In\eta = 1.238 - 0.995\, ln E\gamma \text{----------} \textbf{(eq5)}$$

at $E_\gamma > 100$ KeV

3.7.3 Sample Preparation for Gamma-ray Spectrometry

The coastal sands were air dried in a clean room for 48 hours and oven-dried at 105^{o}C for about 4 hrs. About 1 kg of sand samples were sieved through a 2 mm pore size mesh packed into a 1 litre Marinelli beaker. The weight of the beaker and sand sample was recorded and the beaker was tightly sealed and stored for about 28 days prior to acquisition of the gamma data (IAEA, 1989).

The essence of the 28 days storage was to ensure that secular equilibrium is attained between the long-lived parent radionuclides and short-lived daughter radionuclides in the U-238 and Th-232 decay series.

Counting of the naturally occurring radioactive materials in the sand sample was carried out in a well shielded high purity germanium (HPGe) detector for a period of 36000 seconds. Gamma activity measurement is observed as Gaussian peaks and the peak areas which correspond to radionuclides of interest were used in the estimation of the activity concentrations of the respective radionuclides. The activity concentrations were determined on dry weight basis and reported in Bq/Kg.

The activity concentrations of the coastal sands were determined by computing the equation below on a Microsoft Excel sheet and developing it for the activity concentration calculation. The key radionuclides of interest in the coastal sand samples are U-238, Th-232 and K-40. Their progenies were identified and their average area was recorded and used in the estimation of the activity concentration of the analytes of interest.

$$A_{sp} = \frac{N_D e^{\lambda_p T_d}}{p.T_c.\eta.m} \quad \text{----------(eq 6)}$$

The parameters required are as follows;

A_{sp}: Activity concentration of sample

N: Net counts of the radionuclide in the samples

T_d : Delay time between sampling and counting

P: Gamma emission probability (gamma yield)

η: Absolute counting efficiency of the detector system

T_c : Sample counting time

m: Mass of the sample (kg) or volume (l)

$e^{\lambda_p T_d}$: Decay correction factor for delay between time of sampling and counting

λ_p: Decay constant of the parent radionuclide.

3.8 Chemical Identification and Quantification of Rare Earth Elements using Inductively Coupled Plasma Mass Spectrometry (ICP-MS)

3.8.1 Reagents, Chemicals and the Treatment of Samples

The selected reagents used in this experiment include: ISO 3696- grade water obtained from ReAgent Chemicals Ltd. U.K., and about 125 mL of multi-element standard (Ce, Dy, Er, Eu, Gd, Ho, La, Lu, Nd, Pr, Sm, Sc, Tb, Th, Tm, U, Yb and Y) of concentration 10 μg/mL, were obtained from Inorganic Ventures, Virginia U.S.A. TRU-resin, LN-resin, SR-resin were obtained from TRISKEM International, France; via Separations Pty, Randburg, South Africa. Lithium metaborate was obtained from Chengdu Chemphysics, Sichuan, China (Mainland). OREAS 460 certified reference material was supplied by ORE Research & Exploration, Australia. AMIS0185 was supplied free by African Mineral Standard, Modderfontein, South Africa. Electronic grade HF, analytical reagent (AR) grade $HClO_4$, HNO_3, HCl, were obtained from Fisher Scientific Chemicals.

The beach sand samples retrieved from the particle size sorting process were grouped into three fractions viz: **(i)** coarse fraction (0.5 mm < x < 2 mm) **(ii)** medium fraction

(0.25 mm <x <0.5 mm) and **(iii)** fine fraction (x < 0.25 mm).This resulted in a total of 74 sub-samples which were analysed for rare earth element content using ICP-MS.The different fractions were transferred into a riffle splitter in order to ensure homogenization of the samples. The collected fractions were pulverised using a Fritsch Pulverisette 2 mortar grinder to a size less than 75 μm.

3.8.2 Sample Digestion for REEs Analysis

The standard method (ME-MS81) developed by ALS laboratory was used in the digestion of the beach sand samples. About 200 mg of the pulverised sample was mixed thoroughly with about 900 mg of lithium metaborate ($LiBO_2$) and fused at a temperature of about 1050 ^oC. The fused matrix is allowed to cool and dissolved in 4% HNO_3. The digested sample was filtered and diluted with ISO3696- grade water to the 250 mL mark prior to ICP-MS analysis. About 10 μg/mL of Rh was used as internal standard.

Lab duplicates were prepared using sample CR7M and WR3F. Optimized solutions were used in the calibration of the ICP-MS instrument calibration in order to improve its sensitivity. During sample measurement, a calibration blank was run prior to running of the calibration solutions. The Calibration check solution was analyzed at every batch of the analysis.

Element concentration calculation in aqueous sample was calculated using the formula described in equation 7.

$$\rho = (\rho_1 - \rho_o) f_d f_a \text{----------} \textbf{(7)}$$

In the solid sample, the element concentration was calculated using equation (8).

$$w = (\rho_1 - \rho_o)\, f_a\, V/m \text{----------} \textbf{(8)}$$

Parameters are defined as follows;

ρ = Aqueous sample element concentration (µg/L)

ρ_1 = Test sample element Concentration (µg/L)

ρ_o= Blank element concentration (µg/L)

f_d= Digested sample dilution factor ;f_d=1 in most cases

f_a= Dilution factor of test portion

w = Mass fraction of element in the solid sample (µg/kg)

V = Digested test sample volume (litres)

M = Digested sample mass (kg)

3.9 Separation of Selected Light Rare Earth Elements (LREEs)

3.9.1 Sr, TRU and LN Resins in the Separation of LREEs

The TRU resin is a typical example of an extraction chromatographic resin which is composed of an inert substrate (Amberlite XAD-7), which is adsorbed to (Octyl(phenyl))-N,N diisobutyl-methyl phosphine oxide (CMPO) dissolved in tributyl phosphate (TBP). The particle size of resin is about 50-100 um which happen to be the smallest particle size. TRU resin was developed by Eichrom technologies for adsorption and selective desorption of radionuclides in waste processing with low concentration of acids desorption and minimal waste generated. The TRU resin in this study was used in the sorption and selective desorption of light rare earth elements from the rare earth-containing geological matrix.

The TRU and Sr column were prepared using 4 mm X 20 mm length polyethylene tube described in literature (Pin et al., 1994). The columns were soaked with 10% HNO_3 and rinsed with deionized water and the lower sections were guarded using a polyethylene frit (Míková & Denková, 2007). A volume of about 0.25 mL of preconditioned (*in 0.05 M HNO_3*) TRU resin was transferred into the column and a second frit was used. The strontium resin SR-Spec resin was also preconditioned (*in 0.05 M HNO_3*) prior to transfer into the SR- column.

TRU-Spec and Sr- Spec resin were pre-cleaned by transferring about 0.25 mL of each into different columns (4 mm x 20 mm column), cleaned with about 10 mL deionized water, 2 mL 0.05 M HNO_3, rinsed with about 5 mL deionized water and conditioned with 1 mL of 1 M HNO_3-ascorbic acid. The ascorbic acid concentration used in the experiment was 0.28 M in order to reduce iron (III) in the sample. Fig 3.10 shows a schematic involving the stages for the separation of the REEs. The first stage involves

the digestion of beach sands, while the second stage shows the coupling of the Sr and TRU column. The Sr-TRU column is decoupled in the third stage and the REE fractions are co-eluted on the LN resin in the fourth stage. The TRU-LN is decoupled in the fifth stage and the sixth stage involves the stepwise elution of the REEs.

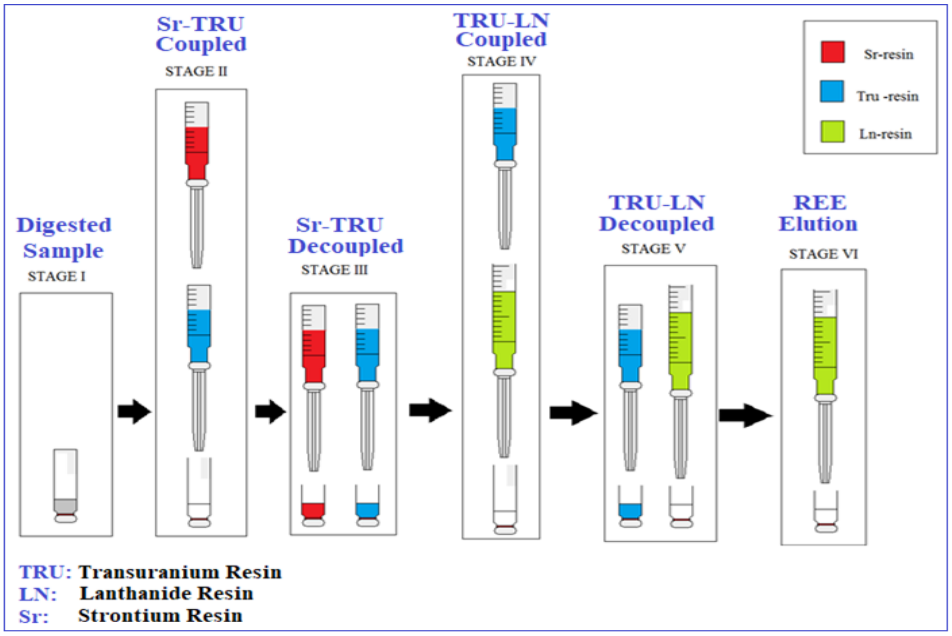

Fig. 3.10: Stages in the separation of LREEs

3.9.2 Digestion of Samples for REEs Separation

About 0.200 g of OREAS-460 certified geological reference material is mixed thoroughly with 1.00 g of lithium metaborate and transferred into a 40 x 40 mm carbon crucible. The fusion was carried out in a Lindberg muffle furnace at a temperature of about 1050 ^{o}C for about 30 minutes. The fusion cake was transferred into a solution of 20 mL HNO_3 (5% v/v), stirred with a magnetic stirrer on a hot plate

and evaporated to dryness and re-constituted with 2 mL of 1 M HNO_3-ascorbic acid ($C_6H_8O_6$). The procedure was also repeated for AMIS-0185 certified reference material. The beach sand samples were prepared under similar conditions as the geological reference materials.

Another portion of about 200 mg beach sand powder sample was digested in 2 mL of 22 M HF and heated in a fume hood at a temperature of about 110 ^oC using the method described by Pin et al. (2014). Similar digestion was carried out on three CRMs (OREAS 460, & AMIS 0185).

Illustrated in Fig. 3.11 is the flow process for the separation of the REEs. The digested sample was loaded on the Sr column which contained about 83 mg of Sr-resin, at a bed height of 2 cm (250 µL) and washed with 2 mL of 7 M HNO_3 for the removal of barium. The Sr column was washed with about 2 mL of 3 M HNO_3 and the REEs were eluted directly on the TRU column with 2 mL of 6 M HCl. The TRU column contains resin of about 83 mg and a bed height of 2 cm. The TRU-Spec column was coupled vertically in tandem with the LN column (4 mm X 60 mm) which contains a about 300 mg of LN resin. The TRU resin was washed on the LN column using 2.5 mL of 0.05 M HCl. The TRU column is decoupled and washed with 0.75 mL of 1 M HNO_3-ascorbic acid, 2.0 mL of 1 M HNO_3, 100 µL of 0.05M HNO_3 and about100µL of 0.05 M HCl. The LN column is rinsed with 0.2 mL of 0.05 M HCl. Stepwise elution of LREE (La-Nd) is carried out with 2 mL of 0.25 M HCl. Sm-Dy is eluted by stepwise elution with about 1.5 mL of 0.75 M HCl. The Pr, Sm, Nd and Eu fractions were retained in readiness for ICP-MS analysis.

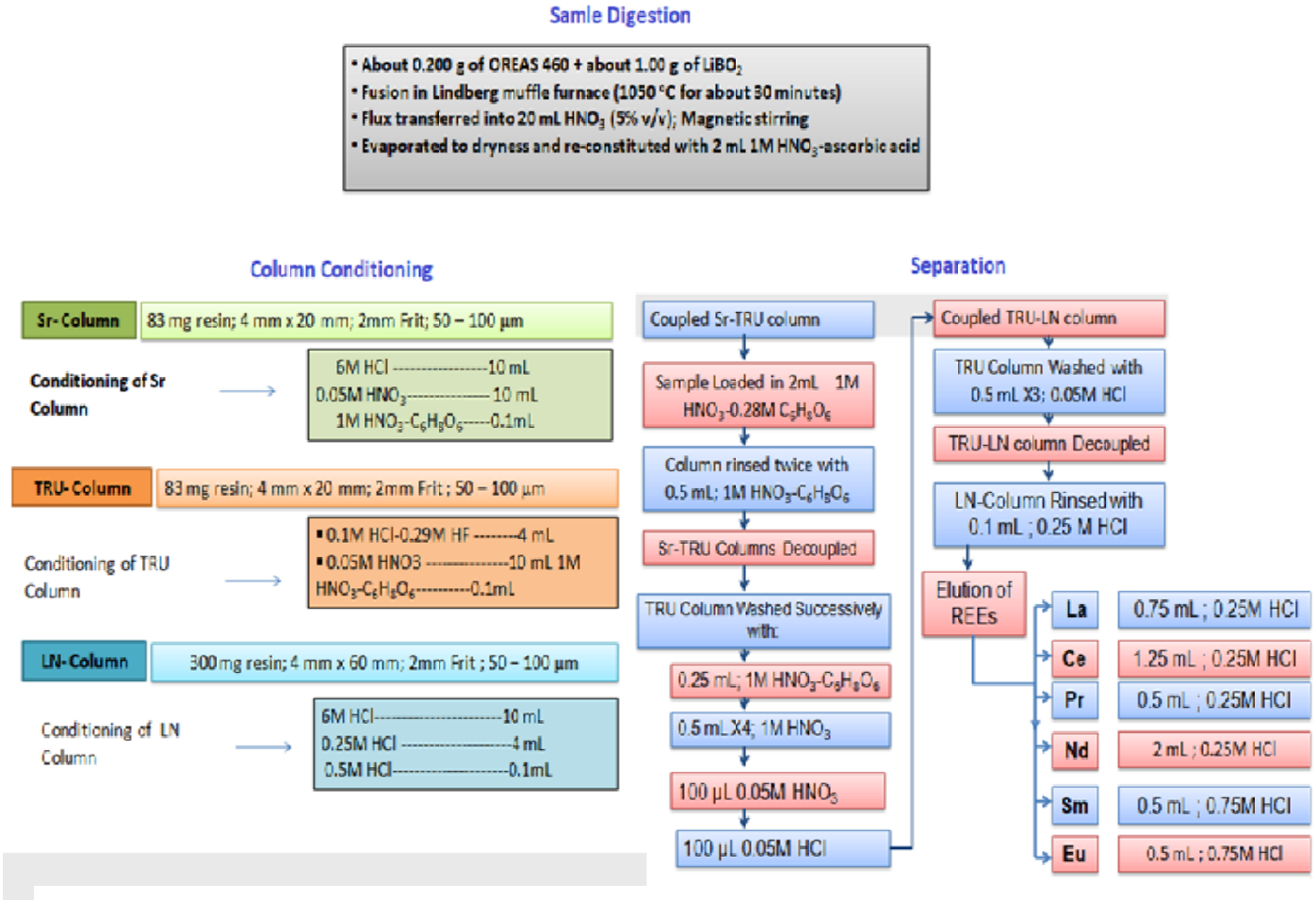

Source: Pin et al. (1994); Pin & Zalduegui (1997); Horwitz & McAlister (2006); Mikova & Denkova, (2007).

Fig.3.11: Schematics for the separation of LREEs

CHAPTER FOUR

RESULTS AND DISCUSSION

4.1 NORMs in Beach Sands of the Central and Western Regions of Ghana

Prior to the investigation of rare earth elements in the beach sands, the selected samples were stored in a Marinelli beaker for about 28 days in order for the samples to attain secular equilibrium (IAEA, 1989). The activity concentration of the natural occurring radionuclides (U-238, Th-232 and K-40) in the beach sands was studied using gamma spectrometry. A total of 25 samples were collected from the beach sands of the Central (15) and Western (10) region. In a bid to ensure data reliability, the Calibration of the HPGe detector was carried out using IAEA Certified Reference Materials (RGU-1(U-ore), RGTh-1 (Th-ore) and RGK-1 (K-ore)) contained in a 1L-Marinelli beaker. The activity concentration of U-238, Th-232 and K-40 in the beach sands of the Central region and Western region are reported in Table 4.1 and Table 4.2 respectively.

The mean activity concentration of U-238, Th-232 and K-40 in the beach sands of the Central and Western regions are shown in Tables 4.1 and 4.2 respectively. The activities range and value are reported on dry weight basis in Bq/Kg. The range of activities in the Central region U-238, Th-232 and K-40 occur as (1.3±0.47 to 31.50±3.31)^{238}U; (0.7±0.04 to 71.70±4.55)^{232}Th; and (73.9±6.72 to 1775.5±28.35) ^{40}K. The range of the activities in the Western region occur as (1.0±0.03 to 5.6±0.24) ^{238}U; (0.8±0.04 to 3.8±0.14)^{232}Th; (18.6±0.23 to 343.2±18.35) ^{40}K. A graphical illustration of the activity concentrations of ^{238}U and ^{232}Th in the beach sands of the Central and Western regions are shown in Fig. 4.1 and Fig. 4.4.

Table 4.1: Activity concentration of ^{238}U, ^{232}Th and ^{40}K in beach sands along the coast of the Central region of Ghana

Sampling Location	Activity Concentration (Bq/Kg)			
	^{238}U	^{232}Th	^{40}K	Ra_{eq}
CR1	2.4±0.11	0.9±0.34	69.2±7.16	8.53
CR2	1.8±0.12	0.8±0.02	88.4±10.96	9.23
CR3	1.8±0.13	0.9±0.11	96.0±5.78	9.79
CR4	3.1±0.22	1.7±0.12	115.9±12.3	13.68
CR5	1.7±0.01	0.9±0.05	129.0±9.80	12.00
CR6	1.7±0.21	0.9±0.01	118.2±10.25	11.17
CR7	31.5±3.31	71.7±4.55	1775.5±28.35	258.21
CR8	4.1±1.13	2.0±0.51	81.6±6.39	12.66
CR9	27.2±58	6.2±1.20	69.7±8.12	33.67
CR10	2.4±0.12	0.7±0.14	142.4±14.15	13.33
CR11	1.5±0.21	0.8±0.21	96.5±11.01	9.35
CR12	1.3±0.47	0.7±0.04	73.9±6.72	7.48
CR13	1.5±0.31	0.7±0.02	84.7±7.61	8.41
CR14	1.4±0.33	0.7±0.07	74.0±8.29	7.50
CR15	1.6±0.21	0.5±0.17	80.2±9.82	8.01

CR1= Gomoa Fetteh; **CR2**= Senya Beraku; **CR3**= Winneba; **CR4**= Mankwadze; **CR5**=Apam; **CR6**=Mumford; **CR7**=Dago; **CR8**= Akra; **CR9**=Ekumpoano; **CR10**=Edumafa;

Table 4.2: Activity concentration of ^{238}U, ^{232}Th and ^{40}K in beach sands along the coast of the Western region of Ghana

Sampling Location	Activity Concentration (Bq/Kg)			
	^{238}U	^{232}Th	^{40}K	Ra_{eq}
WR1	1.0±0.03	0.8±0.04	18.6±0.23	3.56
WR2	2.5±0.23	1.8±0.01	175.1±9.56	17.30
WR3	5.6±0.24	3.8±0.14	343.2±18.35	35.10
WR4	1.6±0.01	1.1±0.32	206.2±15.65	17.56
WR5	4.0±0.12	1.5±0.03	100.5±10.23	13.16
WR6	1.4±0.01	0.5±0.11	61.3±5.42	7.42
WR7	1.0±0.12	0.8±0.12	18.6±2.33	7.54
WR8	3.5±1.25	1.5±0.10	43.7±6.12	8.78
WR9	2.4±0.25	0.7±0.02	34.3±5.36	5.85
WR10	1.1±0.17	0.5±0.03	23.2±3.41	3.45

WR1= Shama; **WR2**= Abuesi; **WR3**= Sekondi; **WR4**= Takoradi; **WR5**=Cape Three Points; **WR6**= Egyembra; **WR7**=Axim; **WR8**= Esiama; **WR9**= Sanzule; **WR10**=Atuabo

Fig. 4.1 shows a gradual increase in the concentration of U-238 for the beach sands of Senya Beraku to the beach sands of Mankwadze, this is followed by a gradual decrease in U-238 towards the beach sands of Apam and Mumford. A decreased U-238 concentration is sandwiched between Dago and Ekumpoano which shows increased concentration of U-238. This trend is similar for Th-232 concentration in the beach sands of the Central region as shown in Fig. 4.2. Concentrations of U-238 and Th-232 in the beach sands of Dago and Ekumpoano exceeds the concentrations found in the beach sands of other locations in the Central region.

Fig. 4.3 shows a gradual increase in the activity concentration of U-238 in the beach sands of Shama, Abuesi and Sekondi in the Western region. This is followed by a sharp decrease in U-238 concentration in the beach sands of Takoradi and a sudden increased concentration in the beach sands of Cape Three Points. A similar trend is observed for the concentrations of Th-232 in the beach sands of Shama, Abuesi, Sekondi and Takoradi as shown in Fig. 4.4. A gradual decrease in the concentration of Th-232 from the beach sands of Cape Three Points towards Egyembra and Axim is shown in Fig 4.4, this is followed by a slight increase in the concentrations of Th-232in the beach sand of Esiama. A gradual decrease in the concentrations of Th-232 and U-238 was observed in the beach sands of Esiama, Sanzule and Atuabo as shown in Fig. 4,3 and Fig. 4.4.

Fig. 4.5 shows the concentrations of U-238 and Th-232 in the beach sands of the Central and Western regions. The U-238 and Th-232 concentration in the beach sands of Dago and Ekumpoano exceeds what was obtained in the beach sands of the other locations in the Central and Western region coastline. Concentration of K-40 in the beach sands of Dago far exceeds the U-238, Th-232 and K-40 concentrations for other locations in the beach sands of the Central and Western region as shown in Fig. 4.6

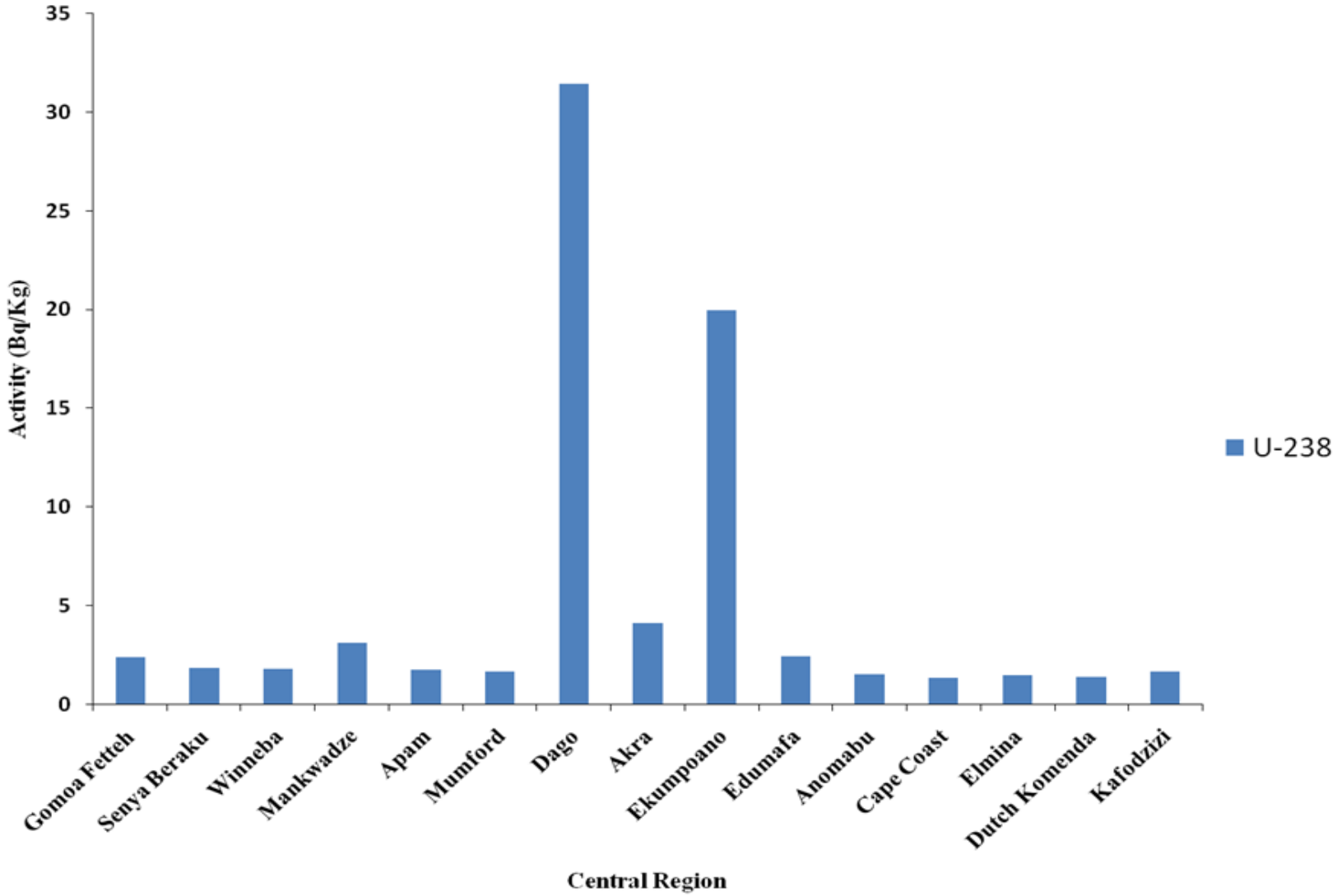

Fig.4.1: Activity concentration of ^{238}U in the beach sands of the Central region of Ghana

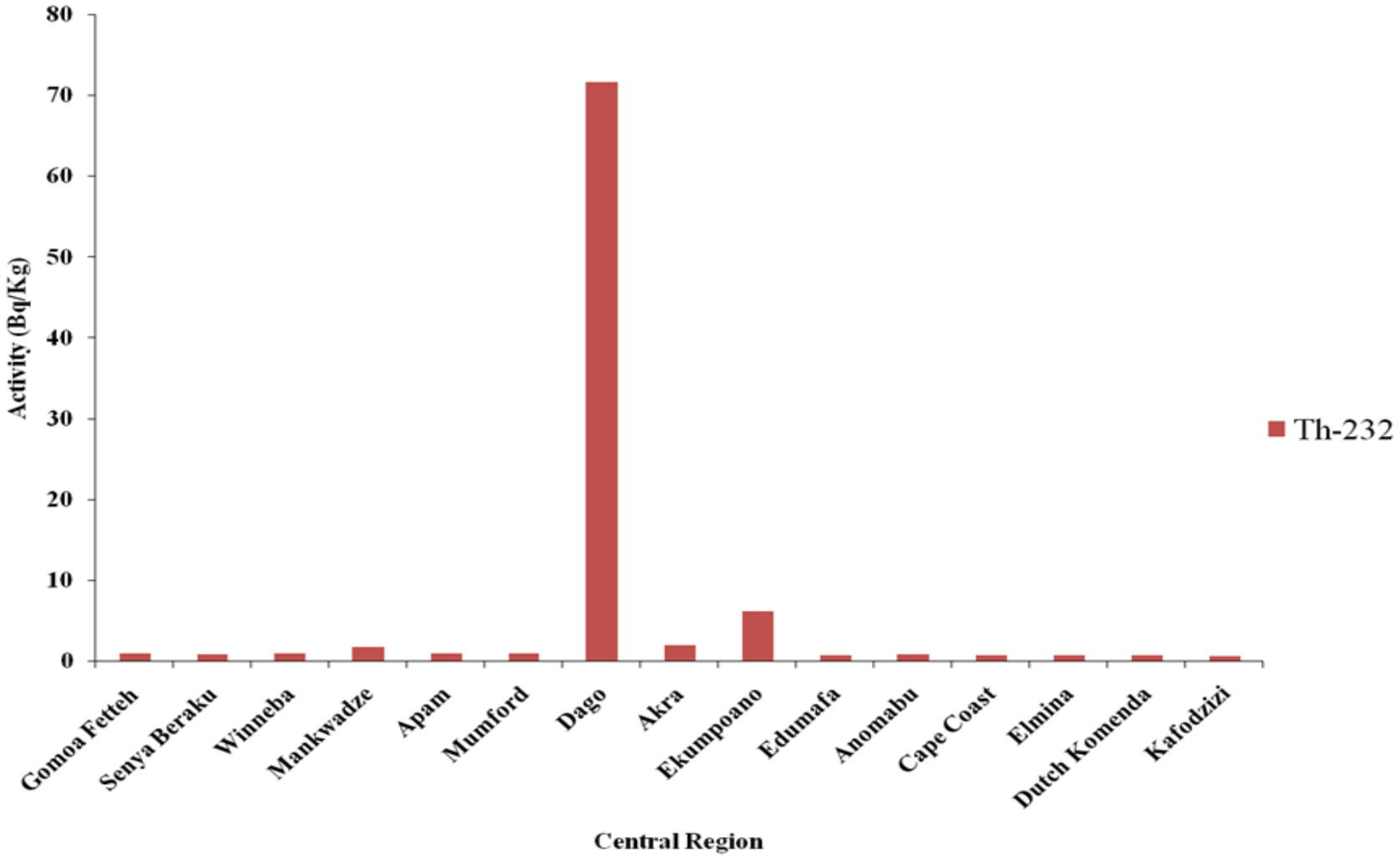

Fig.4.2: Activity concentration of ^{232}Th in the beach sands of the Central region of Ghana

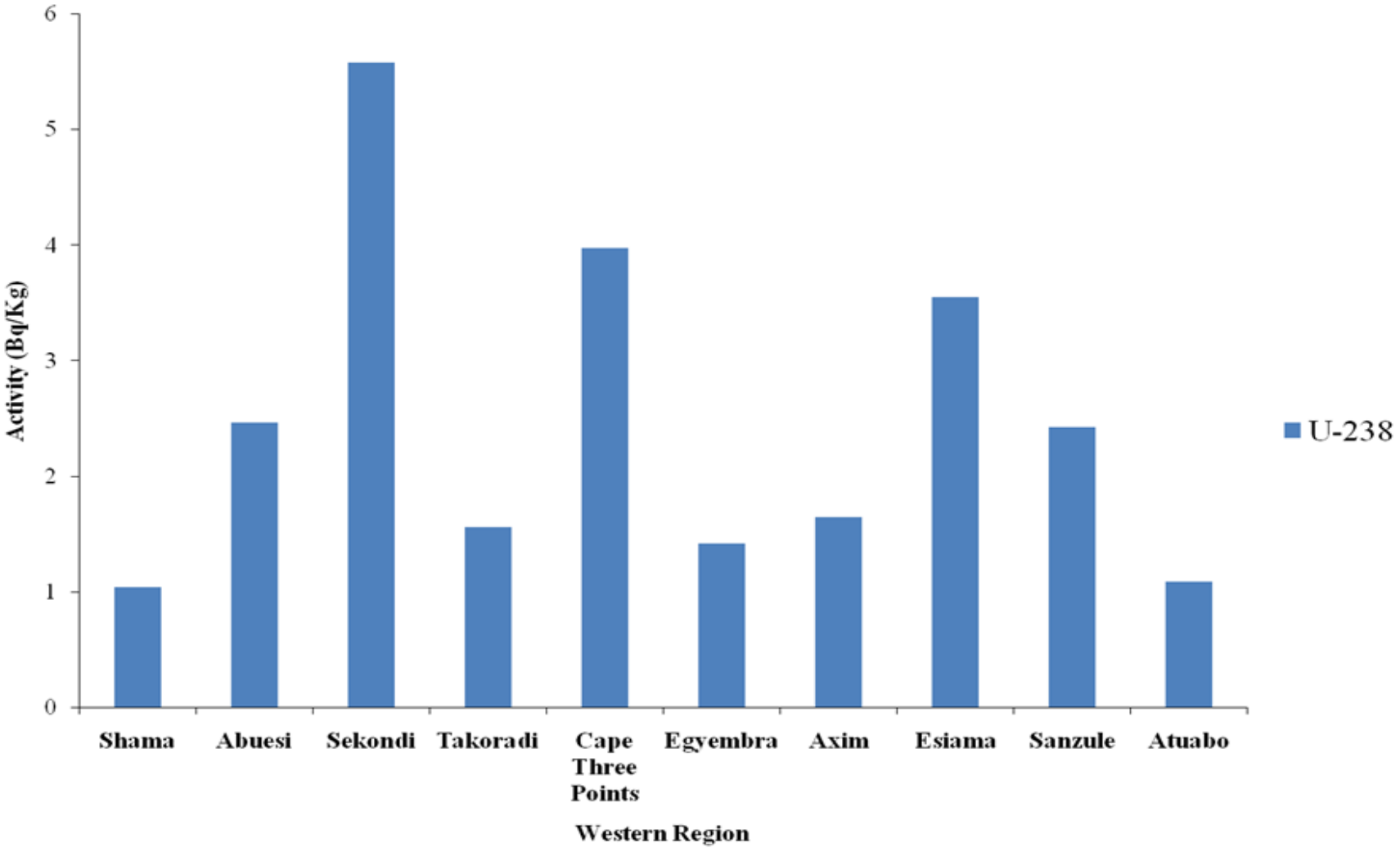

Fig.4.3: Activity concentration of ^{238}U in the beach sands of the Western region of Ghana

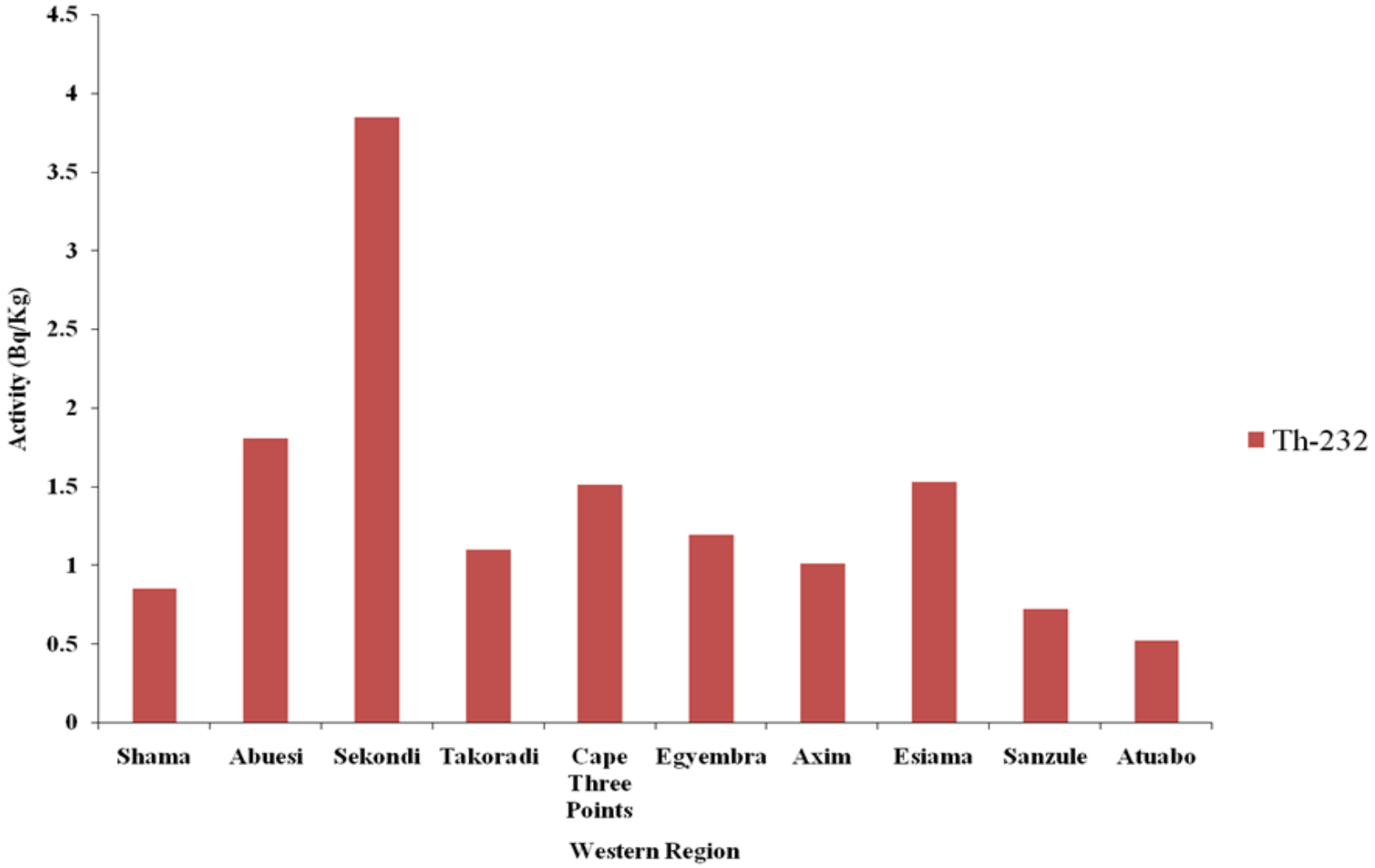

Fig.4.4: Activity concentration of ^{232}Th in the beach sands of the Western region of Ghana

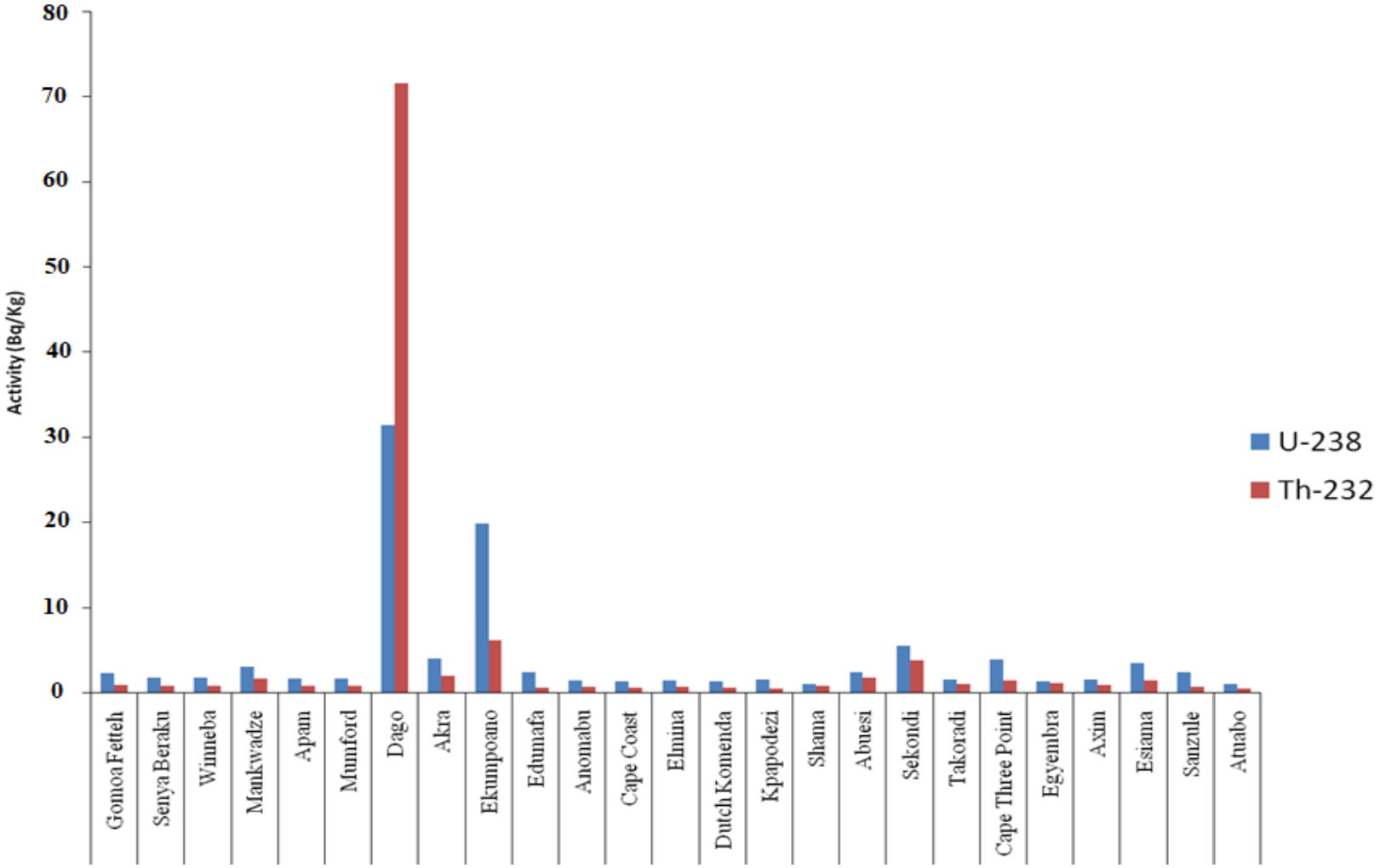

Fig.4.5: Activity concentration of ^{238}U and ^{232}Th in the beach sands of the Central and Western regions of Ghana

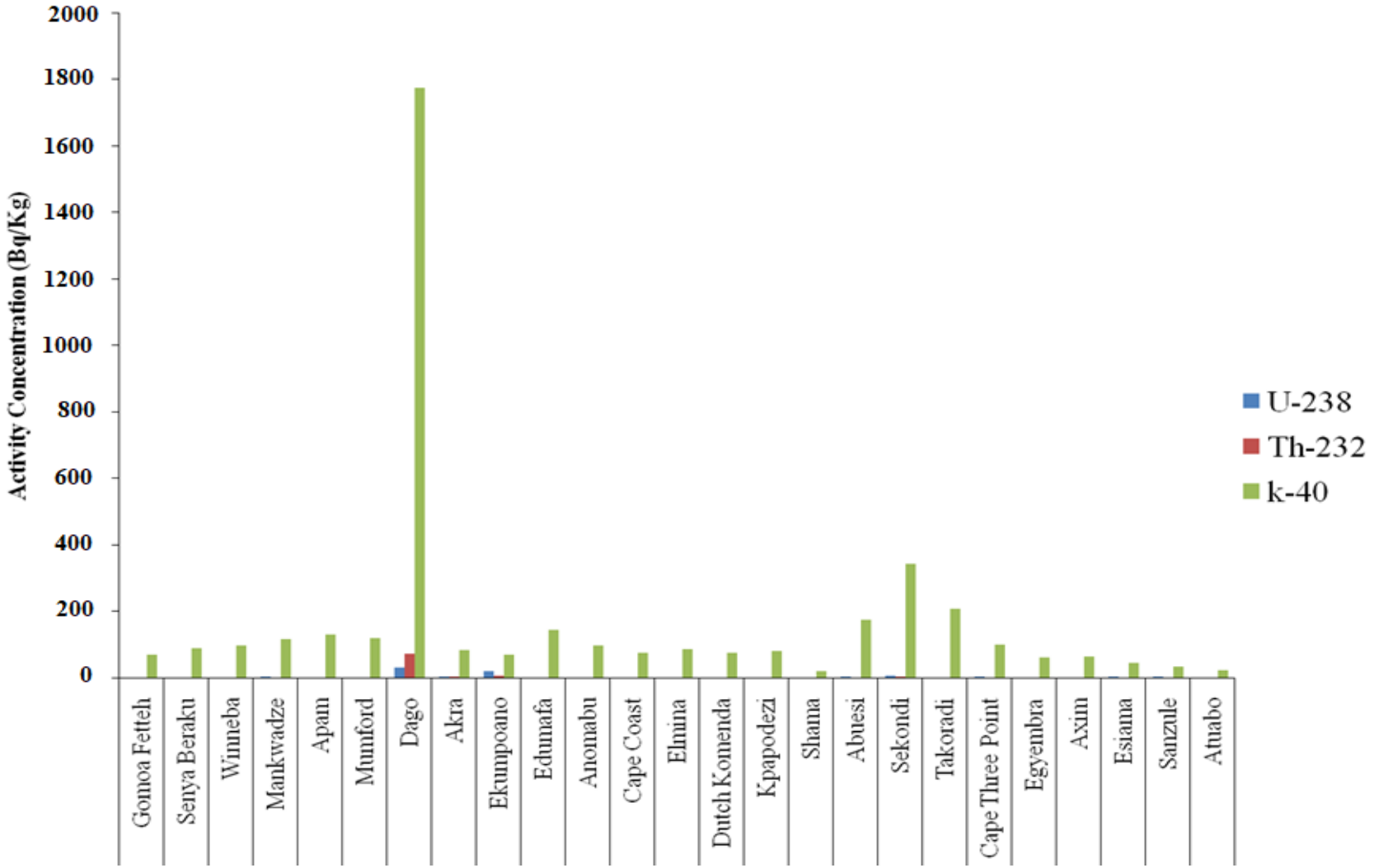

Fig.4.6: Activity concentration of ^{238}U, ^{232}Th and ^{40}K in the beach sands of the Central and Western regions of Ghana

The region of highest concentration for ^{238}U and ^{232}Th in the Central and Western region corresponds to Dago (CR7), followed by the beach sands of Ekumpoano and Sekondi as shown in Fig. 4.6. U-238 concentration in the beach sands of the Central and Western regions are higher than the Thorium concentration, with the exception of the beach sands of Dago which shows high concentration of Thorium-232.

Considering the high level of thorium in the beach sands of Dago as shown in Fig. 4.2 and Fig. 4.6, thorium associated minerals is suspected. Typical selected thorium associated minerals include; thorite, monazite, thorianite, thorogummite, huttonite and thorutite; other relevant minerals are reported in the works of Frondel & Fleischer (1950) & Clifford (1958).

Although the beach sands of Dago, and Ekumpoano are dominated by wacke sediment, sandstones and conglomerates bordered with detrital sediments; the beach sands of Akra are known to comprise of biotite, granitoids, with volacnistic sediments and undifferentiated mica schists (GSD, 2009).

The beach sands of Abuesi, Sekondi, Takoradi, Cape Three Points Esiama and Sanzule showed increased concentrations of U-238 as shown in Fig. 4.1, the beach sands of Sekondi shows that the samples were could contain uranothorite of other thorium uranium associated mineral. The geology of the Sekondi beach area suggests sandstones, interbeded shale.

The basic radiological parameters of the beach sands are discussed further.

4.1.1 Radium Equivalent Activity (Ra_{eq})

In a bid to allow a single index value for the description of the uranium, thorium and potassium component of the beach sands along the coast in the different regions, the following equation was used in the estimation of the radium equivalent (Ra_{eq}).

$$Ra_{eq} = A_U + 1.43A_{Th} + 0.007\ A_K$$

Where A_U, A_{Th} and A_K are the specific activity concentrations of U-238, Th-232 and K-40 respectively. The radium equivalent is a measure of the external gamma dose and internal dose due to radon and its daughters.

The Ra_{eq} range in the beach sands of the Central region occurs in the range of 7.47 Bq/Kg to 258.21 Bq/Kg., while the Ra_{eq} range of the Western region occurs in the range of 3.45 Bq/Kg to 35.10 Bq/Kg (Table 4.3). Activity concentrations obtained in this study compares favourably with studies along the coastal belt of Ghana by Lawluvi et al. (2016) but far lower than the beach sands of Brazil and India as shown in Appendix E.

4.1.2 Absorbed Gamma Dose Rate

The absorbed gamma dose rate in air per unit activity at about 1m height for the naturally occurring radioactive materials in the beach sands were calculated using the UNSCEAR conversion equation (Sivakumar et al., 2014).

$$D_R\ (nGyh^{-1}) = 0.462A_U + 0.604\ A_{Th} + 0.042A_K$$

The conversion factors used in the estimation are 0.462 $nGyh^{-1}$ (^{238}U), 0.604 $nGyh^{-1}$ (^{232}Th); and 0.042 $nGyh^{-1}$ (^{40}K).

The dose rate in the beach sands along the central and Western region is averaged at11.40 ($nGyh^{-1}$) , the Central region occur at a range of 4.13 - 132.39 ($nGyh^{-1}$) and the Western region occur at a range of 1.78 – 19.32 ($nGyh^{-1}$) as shown in Table 4.3.

The mean absorbed dose rate in the beach sands is lower than the world average estimated absorbed mean gamma dose rate of 84 ($nGyh^{-1}$) except that of Dago.

4.1.3 Annual Effective Dose Rate (AEDR)

The estimated annual effective dose rate (AEDR) was calculated from the absorbed dose rate using the formula stated in the equation below;

$$AEDR\ (mSv/y) = D_R\ (nGyh^{-1}) \times 8760\ (h/\ yr^{-1}) \times 0.7 \times (10^3/10^9)\ (mSv/nGy) \times 0.2$$

$$AEDR = D_R \times 1.23 \times 10^{-3}$$

The average annual effective dose rate in the beach sands for the Central and Western regions occur as 0.014 (mSv/y). The dose rate range found in the Central region occur in the range 0.005 – 0.162 (mSv/y) and the Western region occur as 0.002 – 0.024 (mSv/y) (Table 4.3).

4.1.4 Activity Utilization Index (AUI)

The activity utilization index which is a measure of radiation dose rate in air was estimated in the beach sands of the central and western region. The activity per unit mass constants for uranium, thorium and potassium are 50, 50 and 500 Bq/Kg.

The average AUI in the study area along the Central and Western region is 0.102 while the range in the Central region is 0.027 – 1.302 while the Western region ranged between 0.018 – 0.126. This suggests an annual effective dose which is less than 0.3 mSv/y (Table 4.3).

4.1.5 Radiation Hazard Indices (RHI)

The estimation of the radiation hazard index is due to external and internal radiation hazard indices. This is derived from the expression given below:

$Hex = (A_U/370\ Bq/Kg) + (A_{Th}/259 Bq/Kg) + (A_K/4810\ Bq/Kg)$

$Hin = (A_U/185 Bq/Kg) + (A_{Th}/259\ Bq/Kg) + (A_K/4810\ Bq/Kg)$

The average level of the external hazard index is 0.062 for the Central and Western region. The range occur as 0.022 – 0.731 for the Central region and the Western region 0.010 – 0.101.

The average level of the internal hazard index is 0.073for the Central and Western region, while that of the Central region ranged from 0.025 – 0.816 and the Western region occur as 0.013 – 0.116 (Table 4.3).

4.1.6 Gamma Radiation Representative Level Index (RLI)

This is estimated from the average concentration of uranium, thorium and potassium present in the beach sands. The expression used in the estimation is shown in the equation below.

$$RLI = (A_U(1/150) + A_{Th}(1/100) + A_K(1/1500))$$

The average RLI estimated in the beach sands along the Central and Western region is 0.18. The range for the Central region is 0.065 – 2.110 and the Western region occur in the range 0.028- 0.304. The RLI value average is less than 1. This implies an annual effective dose lower than 1 mSv/y. The highest value obtained in the beach sands of Dago (CR7) which is 2.110, suggests a relatively higher annual effective dose (Table 4.3).

A comparison of the activity concentration of the beach sands in this study with those found in other places around the world is shown in *Appendix E*. The average activity in the Central region for ^{238}U, ^{232}Th, and ^{40}K is 5.18, 6.00 and 206.36 Bq/Kg. The average activity concentration in the Western region for ^{238}U, ^{232}Th, and ^{40}K is respectively 2.5, 1.4 and 107 Bq/Kg. The world average for ^{238}U, ^{232}Th, and ^{40}K is 35, 30 & 400 Bq/Kg.

Table 4.3: Radiological parameters in the coastal sands of the Central and Western regions of Ghana

Location	DR (nGy/h)	Annual Effective Dose Rate ($mSvy^{-1}$)	Activity Utilization Index (AUI)	RHI_{ex}	RHI_{Int}	RLI_{γ}
CR1	4.56	0.006	0.039	0.024	0.031	0.07
CR2	5.07	0.006	0.034	0.027	0.032	0.08
CR3	5.40	0.007	0.035	0.028	0.033	0.08
CR4	7.34	0.009	0.059	0.039	0.047	0.12
CR5	6.74	0.008	0.037	0.035	0.039	0.11
CR6	6.25	0.008	0.035	0.032	0.037	0.10
CR7	132.39	0.162	1.302	0.731	0.816	2.11
CR8	6.53	0.008	0.069	0.036	0.047	0.10
CR9	15.88	0.019	0.265	0.092	0.146	0.24
CR10	7.50	0.009	0.042	0.039	0.045	0.12
CR11	5.21	0.006	0.031	0.027	0.031	0.08
CR12	4.13	0.005	0.027	0.022	0.025	0.06
CR13	4.66	0.006	0.029	0.024	0.028	0.07
CR14	4.14	0.005	0.027	0.022	0.025	0.07
CR15	4.44	0.005	0.028	0.023	0.028	0.07
WR1	1.78	0.002	0.021	0.010	0.013	0.03
WR2	9.58	0.012	0.059	0.050	0.057	0.15
WR3	19.32	0.024	0.126	0.101	0.116	0.30
WR4	10.04	0.012	0.045	0.051	0.056	0.16
WR5	6.97	0.009	0.063	0.037	0.048	0.11
WR6	3.95	0.005	0.033	0.021	0.025	0.06
WR7	4.04	0.005	0.033	0.022	0.026	0.06
WR8	4.39	0.005	0.055	0.025	0.034	0.07
WR9	3.00	0.004	0.034	0.016	0.023	0.05
WR10	1.79	0.002	0.018	0.010	0.013	0.03
Average	**11.40**	**0.014**	**0.102**	**0.062**	**0.073**	**0.18**

RHI_{ex}: External Radiation Hazard Index
RHI_{int}: External Radiation Hazard Index
RLI_{γ}: Gamma Radiation Representative Level Index

4.2 Grain Size Distribution of Coastal Sands in the Central and Western Region of Ghana

4.2.1 Distribution in Coastal Sands of Central Region

The coastline of Ghana covers a stretch of approximately 539 km (~335 miles) starting from the Togo border (Aflao) on the east towards the Ivory Coast (Cote d'Ivoire) to the west. The Central region coastline spans across a distance of approximately 220 km (~137 miles), sandwiched between the Greater Accra Region to the east and the Western Region to the west.

The coastal environment of Ghana holds information about the rich history of Ghana with different tourism sites, the beaches serve for recreational purposes and the Gulf of Guinea (North Atlantic Ocean) influenced the occupation of the coastal settlers who are engage mostly in fishing.

The coastal sand holds a lot of information about radioactive sands which were first reported by Layton (1958). Beach sands from the sub-littoral zone along the coast of the Central region of Ghana were collected from 15 sites and considered for particle size studies. Different critical contributors are known to affect the particle size of sands along the coastal zone. Factors such as fluvial discharges, long range transport, waves and tidal processes all influence the particle size of the beach sand in the detrital environment (Armstrong-Altrin et al., 2012). The beach sands of the Central region can be classified based on their textural group as slightly gravelly sand and are composed mostly of slightly very fine gravelly medium sands.

Table 4.4 shows the textural group and name classification of the coastal sands along the Central region. The coastal sands are mostly trimodal-moderately well sorted with

the exception of sands from Apam, Senya, and Fetteh which are Polymodal-moderately-sorted, unimodal-well sorted and Bimodal-well sorted respectively. Textural group information obtained suggests that the beach sands are slightly gravelly sand, broadly slightly-very fine-gravelly-medium-sand with the exception of Senya which is composed of slightly gravelly sand. Observations from the textural group suggest a progression of trimodal moderately well sorted sand occurs from Akra to Edumafa. Sand samples with different property such as that of Senya occur as unimodal, well sorted; samples from Fetteh, Anomabu and Kafodzizi are mostly Bimodal, while samples from Apam sands are Polymodal.

The challenge with this aspect of the sand distribution is that of the unimodal samples, a set of grain size predominates. The sieve size used include 1000 µm, 500 µm, 250 µm, 125 µm and 63 µm. Statistical details for the sorting Central region are reported *(Appendix B)*.

The Western region coastline occupies a distance of approximately 192 km (~119 miles), sandwiched between the Central Region to the east and the Ivory Coast (Cote d`Ivoire) to the west. The coastal stretch is essentially been described to have a narrow shelf , steep shoreline and severe Climate (Malvárez, 2012).

Table 4.5 shows the classification of the sediments in the beach sands. The sand samples collected along the 10 sample sites along the western region were analyzed using GRADISTAT Ver. 9.0 and the resulting information are discussed as follows. Statistical details retrieved from the GRADISTAT Ver. 9.0 application are reported. *(Appendix B)*.

Table 4.4: Sediment Name and Textural Group of Selected Coastal Sands along the Central Region of Ghana

Location	Sample Type	Textural Group	Sediment Name
Gomoa Fetteh	Bimodal, Well Sorted	Slightly Gravelly Sand	Slightly Very Fine Gravelly Medium Sand
SenyaBeraku	Unimodal, Well Sorted	Slightly Gravelly Sand	Slightly Gravelly Sand
Winneba	Trimodal, Moderately Sorted	Slightly Gravelly Sand	Slightly Very Fine Gravelly Medium Sand
Mankwadze	Trimodal, Moderately Well Sorted	Slightly Gravelly Sand	Slightly Very Fine Gravelly Medium Sand
Apam	Polymodal, Moderately Sorted	Slightly Gravelly Sand	Slightly Very Fine Gravelly Medium Sand
Mumford	Trimodal, Moderately Well Sorted	Slightly Gravelly Sand	Slightly Very Fine Gravelly Medium Sand
Dago	Trimodal, Moderately Sorted	Slightly Gravelly Sand	Slightly Very Fine Gravelly Medium Sand
Akra	Trimodal, Moderately Well Sorted	Slightly Gravelly Sand	Slightly Very Fine Gravelly Medium Sand
Ekumpoano	Trimodal, Moderately Well Sorted	Slightly Gravelly Sand	Slightly Very Fine Gravelly Medium Sand
Edumafa	Trimodal, Moderately Well Sorted	Slightly Gravelly Sand	Slightly Very Fine Gravelly Medium Sand
Anomabu	Bimodal, Moderately Sorted	Slightly Gravelly Sand	Slightly Very Fine Gravelly Medium Sand
Cape Coast	Trimodal, Moderately Sorted	Slightly Gravelly Sand	Slightly Very Fine Gravelly Medium Sand
Elmina	Trimodal, Moderately Well Sorted	Slightly Gravelly Sand	Slightly Very Fine Gravelly Medium Sand
Dutch Komenda	Trimodal, Moderately Sorted	Slightly Gravelly Sand	Slightly Very Fine Gravelly Medium Sand
Kafodzizi	Bimodal, Moderately Well Sorted	Slightly Gravelly Sand	Slightly Very Fine Gravelly Medium Sand

Table 4.5: Sediment Name and Textural Group of Selected Coastal Sands along the Western Region of Ghana

Location	Sample Type	Textural Group	Sediment Name
Shama	Trimodal, Moderately Well Sorted	Slightly Gravelly Sand	Slightly Very Fine Gravelly Coarse Sand
Abuesi	Bimodal, Moderately Well Sorted	Slightly Gravelly Sand	Slightly Very Fine Gravelly Medium Sand
Sekondi	Bimodal, Moderately Well Sorted	Slightly Gravelly Sand	Slightly Very Fine Gravelly Medium Sand
Takoradi	Bimodal, Moderately Well Sorted	Sand	Moderately Well Sorted Medium Sand
Cape Three Points	Polymodal, Poorly Sorted	Slightly Gravelly Sand	Slightly Very Fine Gravelly Medium Sand
Egyembra	Trimodal, Moderately Sorted	Slightly Gravelly Sand	Slightly Very Fine Gravelly Medium Sand
Axim	Polymodal, Poorly Sorted	Gravelly Sand	Very Fine Gravelly Medium Sand
Esiama	Polymodal, Poorly Sorted	Slightly Gravelly Sand	Slightly Very Fine Gravelly Medium Sand
Sanzule	Polymodal, Poorly Sorted	Slightly Gravelly Sand	Slightly Very Fine Gravelly Medium Sand
Atuabo	Trimodal, Moderately Well Sorted	Slightly Gravelly Sand	Slightly Very Fine Gravelly Medium Sand

4.3 Heavy Minerals in Beach Sands of the Central and Western Regions of Ghana

Due to abrasion and weathering of parent rocks in the coastal environment, mineral fragments are gradually transported by the sea waves and are deposited in the beach sands along the coastal environment. Accumulation of the heavy minerals in beach sands could lead to the formation of placers which spans a wide distance and are often deep seated in the sand bed.

The beach sand in the Central and Western region of the Ghana were studied for heavy mineral presence. The minerals found in the beach sands are shown in Fig. 4.7 a-f and *Appendix G*. Typical minerals identified within the beach sands of the Central region include; rutile, tourmaline, zircon, biotite, hornblende, staurolite, and biotite. Zircon is known to be found in silisic igneous rocks and they occur in beach sands and placers. The beach sands of Ekumpoano and Dago contained zircon which is a known host of rare earth elements. Apatite was observed in the beach sands of Edumafa, while the beach sands of Fetteh showed traces of biotites and epidotes.

The beach sands of Atuabo in the Western region contained some zircon, while zircon, rutile, staurolite and tourmaline were found in the beach sands of Sanzule. Beach sands of Sekondi also contained some rutile, tourmaline and zircons. Egyembra and Cape Three Points contained minerals such as biotite, tourmaline and zircon. The beach sands of Esiama and Shama showed traces of zircon, tourmaline and pyroxene.

(a)

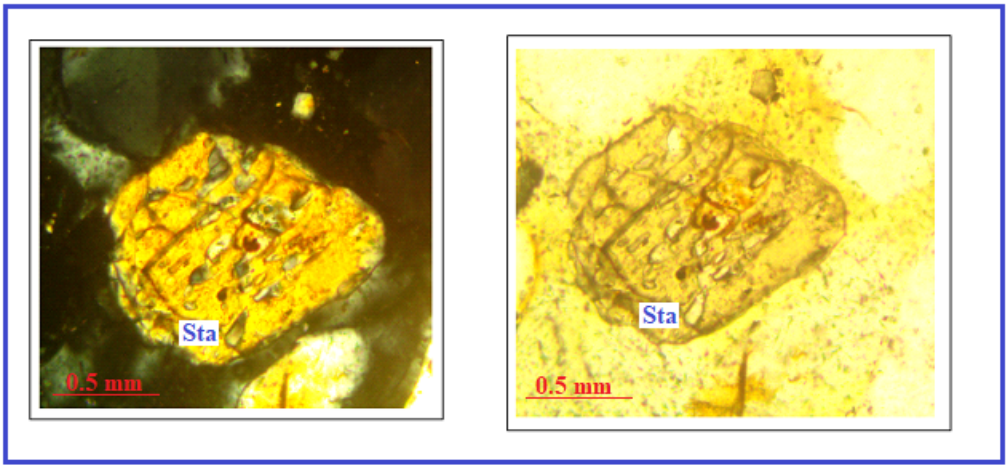

(b)

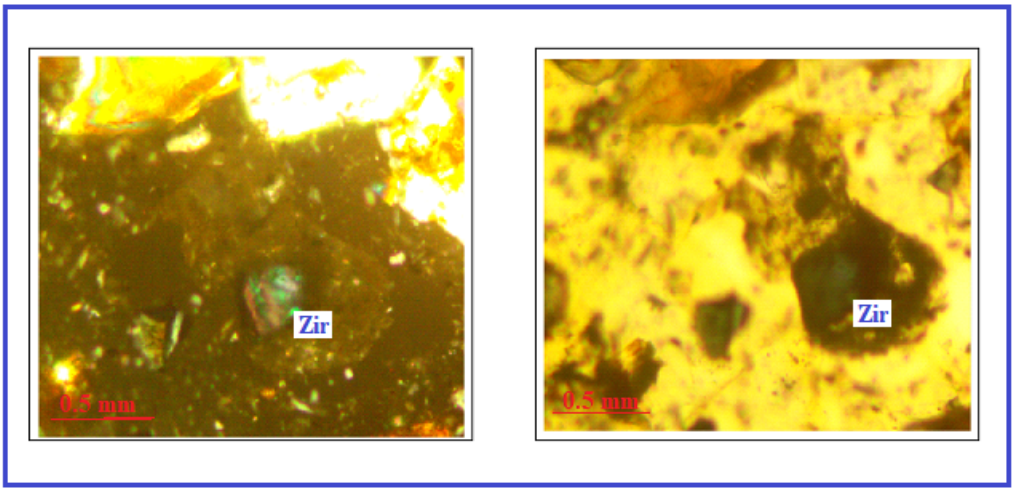

(c)

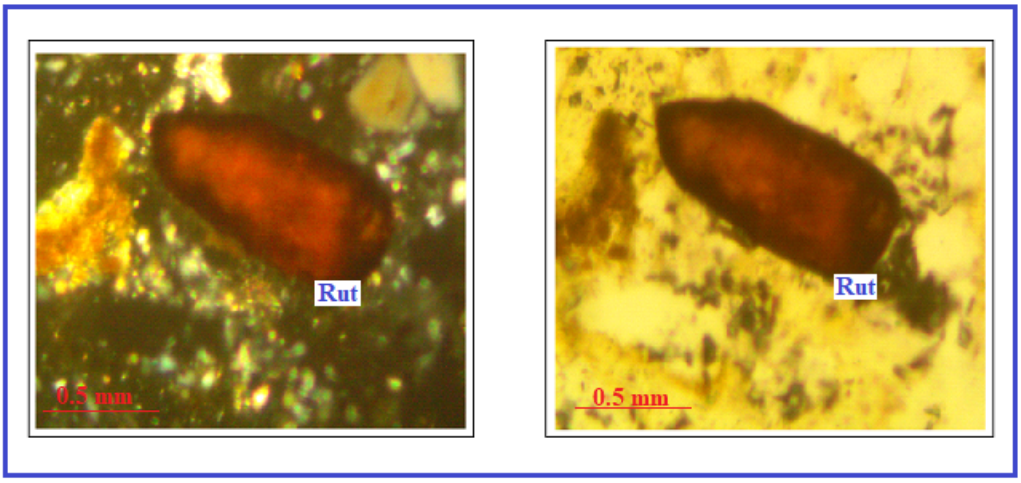

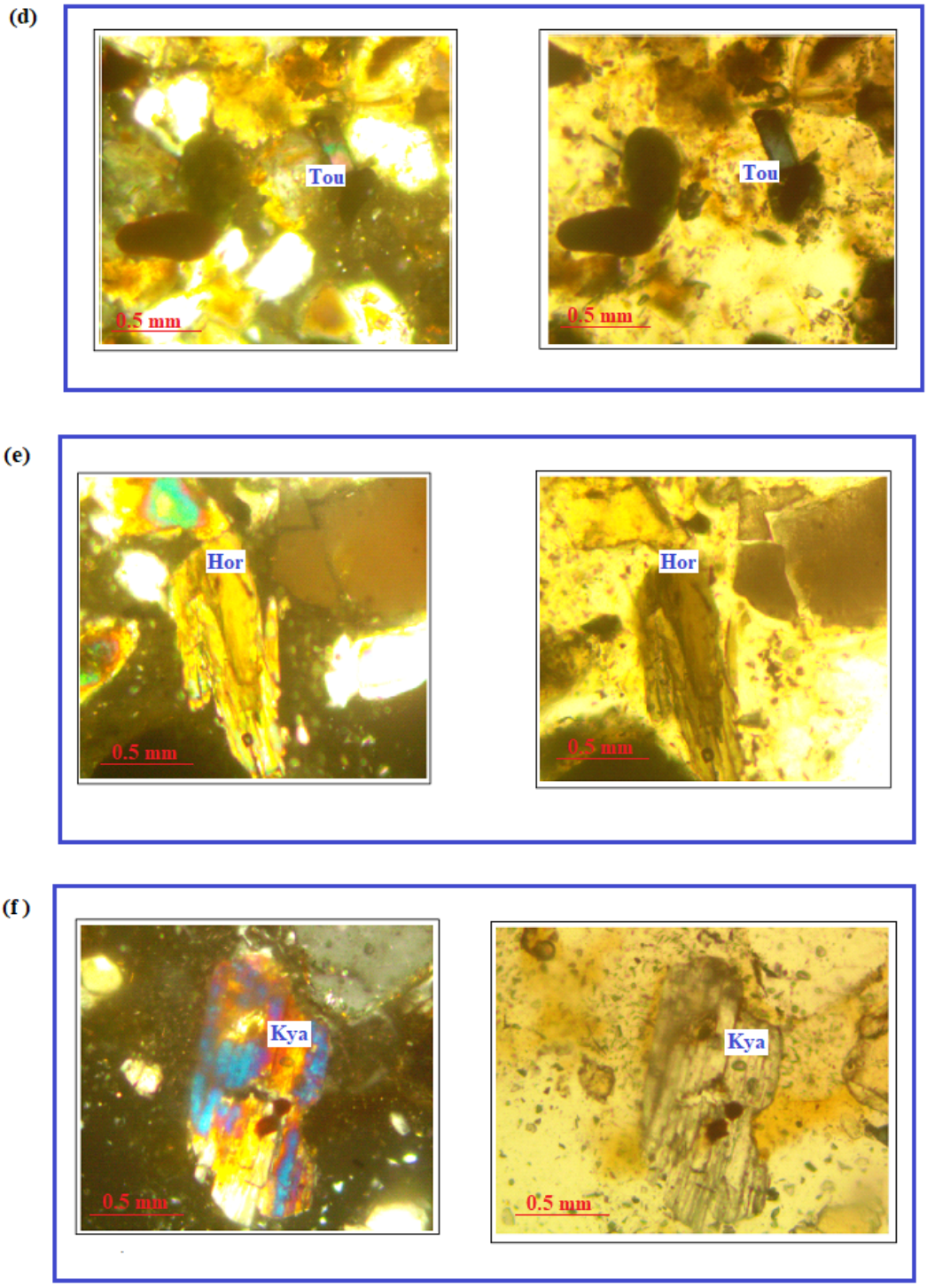

Fig. 4.7: Photomicrograph of selected minerals in beach sand of Central and Western regions of Ghana: (*Left image*) cross polarized light and (*Right image*) plane-polarized light (a) Staurolite (b) Zircon (c) Rutile (d) Tourmaline (e) Hornblende (f) Kyanite

4.4 Rare Earth Elements Distribution in Coastal Sands of the Central and Western Region of Ghana

4.4.1 Distribution of Rare Earth Elements in Beach Sands of the Central Region

Results obtained from the analysis of the rare earth elements in the beach sands are considered based on their particle size i.e coarse, medium and fine sands; the result spans across Fetteh to Kafodzizi in the Central region. Table 4.6 shows the distribution of rare earth elements concentration in coarse fractions of the beach sands of the central region.

The sum of the REEs in the coarse sand fraction occurs in the range 6.35 to 13.30 ppm and the highest concentration is observed in the beach sands of Dago (CR7), while the lowest occurs in the beach sands of Anomabu (CR11) and Akra (CR8).

The sum of the LREEs in the coarse sand fraction along the Central region occur in the range 5.56 – 11.7 ppm, where the beach sands from Dago (CR7) shows increased concentration in LREEs in relation to the least occurring in the beach sands of Anomabu (CR11) (Fig. 4.8).

The sum of HREEs in the coarse sands ranged between 0.64 – 1.53 ppm with the lowest in Akra sands and the highest concentration in the Dago (CR7) sands (Fig. 4.9). A ratio of the LREEs to HREEs is 5.81 – 9.89 ppm with the highest concentration observed in the beach sands of Senya (CR2) and lowest in the sands of Ekumpoano (CR9); this suggests enrichment in LREEs in the beach sands of Senya (Table 4.6). Fig. 4.10 shows the trend in the distribution of the total REEs in the coarse fraction of the beach sands of the Central region. Total REEs was lowest in the coarse fraction. *(Appendix D for summary data and Appendix F for YHREE chart representation).*

Table 4.6: Rare earth elements concentration (ppm) in coarse fractions of the beach sands of the Central region

Code	La	Ce	Pr	Nd	Sm	Eu	Gd	Tb	Dy	Ho	Er	Tm	Yb	Lu	Y	LREE	HREE	∑REE	L/H
DL	**0.5**	**0.5**	**0.03**	**0.1**	**0.03**	**0.03**	**0.05**	**0.01**	**0.05**	**0.01**	**0.03**	**0.01**	**0.03**	**0.01**	**0.5**				
CRC1	1.40	2.06	0.30	1.20	0.24	0.05	0.16	0.03	0.17	0.03	0.12	0.02	0.13	0.02	1.00	5.79	0.68	6.47	8.51
CRC2	1.70	3.30	0.37	1.40	0.31	0.04	0.22	0.04	0.19	0.03	0.11	0.02	0.1	0.01	1.00	7.12	0.72	7.84	9.89
CRC3	1.40	2.90	0.33	1.30	0.27	0.07	0.26	0.04	0.23	0.05	0.13	0.03	0.13	0.02	1.40	6.27	0.89	7.16	7.04
CRC4	2.20	4.30	0.51	1.90	0.33	0.10	0.32	0.06	0.34	0.07	0.18	0.02	0.18	0.03	1.80	9.34	1.20	10.54	7.78
CRC5	1.90	3.70	0.46	1.60	0.33	0.06	0.30	0.04	0.29	0.05	0.14	0.03	0.16	0.03	1.60	8.05	1.04	9.09	7.74
CRC6	1.80	3.70	0.41	1.60	0.24	0.06	0.30	0.05	0.19	0.04	0.12	0.02	0.12	0.02	1.30	7.81	0.86	8.67	9.08
CRC7	2.70	5.80	0.59	2.20	0.42	0.06	0.36	0.06	0.38	0.09	0.26	0.03	0.31	0.04	2.10	11.77	1.53	13.3	7.69
CRC8	1.30	2.70	0.34	1.10	0.24	0.03	0.20	0.02	0.16	0.03	0.11	0.01	0.09	0.02	0.80	5.71	0.64	6.35	8.92
CRC9	1.50	3.10	0.33	1.20	0.27	0.05	0.26	0.04	0.27	0.05	0.23	0.02	0.21	0.03	1.60	6.45	1.11	7.56	5.81
CRC10	1.40	2.90	0.35	1.20	0.27	0.05	0.17	0.04	0.16	0.04	0.1	0.02	0.12	0.02	1.10	6.17	0.67	6.84	9.21
CRC11	1.30	2.60	0.29	1.10	0.23	0.04	0.21	0.04	0.21	0.03	0.12	0.02	0.14	0.02	1.00	5.56	0.79	6.35	7.04
CRC12	1.30	2.70	0.31	1.10	0.24	0.05	0.19	0.03	0.15	0.03	0.13	0.02	0.12	0.01	0.90	5.70	0.68	6.38	8.38
CRC13	1.70	3.30	0.39	1.50	0.30	0.06	0.25	0.03	0.19	0.03	0.07	0.02	0.15	0.02	1.00	7.25	0.76	8.01	9.54
CRC14	1.20	2.70	0.31	1.20	0.22	0.05	0.23	0.04	0.2	0.02	0.12	0.02	0.12	0.02	0.90	5.68	0.77	6.45	7.38
CRC15	1.30	2.70	0.29	1.10	0.22	0.07	0.21	0.02	0.13	0.04	0.10	0.01	0.13	0.01	0.90	5.68	0.65	6.33	8.74

CR1= Gomoa Fetteh; **CR2**= Senya Beraku; **CR3**= Winneba; **CR4**= Mankwadze; **CR5**=Apam; **CR6**=Mumford; **CR7**=Dago; **CR8**= Akra; **CR9**=Ekumpoano; **CR10**=Edumafa; **CR11**=Anomabu; **CR12**=Cape Coast; **CR13**=Elmina; **CR14**=Dutch Komenda; **CR15**=Kafodzizi

DL: Detection Limit

The medium fraction of the beach sands along the coast of the Central region contain a total REE distribution ranged between 8.56 to 53.15 ppm with the lowest concentration in the beach sands of Anomabu (CR11) highest concentration observed in the beach sands of Dago (CR7). The values recorded for the total REEs in the medium sands exceeded the concentrations obtained in the coarse fraction of the beach sands (Table 4.6).

HREE distribution in the medium beach sand fractions of the Central region shows that Dago (CR7) has the highest (5.02 ppm) concentration of HREEs and the lowest (0.84 ppm) concentration is found in the beach sands of Anomabu (CR11) (Fig. 4.9).

LREEs in the medium fraction of the beach sands of the Central region shows values ranging from 7.72 to 48.13 ppm with the lowest occurring in the Anomabu (CR11) beach sands and the highest in the beach sands of Dago (CR7). The ratio of light to heavy REEs in the medium sands shows the beach sands of Ekumpoano (CR9) 5.83 as the lowest and Elmina (CR13) 9.95 as the highest (Table 4.7).

Ratio of LREE to HREE in medium sand fraction of the beach sands in the Central region of the range 5.83 – 9.95 and a higher value is obtained in the beach sands of Elmina (CR13) and the lowest in Ekumpoano (CR9) beach sands (Table 4.7).

Fine sand fraction of the beach sands suggest an increased concentration of the REEs when compared with that observed in the coarse and medium fraction. Total REEs across the fine sands in the Central region occurs in the range 16.67 to 795.01 ppm, with the lowest occurring in the beach sands of Edumafa (CR10) and the highest concentration observed in beach sands of Dago (CR7). A comparison of total REEs

Table 4.7: Rare earth elements concentration (ppm) in medium fractions of beach sands in the Central region

Code	La	Ce	Pr	Nd	Sm	Eu	Gd	Tb	Dy	Ho	Er	Tm	Yb	Lu	Y	LREE	HREE	∑REE	L/H
DL	**0.5**	**0.5**	**0.03**	**0.1**	**0.03**	**0.03**	**0.05**	**0.01**	**0.05**	**0.01**	**0.03**	**0.01**	**0.03**	**0.01**	**0.5**				
CRM1	2.00	4.00	0.44	1.8	0.36	0.08	0.35	0.04	0.29	0.06	0.15	0.03	0.16	0.02	1.50	8.68	1.10	9.78	7.89
CRM2	2.10	4.20	0.48	2.00	0.36	0.10	0.36	0.06	0.39	0.08	0.20	0.03	0.24	0.03	2.10	9.24	1.39	10.63	6.65
CRM3	2.80	5.40	0.66	2.40	0.48	0.10	0.39	0.05	0.31	0.07	0.19	0.02	0.19	0.03	1.80	11.84	1.25	13.09	9.47
CRM4	2.60	5.30	0.62	2.50	0.42	0.12	0.43	0.06	0.41	0.09	0.26	0.04	0.23	0.04	2.20	11.56	1.56	13.12	7.41
CRM5	3.10	6.60	0.76	3.10	0.60	0.11	0.46	0.07	0.45	0.07	0.23	0.04	0.21	0.04	2.20	14.27	1.57	15.84	9.09
CRM6	3.60	7.40	0.85	3.10	0.63	0.14	0.55	0.09	0.53	0.11	0.30	0.05	0.32	0.04	2.90	15.72	1.99	17.71	7.90
CRM7	11.30	22.90	2.55	9.40	1.84	0.14	1.48	0.18	1.06	0.23	0.87	0.13	0.91	0.16	6.30	48.13	5.02	53.15	9.59
CRM8	2.80	5.60	0.65	2.30	0.49	0.09	0.36	0.06	0.34	0.09	0.26	0.03	0.31	0.04	2.10	11.93	1.49	13.42	8.01
CRM9	3.00	5.90	0.67	2.50	0.48	0.11	0.41	0.08	0.51	0.12	0.38	0.07	0.53	0.07	3.40	12.66	2.17	14.83	5.83
CRM10	1.90	4.00	0.46	1.80	0.33	0.09	0.32	0.04	0.28	0.06	0.17	0.03	0.19	0.03	1.70	8.58	1.12	9.70	7.66
CRM11	1.90	3.60	0.40	1.50	0.25	0.07	0.26	0.04	0.21	0.03	0.12	0.02	0.14	0.02	1.10	7.72	0.84	8.56	9.19
CRM12	2.10	4.90	0.46	1.70	0.30	0.08	0.35	0.06	0.32	0.07	0.28	0.03	0.24	0.04	2.10	9.54	1.39	10.93	6.86
CRM13	2.30	4.80	0.53	2.00	0.32	0.10	0.34	0.04	0.26	0.05	0.12	0.02	0.16	0.02	1.20	10.05	1.01	11.06	9.95
CRM14	2.00	4.10	0.44	1.70	0.33	0.11	0.31	0.04	0.23	0.05	0.16	0.02	0.16	0.02	1.30	8.68	0.99	9.67	8.77
CRM15	1.80	3.80	0.41	1.80	0.33	0.08	0.27	0.04	0.22	0.04	0.15	0.04	0.18	0.02	1.30	8.22	0.96	9.18	8.56

CR1= Gomoa Fetteh; **CR2**= Senya Beraku; **CR3**= Winneba; **CR4**= Mankwadze; **CR5**=Apam; **CR6**=Mumford; **CR7**=Dago; **CR8**= Akra; **CR9**=Ekumpoano; **CR10**=Edumafa; **CR11**=Anomabu; **CR12**=Cape Coast; **CR13**=Elmina; **CR14**=Dutch Komenda; **CR15**=Kafodzizi

DL: Detection Limit

Table 4.8: Rare earth elements concentration (ppm) in fine fractions of beach sand in the Central region

Code	La	Ce	Pr	Nd	Sm	Eu	Gd	Tb	Dy	Ho	Er	Tm	Yb	Lu	Y	LREE	HREE	∑REE	L/H
DL	**0.5**	**0.5**	**0.03**	**0.1**	**0.03**	**0.03**	**0.05**	**0.01**	**0.05**	**0.01**	**0.03**	**0.01**	**0.03**	**0.01**	**0.5**				
CRF1	2.00	4.00	0.44	1.80	0.36	0.08	0.35	0.04	0.29	0.06	0.15	0.03	0.16	0.02	1.50	27.11	3.74	30.85	7.25
CRF2	2.10	4.20	0.48	2.00	0.36	0.10	0.36	0.06	0.39	0.08	0.20	0.03	0.24	0.03	2.10	32.83	3.94	36.77	8.33
CRF3	2.80	5.40	0.66	2.40	0.48	0.10	0.39	0.05	0.31	0.07	0.19	0.02	0.19	0.03	1.80	30.89	3.79	34.68	8.15
CRF4	2.60	5.30	0.62	2.50	0.42	0.12	0.43	0.06	0.41	0.09	0.26	0.04	0.23	0.04	2.20	26.08	4.21	30.29	6.19
CRF5	3.10	6.60	0.76	3.10	0.60	0.11	0.46	0.07	0.45	0.07	0.23	0.04	0.21	0.04	2.20	27.96	3.33	31.29	8.40
CRF6	3.60	7.40	0.85	3.10	0.63	0.14	0.55	0.09	0.53	0.11	0.30	0.05	0.32	0.04	2.90	19.77	2.80	22.57	7.06
CRF7	11.30	22.90	2.55	9.40	1.84	0.14	1.48	0.18	1.06	0.23	0.87	0.13	0.91	0.16	6.30	727.56	67.45	795.01	10.79
CRF8	2.80	5.60	0.65	2.30	0.49	0.09	0.36	0.06	0.34	0.09	0.26	0.03	0.31	0.04	2.10	96.57	18.25	114.82	5.29
CRF9	3.00	5.90	0.67	2.50	0.48	0.11	0.41	0.08	0.51	0.12	0.38	0.07	0.53	0.07	3.40	375.78	74.53	450.31	5.04
CRF10	1.90	4.00	0.46	1.80	0.33	0.09	0.32	0.04	0.28	0.06	0.17	0.03	0.19	0.03	1.70	14.98	1.69	16.67	8.86
CRF11	1.90	3.60	0.40	1.50	0.25	0.07	0.26	0.04	0.21	0.03	0.12	0.02	0.14	0.02	1.10	30.01	5.08	35.09	5.91
CRF12	2.10	4.90	0.46	1.70	0.30	0.08	0.35	0.06	0.32	0.07	0.28	0.03	0.24	0.04	2.10	20.22	3.14	23.36	6.44
CRF13	2.30	4.80	0.53	2.00	0.32	0.10	0.34	0.04	0.26	0.05	0.12	0.02	0.16	0.02	1.20	21.33	4.81	26.14	4.43
CRF14	2.00	4.10	0.44	1.70	0.33	0.11	0.31	0.04	0.23	0.05	0.16	0.02	0.16	0.02	1.30	31.02	4.55	35.57	6.82
CRF15	1.80	3.80	0.41	1.80	0.33	0.08	0.27	0.04	0.22	0.04	0.15	0.04	0.18	0.02	1.30	24.85	4.64	29.49	5.36

CR1= Gomoa Fetteh; **CR2**= Senya Beraku; **CR3**= Winneba; **CR4**= Mankwadze; **CR5**=Apam; **CR6**=Mumford; **CR7**=Dago; **CR8**= Akra; **CR9**=Ekumpoano; **CR10**=Edumafa; **CR11**=Anomabu; **CR12**=Cape Coast; **CR13**=Elmina; **CR14**=Dutch Komenda; **CR15**=Kafodzizi

DL: Detection Limit

in the coarse, medium and fine sand fractions from the beach sand from Dago shows about 92% increase in the fine fraction (Fig. 4.10).

The total REEs in the fine sand fraction of the beach sands in two locations Akra (CR8) and Ekumpoano (CR9) shows total REE concentration exceeding 100 ppm. Westward movement from the beach sands of Dago (CR7) shows a slight decrease in the total REEs at Akra (CR8) and an abrupt increase in the total REEs observed in fine fractions of the beach sands of Ekumpoano (CR9).

The LREE concentration in the fine fractions of the beach sands occurs in the range 14.98 – 727 ppm with the least concentration found in the beach sands of Edumafa (**CR10**) and the highest concentration found in the beach sands of Dago (CR7) *(Appendix D)*. The perimeter surrounding Akra (CR8) extending from Dago (CR7) to Ekumpoano (CR9) shows conspicuous concentration of LREEs.

HREE concentration in the fine fractions of the beach sands in the Central region are in the range 1.69 – 74.53 ppm, where Edumafa (CR10) had the lowest HREE content and the highest occurring in the beach sands of Ekumpoano (CR9) *(Appendix D)*.

The ratio of LREE to HREE shows the beach sands of Dago (CR7) have the highest value (10.79) and the lowest value was found in Elmina beach sands (CR13).

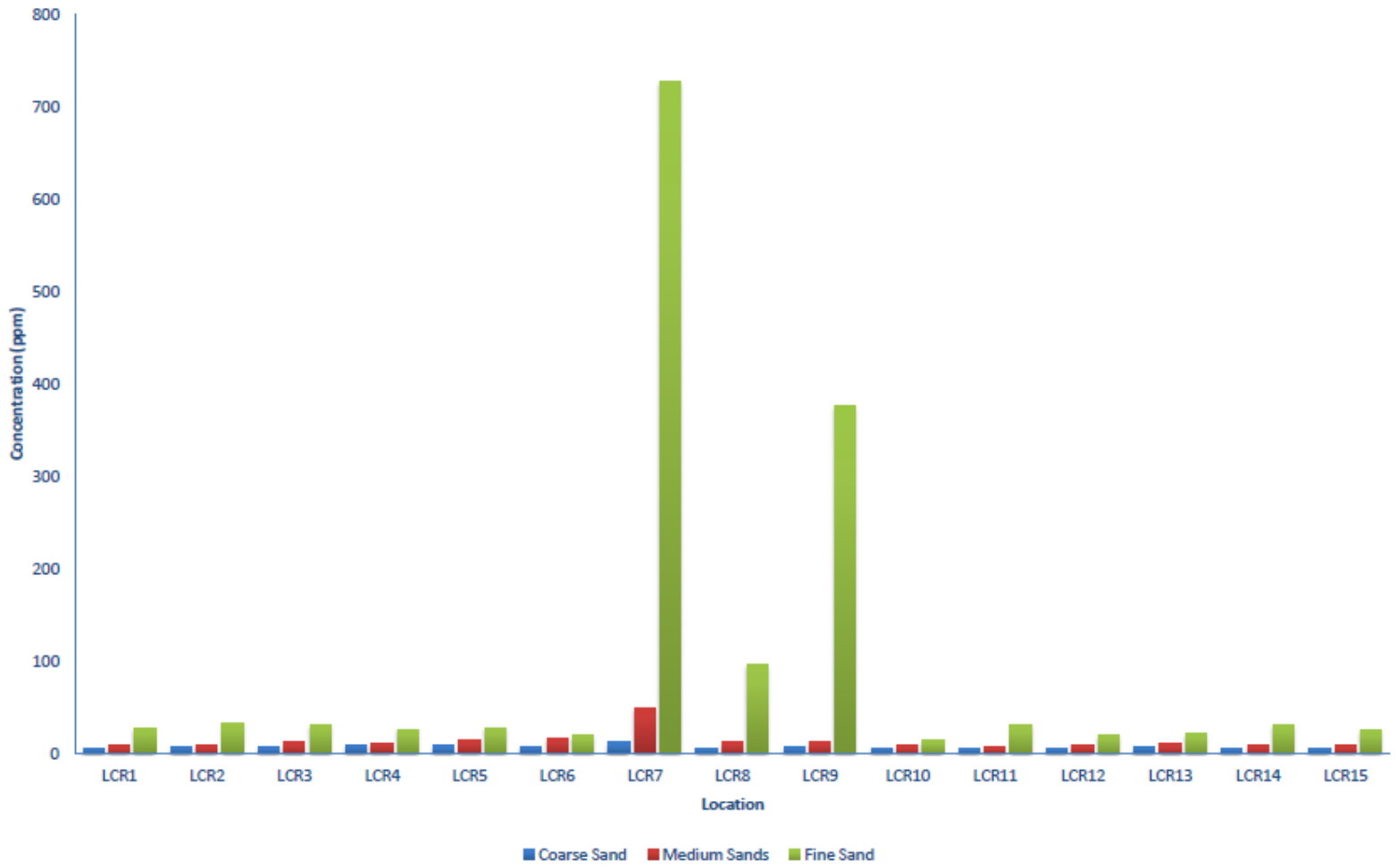

LCR1= Gomoa Fetteh; **LCR2**= Senya Beraku; **LCR3**= Winneba; **LCR4**= Mankwadze; **LCR5**=Apam; **LCR6**=Mumford; **LCR7**=Dago; **LCR8**= Akra; **LCR9**=Ekumpoano; **LCR10**=Edumafa; **LCR11**=Anomabu; **LCR12**=Cape Coast; **LCR13**=Elmina; **LCR14**=Dutch Komenda; **LCR15**=Kafodzizi

Fig. 4.8: Distribution of LREEs (La - Eu) in the coarse, medium and fine fraction of beach sands in the Central Region of Ghana.

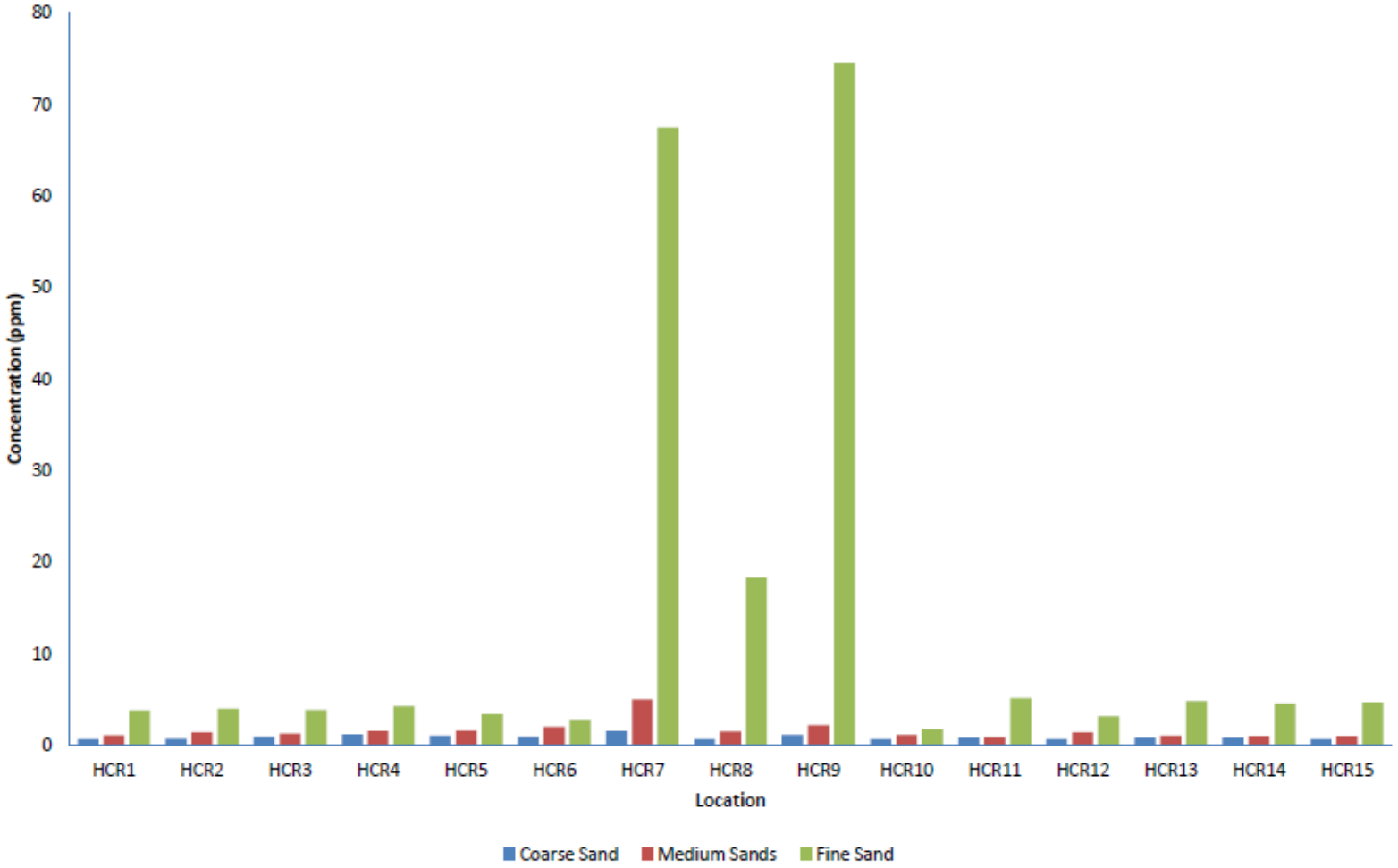

HCR1= Gomoa Fetteh; **HCR2**= Senya Beraku; **HCR3**= Winneba; **HCR4**= Mankwadze; **HCR5**=Apam; **HCR6**=Mumford; **HCR7**=Dago; **HCR8**= Akra; **HCR9**=Ekumpoano; **HCR10**=Edumafa **HCR11**=Anomabu; **HCR12**=Cape Coast; **HCR13**=Elmina; **HCR14**=Dutch Komenda; **HCR15**=Kafodzizi

Fig. 4.9: Distribution of HREEs (Gd –Lu) in the coarse, medium and fine fraction of beach sands in the Central Region of Ghana

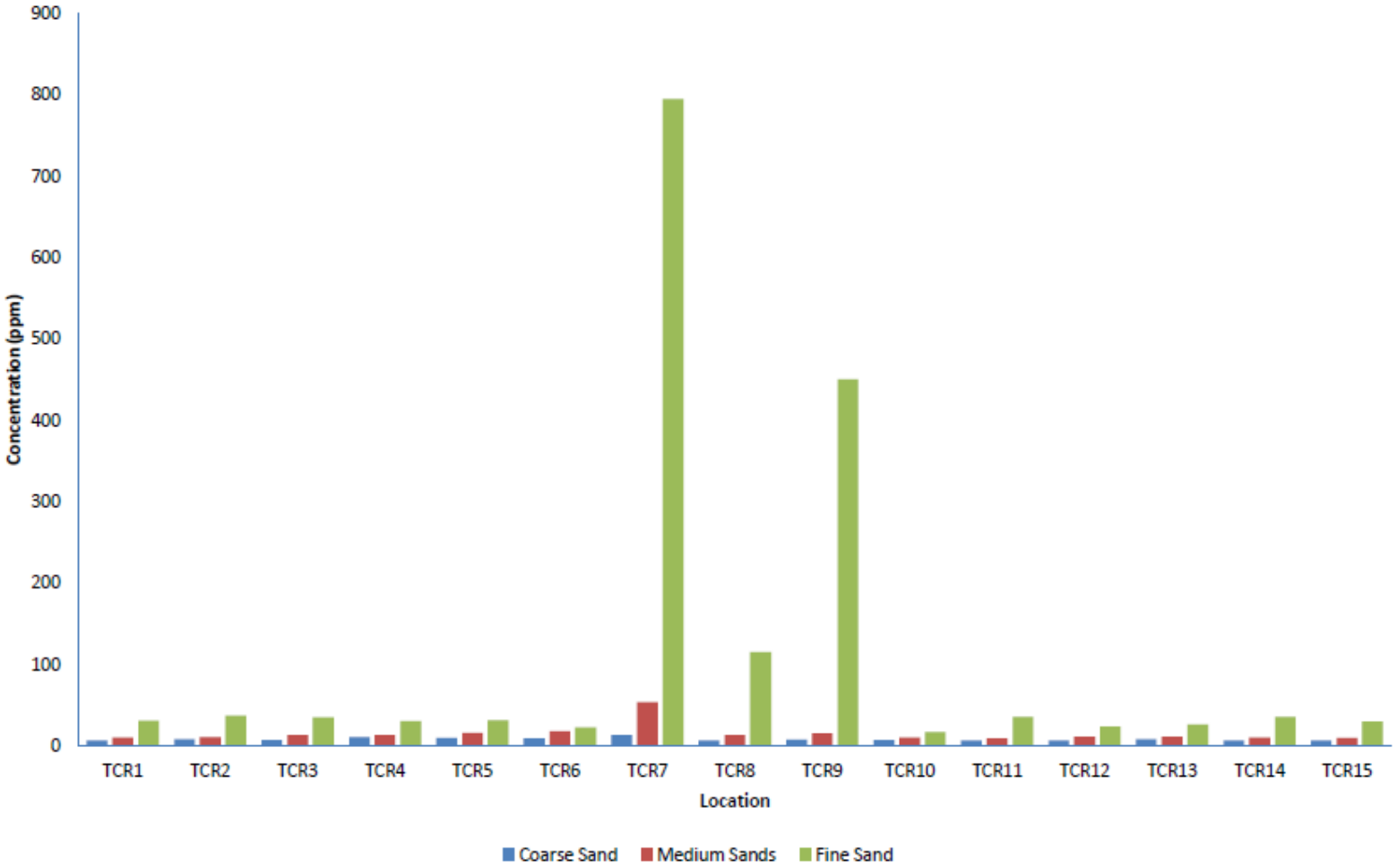

TCR1= Gomoa Fetteh; **TCR2**= Senya Beraku; **TCR3**= Winneba; **TCR4**= Mankwadze; **TCR5**=Apam; **TCR6**=Mumford; **TCR7**=Dago; **TCR8**= Akra; **TCR9**=Ekumpoano; **TCR10**=Edumafa; **TCR11**=Anomabu; **TCR12**=Cape Coast; **TCR13**=Elmina; **TCR14**=Dutch Komenda; **TCR15**=Kafodzizi

Fig. 4.10: Distribution of total REEs (La – Lu) in the coarse, medium, and fine fraction of beach sands in the Central Region of Ghana.

4.4.2 Distribution of Rare Earth Elements in Beach Sands of the Western Region

Rare Earth element data obtained from the analysis of beach sands of ten locations along the Western region of Ghana are reported based on their fractions (coarse, medium and fine). The sampling covers the stretch from Shama to Atuabo. Fig. 4.11 to 4.13 shows the distribution of rare earth elements concentration in the beach sands of the Western region.

The sum of the LREEs in the coarse fraction of the beach sands in the western region occurs in the range 5.07 to 26.08 ppm, with the least occurring in the sands of Egyembra (WR6) and highest concentration in the beach sand of Axim (WR7) (Table 4.9). The beach sands of Sekondi (WR3) are composed mostly of very fine sands with no coarse fractions in the samples collected (Table 4.5).

The sum of HREE in the coarse fraction of the beach sands in the Western region shows concentration ranging between 0.62 to 3.70 ppm, with the least found in the beach sands of Egyembra (WR6), highest concentration in the beach sand of Axim (WR7) (Table 4.9).

The total REE distribution in the coarse fraction is in the range 5.69 to 29.78 ppm and pattern of concentration follows what was observed in the respective locations of Egyembra (WR6) and Axim (WR7) (Fig. 4.13). Ratio of LREE to HREE in the coarse fraction of the beach sands in the Western region ranges from the lowest 6.67 in Shama (WR1) to 10.11 in Takoradi (WR4) (Table 4.9).

A comparison of the total REE in the coarse fraction of the beach sands of the Western region shows appreciable quantity of REE in reference to the coarse sands of the Central region; the highest concentration in Western region was found in Axim (WR7) and that of the Central region was found in Dago (CR7).

Table 4.9: Rare earth elements concentration in coarse fractions of beach sand in the Western region

Code	La	Ce	Pr	Nd	Sm	Eu	Gd	Tb	Dy	Ho	Er	Tm	Yb	Lu	Y	LREE	HREE	∑REE	L/H
DL	**0.5**	**0.5**	**0.03**	**0.1**	**0.03**	**0.03**	**0.05**	**0.01**	**0.05**	**0.01**	**0.03**	**0.01**	**0.03**	**0.01**	**0.5**				
WRC1	2.30	5.20	0.53	2.10	0.37	0.11	0.37	0.06	0.37	0.08	0.32	0.04	0.31	0.04	2.40	10.61	1.59	12.2	6.67
WRC2	3.10	5.90	0.70	2.40	0.56	0.11	0.39	0.06	0.36	0.07	0.22	0.03	0.24	0.03	2.10	12.77	1.40	14.17	9.12
WRC3	-	-	-	-	-	-	-	-	-	-	-	-	-	-	-	-	-	-	-
WRC4	4.70	8.30	1.05	4.10	0.68	0.17	0.63	0.09	0.52	0.09	0.25	0.03	0.23	0.04	2.70	19.00	1.88	20.88	10.11
WRC5	3.30	5.60	0.84	3.40	0.68	0.19	0.64	0.09	0.58	0.12	0.31	0.05	0.27	0.04	3.80	14.01	2.10	16.11	6.67
WRC6	1.10	2.20	0.29	1.20	0.23	0.05	0.18	0.03	0.14	0.02	0.11	0.01	0.11	0.02	0.90	5.07	0.62	5.69	8.18
WRC7	5.20	13.30	1.26	5.00	1.03	0.29	1.05	0.17	0.97	0.24	0.62	0.08	0.5	0.07	5.70	26.08	3.70	29.78	7.05
WRC8	1.80	3.80	0.43	1.60	0.30	0.05	0.27	0.03	0.2	0.04	0.14	0.02	0.14	0.02	1.10	7.98	0.86	8.84	9.28
WRC9	1.50	3.00	0.32	1.30	0.22	0.05	0.18	0.03	0.19	0.04	0.09	0.01	0.13	0.02	1.00	6.39	0.69	7.08	9.26
WRC10	1.60	3.20	0.39	1.30	0.25	0.06	0.23	0.04	0.14	0.03	0.11	0.02	0.12	0.02	0.90	6.80	0.71	7.51	9.58

WR1= Shama; **WR2**= Abuesi; **WR3**= Sekondi; **WR4**= Takoradi; **WR5**=Cape Three Points; **WR6**= Egyembra; **WR7**=Axim; **WR8**= Esiama; **WR9**= Sanzule; **WR10**=Atuabo

DL: Detection Limit

LREE in medium fraction of the beach sands in the Western region shows a range of 8.47 to 76.8 ppm, this corresponds to the sum of the LREE least concentration in the beach sands of Atuabo (WR10) and the highest in the beach sands of Sekondi (WR3) (Table 4.10).

Heavy REEs in the medium fraction beach sands of the Western region occur in the range 1.04 – 8.78 ppm, high concentration was observed in the Sekondi (WR3) where the least concentration was found in the beach sands of Sanzule (WR9) and Atuabo (WR10) (Table 4.10).

Total REEs in the medium fraction beach sands of the Western region occur in the range 9.51- 85.58 ppm, with the highest concentration recorded in the Sekondi (WR3) beach sands and the lowest in the Atuabo beach sands. Ratio of the LREE to the HREE in the medium fraction occurs in the range 3.97 – 9.56 which corresponds to Shama (WR1) and Esiama (WR8) respectively (Table 4.10).

Fine sands fraction in the beach of LREE in the Western region occur in the range of 21.6 - 77.46 ppm, where the least corresponds to the Takoradi (WR4) beach sands and the most concentration found in the Sekondi (WR3) beach sands. The LREE in the fine sand is relatively higher compared to what was observed in the coarse and medium fraction of beach sands in the Western region (Table 4.11).

HREEs found in the fine fraction beach sands in the Western region occur in the range of 2.70 – 17.63 ppm, with the Esiama (WR8) beach sands having the highest concentration of HREEs and the lowest observed in the beach sands of Takoradi (WR4) (Table 4.11).

Total REEs found in the beach sands of the Western region occur in the range 24.3 – 86.28 ppm, the highest concentration was found in the beach sands of Sekondi (WR3) and the least found in the beach sands of Takoradi. Fig. 4.11 – 4.13 shows the graphical illustration of the LREE, HREE and TREE distribution in the beach sands of the Western region *(Appendices D and F).*

Table 4.10: Rare earth elements concentration in medium fractions of beach sand in the Western region

Code	La	Ce	Pr	Nd	Sm	Eu	Gd	Tb	Dy	Ho	Er	Tm	Yb	Lu	Y	LREE	HREE	∑REE	L/H
DL	**0.5**	**0.5**	**0.03**	**0.1**	**0.03**	**0.03**	**0.05**	**0.01**	**0.05**	**0.01**	**0.03**	**0.01**	**0.03**	**0.01**	**0.5**				
WRM1	3.40	8.70	0.84	3.30	0.61	0.16	0.66	0.14	1.03	0.25	0.76	0.12	0.99	0.16	6.70	16.31	4.11	20.42	3.97
WRM2	4.00	7.90	0.93	3.40	0.67	0.14	0.55	0.08	0.45	0.10	0.27	0.04	0.29	0.04	2.80	17.04	1.82	18.86	9.36
WRM3	18.00	30.0	4.84	19.40	3.74	0.82	3.09	0.42	2.11	0.45	1.27	0.16	1.13	0.15	13.90	76.80	8.78	85.58	8.75
WRM4	3.60	6.90	0.81	3.10	0.59	0.14	0.54	0.09	0.47	0.09	0.27	0.04	0.30	0.04	2.90	15.14	1.84	16.98	8.23
WRM5	8.10	14.70	2.08	8.30	1.83	0.46	1.67	0.25	1.40	0.29	0.80	0.11	0.57	0.08	8.80	35.47	5.17	40.64	6.86
WRM6	2.70	5.50	0.67	2.40	0.43	0.11	0.41	0.06	0.36	0.07	0.22	0.03	0.20	0.03	2.20	11.81	1.38	13.19	8.56
WRM7	6.70	16.00	1.74	6.70	1.32	0.33	1.09	0.17	0.95	0.18	0.48	0.08	0.43	0.06	5.10	32.79	3.44	36.23	9.53
WRM8	3.10	6.70	0.76	2.90	0.49	0.11	0.37	0.07	0.38	0.08	0.26	0.04	0.24	0.03	2.20	14.06	1.47	15.53	9.56
WRM9	2.30	4.50	0.56	1.90	0.37	0.09	0.35	0.05	0.26	0.05	0.15	0.02	0.14	0.02	1.30	9.72	1.04	10.76	9.35
WRM10	2.00	4.00	0.45	1.60	0.35	0.07	0.32	0.05	0.28	0.06	0.15	0.02	0.13	0.03	1.60	8.47	1.04	9.51	8.14

WR1= Shama; **WR2**= Abuesi; **WR3**= Sekondi; **WR4**= Takoradi; **WR5**=Cape Three Points; **WR6**= Egyembra; **WR7**=Axim; **WR8**= Esiama; **WR9**= Sanzule; **WR10**=Atuabo

DL: Detection Limit

Table 4.11: Rare earth elements concentration in fine fractions of beach sand in the Western region

Code	La	Ce	Pr	Nd	Sm	Eu	Gd	Tb	Dy	Ho	Er	Tm	Yb	Lu	Y	LREE	HREE	∑REE	L/H
DL	**0.50**	**0.50**	**0.03**	**0.10**	**0.03**	**0.03**	**0.05**	**0.01**	**0.05**	**0.01**	**0.03**	**0.01**	**0.03**	**0.01**	**0.50**				
WRF1	14.40	29.5	3.19	11.80	2.26	0.41	2.09	0.40	2.99	0.82	2.64	0.47	3.26	0.49	22.80	61.56	13.16	74.72	4.68
WRF2	7.40	15.80	1.85	6.70	1.36	0.33	1.19	0.19	1.12	0.24	0.66	0.11	0.72	0.10	6.10	33.44	4.33	37.77	7.72
WRF3	16.40	34.90	4.43	17.50	3.44	0.79	2.90	0.41	2.37	0.45	1.27	0.17	1.09	0.16	12.80	77.46	8.82	86.28	8.78
WRF4	5.00	9.80	1.17	4.60	0.78	0.25	0.77	0.12	0.71	0.16	0.43	0.06	0.39	0.06	4.10	21.60	2.70	24.30	8.00
WRF5	8.40	15.10	2.20	9.30	1.90	0.54	1.85	0.30	1.75	0.36	1.07	0.13	0.94	0.14	10.50	37.44	6.54	43.98	5.72
WRF6	7.90	16.10	1.92	7.20	1.36	0.33	1.23	0.20	1.16	0.26	0.81	0.12	0.84	0.14	7.30	34.81	4.76	39.57	7.31
WRF7	8.90	19.70	2.32	8.90	1.81	0.43	1.52	0.24	1.29	0.25	0.70	0.10	0.74	0.12	7.30	42.06	4.96	47.02	8.48
WRF8	10.80	22.70	2.63	9.70	2.12	0.67	2.81	0.61	5.04	1.20	3.68	0.54	3.35	0.40	34.30	48.62	17.63	66.25	2.76
WRF9	7.20	14.90	1.72	6.10	1.31	0.39	1.28	0.26	1.77	0.43	1.34	0.21	1.26	0.18	12.60	31.62	6.73	38.35	4.70
WRF10	10.60	18.30	2.16	7.60	1.52	0.35	1.76	0.37	2.86	0.67	2.08	0.29	1.95	0.28	18.80	40.53	10.26	50.79	3.95

WR1= Shama; **WR2**= Abuesi; **WR3**= Sekondi; **WR4**= Takoradi; **WR5**=Cape Three Points; **WR6**= Egyembra; **WR7**=Axim; **WR8**= Esiama; **WR9**= Sanzule; **WR10**=Atuabo

DL: Detection Limit

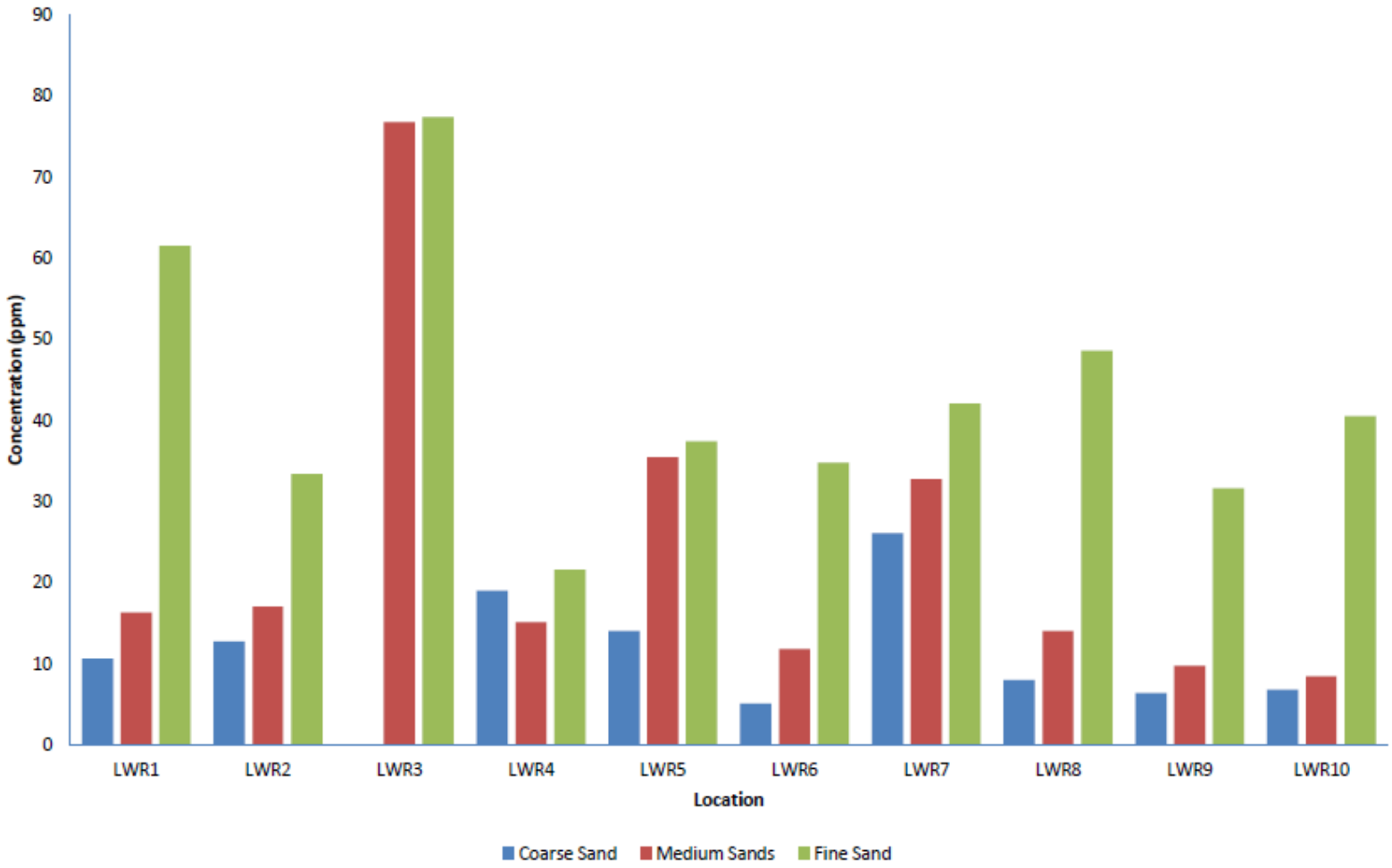

LWR1= Shama; **LWR2**= Abuesi; **LWR3**= Sekondi; **LWR4**= Takoradi; **LWR5**=Cape Three Points; **LWR6**= Egyembra; **LWR7**=Axim; **LWR8**= Esiama; **LWR9**= Sanzule; **LWR10**=Atuabo

Fig.4.11: Distribution of LREEs (La - Eu) in the coarse, medium and fine fraction of beach sands in the Western Region of Ghana

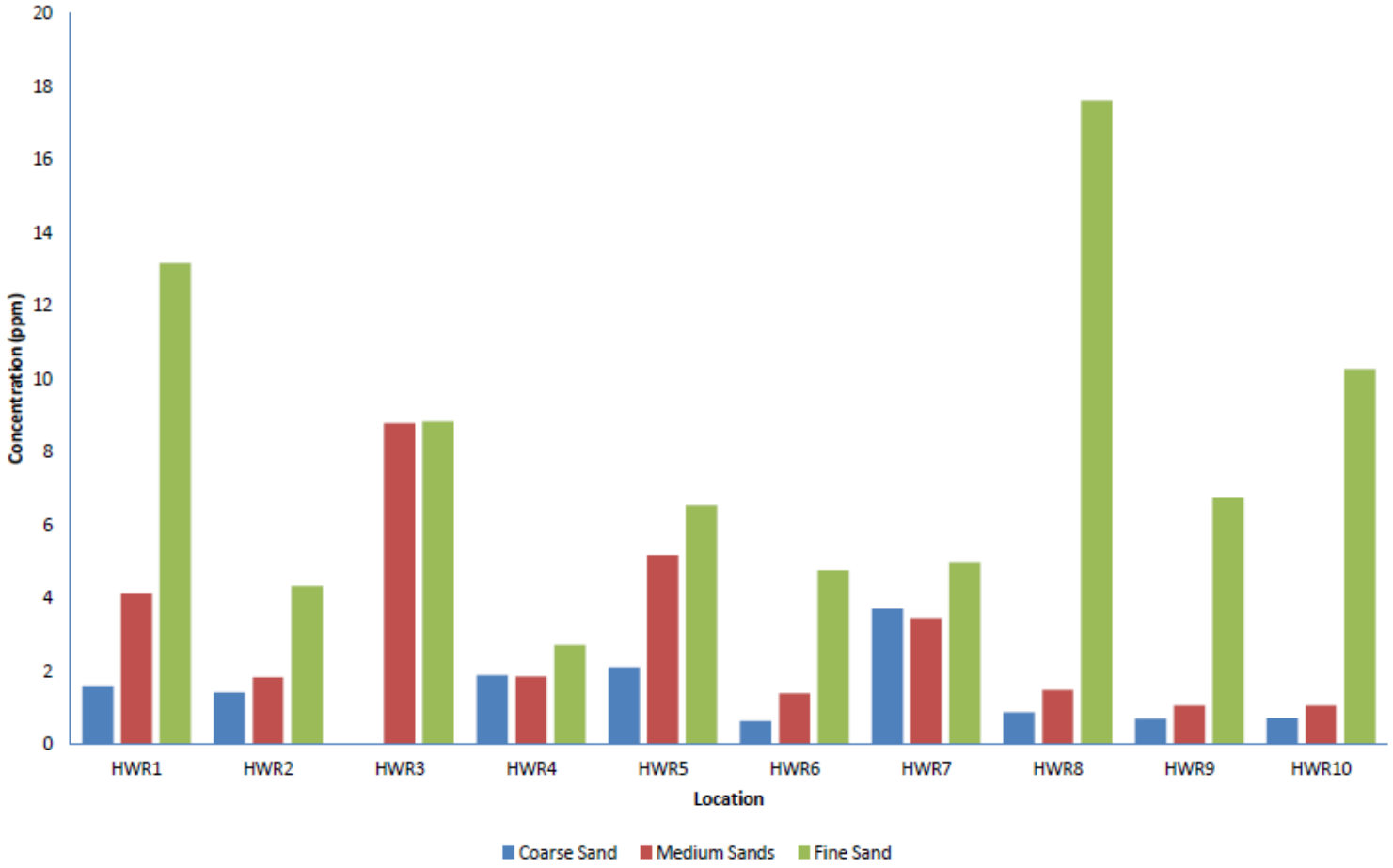

HWR1= Shama; **HWR2**= Abuesi; **HWR3**= Sekondi; **HWR4**= Takoradi; **HWR5**=Cape Three Points; **HWR6**= Egyembra; **HWR7**=Axim; **HWR8**= Esiama; **HWR9**= Sanzule; **HWR10**=Atuabo

Fig. 4.12: Distribution of HREEs (Gd - Lu) in the coarse, medium and fine fraction of beach sands in the Western Region of Ghana

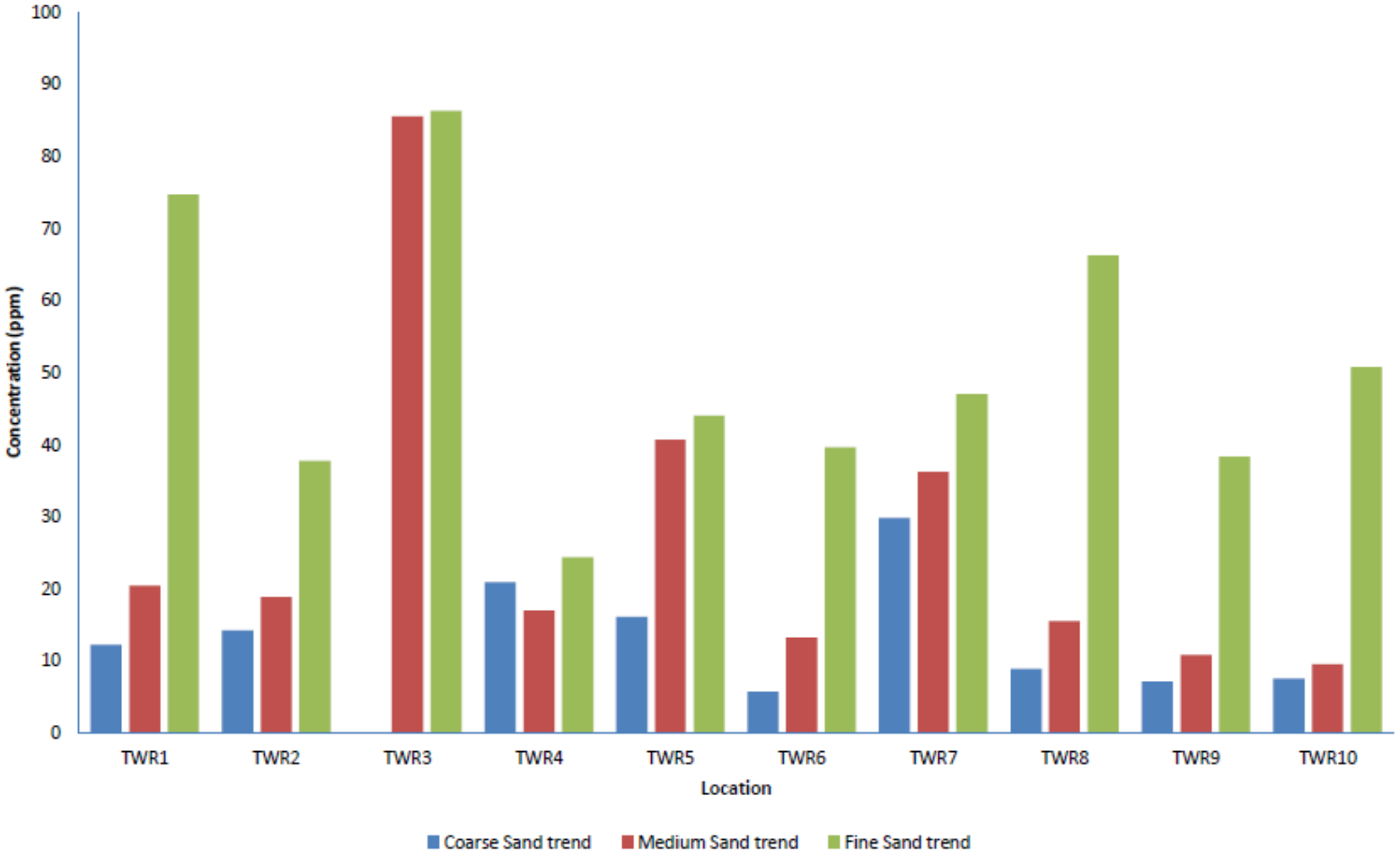

TWR1= Shama; **TWR2**= Abuesi; **TWR3**= Sekondi; **TWR4**= Takoradi; **TWR5**=Cape Three Points; **TWR6**= Egyembra; **TWR7**=Axim; **TWR8**= Esiama; **TWR9**= Sanzule; **TWR10**=Atuabo

Fig. 4.13: Distribution of total REEs (La – Lu) in the coarse, medium and fine fraction of beach sands in the Western Region of Ghana

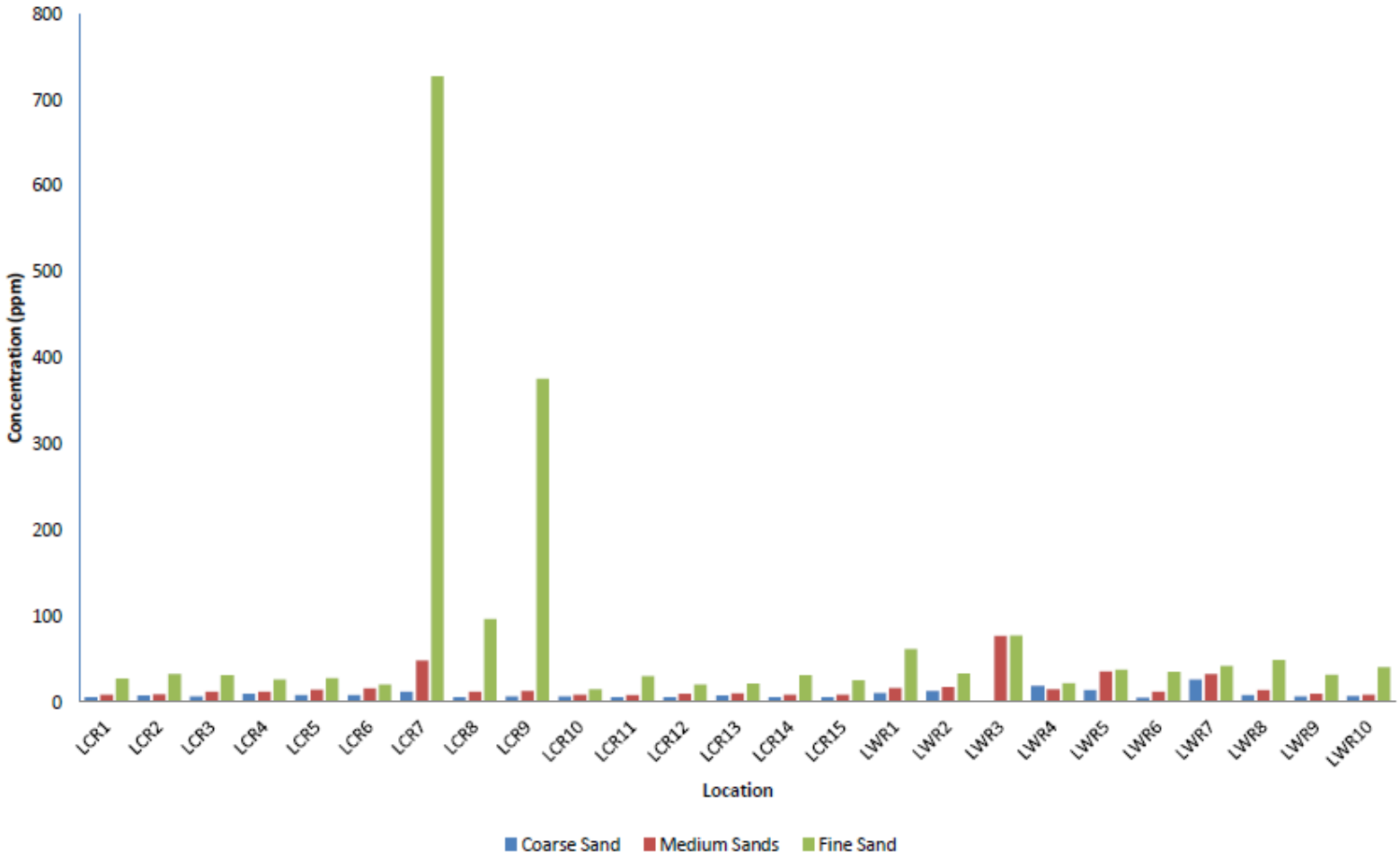

Fig. 4.14: Distribution of LREEs (La – Eu) in the coarse, medium and fine fraction of beach sands in the Central and Western Regions of Ghana

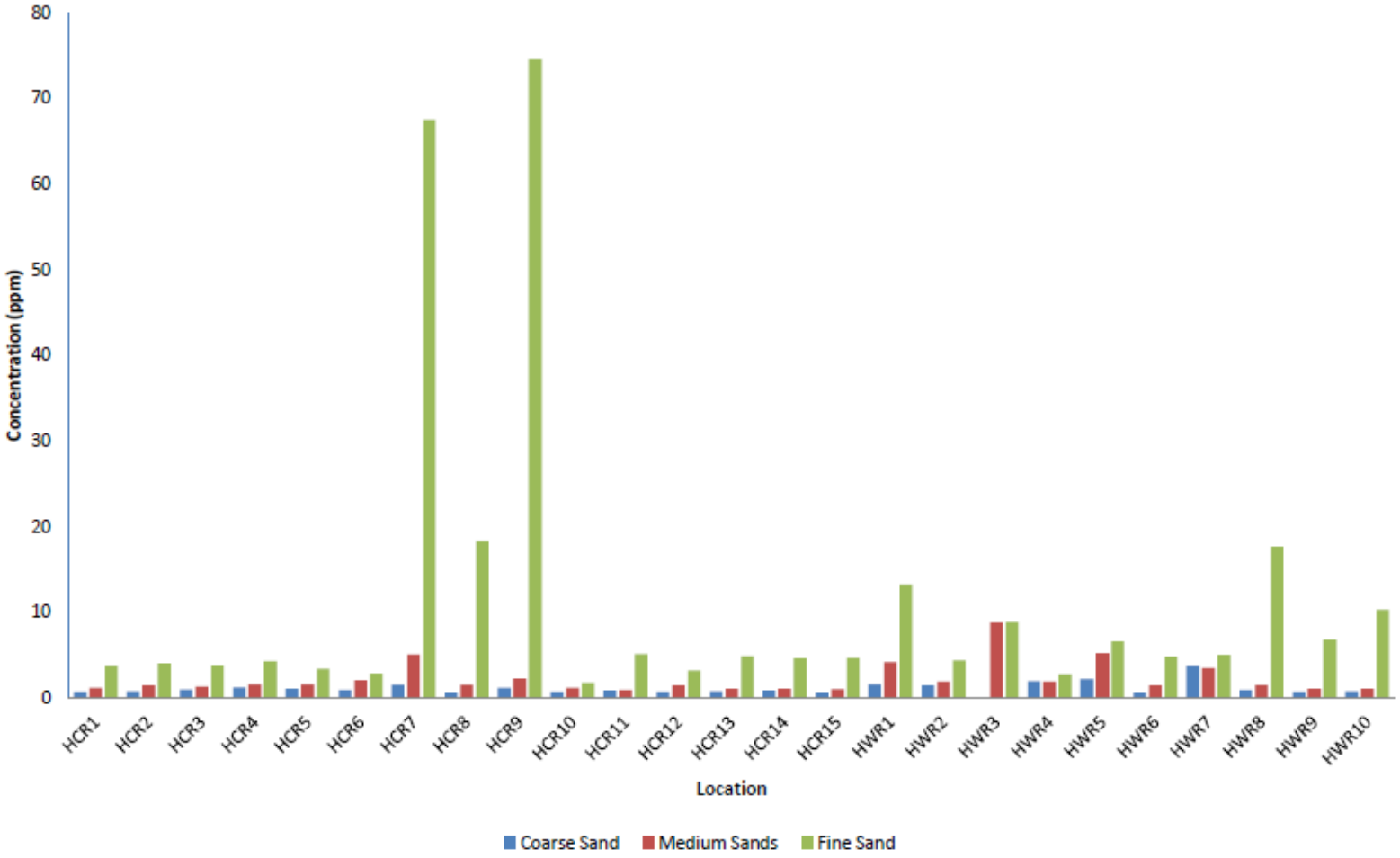

Fig. 4.15: Distribution of HREEs (Gd – Lu) in the coarse, medium and fine fraction of beach sands in the Central and Western Regions of Ghana.

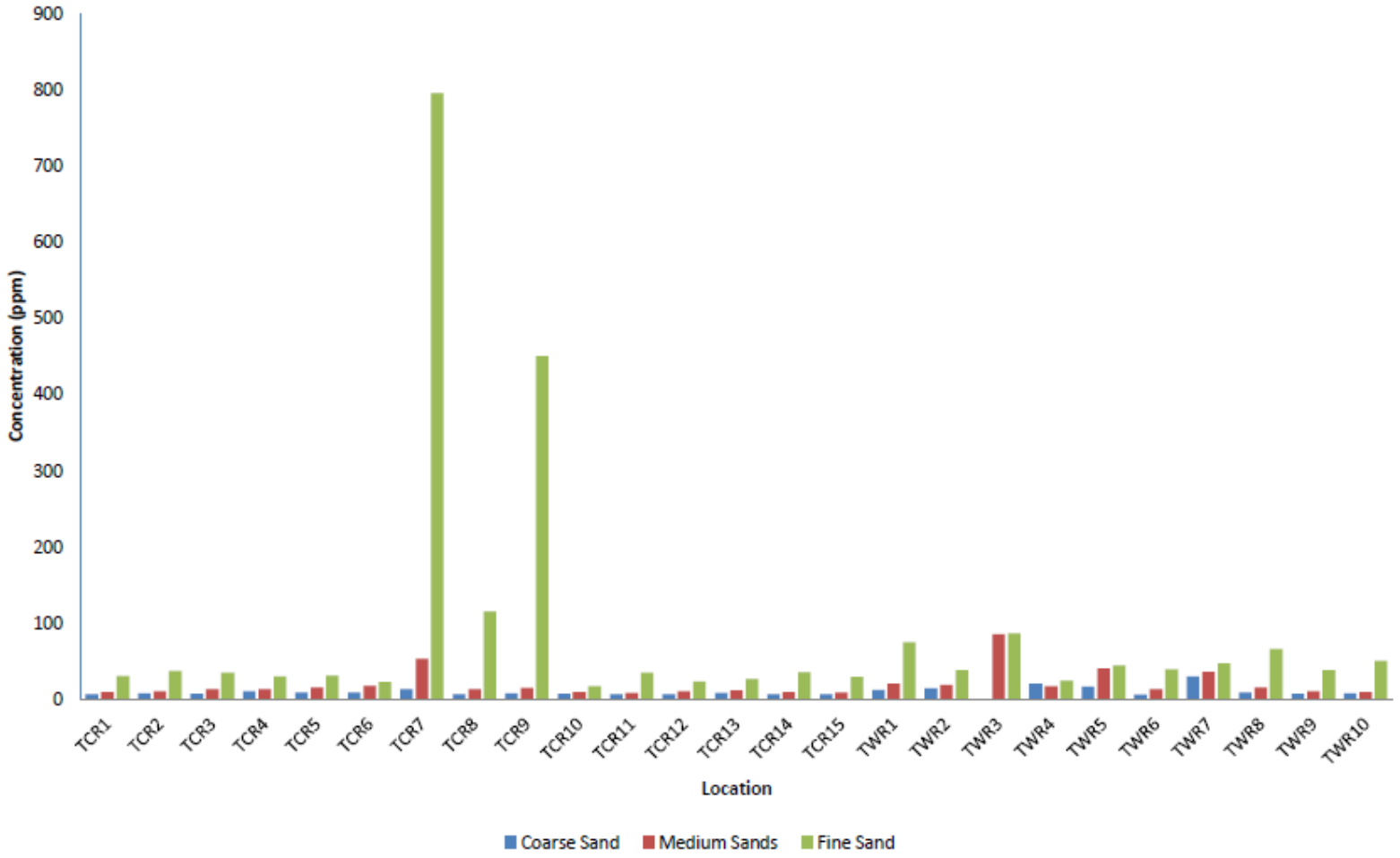

Fig. 4.16: Distribution of total REEs (La – Lu) in the coarse, medium and fine fraction of beach sands in the Central and Western regions of Ghana

4.5 Elemental Concentration (ppm) of Thorium and Uranium in Relation to Rare Earth Elements in Beach Sands of the Central and Western Region of Ghana

4.5.1 Elemental Concentration (ppm) of Thorium and Uranium in Relation to Rare Earth Elements in Beach Sands of the Central Region of Ghana

The beach sands in the Central region were analysed for the elemental thorium and uranium concentration of the coarse, medium and fine fractions. The concentration of thorium in the beach sands shown in Table 4.12 ranged as coarse (0.34 to 1.00 ppm); medium (0.38 to 4.74 ppm); and fine (0.85 to 75.2 ppm). The highest concentration of thorium was observed in the beach sands of Dago for the three fractions (coarse, medium and fine). The mean concentrations of thorium along the locations in the Central region were found for the coarse, medium and fine fraction as; (0.492 ppm; 0.84 ppm; and 9.32 ppm).

The elemental uranium concentration in the beach sands of the Central region ranged for coarse (0.26 to 0.58 ppm); medium (0.20 to 1.54 ppm); and fine (0.33 to 14.1 ppm). The highest uranium concentrations in the three fractions were; Senya (0.58 ppm- coarse); Dago (1.54 ppm- medium) and Ekumpoano (14.1 ppm- Fine). The mean concentrations of uranium along the locations in the Central region were found for the coarse medium and fine fraction as; (0.36 ppm; 0.39 ppm; and 2.45 ppm).

A ternary diagram of the relation in the coarse, medium and fine fractions vis-à-vis the LREE-Th-HREE and LREE-U-HREE for the Central region are shown in Fig. 4.17. The diagram shows that the LREEs are more associated with uranium and thorium in the beach sands.

Table 4.12: Elemental concentration (ppm) of Thorium and Uranium in relation to Rare Earth Elements in beach sands of the Central region of Ghana

Wt (ppm)	*C1	*C2	*C3	*C4	*C5	*C6	*C7	*C8	*C9	*C10	*C11	*C12	*C13	*C14	*C15
Th	0.37	0.54	0.34	0.56	0.45	0.4	1	0.61	0.49	0.45	0.42	0.45	0.5	0.39	0.41
U	0.38	0.58	0.40	0.42	0.39	0.5	0.42	0.31	0.29	0.32	0.3	0.27	0.39	0.28	0.26

Wt (ppm)	*M1	*M2	*M3	*M4	*M5	*M6	*M7	*M8	*M9	*M10	*M11	*M12	*M13	*M14	M15
Th	0.54	0.46	0.55	0.53	0.55	1	4.74	0.91	0.79	0.45	0.39	0.41	0.44	0.38	0.46
U	0.3	0.33	0.3	0.32	0.36	0.44	1.54	0.36	0.57	0.23	0.24	0.26	0.24	0.2	0.23

Wt (ppm)	*F1	*F2	*F3	*F4	*F5	*F6	*F7	*F8	*F9	*F10	*F11	*F12	*F13	*F14	F15
Th	1.75	2.96	1.91	1.76	1.40	1.12	75.2	9.54	44.6	0.85	1.81	1.23	1.19	1.38	1.24
U	0.75	0.83	0.66	0.65	0.5	0.58	13.85	3.29	14.1	0.33	0.76	0.57	0.53	0.59	0.65

*C: Coarse, *M: Medium, *F: Fine

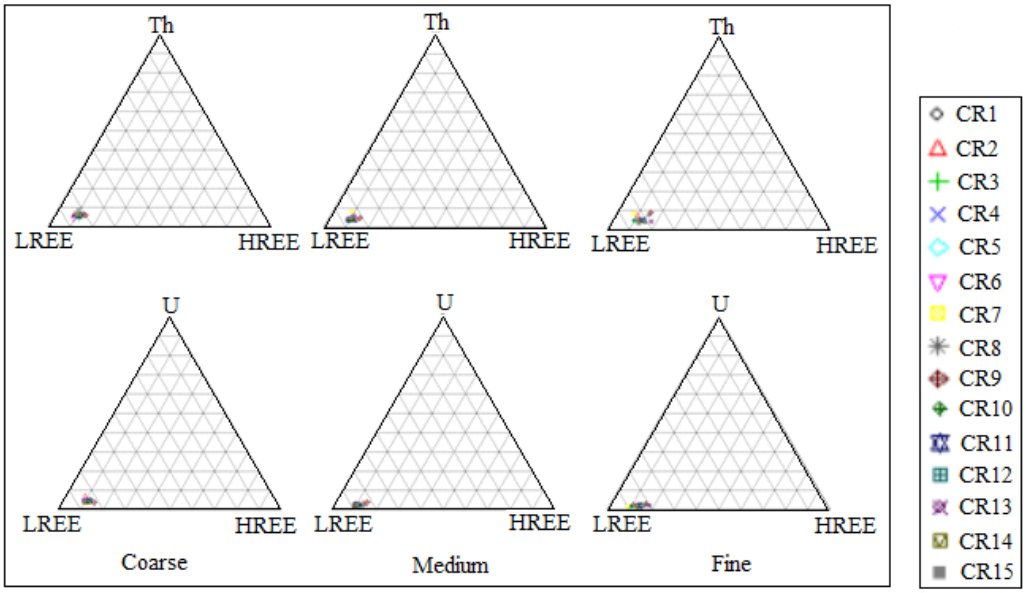

Fig. 4.17: LREE-HREE U, Th ternary diagram for the Central region of Ghana

4.5.2 Elemental Concentration (ppm) of Thorium and Uranium in Beach Sands of the Western Region of Ghana

The beach sands in the Western region were analysed for elemental thorium and uranium concentration of the coarse, medium and fine fractions. The concentration of thorium in the beach sands shown in Table 4.13 ranged as coarse (0.23 to 1.59 ppm); medium (0.32 to 1.48 ppm); and fine (0.98 to 5.52 ppm). The highest concentrations of thorium were found in the beach sands of Axim (1.59 ppm), Sekondi (1.48 ppm) and Shama (5.52 ppm) for coarse, medium and fine fractions. The mean concentrations of thorium along the locations in the Central region were found for the coarse medium and fine fraction as; (0.52 ppm; 0.70 ppm; and 2.10 ppm).

The elemental uranium concentration in the beach sands of the Western region ranged for coarse (0.15 to 0.74 ppm); medium (0.21 to 1.03 ppm); and fine (0.49 to 2.28 ppm). The highest uranium concentrations in the three fractions were found in; Axim (0.74 ppm- coarse); Sekondi (1.03 ppm- medium) and Shama (2.28 ppm- Fine). The mean concentrations of uranium along the locations in the Western region were found for the coarse medium and fine fraction as; (0.36 ppm; 0.44 ppm; and 1.01 ppm).

A ternary diagram of the relation in the coarse, medium and fine fractions vis-à-vis the LREE-Th-HREE and LREE-U-HREE for the Western region are shown in Fig. 4.18. The diagram shows that the LREEs are more associated with uranium and thorium in the beach sands.

Table 4.13: Elemental concentration (ppm) of thorium and uranium in relation to rare earth elements in beach sands of the Western region of Ghana

Wt (ppm)	#C1	#C2	#C3	#C4	#C5	#C6	#C7	#C8	#C9	#C10
Th	0.49	0.43		0.71	0.27	0.23	1.59	0.39	0.27	0.34
U	0.3	0.39		0.56	0.42	0.15	0.74	0.25	0.18	0.23
Wt (ppm)	**#M1**	**#M2**	**#M3**	**#M4**	**#M5**	**#M6**	**#M7**	**#M8**	**#M9**	**#M10**
Th	0.84	0.88	1.48	0.74	0.78	0.36	0.7	0.51	0.35	0.32
U	0.51	0.33	1.03	0.43	0.58	0.21	0.54	0.28	0.23	0.21
Wt (ppm)	**#F1**	**#F2**	**#F3**	**#F4**	**#F5**	**#F6**	**#F7**	**#F8**	**#F9**	**#F10**
Th	5.52	1.97	2.81	0.98	1.02	1.68	1.23	2.11	1.37	2.28
U	2.28	0.68	1.15	0.49	0.77	0.86	0.84	1.25	0.7	1.04

#C: Coarse, **#M:** Medium, **#F:** Fine

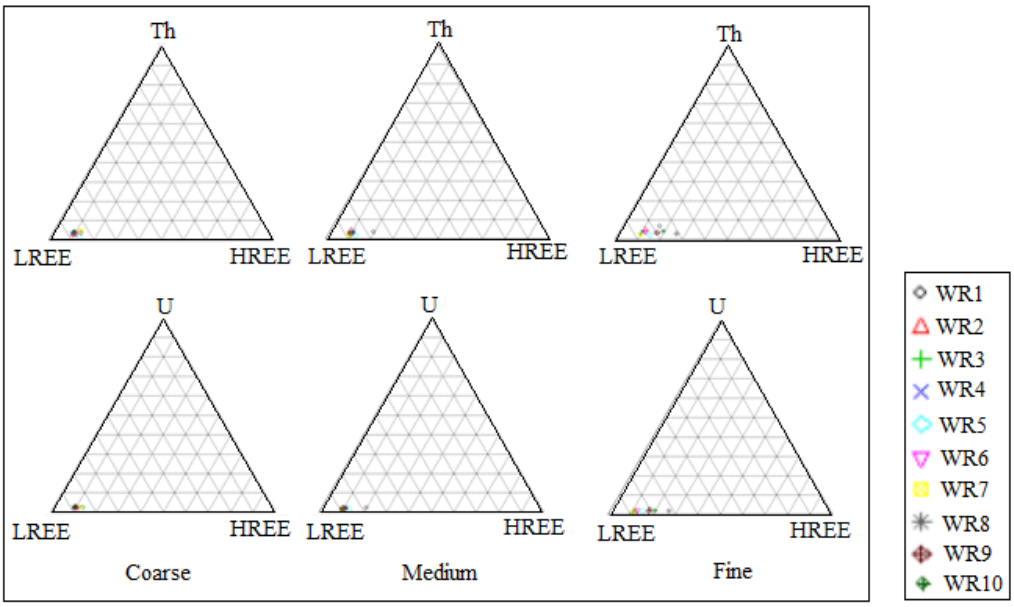

Fig. 4.18: LREE-HREE U, Th ternary diagram for the Western region of Ghana.

4.6 Dendogram Hierarchical Clustering Studies of the Rare Earth Elements in Beach Sands of the Central and Western Regions of Ghana

4.6.1 Hierarchical Clustering of REEs in Beach Sands of the Central Region

The results obtained from the concentration of the REES as discussed earlier gives a broad classification of the REEs in their individual environment. Although sampling was conducted along the coast, the information associated with the proximity of the REEs viz-a- viz their location is crucial in elucidating locations that share similar properties in their REEs. Statistical package for social scientist version 16.0 was used in the analysis of the Dendogram. Fig. 4.19a shows the dendogram of the REEs in coarse fraction of the beach sands.

The coarse fraction dendogram of REEs in the 15 locations along the beach sand of the Central region shown in Fig. 4.19a clusters into 3 sub-groups (CRC6, CRC13, CRC2; CRC3, CRC5, CRC9), (CRC11, CRC14, CRC1, CRC10, CRC12, CRC8, CRC15) and (CRC4, CRC7). This suggests similarity in the concentrations of the REEs in the major clusters.

Since the concentration of the REEs increases with decrease in particle size, the dendogram information from the medium sands is expected to give a clearer picture of the associative environments of the REEs in the beach sands. Fig. 4.19b shows the dendogram information in the medium sands of the Central region. CRM 7 which is sand collected from Dago comes out as an outlier in the medium fraction cluster analysis. The REEs from (CR4, CR5, CR6, CR9) shows similarity in the concentration of their REEs. Hence the rest of the locations share common association in their REE concentration for the medium sands in the Central region. The clusters in

the fine sands (Fig. 4.19c) of the Central region are broadly grouped into two clusters, while CR7 and CR9 show similarity in REE concentration.

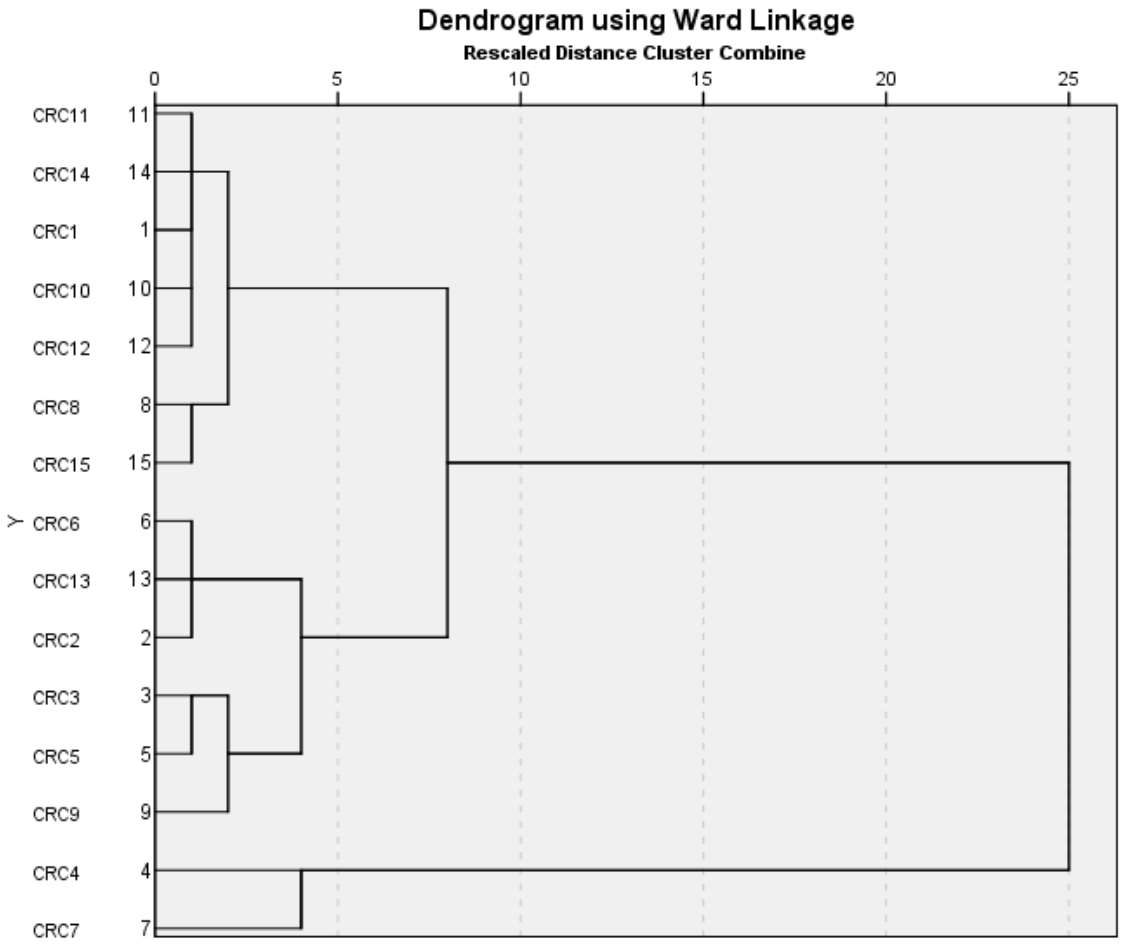

Fig. 4.19a: Hierarchical Clustering Studies of REEs and Y in coarse fraction beach sands of the Central region of Ghana.

CR1= Gomoa Fetteh; **CR2**= Senya Beraku; **CR3**= Winneba; **CR4**= Mankwadze; **CR5**=Apam; **CR6**=Mumford; **CR7**=Dago; **CR8**= Akra; **CR9**=Ekumpoano; **CR10**=Edumafa; **CR11**=Anomabu; **CR12**=Cape Coast; **CR13**=Elmina; **CR14**=Dutch Komenda; **CR15**=Kafodzizi

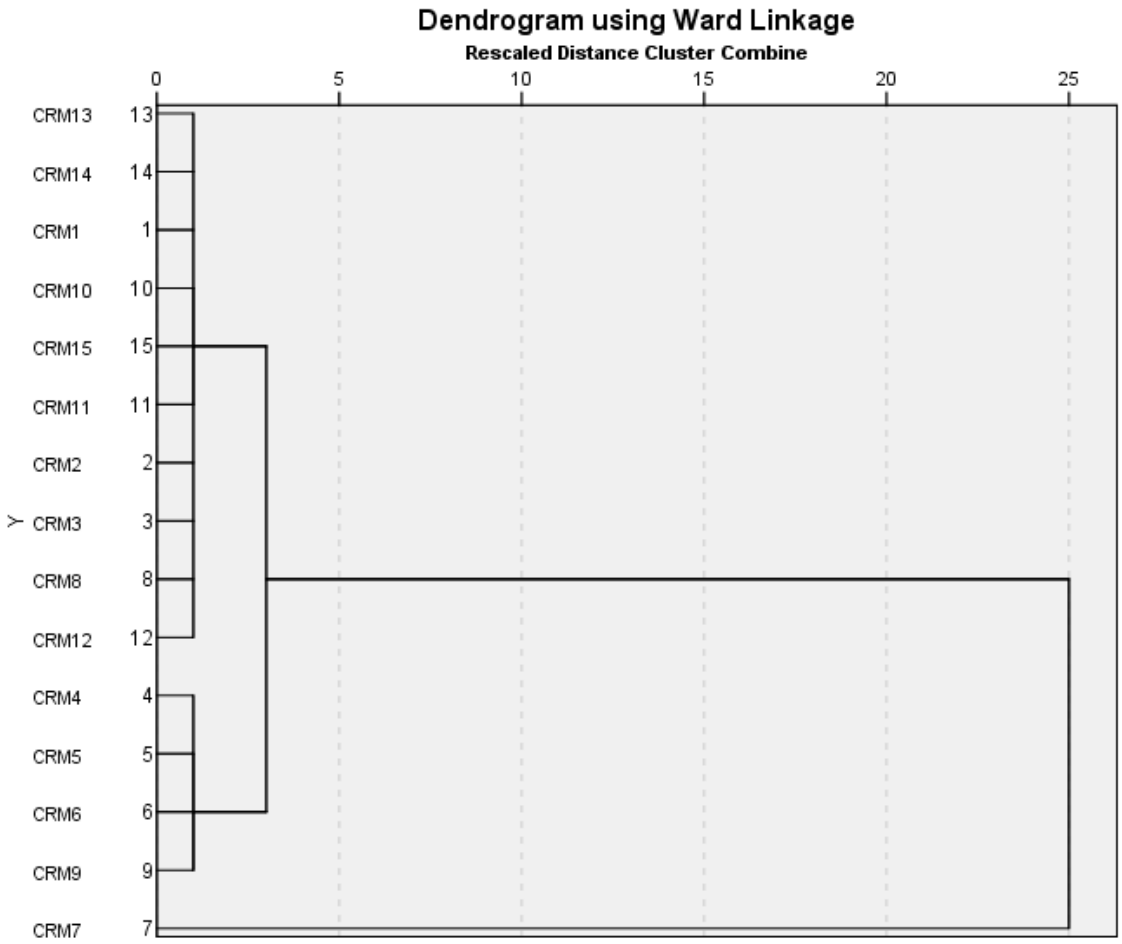

Fig. 4.19b: Hierarchical Clustering Studies of REEs and Y in medium fraction beach sands in the Central region of Ghana.

CR1= Gomoa Fetteh; **CR2**= Senya Beraku; **CR3**= Winneba; **CR4**= Mankwadze; **CR5**=Apam; **CR6**=Mumford; **CR7**=Dago; **CR8**= Akra; **CR9**=Ekumpoano; **CR10**=Edumafa; **CR11**=Anomabu; **CR12**=Cape Coast; **CR13**=Elmina; **CR14**=Dutch Komenda; **CR15**=Kafodzizi

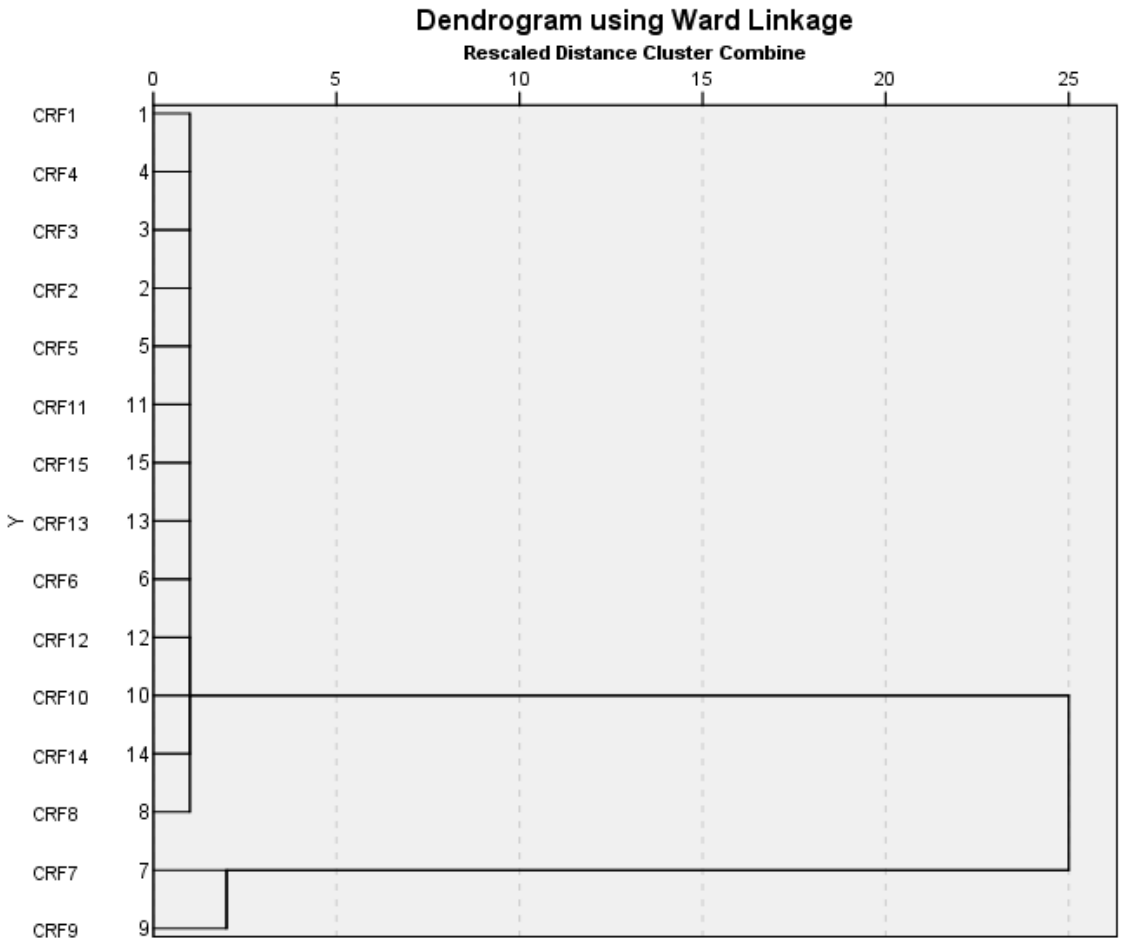

Fig. 4.19c: Hierarchical Clustering Studies of REEs and Y in fine fraction beach sands of the Central region of Ghana.

CR1= Fetteh; **CR2**= Senya; **CR3**= Winneba; **CR4**= Mankwadze; **CR5**=Apam; **CR6**=Mumford; **CR7**=Dago; **CR8**= Akra; **CR9**=Ekumpoano; **CR10**=Edumafa; **CR11**=Anomabu; **CR12**=Cape Coast; **CR13**=Elmina; **CR14**=Dutch Komenda; **CR15**=Kafodzizi

4.6.2 Hierarchical Clustering of REEs in Beach Sands of the Western Region of Ghana

The clustering of the REEs in the Western region was considered based on the coarse, medium and fine fractions. The dendogram information obtained for the coarse fraction of beach sands in the Western region shows WRC7 as an outlier (Fig. 4.20a). This suggests that the concentration of the REEs in the WRC7 location differs from the other two major clusters.

The increase in concentration of the REEs from the Coarse, to medium implies affects the dendogram outcome for the medium sands as shown in Fig. 4.20b. The medium sands are ordered into two main clusters which suggest that REE concentrations in locations WR5, WR7 and WR1 share similar characteristic in their REE concentrations.

The Dendogram output for the fine sands in the Western region (Fig. 4.20c) shows a group cluster of WRF1, WRF8 and WRF3. The geology of the various sampling location is believed to have an influence on the concentrations of the REEs in the different beach sand fractions from both the Central and Western region.

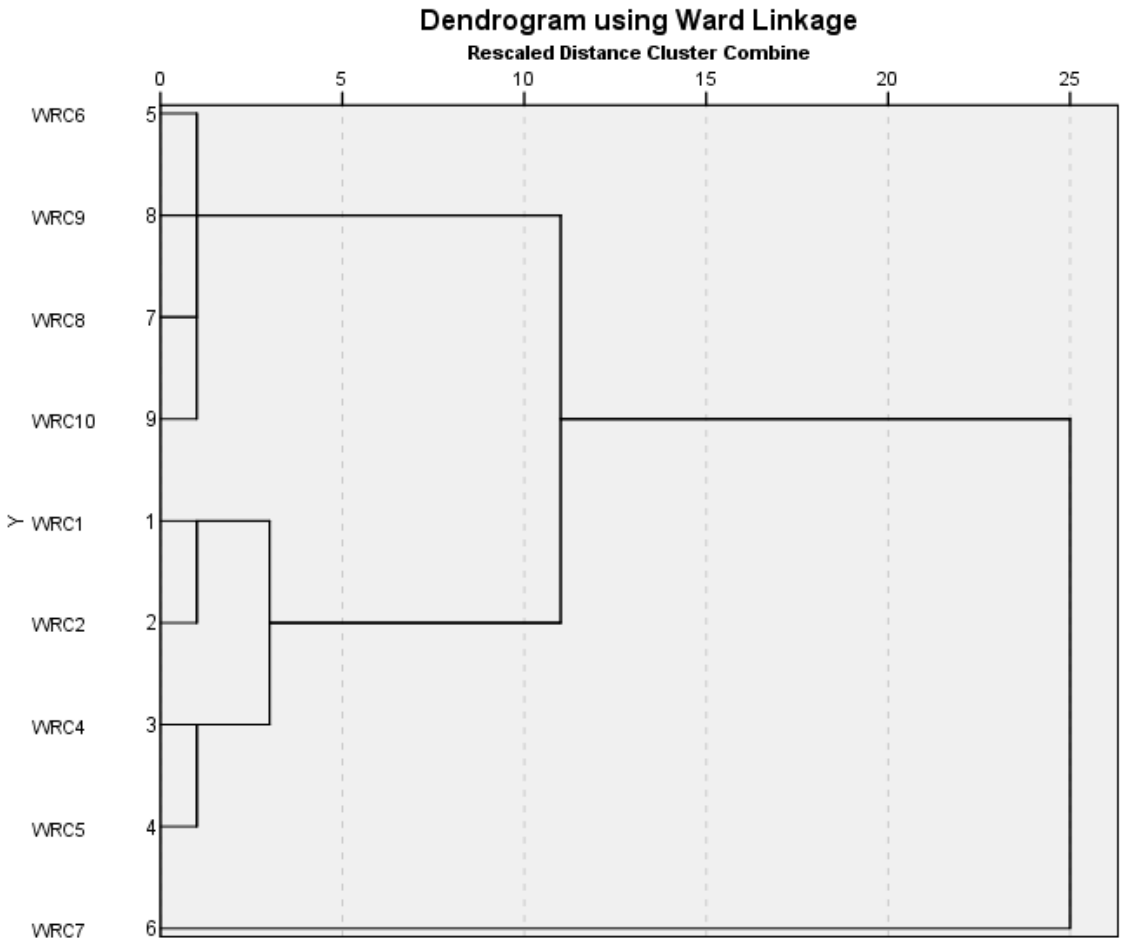

Fig. 4.20a: Hierarchical Clustering Studies of REEs and Y in coarse fraction beach sands of the Western region of Ghana.

WR1= Shama; **WR2**= Abuesi; **WR3**= Sekondi; **WR4**= Takoradi; **WR5**=Cape Three Point; **WR6**= Egyembra; **WR7**=Axim; **WR8**= Esiama; **WR9**= Sanzule; **WR10**=Atuabo

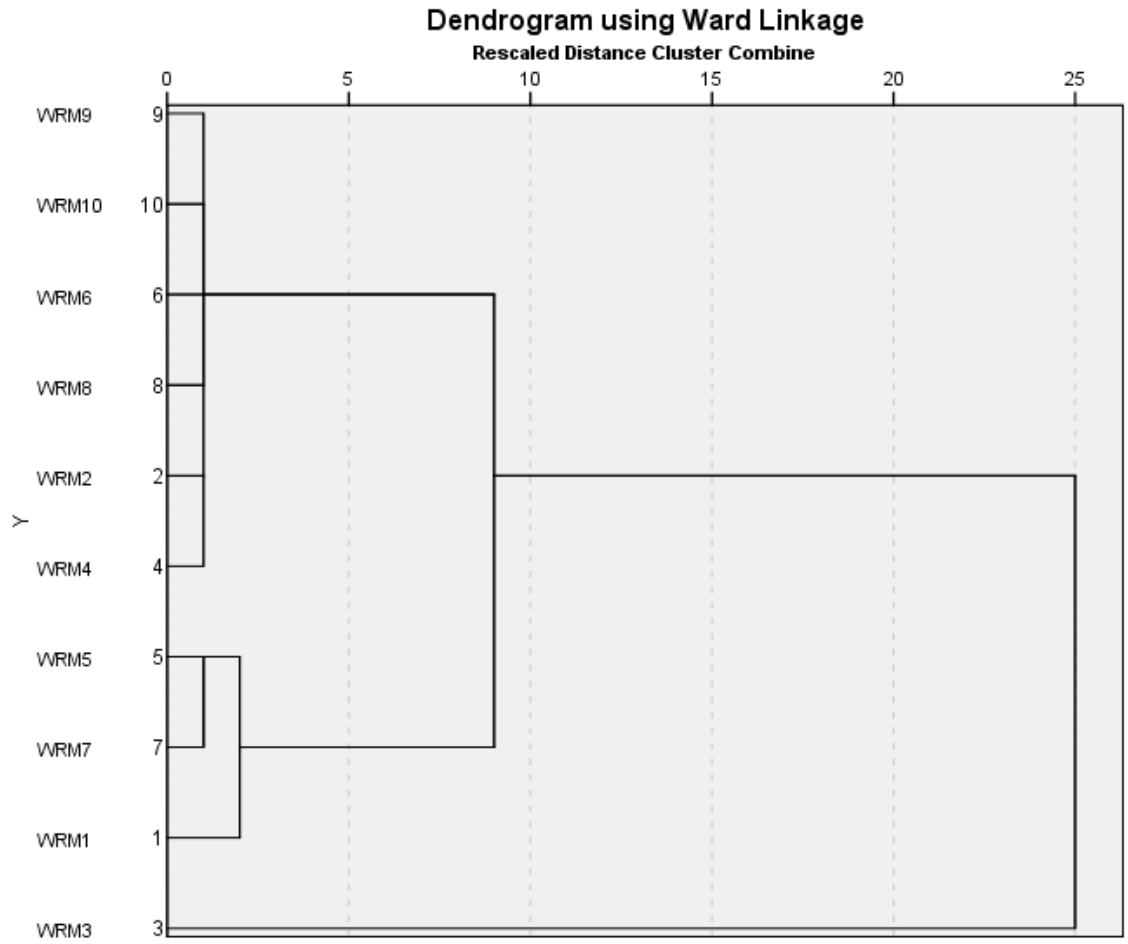

Fig. 4.20b: Hierarchical Clustering Studies of REEs and Y in medium fraction beach sands of the Western region of Ghana.

WR1= Shama; **WR2**= Abuesi; **WR3**= Sekondi; **WR4**= Takoradi; **WR5**=Cape Three Point; **WR6**= Egyembra; **WR7**=Axim; **WR8**= Esiama; **WR9**= Sanzule; **WR10**=Atuabo

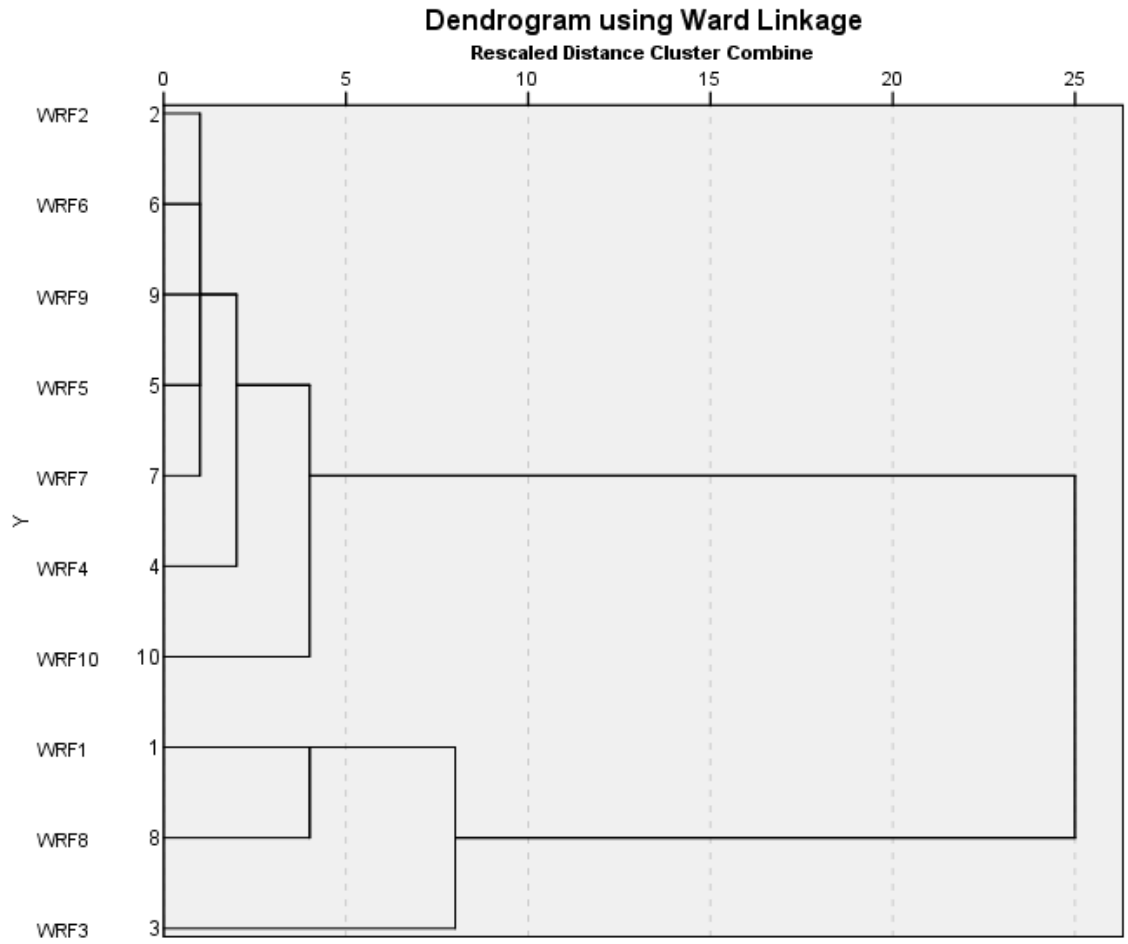

Fig. 4.20c: Hierarchical Clustering Studies of REEs and Y in fine fraction beach sands of the Western region of Ghana.

WR1= Shama; **WR2**= Abuesi; **WR3**= Sekondi; **WR4**= Takoradi; **WR5**=Cape Three Points; **WR6**= Egyembra; **WR7**=Axim; **WR8**= Esiama; **WR9**= Sanzule; **WR10**=Atuabo

4.7 Geospatial Elucidation of the REEs in the Coastal Environment

The observations in the Dendogram analysis of the REEs in the coastal environment show the close association of REEs in specific locations. However, the reasons why extremely high concentration of REEs were observed in the beach sands of Dago (CR7), Akra (CR8) and Ekumpoano (CR9) could not be well explained despite the fact that the locations were along the same terrain along the coast of the Central region.

Probing further into the use of geospatial analysis of the locations, a three dimensional (3D) visualization using ArcScene® gives a clear visual perspective of the nature of the geological environment where the REEs occur in the Central and Western region. Fig. 4.21a,b; and Fig. 4.22a,b show the 3D representation of the data set from the locations where the samples were picked from in the Central region.

Digital elevation models and raster data were generated from the United States Geological Survey (USGS) database. The Central and Western region data shape files and geology data were obtained from the Remote Sensing and Geographic Information System (RS/GIS). The locations identified in the Central and Western region gives information about the geology of the different sample location.

Tables 4.14 and 4.15 shows a summary statistics of the REEs in the Central and Western region. The observations in the changes in the REEs concentration while traversing from CR7, CR8 and CR9 suggests a geological complexity.

Table 4.14: Summary statistics of the REEs in the Central region of Ghana

Coarse	CR1	CR2	CR3	CR4	CR5	CR6	CR7	CR8	CR9	CR10	CR11	CR12	CR13	CR14	CR15
∑LREE	5.79	7.12	6.27	9.34	8.05	7.81	11.77	5.71	6.45	6.17	5.56	5.7	7.25	5.68	5.68
∑HREE	0.68	0.72	0.89	1.20	1.04	0.86	1.53	0.64	1.11	0.67	0.79	0.68	0.76	0.77	0.65
∑REE	6.47	7.84	7.16	10.54	9.09	8.67	13.3	6.35	7.56	6.84	6.35	6.38	8.01	6.45	6.33
∑(Y+HREE)	1.68	1.72	2.29	3.00	2.64	2.16	3.63	1.44	1.55	1.77	1.79	1.58	1.76	1.67	1.55
∑(Y+REE)	7.47	8.84	8.56	12.34	10.69	9.97	15.4	7.15	9.16	7.94	7.35	7.28	9.01	7.35	7.23
%LREE	5.55	6.82	6.01	8.95	7.71	7.48	11.28	5.47	6.18	5.91	5.33	5.46	6.95	5.44	5.44
%HREE	5.23	5.54	6.85	9.24	8.01	6.62	11.78	4.93	8.55	5.16	6.08	5.23	5.85	5.93	5.00
%YHREE	5.35	5.48	7.30	9.56	8.41	6.88	11.56	4.59	8.63	5.64	5.70	5.03	5.61	5.32	4.94
%YTREE	5.50	6.51	6.31	9.09	7.88	7.34	11.35	5.27	6.75	5.85	5.41	5.36	6.64	5.41	5.33
Medium															
∑LREE	8.68	9.24	11.84	11.56	14.27	15.72	48.13	11.93	12.66	8.58	7.72	9.54	10.05	8.68	8.22
∑HREE	1.10	1.39	1.25	1.56	1.57	1.99	5.02	1.49	2.17	1.12	0.84	1.39	1.01	0.99	0.96
∑REE	9.87	10.63	13.09	13.12	15.84	17.71	53.15	13.42	14.83	9.70	8.56	10.93	11.06	9.67	9.18
∑(Y+HREE)	2.60	3.49	3.05	3.76	3.77	4.89	11.32	3.59	5.57	2.82	1.94	3.49	2.21	2.29	2.26
∑(Y+REE)	11.28	12.73	14.89	15.32	18.04	20.61	59.45	15.52	18.23	11.40	9.66	13.03	12.26	10.97	10.48
%LREE	4.41	4.69	6.02	5.87	7.25	7.99	24.45	6.06	6.43	4.36	3.92	4.85	5.11	4.41	4.18
%HREE	4.61	5.83	5.24	6.54	6.58	8.34	21.05	6.25	9.10	4.70	3.52	5.83	4.23	4.15	4.03
%YHREE	4.56	6.12	5.35	6.59	6.61	8.57	19.84	6.29	9.76	4.94	3.40	6.12	3.87	4.01	3.96
%YTREE	4.44	5.01	5.87	6.03	7.11	8.12	23.42	6.11	7.18	4.49	3.81	5.13	4.83	4.32	4.13
Fine															
∑LREE	27.11	32.83	30.89	26.08	27.96	19.77	727.56	96.57	375.78	14.98	30.01	20.22	21.33	31.02	24.85
∑HREE	3.74	3.94	3.79	4.21	3.33	2.80	67.45	18.25	74.53	1.69	5.08	3.14	4.81	4.55	4.64
∑REE	30.85	36.77	34.68	30.29	31.29	22.57	795.01	114.82	450.31	16.67	35.09	23.36	26.14	35.57	29.49
∑(Y+HREE)	9.04	9.64	8.99	10.11	8.03	6.60	157.15	47.85	199.53	3.99	13.18	7.44	12.91	10.75	11.14
∑(Y+REE)	36.15	42.47	39.88	36.19	35.99	26.37	884.71	144.42	575.31	18.97	43.19	27.66	34.24	41.77	35.99
%LREE	1.80	2.18	2.05	1.73	1.86	1.31	48.28	6.41	24.94	0.99	1.99	1.34	1.42	2.06	1.65
%HREE	1.82	1.91	1.84	2.04	1.62	1.36	32.75	8.86	36.19	0.82	2.47	1.52	2.34	2.21	2.25
%YHREE	1.75	1.87	1.74	1.96	1.56	1.28	30.43	9.27	38.64	0.77	2.55	1.44	2.50	2.08	2.16
%YTREE	1.79	2.10	1.97	1.79	1.78	1.30	43.73	7.14	28.43	0.94	2.13	1.37	1.69	2.06	1.78

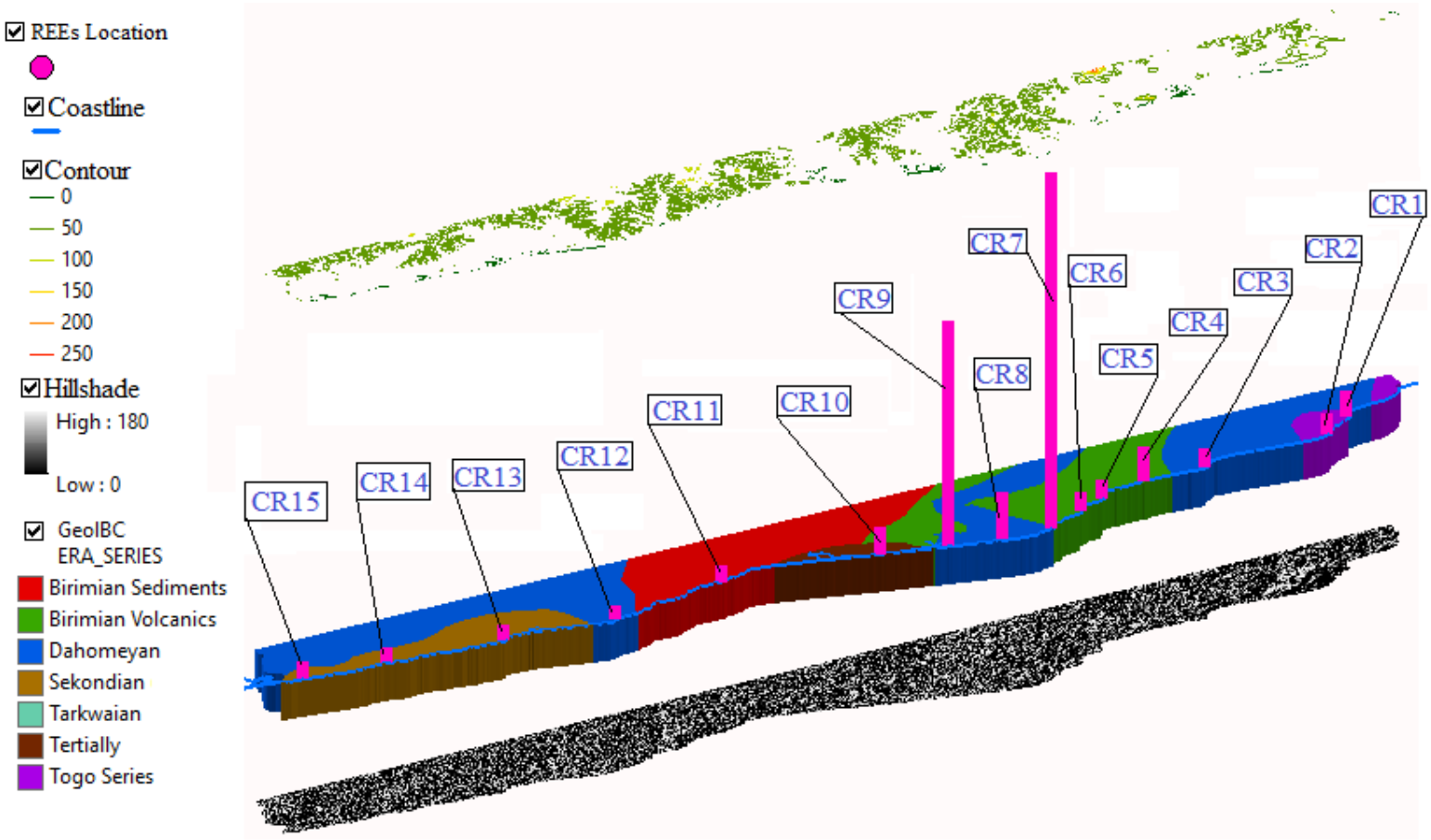

CR1= Gomoa Fetteh; **CR2**= Senya Beraku; **CR3**= Winneba; **CR4**= Mankwadze; **CR5**=Apam; **CR6**=Mumford; **CR7**=Dago; **CR8**= Akra; **CR9**=Ekumpoano; **CR10**=Edumafa; **CR11**=Anomabu; **CR12**=Cape Coast; **CR13**=Elmina; **CR14**=Dutch Komenda; **CR15**=Kafodzizi

Fig. 4.21a: Geospatial representation of the geology in the Central region

Observations from the Geospatial representation of the sampling locations show that CR7 and CR9 occur on the boundary geology between the Dahomeyan and the Birimian Volcanics, While CR8 occurs on the Dahomeyan. A comparison of CR3, CR8 and CR12 which lies on the Dahomeyan shows slight similarity in their REE concentration. Fig. 4.21b shows Wacke sediment shown in the geospatial representation of the beach sands of Dago, this also reflects in the beach sands of Ekumpoano. This suggest probable geologic fault within the area of REE prominence. The detrital sediments of the Akra beach sands are mostly sandstone and conglomerates. The tendency of the material transport from the beach sand of Dago where we have high concentration of REEs to Akra and Ekumpoano is possible, but must be investigated further.

The beach sands of Sekondi which has characteristics property of granitoids shows promising potential for HREEs (Fig. 4.22b; Table 4.15). Tables 4.14 and 4.15 shows the summary statistics of the YREEs in the Central and Western region. Corresponding pie chart representation shown in Appendix D and F provides better elucidation of the YREEs in the beach sands of the Central and Western region of Ghana. The beach sands of Shama, Esiama and Atuabo show relatively high percentage of YHREE which are critical for high power magnets in wind mills and motors.

A spline linkage of the REEs geospatial distribution along the Western region and Central regions shows a bell-shaped curve in areas of high REE concentrations (Fig 4.23).

Table 4.15: Summary statistics of the REEs in the Western region of Ghana

Coarse	WR1	WR2	WR3	WR4	WR5	WR6	WR7	WR8	WR9	WR10
∑LREE	10.61	12.77		19.00	14.01	5.07	26.08	7.98	6.39	6.80
∑HREE	1.59	1.40		1.88	2.10	0.62	3.70	0.86	0.69	0.71
∑REE	12.20	14.17		20.88	16.11	5.69	29.78	8.84	7.08	7.51
∑(Y+HREE)	3.99	3.50		4.58	5.90	1.52	9.4	1.96	1.69	1.61
∑(Y+REE)	14.60	16.27		23.58	19.91	6.59	35.48	9.94	8.08	8.41
%LREE	9.76	11.75		17.48	12.89	4.66	23.99	7.34	5.88	6.26
%HREE	11.73	10.33		13.87	15.50	4.58	27.31	6.35	5.09	5.24
%YHREE	11.68	10.25		13.41	17.28	4.45	27.53	5.74	4.95	4.71
%YTREE	10.22	11.39		16.51	13.94	4.61	24.84	6.96	5.66	5.89
Medium										
∑LREE	16.31	17.04	76.80	15.41	35.47	11.81	32.79	14.06	9.72	8.47
∑HREE	4.11	1.82	8.78	1.84	5.17	1.38	3.44	1.47	1.04	1.04
∑REE	20.42	18.86	85.58	16.98	40.64	13.19	36.23	15.53	10.76	9.51
∑(Y+HREE)	10.81	4.62	22.68	4.74	13.97	3.58	8.54	3.67	2.34	2.64
∑(Y+REE)	27.12	21.66	99.48	19.88	49.44	15.39	41.33	17.73	12.06	11.11
%LREE	6.86	7.17	32.32	6.37	14.93	4.97	13.80	5.92	4.09	3.56
%HREE	13.66	6.05	29.18	6.11	17.18	4.59	11.43	4.89	3.46	3.46
%YHREE	13.93	5.95	29.23	6.11	18.00	4.61	11.01	4.73	3.02	3.40
%YTREE	8.60	6.87	31.56	6.31	15.69	4.88	13.11	5.63	3.83	3.52
Fine										
∑LREE	61.56	33.44	77.46	21.6	37.44	34.81	42.06	48.62	31.62	40.53
∑HREE	13.16	4.33	8.82	2.70	6.54	4.76	4.96	17.63	6.73	10.26
∑REE	74.72	37.77	86.28	24.3	43.98	39.57	47.02	66.25	38.35	50.79
∑(Y+HREE)	35.96	10.43	21.62	6.80	17.04	12.06	12.26	51.93	19.33	29.06
∑(Y+REE)	97.52	43.87	99.08	28.4	54.48	46.87	54.32	100.55	50.95	69.59
%LREE	14.34	7.79	18.05	5.03	8.72	8.11	9.80	11.33	7.37	9.44
%HREE	16.47	5.42	11.04	3.38	8.19	5.96	6.21	22.07	8.42	12.84
%YHREE	16.61	4.82	9.99	3.14	7.87	5.57	5.66	23.99	8.93	13.42
%YTREE	15.10	6.79	15.35	4.40	8.44	7.26	8.41	15.57	7.89	10.78

WR1= Shama; **WR2**= Abuesi; **WR3**= Sekondi; **WR4**= Takoradi; **WR5**=Cape Three Points; **WR6**= Egyembra; **WR7**=Axim; **WR8**= Esiama; **WR9**= Sanzule; **WR10**=Atuabo

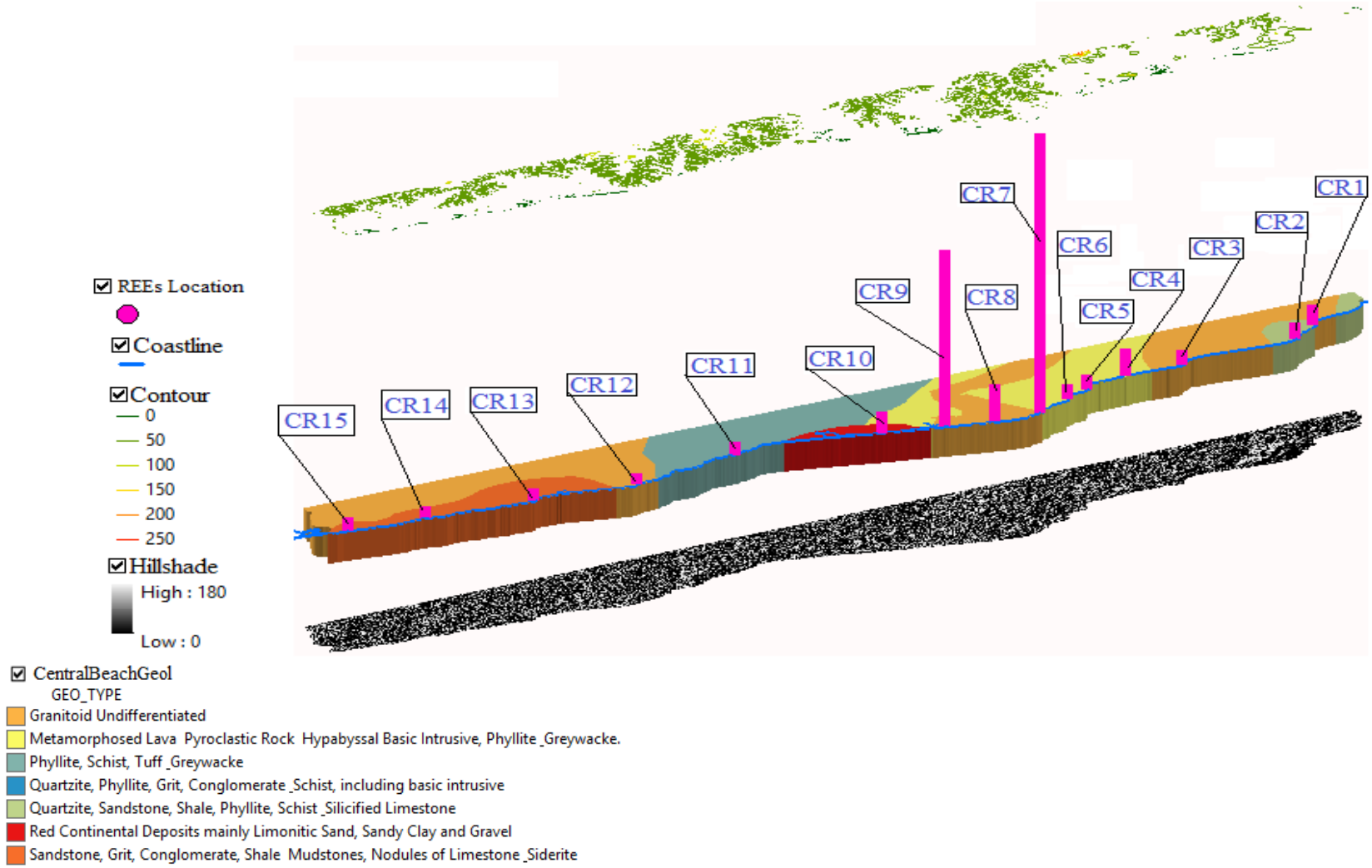

CR1= Gomoa Fetteh; **CR2**= Senya Beraku; **CR3**= Winneba; **CR4**= Mankwadze; **CR5**=Apam; **CR6**=Mumford; **CR7**=Dago; **CR8**= Akra; **CR9**=Ekumpoano; **CR10**=Edumafa; **CR11**=Anomabu: **CR12**=Cape Coast: **CR13**=Elmina: **CR14**=Dutch Komenda: **CR15**=Kafodzizi

Fig. 4.21b: Geospatial representation of the geology in the Central region.

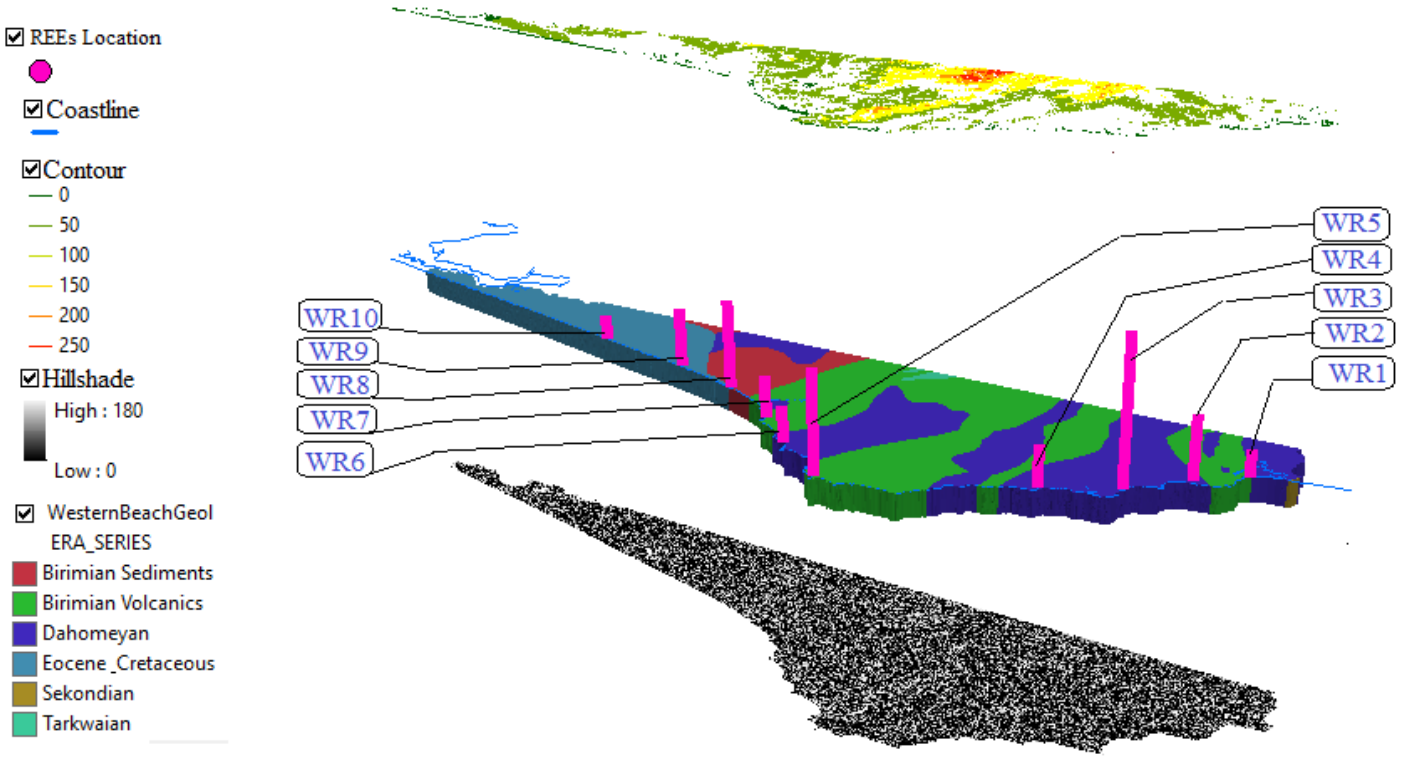

WR1= Shama; **WR2**= Abuesi; **WR3**= Sekondi; **WR4**= Takoradi; **WR5**=Cape Three Points; **WR6**= Egyembra; **WR7**=Axim; **WR8**= Esiama; **WR9**= Sanzule; **WR10**=Atuabo

Fig. 4.22a: Geospatial representation of the geology in the Western region of Ghana.

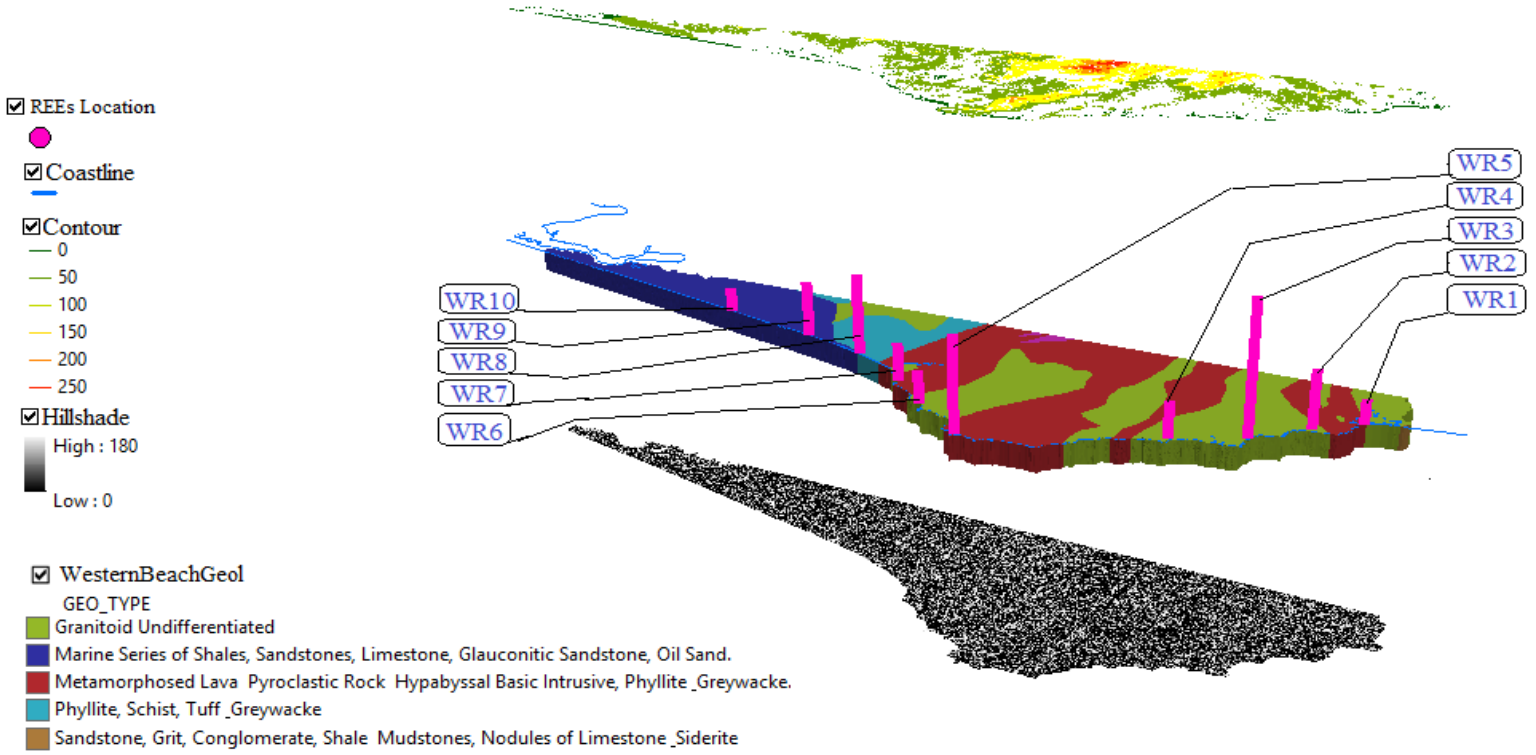

WR1= Shama; **WR2**= Abuesi; **WR3**= Sekondi; **WR4**= Takoradi; **WR5**=Cape Three Points; **WR6**= Egyembra; **WR7**=Axim; **WR8**= Esiama; **WR9**= Sanzule; **WR10**=Atuabo

Fig. 4.22b: Geospatial representation of the geology in the Western region of Ghana.

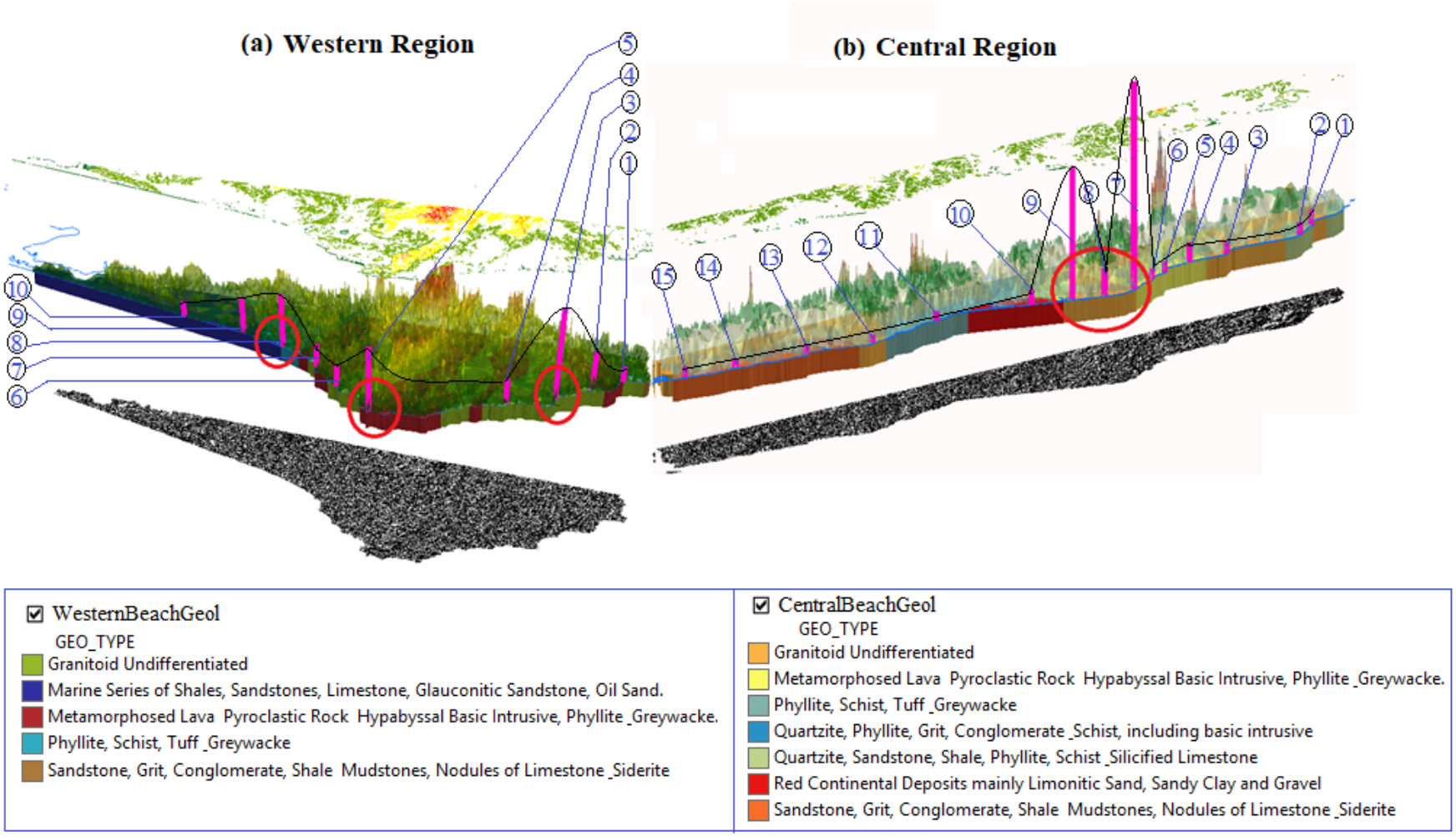

WR1= Shama; **WR2**= Abuesi; **WR3**= Sekondi; **WR4**= Takoradi; **WR5**=Cape Three Points; **WR6**= Egyembra; **WR7**=Axim; **WR8**= Esiama; **WR9**= Sanzule; **WR10**=Atuabo
CR1= Gomoa Fetteh; **CR2**= Senya Beraku; **CR3**= Winneba; **CR4**= Mankwadze; **CR5**=Apam; **CR6**=Mumford; **CR7**=Dago; **CR8**= Akra; **CR9**=Ekumpoano; **CR10**=Edumafa;
CR11=Anomabu; **CR12**=Cape Coast; **CR13**=Elmina; **CR14**=Dutch Komenda; **CR15**=Kafodzizi

Fig. 4.23: Interconnecting spline linkage of REE geospatial distribution pattern in the; **(a)** Western and **(b)** Central regions of Ghana.

4.8 Rare Earth Elements Separation in Selected Beach Sands

The sample decomposition using lithium metaborate fusion showed inconsistencies during the separation process. The blockage of the resin was conspicuous and this increased the amount of acid volume required during the experiment (Pin & Zalduegui, 1997). This is basically due to the large amount of flux required for complete fusion of the sample. The use of hydrofluoric acid and nitric acid served as an alternative during the digestion process. Reduction of iron was achieved using ascorbic acid, which aids the sorption of iron on the TBP-CMPO and efficient release of the rare earth elements (Pin & Zalduegui, 1997).

Higher concentration of HNO_3 is responsible for reduced recoveries of LREEs in the separation process; hence the use of lower concentration of 1 M HNO_3 in line with studies by Pin et al. (2014). This reduced the extent to which LREEs is lost during the separation process.

The concentrations of the selected separated LREE (Pr, Nd, Sm and Eu) into their different components in Certified Reference Materials; OREAS 460 [carbonatite supergene REE-Nb ore (treo 0.53%)] and AMIS 0185, as well as samples CRF7, CRF8, WR7 and WRF3 are presented in Table 4.16. Values obtained after the chemical separation were relatively close to the initial concentrations of the selected REEs.

Table 4.16: Data for Pr, Nd, Sm and Eu concentration (ppm) after chemical separation

Sample	Pr	Nd	Sm	Eu
OREAS 460	244±8[a]	781±47[a]	107±3[a]	22.7±0.96[a]
a	235.04	740.23	100.03	20.04
b	235.00	743.22	100.01	20.02
c	236.01	747.31	100.09	20.15
AMIS 0185	3471±343[b]	9238±1033[b]	556±48[b]	94.2±12.1[b]
a	3420	8040.23	550.35	90.32
b	3460	8043.55	543.24	92.14
c	3432	8033.34	543.30	90.12
CRF7	2.52	9.14	1.83	0.14
a	2.50	9.34	1.85	0.10
b	2.51	9.30	1.82	0.12
CRF8	0.65	2.34	0.49	0.09
a	0.63	2.32	0.44	0.06
b	0.68	2.35	0.47	0.05
WRF3	4.43	17.45	3.44	0.79
a	4.40	17.40	3.42	0.75
b	4.10	17.42	3.38	0.73
WRF7	2.32	8.90	1.81	0.43
a	2.37	8.51	1.88	0.42
b	2.35	8.36	1.84	0.45

[a]Origin of Standard**:** Certified Reference Material, Oreas 460 [carbonatite supergene REE-Nb ore (treo 0.53%)]

[b]AMIS0185: Wigu Carbonatite Complex, Tanzania.

CHAPTER FIVE

CONCLUSIONS AND RECOMMENDATIONS

5.1 Conclusions

5.1.1 Radioactivity Distribution Assessment (NORMS)

Assessment of gamma spectrometry data of the beach sands in the Central and Western regions of Ghana showed variation in the activity concentrations of the beach sands *vis-à-vis* their respective locations. The average concentrations of ^{238}U, ^{232}Th and ^{40}K found in the beach sands of the Central and Western regions of Ghana were found to contain permissible levels of radionuclides with mean activity occurring in the range 1.3 ± 0.47 to 31.50± 3.31 Bq/Kg (^{238}U)**;** 0.7± 0.04 to 71.70± 4.55 Bq/Kg (^{232}Th)**;** 73.9± 6.72 to 1775.5± 28.35 (^{40}K) for the Central region. The Western region ranged as 1.0 ± 0.03 to 5.6± 0.24 Bq/Kg (^{238}U)**;** 0.8± 0.04 to 3.8± 0.14 Bq/Kg (^{232}Th); and 18.6± 0.23 to 343.2± 18.35 (^{40}K).

Dose rate in the Central region ranged between 4.13 to 132.39 (nGy/hr) and 1.78 to 19.32 (nGy/hr) and total average across the two region is 11.40 (nGy/hr).

The annual effective dose in the Central region ranged between 0.0051 to 0.1624 and 0.002 to 0.024 for the Western region and a total average of 0.014 mSv/Yr.

The activity utilization index (AUI) in the Central region ranged between 0.027 to 1.302 and 0.018 to 0.126 for the Western region; and a total average of 0.102.

External radiation hazard indices in the Central region occur in the range 0.022 to 0.731 and 0.010 to 0.101 for the Western region; and a total average of 0.062.

Internal radiation hazard indices in the Central region occur in the range 0.025 to 0.816 and 0.013 to 0.116 in the Western region; and a total average of 0.073.

Representative level index in the Central region beach sands occur in a range of 0.065 to 2.110 and 0.028-0.304 in the Western region. The average activity in the Central region for ^{238}U, ^{232}Th and ^{40}K are 5.18, 6.00 and 206.36 Bq/Kg.

The high radioactivity (Bq/Kg) levels (^{238}U, ^{232}Th, ^{40}K, Ra_{eq}) in the beach sands of Dago (31.5±3.31; 71.7±4.55; 1775.5±28.35; 258.21); Akra (4.1±1.13; 2.0±0.51; 81.6±6.39; 12.66); Ekumpoano (27.2±5.8; 6.2±1.20; 69.7±8.12; 33.67) in the Central region suggests a potential hot zone for radioactive minerals which hold information to potential radioactive minerals.

The high radioactivity (Bq/Kg) in the beach sands of Abuesi (2.5±0.23; 1.8±0.01; 175.1±9.56; 17.30); Sekondi (5.6±0.24; 3.8±0.14; 343.2±18.35; 35.10); Cape Three points (4.0±0.12; 1.5±0.03; 100.5±10.23; 13.16); Esiama (3.5±1.25; 1.5±0.10; 43.7±6.12; 8.78); and Sanzule (2.4±0.25; 0.7±0.02; 34.3±5.36; 5.85) in the Western region suggests potential hot zones for radioactive minerals. The average activity concentration in the Western region for ^{238}U, ^{232}Th and ^{40}K are 2.5, 1.4 and 107 Bq/Kg

Although comparative observation of the radioactivity data from the beach sands of the Central and Western region clearly shows the prominence of ^{238}U, ^{232}Th and ^{40}K in the beach sands of the Central region.; the geology of the locations suggest a greater contributory factor to the levels of thorium and uranium in the beach sand. Thus a fingerprint for potential radioactive minerals has been found.

5.1.2 Rare Earth Elements Fingerprints

Rare earth elements (La, Ce, Pr, Nd, Sm, Eu, Gd, Tb, Dy, Ho, Er, Tm, Yb, Lu and Y) were found in the beach sands of the Western and Central region.

The total rare earth element distribution in the beach sands of the Central region show ranges for coarse fraction (6.33 to 13.30 ppm); medium fraction (8.56 to 53.15 ppm) and fine (16.67 to 795.01 ppm) fraction.

The sum of light rare earth elements (LREE); heavy rare earth (HREE); and ratio of light to heavy rare earth (LREE/HREE) distribution in the Central region ranged from coarse fraction (5.56 to 11.77 ppm; 0.64 to 1.53 ppm; 5.81to 9.89); medium fraction (7.72 to 48.13 pm; 0.84 to 5.02 ppm; 5.83 to 9.95); and fine fraction (14.98 to 727 ppm; 1.69 to 74.53 ppm; 4.43 to 10.79).

The sum of rare earth elements distribution in the beach sands of the Western region for coarse (5.69 to 29.78 ppm); medium (9.51 to 85.58 ppm) and fine (24.3 to 86.28) fraction.

The sum of light rare earth elements (LREE); heavy rare earth (HREE); and ratio of light to heavy rare earth (LREE/HREE) distribution in the Western region ranged from coarse fraction (5.07 to 26.08 ppm; 0.62 to 3.70 ppm; 6.67 to 10.11); medium fraction (8.47 to 76.8 ppm; 1.04 to 8.78 ppm; 3.97 to 9.56) and fine fraction (21.6 to 77.46 ppm; 2.7 to 17.63 ppm; 2.76 to 8.78).

A critical look at the concentrations of the REEs in the coarse, medium and fine fractions showed an increase of REEs from the coarse to medium and fine fraction. The concentrations of REEs in the Beach sands of the Central region showed Dago, Akra and Ekumpoano as potential hotspots with high levels of REEs.

The concentrations of the REEs in the Western region showed the beach sands of Sekondi as potential location for REEs.

5.1.3 Geospatial Observation

The assessment of the geospatial distribution follows a dome-shaped pattern in the Central region; and a wavy pattern in the Western region. Despite the prominence of REE- fingerprints in the beach sands of Dago, Akra and Ekumpoano which are peak points in the Central region, the corresponding increase in radioactivity concentrations in the locations (Dago, Akra and Ekumpoano) beach sands suggest a strong influence of the geology in the elevated concentration observed. The sharp decrease in the concentration of total REEs in the beach sands of Akra shows an anomaly despite the fact that the sampling points are along the same trend. The geospatial observation showed that the sampling location at Dago and Ekumpoano are on probable geological faults and differing geology.

The studies concluded that the radioactivity distribution in the beach sands serves as pathfinders to potential rare earth elements deposits in the Central region. Although heavy REEs are found in relatively higher concentration in the beach sands of the Western regions, the REEs in the fine fractions of the Central region exceeds that of the Western region. Heavy minerals such as Zircon, Rutile and Amphiboles were identified in the beach sand of the Central and Western regions. The minerals found are known to concentrate REEs. This is in agreement with minerals found in similar studies on the beach sands along the Ghana coastline; and are indicative of shore-derived minerals; suggesting mineral sand contribution from inland sources.

The peak areas observed in this study could be pointers to huge deposits of REEs which are of great economic importance to the global technology industry. Thus, the

renewable energy target which relies on selected rare earth elements is achievable if more resources are committed towards potential sources of the REEs in-land.

5.2 Recommendations

(1) Based on the high concentrations obtained from the radioactivity studies in beach sands from Dago, Akra and Ekumpoano, further research should be carried out on the radiological characterization and rare earth elements studies of the in-land soils; hydrogeochemical studies of the groundwater; and characterization of the heavy minerals of the beach rocks at the three towns.

(2) Further studies should be conducted on the beach rocks of Shama, Sekondi, and Esiama for heavy rare earth elements.

(3) There is the need to extend the studies to cover other coastal regions of Ghana.

(4) Further studies should be carried out on the levels of heavy metals on the beach sands along the coast of Ghana, due to the huge tourism potential of the beaches in Ghana.

(5) Research should be conducted on the efficient separation of the light and heavy rare earth elements (LREEs and HREEs) for the development of isotopic signatures for beach sands.

(6) Monitoring of radioactivity levels along the coast of Ghana should be instituted by stakeholder governmental agencies, in view of the relatively high levels of Uranium and Thorium in some sampling locations used for the study.

REFERENCES

ACC. (2014). *The Economic Benefits of the North American Rare Earths Industry*. Retrieved from http://www.rareearthtechalliance.com/Resources/The-Economic-Benefits-of-the-North-American-Rare-Earths-Industry.pdf

Adam Jordens, R. S. S., & Neil A. Rowson, K. E. W. (2014). Processing a rare earth mineral deposit using gravity and magnetic separation. *Minerals Engineering* , *62*, 9–18.

Ahankoub, M., Jamshidi, F., & Sheikhi, R. (2015). Investigated the occurrence of iron ore, magnetite, carbonate sediments in the Oligocene North Bijar(NW of Iran). *Technical Journal of Engineering and Applied Sciences*,5, 172–181.

Akira Koshimoto, Tatsuya Oshima, Keisuke Ohto, and Y. B. (2011a). Synthesis of Phosphonic Acid Extractants and Selective Extraction of In(III) and Ga(III) from Acidic Media Containing Zn(II). *Solvent Extraction Research and Development, Japan*,*18*, 137–147.

Albarede, F. (2011). Lithophile Elements. In *Encyclopedia of Astrobiology* (pp. 931–931). Berlin, Heidelberg: Springer Berlin Heidelberg. http://doi.org/10.1007/978-3-642-11274-4_900

Alcidio Abrao , Antonio Alves de Freitas, F. M. S. de C. (2001). Preparation of highly pure thorium nitrate via thorium sulfate and thorium peroxide. *Journal of Alloys and Compounds*, *323-324*, 53–56.

Alexander Frank Wells. (1975). *Structural Inorganic Chemistry - Alexander Frank Wells - Google Books* (4th ed.). Clarendon Press Oxford.

Ali, S., & H., S. (2014). Social and Environmental Impact of the Rare Earth Industries. *Resources*, *3*(1), 123–134. http://doi.org/10.3390/resources3010123

Allen Alper. (2016). Metals News - Peak Resources (ASX: PEK) Advances Ngualla Rare Earth Deposit toward Production with High Grades and Low Capex in Tanzania. Retrieved June 25, 2017, from http://www.metalsnews.com/

Amekudzie, A., Emi-Reynolds, G., Faanu, A., Darko, E. O., Awudu, A. R., Adukpo, O., Ibrahim, A. (2011). Natural radioactivity concentrations and dose assessment in shore sediments along the coast of greater Accra, Ghana. *World Applied Sciences Journal*, *13*(11), 2338–2343.

Andrej Szytula, J. L. (1994). *Handbook of Crystal Structures and Magnetic Properties of Rare Earth* (1st Ed.). CRC Press Inc. London.

Araque, J. C., Hettige, J. J., & Margulis, C. J. (2015). Modern Room Temperature Ionic Liquids, a Simple Guide to Understanding Their Structure and How It May Relate to Dynamics. *The Journal of Physical Chemistry B*, *119* (40), pp 12727–12740

Armstrong-Altrin, J. S., Lee, Y. Il, Kasper-Zubillaga, J. J., Carranza-Edwards, A., Garcia, D., Eby, G. N., Cruz-Ortiz, N. L. (2012). Geochemistry of beach sands along the western Gulf of Mexico, Mexico: Implication for provenance. *Chemie Der Erde - Geochemistry*, *72*(4), 345–362.

Atanassova, M., & Dukov, I. L. (2006). Solvent extraction and separation of lanthanoids with mixtures of chelating extractant and 1-(2-pyridylazo)-2-naphthol. *Separation and Purification Technology*, *49*(1), 101–105.

Barry C. Moring; Margo I. Toth, Rebecca G. Stoneman, and H. Richard Blank, J. (1988). Mineral Resources of the Clover Mountains Wilderness Study Area, Lincoln; (1st Ed.) *US Geological Survey Bulletin 1728-B*.

Bell, K. (2009). Carbonatite occurrences of the world: map and database, by A. R. Woolley and B. A. Kjarsgaard. *Journal of Petrology*, *50*(1), 195–196. http://doi.org/10.1093/petrology/egn080

Botwe, B. O., Schirone, A., Delbono, I., Barsanti, M., Delfanti, R., Kelderman, P., Lens, P. N. L. (2017). Radioactivity concentrations and their radiological significance in sediments of the Tema Harbour (Greater Accra, Ghana). *Journal of Radiation Research and Applied Sciences*, *10*(1), 63–71. http://doi.org/10.1016/j.jrras.2016.12.002

Braatz, A. D., Antonio, M. R., Nilsson, M., Jestin, J., Pellet-Rostaing, S., Zemb, T., Schlossman, M. L. (2017). Structural study of complexes formed by acidic and neutral organophosphorus reagents. *Dalton Trans.*, *46*(4), 1194–1206. http://doi.org/10.1039/C6DT04305D

Broom-Fendley, S., Brady, A. E., Wall, F., Gunn, G., & Dawes, W. (2017). REE minerals at the Songwe Hill carbonatite, Malawi: HREE-enrichment in late-stage apatite. *Ore Geology Reviews*, *81*, 23–41. http://doi.org/10.1016/j.oregeorev.2016.10.019

Caro, G., Bourdon, B., Halliday, A. N., & Quitt, G. (2008). Super-chondritic Sm/Nd ratios in Mars, the Earth and the Moon. *Nature*, *452*(7185), 336–339. http://doi.org/10.1038/nature06760

CEID, (2015). Centre for Economic Information and Documentation Bucharest. The rare earth economy a new branch of economics; (1st Ed.) Pp.75. CNCSIS: cod 045/2006 Bucureşti, România,

Cerny, P., & Ercit, T. S. (2005). The classification of granitic pegmatites revisited. *The Canadian Mineralogist*, *43*(6), 2005–2026. http://doi.org/10.2113/gscanmin.43.6.2005

Chayavadhanangkul, C., Milaho, H., & Chuoykaew, P. (2009). The alkaline digestion of monazite. *Conference on Nuclear Science and Technology; Bangkok (Thailand); 2-3 Jul* .

Cherniak, D. J. (2010). Diffusion in Accessory Minerals: Zircon, Titanite, Apatite, Monazite and Xenotime. *Reviews in Mineralogy and Geochemistry, 72*(1) :827-869.

CISCAG; Cornwall and Isles of Scilly Coastal Advisory Group. (2011). *Cornwall and Isles of Scilly SMP2 Review of Coastal Processes and Geomorphology*. Isles of Scilly. Technical report Bodmin/303478 (1st Ed), Cornwall Council, UK.

Clark, A. M. (1983) "Mineralogy of the rare earth elements," in *Rare Earth Element Geochemistry*, P. Henderson, Ed., pp. 33–54, Elsevier Science, New York, NY, USA.

Clifford Frondel. (1958). *Systematic Mineralogy of Uranium and Thorium - Clifford Frondel - Geological Survey Bulletin 1064*. US Government Printing Office.

Conafric. (2000). Ghana: we mean business; Business and Economics (1st Ed) Conafric Ghana Ltd.

Dampare, S. B., Asiedu, D. K., Osae, S., Nyarko, B. J. B., & Banoeng-Yakubo, B. (2005). Determination of rare earth elements by neutron activation analysis in altered ultramafic rocks from the Akwatia District of the Birim diamondiferous field, Ghana. *Journal of Radioanalytical and Nuclear Chemistry, 265*(1), 101–106. http://doi.org/10.1007/s10967-005-0801-y

Deb, M and Sarkar, S.C. (2017). How Do Mineral Deposits Form and Transform? A Systematic Approach. In *Minerals and Allied Natural Resources and their Sustainable Development*. Springer Geology. http://doi.org/10.1007/978-981-10-4564-6_2

Debashish Sengupta. (2016). Chapter 4- Placer-Type Rare Earth Element Deposits, In book: *Reviews in Economic Geology*, (1st Ed), 18, pp.81-100 Society of Economic Geologists

Dickson, K. B. (1969). *A historical geography of Ghana*. Cambridge University Press.

Dill, H. G. (2010). The "chessboard" classification scheme of mineral deposits: Mineralogy and geology from aluminum to zirconium. *Earth-Science Reviews, 100*(1-4), 1–420. http://doi.org/10.1016/j.earscirev.2009.10.011

Don L. Anderson. (2007). *New Theory of the Earth - Don L. Anderson - Google Books* (1st Ed). California: Cambridge University Press.

Dorenbos .P. (2000). The 5d level positions of the trivalent lanthanides in inorganic compounds. *Journal of Luminescence, 91*, 155–176.

Dulski, T. R. (1999). *Trace elemental analysis of metals : methods and techniques*. M(1stEd). Marcel Dekker Inc. New York USA.

Edwards, R., & Atkinson, K. (1986). The design and implementation of exploration programmes. In *Ore Deposit Geology and its Influence on Mineral Exploration*(pp. 400–425). Dordrecht: Springer Netherlands. http://doi.org/10.1007/978-94-011-8056-6_11

Esro, M., Mazzocco, R., Vourlias, G., Kolosov, O., Krier, A., Milne, W. I., & Adamopoulos, G. (2015). Solution processed lanthanum aluminate gate dielectrics for use in metal oxide-based thin film transistors. *Applied Physics Letters*, *106*(20), 203507. http://doi.org/10.1063/1.4921262

Fabian Cassan (2013). *Rocks and minerals.* Encyclopaedia Britannica, inc. Encyclopaedia Britannica, Inc. 101 pp

Fan, H.-R., Yang, K.-F., Hu, F.-F., Liu, S., & Wang, K.-Y. (2016). The giant Bayan Obo REE-Nb-Fe deposit, China: Controversy and ore genesis. *Geoscience Frontiers*, *7*(3), 335–344. http://doi.org/10.1016/j.gsf.2015.11.005

Farooq .S. (2017.). Hydrothermal and Skarn Deposits. Retrieved June 11, from http://www.angelfire.com/sc3/farooqs/notes/b3-3-4.htm

Fathi Habashi. (1997a). *Handbook of Extractive Metallurgy, Volume 3*. (1st Ed.). Wiley. Retrieved from https://works.bepress.com/fathi_habashi/23/

Frondel, J. W., & Fleischer, M. (1950). A glossary of uranium- and thorium-bearing minerals. (3rd Ed.) *Geological Survey Circular 74; 1009-F.*

GCM, (2017). Ghana Chamber of Mines Report: Ghana Mining and Energy Summit (GMES), 31st May - 2nd June, International Conference Centre, Accra, Ghana.

Ghana Immigration (2017). *Facts about Ghana*. Retrieved from http://www.ghanaimmigration.org.

Gharibyan, N., Dailey, A., McLain, D. R., Bond, E. M., Moody, W. A., Happel, S., & Sudowe, R. (2014). Extraction Behavior of Americium and Curium on Selected Extraction Chromatography Resins from Pure Acidic Matrices. *Solvent Extraction and Ion Exchange*, *32*(4), 391–407. http://doi.org/10.1080/07366299.2014.884888

Gilbert N. Hanson. (1980). Rare Earth Elements in Petrogenetic Studies of Igneous System. *Ann. Rev. Earth Planet Sci.*, *8*, 371–406.

GMI, (2018). Global Market Insights, Inc, Rare Earth Metals Market Share & Forecast, 2017 – 2024 *Market Research Reports. Retrieved from https://www.gminsights.com*

Gosen, B. S. Van, Fey, D. L., Shah, A. K., Verplanck, P. L., & Hoefen, T. M. (2014). *Deposit model for heavy-mineral sands in coastal environments: Chapter L in* Mineral deposit models for resource assessment. *Scientific Investigations Report*. Retrieved from https://pubs.er.usgs.gov/publication/sir20105070L

Gschneidner, K. A., Bunzli, J.-C. G., & Pecharsky, V. K. (2006). *Handbook on the physics and chemistry of rare earths*. North Holland Pub. Co.

Gschneidner, K. A., & Eyring, L. (1978). *Handbook on the physics and chemistry of rare earths*. (1st Ed.) North-Holland.

GSD [Geological Survey Department] (2009). *Geological Map of Ghana 1: 1 000 000*.

Guilbert, J. M., & Park, C. F. (1986). *The geology of ore deposits*. (4th Ed.) New York : W.H. Freeman.

Guilbert, J. M., & Park, C. F. (2007). *The geology of ore deposits*. Waveland Press Inc.

Hacker, B. R., Kelemen, P. B., & Behn, M. D. (2015). Continental Lower Crust. *Annu. Rev. Earth Planet. Sci*, *43*, 167–205. http://doi.org/10.1146/annurev-earth-050212-124117

Haoqing, W. & Lijun W. (2003). Carbon film and LiFePO4 composite nm conductive material and its synthesis method. Google patents CN1442917A.

Harb, S. (2008). Natural radioactivity and external gamma radiation exposure at the coastal Red Sea in Egypt. *Radiation Protection Dosimetry*, *130*(3), 376–384. http://doi.org/10.1093/rpd/ncn064

Harb, S., El-Kamel, A. H., Zahran, A. M., Abbady, A., & As-Subaihi, F. A. A. (2012). Measurement of Natural Radioactivity in Beach Sediments From Aden Coast on Gulf of Aden, South of Yemen. In *XI Radiation Physics & Protection Conference*.

Hart, C. A. (2013). Climate Change and the Private Sector;Scaling up Private Sector Response to Climate Change. *Exploration in Environmental Economics.(1st Ed.)Abingdon, Oxfordshire, UK Routledge Publishers.*

Hart, S.R. and Zindler, A. (1986). GERM Reservoir Database; In search of a bulk-Earth composition. *Chemical Geology*, *57*(3-4), 247–267.

Hayford, M. S., Akiti, T. T., Serfor-Armah, Y., & Dampare, S. B. (2013). Investigaton of Kpong carbonatite as a potential source for rare earth elements (REEs) using instrumental neutron activation analysis (INAA). *Radiochimica Acta*, *101*(11), 739–744. http://doi.org/10.1524/ract.2013.2107

He C, Lei Y, Ge J (2014). Assessment of Trading Partners for China's Rare Earth Exports Using a Decision Analytic Approach. *PLoS ONE* 9(7): e102870. https://doi.org/10.1371/journal.pone.0102870

Hedrick, S. B. C. and J. B. (2006). Industrial Minerals & Rocks: Commodities, Markets, and Uses. In Kogel, E.J., Nikhil C. T., James M. B., Stanly T. K, *Rare Earth Elements* (7th ed., p. 1565). Colorado, USA.

Hofstra, A. H., Meighan, C. J., Song, X., Samson, I., Marsh, E. E., Lowers, H. A., Hunt, A. G. (2016). Mineral Thermometry and Fluid Inclusion Studies of the Pea Ridge Iron Oxide-Apatite–Rare Earth Element Deposit, Mesoproterozoic St. Francois Mountains Terrane, Southeast Missouri, USA. *Economic Geology*, *111*(8), 1985–2016. http://doi.org/10.2113/econgeo.111.8.1985

Holland, H. D., & Turekian, K. K. (2004). The Crust. *Treatise on Geochemistry*. (1st Ed.) Vol.3, Oxord, UK. Elsevier Ltd.

Horwitz, E. P., McAlister, D. R., Bond, A. H., & Barrans, R. E. (2005). Novel Extraction of Chromatographic Resins Based on Tetraalkyldiglycolamides: Characterization and Potential Applications. *Solvent Extraction and Ion Exchange*, *23*(3), 319–344. http://doi.org/10.1081/SEI-200049898

Hu, Z., Haneklaus, S., Sparovek, G., & Schnug, E. (2006). *Rare Earth Elements in Soils. Communications in Soil Science and Plant Analysis* 37,(9-10). 1381-1420. http://doi.org/10.1080/00103620600628680

Huang, C., & Bian, Z. (2010). Introduction. In *Rare Earth Coordination Chemistry* (pp. 1–39). Chichester, UK: John Wiley & Sons, Ltd. http://doi.org/10.1002/9780470824870.ch1

Huang, S., Jacobsen, S. B., & Mukhopadhyay, S. (2013). Nd systematics of Earth are inconsistent with a superchondritic Sm/Nd ratio. *Proceedings of the National Academy of Sciences of the United States of America* , *110*(13), 4929–4934. http://doi.org/10.1073/pnas.1222252110

IAEA [International Atomic Energy Agency] (1989). *Measurement of Radionuclides in Food and the Environment: A Guidebook. Technical Reports Series No. 295* Vienna.

IAEA [International Atomic Energy Agency] (1993). Uranium Extraction Technology *Technical Reports Series* No. 359. Vienna.

IBP [International Business Publications] (2008). *Ghana mining laws and regulations handbook.* (1st Ed) Vol. 1. Intl Business Pubns Usa.

Inoue, S., Ordonez, C. F., & Freiser, H. (1985). Mixed Ligand Chelate Extraction of Lanthanides With N-M-Trifluoromethylbenzoyl-Phenylhydroxylamine Systems. *Solvent Extraction and Ion Exchange*, *3*(6), 839–855. http://doi.org/10.1080/07366298508918543

IRENA [Renewable Energy Agency] (2015). *Africa 2030: Roadmap for a Renewable Energy Future.* Retrieved from http://www.irena.org/Document Downloads /Publications/IRENA_Africa_2030_REmap_2015_low-res.pdf

Irving, M., D. G., Richardson (1992). *Geological Survey of Canada, Open File 2484 - Canada-Northwest Territories Mineral Development Subsidiary Agreement 1987-1991-Google Books*. (D.G Richardson; M. Irving, Ed.). Canada Northwest.

Izatt, S. R., Mckenzie, J. S., Izatt, N. E., Bruening, R. L., Krakowiak, K. E., & Izatt, R. M. (2016). Molecular Recognition Technology: A Green Chemistry Process For Separation of Individual Rare Earth Metals. Retrieved from http://ucore.com/documents/WhitePaper_REE_Separations.pdf

Jack Zhang, Baodong Zhao, B. S. (2016). *Separation Hydrometallurgy of Rare Earth Elements - Jack Zhang, Baodong Zhao, Bryan Schreiner - Google Books*. Springer International Publishing. http://doi.org/10.1007/978-3-319-28235-0

Jahns, R. H., & Burnham, C. W. (1969). Experimental studies of pegmatite genesis; l, A model for the derivation and crystallization of granitic pegmatites. *Economic Geology*, *64*(8), 843–864. http://doi.org/10.2113/gsecongeo.64.8.843

Jones, A. P., Genge, M., & Carmody, L. (2013). Carbonate Melts and Carbonatites. *Reviews in Mineralogy and Geochemistry*, *75*(1), 289–322. http://doi.org/10.2138/rmg.2013.75.10

Jones, G. (2009). Mineral Sands: An Overview of the Industry. *Iluka (unpublished)*, (April), 38–41.

Jordens, A., Cheng, Y. P., & Waters, K. E. (2013). A review of the beneficiation of rare earth element bearing minerals. *Minerals Engineering*, *41*, 97–114. http://doi.org/10.1016/j.mineng.2012.10.017

Kanazawa, Y., & Kamitani, M. (2006). Rare earth minerals and resources in the world. *Journal of Alloys and Compounds*, *408-412*, 1339–1343. http://doi.org/10.1016/j.jallcom.2005.04.033

Kannan, V., Rajan, M. P., Iyengar, M. A. R., & Ramesh, R. (2002). Distribution of natural and anthropogenic radionuclides in soil and beach sand samples of Kalpakkam (India) using hyper pure germanium (HPGe) gamma ray spectrometry. *Applied Radiation and Isotopes*, *57*, 109–119. http://doi.org/10.1016/S0969-8043(01)00262-7

Kazuhiro Kato, Toshiaki Yoshioka, and, & Okuwaki, A. (2000). Study for Recycling of Ceria-Based Glass Polishing Powder. http://doi.org/10.1021/IE990622X

Kinnaird, J. A., & Bowden, P. (1991). Magmatism and Mineralization Associated with Phanerozoic Anorogenic Plutonic Complexes of the African Plate. In *Magmatism in Extensional Structural Settings* (pp. 410–485). Berlin, Heidelberg: Springer Berlin Heidelberg. http://doi.org/10.1007/978-3-642-73966-8_16

Komorova.L, & Tran H. N. (1992). Synergetic Effects in the Extraction of Rare-Earth Ions by Mixed Organic Solvents, *Chem. Papers 46*(3), 174–177.

Krebs, R. E. (2006). *The History and Use of Our Earth's Chemical Elements: A Reference Guide*. Greenwood Publishing Group. Retrieved from https://books.google.com/

Krishnamurthy, N., & Gupta, C. K. (2004). *Extractive Metallurgy of Rare Earths*. CRC Press. Retrieved from https://books.google.com/books

Kruchten Eugene Marie Godfried Andre Van. (1998). Catalytic hydrolysis of alkylene oxides. Retrieved from http://www.google.com.na/patents/EP1034158A1?cl=en

Kumar, V., Jha, M. K., Kumari, A., Panda, R., Kumar, J. R., & Lee, J. Y. (2014). Recovery of Rare Earth Metals (REMs) from Primary and Secondary Resources: A Review. In *Rare Metal Technology 2014* (pp. 81–88). Hoboken, NJ, USA: John Wiley & Sons, Inc. http://doi.org/10.1002/9781118888551.ch16

Lawluvi, H. (2016). *Multivariate Statistical Classification of Beach Sands along the Coastal Belt of Ghana using Natural Radioactivity Data*. PhD Thesis submitted to the University of Ghana.

Layton, W. (1958). *The geology of 1/4` field sheet 32. of Southern Ghana. Ghana Geol.Surv. Bull.* **24**,. pp66

Lehto, J., & Hou, X. (2011). *Chemistry and Analysis of Radionuclides : Laboratory Techniques and Methodology*. Wiley.

Liang, T., Li, K., & Wang, L. (2013). State of rare earth elements in different environmental components in mining areas of China. *Jounal of Environmental Monitoring and Assessment*, 186 (3), 1499–1513. http://doi.org/10.1007/s10661-013-3469-8

Liao, B. Q., Wang, J., & Wan, C. R. (2005). Separation and Recovery of Rare Earths in Reciprocating Extraction Columns. *Separation Science and Technology*, *40*(8), 1685–1700. http://doi.org/10.1081/SS-200059604

Lima-de-Faria, J. (2001). *Structural Classification of Minerals : Volume I: Minerals with A, Am Bn and ApBqCr General Chemical Formulas*. Springer Netherlands.

Linnen, R. L., Van Lichtervelde, M., & Černý, P. (2012). Granitic Pegmatites as Sources of Strategic Metals. *Elements* 8 (4): 275-280.

Littlejohn, P. (2007). Technical Review – Copper Solvent Extraction in Hydrometallurgy. Pp 64. Retrieved from Pennsylvania State University, USA.

Locock, J. Andrew & Burns, C. Peter (2003). The Crystal Structure of Synthetic Autunite. *American Mineralogist,* 88, pp 240–244.

Long, K. R., Van Gosen, B. S., Foley, N. K., & Cordier, D. (2012). The Principal Rare Earth Elements Deposits of the United States: A Summary of Domestic Deposits and a Global Perspective. In *Non-Renewable Resource Issues* (pp. 131–155). Dordrecht: Springer Netherlands.

Lu, X., Zhang, X., & Wang, F. (2008). Natural radioactivity in sediment of Wei River, China. *Environmental Geology*, *53*(7), 1475–1481. http://doi.org/10.1007/s00254-007-0756-0

Lynascorp. (2006). The LAMP, Kuantan, Malaysia. Retrieved August 10, 2017, from https://www.lynascorp.com/Pages/Kuantan-Lynas-Advanced-Materials-Plant.aspx

Maischak, S., & Fachinger, J. (2001). Solid-Phase Extraction for the Separation of Actinides from Radioactive Waste. WM'01 Conference, February 25-March 1, 2001, Tucson, AZ.

Malvárez, G. C. (2012). The History of Shoreline Stabilization on the Spanish Costa del Sol (pp. 235–249). Springer, Dordrecht. http://doi.org/10.1007/978-94-007-4123-2_14

Marc Humphries. (2010). Rare Earth Elements: The Global Supply Chain - *U.S Congresssional Research Service. 7-5700; R41347*. Retrieved December 28, 2016.

Marco T. Einaudi and Naomi Oreskes. (1983). *Progress Toward An Occurrence Model for Proterozoic Iron Oxide Deposits- A comparison between the ore province of South Australia and Southeast Missouri. Depositional Controls, Distribution, and Effectiveness of World's Petroleum. - Gregory F. Ulmishek, H. Douglas Klemme U.S Geological Survey Bulletin.*

Maria A. Petrova, Vanya B. Kurteva, and Lubomir A. Lubenov. (2011). Synergistic Effect in the Solvent Extraction and Separation of Lanthanoids by 4-(4-Fluorobenzoyl)-3-methyl-1-phenyl-pyrazol- 5-one in the Presence of Monofunctional Neutral Organophosphorus Extractants. *Ind. Eng. Chem. Res.*, *50*, 12170–12176.

Maurer, M. A. Mm. H. F. W. (1992). *Heavy Minerals in Colour*. Chapman & Hall, 2-6 Boundary Row, London SE18HN.

McColl, R. W. (2005). *Encyclopedia of world geography. Volume I, A-G*. Facts On File. Infobase Publishing 433 Pp.

McDonough, W. F., and S.-S. S. (1995). The composition of the Earth,. *Chem. Geol.*, *120*, 223 – 253.

McGlade, J.M., Cury .P., Koranteng K.A., Hardman-Mountford N.J. (2002). *The Gulf of Guinea large marine ecosystem : environmental forcing & amp; sustainable development of marine resources.* Elsevier, Amsterdam, Netherlands.

McKenzie, Dan, & O'Nions RK (1991). Partial melt distributions from inversion of rare earth element concentrations. *J. Pet.*, *32*, 1021 – 1091.

Mckeough, M. A., Lentz, D. R., Mcfarlane, C. R. M., & Brown, J. (2013). Geology and evolution of pegmatite-hosted U–Th ± REE–Y–Nb mineralization, Kulyk,

Eagle, and Karin Lakes region, Wollaston Domain, northern Saskatchewan, Canada: examples of the dual role of extreme fractionation and hybridization processes. *Journal of Geosciences*, *58*, 321–346. http://doi.org/10.3190/jgeosci.153

Mike Kellow. (2010). Nkombwa Hill Rare Earths and Phosphate Project, Zambia – Vast Resources. Retrieved July 29, 2017, from http://www.vastresourcesplc.com/news/nkombwa-hill-rare-earths-and-phosphate-project-zambia/

Míková, J., & Denková, P. (2007). Modified chromatographic separation scheme for Sr and Nd isotope analysis in geological silicate samples. *Journal of Geosciences*, *52*(3-4), 221–226. http://doi.org/10.3190/jgeosci.015

Miller, R. R. (2015). Pantellerite-hosted rare earth element mineralization in southeast Labrador: The Foxtrot deposit. Symposium on critical and strategic materials. *British Columbia Geological Survey Paper 2015-3.*

Misra, V. N., Das, S. C., Subbaiah, T., Council of Scientific & Industrial Research (India). Regional Research Laboratory (Bhubaneswar, I., Indian Institute of Metals. Bhubaneswar Chapter., & Indian Institute of Mineral Engineers. Bhubaneswar Chapter. (2005). *International Conference on Emerging Trends in Mineral Processing and Extractive Metallurgy : ICME 2005, 13-14 June 2005*. Allied Publishers.

Mitchell, R. H. (2005). Carbonatites and carbonatites and carbonatites. In *Canadian Mineralogist* 43, pp. 2049–2068). http://doi.org/10.2113/gscanmin.43.6.2049

Mortimer H. Staaz. (1979). Geology and Description of Thorium and Rare Earth Veins in the Laughlin Peak Area, Colfax County, New Mexico. *Geological Survey Professional Paper:Geology and Resources of Thorium in the United States*, *1049*, E1–E32.

Neikov, O., Naboychenko, S., & Mourachova, I. (2009). *Handbook of Non-Ferrous Metal Powders : Technologies and Applications.* (1st Ed.) Elsevier, Oxford, U.K.

NewsGhana. (2017). Central Region | News Ghana. Retrieved July 30, 2017, from https://www.newsghana.com.gh/ghana/regions-of-ghana/central-region/

Nockemann, P., Thijs, B., Pittois, S., Thoen, J., Glorieux, C., Van Hecke, K., Binnemans, K. (2006). Task-Specific Ionic Liquid for Solubilizing Metal Oxides. *The Journal of Physical Chemistry B*, *110*(42), 20978–20992. http://doi.org/10.1021/jp0642995

Norton, P. B., & Esposito, J. J., (2003). *The new encyclopaedia Britannica*. Encyclopaedia Britannica (5).

NPS (2006). National Park Museum Handbook on Radioactive Minerals, Part 1, Chapter 11 and Appendix H, Curatorial Health and Safety and COG 2/5 Fossil Vertebrates as Radon Source. Health Pp.1376

Obolenskiy, B. A. A., Rodionov, S. M., Ariunbileg, S., Dejidmaa, G., Distanov, E. G., Dorjgotov, D., Gotovsuren, A. (2007). *Mineral-Deposit Models for Northeast Asia*. *U.S. Geological Survey Professional Paper 1765*.

Oliveira, D., & Inverno, C. (2014). Classification of rare earth deposit and occurrence types: what's new? Classificação de depósitos e ocorrências de terras raras: uma nova perspectiva. *Comunicações Geológicas Especial II*, *101*, 821–823. Retrieved from http://www.lneg.pt/iedt/unidades/16/paginas/26/30/185

Olivier-Bourbigou, H., Magna, L., & Morvan, D. (2010). Ionic liquids and catalysis: Recent progress from knowledge to applications. *Applied Catalysis A: General*, *373*(1-2), 1–56. http://doi.org/10.1016/j.apcata.2009.10.008

Oliver N. H. S., Pearson P. J., Holcombe R. J. , & Ord A. (2010). Mary Kathleen metamorphic hydrothermal uranium — rare-earth element deposit: Ore genesis and numerical model of coupled deformation and fluid flow. *International Geoscience Journal of the Geological Society of Australia* 46 (3), 467-484

Onghena, B., & Binnemans, K. (2015). Recovery of Scandium(III) from Aqueous Solutions by Solvent Extraction with the Functionalized Ionic Liquid Betainium Bis(trifluoromethylsulfonyl)imide. *Industrial & Engineering Chemistry Research*, *54*(6), 1887–1898. http://doi.org/10.1021/ie504765v

Orris, G. J., & Grauch, R. I. (2002). *Rare Earth Element Mines, Deposits, and Occurrences*. pp 1-174, U.S. Geological Survey. Denver, CO.

Ostapenko, V., Vasiliev, A., Lapshina, E., Ermolaev, S., Aliev, R., Totskiy, Y., Kalmykov, S. (2015). Extraction chromatographic behavior of actinium and REE on DGA, Ln and TRU resins in nitric acid solutions. *Journal of Radioanalytical and Nuclear Chemistry*, *306*(3), 707–711. http://doi.org/10.1007/s10967-015-4331-y

Paul Mann, L. G. M. B. G. (2003). Tectonic Setting of the World's Giant Oil and Gas Fields, 15–105. *The AAPG/Datapages Combined Publications Database*.

Pereira, C., Santos, T., Rocha, Z., Oliveira, A., de B. C. Menezes, M., & Vasconcelos, D. (2011). Determination of natural radioactivity in beach sand in the extreme south of Bahia, Brazil, using gamma spectrometry. *Radiation Protection and Environment*, *34*(3), 178-184. http://doi.org/10.4103/0972-0464.101714

Philip Horwitz, E., McAlister, D. R., & Dietz, M. L. (2006). Extraction Chromatography Versus Solvent Extraction: How Similar are They? *Separation Science and Technology*, *41*(10), 2163–2182. http://doi.org/10.1080/01496390600742849

Pin, C., Briot, D., Bassin, C., & Poitrasson, F. (1994). Concomitant separation of strontium and samarium-neodymium for isotopic analysis in silicate samples, based on specific extraction chromatography. *Analytica Chimica Acta*, *298*(2), 209–217. http://doi.org/10.1016/0003-2670(94)00274-6

Pin, C., & Gannoun, A. (2017). Integrated Extraction Chromatographic Separation of the Lithophile Elements Involved in Long-Lived Radiogenic Isotope Systems (Rb–Sr, U–Th–Pb, Sm–Nd, La–Ce, and Lu–Hf) Useful in Geochemical and Environmental Sciences. *Analytical Chemistry*, *89*(4), 2411–2417. http://doi.org/10.1021/acs.analchem.6b04289

Pin, C., Gannoun .A., & Dupont .A. (2014). Rapid, simultaneous separation of Sr, P, and Nd by extraction chromatography prior to isotope ratios determination by TIMS and MC-ICP-MS. *J. Anal. At. Spectrom.*, *29, 1858-1870*.

Pin, C., & Zalduegui, J. S. (1997). Sequential separation of light rare-earth elements, thorium and uranium by miniaturized extraction chromatography: Application to isotopic analyses of silicate rocks. *Analytica Chimica Acta*, *339*(1-2), 79–89. http://doi.org/10.1016/S0003-2670(96)00499-0

Pingitore, N., Clague, J., & Gorski, D. (2014). Round Top Mountain rhyolite (Texas, USA), a massive, unique Y-bearing-fluorite-hosted heavy rare earth element (HREE) deposit. *Journal of Rare Earths*, *32*(1), 90–96. http://doi.org/10.1016/S1002-0721(14)60037-5

Pisecny, P., Husekova, K., Frohlich, K., Harmatha, L., Soltys, J., Machajdik, D., Jakabovic, J. (2004). Growth of lanthanum oxide films for application as a gate dielectric in CMOS technology. In *Materials Science in Semiconductor Processing* 7(4): 231–236.

Radhakrishna, A. P., Somashekarappa, H. M., Narayana, Y., & Siddappa, K. (1993). A new natural background radiation area on the southwest coast of India. *Health Physics*, *65*(4), 390–395. Retrieved from http://www.ncbi.nlm.nih.gov/pubmed

Rajendran, J., Balasubramanian, G., & Thampi, P. K. (2008). Determination of rare earth elements in Indian coastal monazite by ICP-AES and ICP-MS analysis and their geochemical significance. *Current Science*, *94*(10), 1296–1302.

Ramasamy, V., Sundarrajan, M., Suresh, G., Paramasivam, K., & Meenakshiundaram, V. (2014). Role of light and heavy minerals on natural radioactivity level of high background radiation area, Kerala, India. *Applied Radiation and Isotopes : Including Data, Instrumentation and Methods for Use in Agriculture, Industry and Medicine*. http://doi.org/10.1016/j.apradiso.2013.11.119

Reddy, M. L., Sujatha, S., Varma, R. L., Ramamohan, T. R., Rao, T. P., Iyer, C. S., & Damodaran, A. D. (1997). Mixed-ligand chelate extraction of trivalent lanthanides with 4,4,4-trifluoro-1-phenyl-1,3-butanedione and neutral oxo-donors. *Talanta*, *44*(1), 97–103. Retrieved from http://www.ncbi.nlm.nih.gov/pubmed/18966721

Richard B. Stewart, Benedict Kingsbury, B. R. (2009). *Climate Finance: Regulatory and Funding Strategies for Climate Change and Global Development*. NYU Press. New York and London. Retrieved from http://books.google.com

Robin D. Rogers, & Kenneth R. Seddon. (2002). *Ionic Liquids*. (R. D. Rogers & K. R. Seddon, Eds.) (Vol. 818). Washington, DC: American Chemical Society. http://doi.org/10.1021/bk-2002-0818

Rudnick, R. L., & Gao, S. (2003). Composition of the Continental Crust. In *Treatise on Geochemistry* 3:1–64. Elsevier. http://doi.org/10.1016/B0-08-043751-6/03016-4

Saad, H. R., & Al-Azmi, D. (2002). Radioactivity concentrations in sediments and their correlation to the coastal structure in Kuwait. *Applied Radiation and Isotopes : Including Data, Instrumentation and Methods for Use in Agriculture, Industry and Medicine*, *56*(6), 991–997.

Saji, N. S., Wielandt, D., Paton, C., & Bizzarro, M. (2016). Ultra-high-precision Nd-isotope measurements of geological materials by MC-ICPMS. *Journal of Analytical Atomic Spectrometry*, *31*(7), 1490–1504. http://doi.org/10.1039/C6JA00064A

Salama, E., Diab, H. M., El-Fiki, S. A., & Ibrahim, A. (2015). Distribution of Radionuclides in Soil and Beach Samples of the Western Coast of Suez Gulf, Egypt. *Arab Journal of Nuclear Science and Applications*, *48*(2), 63–69.

Samares Kar. (2013). *High Permittivity Gate Dielectric Materials; Springer Series in Advanced Microelectronics 43*. (1st Ed.). Springer Heidelberg, New York, London.

Santhi, P. B., Reddy, M. L. P., Ramamohan, T. R., & Damodaran, A. D. (1994). Mixed-ligand chelate extraction of neodymium(III) with thenoyltrifluoroacetone and various sulphoxides. *Talanta*, *41*(1), 9–14. http://doi.org/10.1016/0039-9140(94)80162-2

Sarbas, B., & Töpper, W. (2013). *Gmelin handbook of inorganic chemistry. Sc, Y, La-Lu, Rare earth elements, A6b, Y, La, and the lanthanoids : Geochemistry: hydrosphere, atmosphere. Cosmo- and geochemical cycles* (8th Ed.). Springer Science & Business Media.

Schnetzler, C. C., Philpotts, J. A., & Thomas, H. H. (1967). Rare-earth and barium abundances in Ivory Coast tektites and rocks from the Bosumtwi Crater area, Ghana. *Geochimica et Cosmochimica Acta*, *31*(10), 1987–1993. http://doi.org/10.1016/0016-7037(67)90138-X

Sen Gupta, R., & Desa, E. (2001). *The Indian Ocean : A perspective*. 2: 817-868. Balkema Publishers, Tokyo.

Simmons, S. (2007). Pegmatite Genesis: Recent Advances and Areas for Future Research. Granitic Pegmatites: The State of the Art – International Symposium. 6th – 12th May, Porto, Portugal.

Sinding-Larsen, R., & Wellmer, F.-W. (2010). *Non-renewable resource issues : geoscientific and societal challenges*. Springer, London, NY.

Sivakumar, S., Chandrasekaran, A., Ravisankar, R., Ravikumar, S. M., Prince Prakash Jebakumar, J., Vijayagopal, P., Jose, M. T. (2014). Measurement of natural radioactivity and evaluation of radiation hazards in coastal sediments of east coast of Tamilnadu using statistical approach. *Journal of Taibah University for Science*, *8*(4), 375–384. http://doi.org/10.1016/j.jtusci.2014.03.004

Sliwa, A. S. (1991). Phosphate resources of Zambia and progress in their exploration. *Fertilizer Research*, *30*(2-3), 203–212. http://doi.org/10.1007/BF01048655

Spiro D. Alexandratos and Ripperger, K. P. (1998). Synthesis and Characterization of High-Stability Solvent-Impregnated Resins. http://doi.org/10.1021/IE9804780

Spitsyn, V. I., & Katz, J. J. Joseph J. (1976). *Chemistry of transuranium elements : proceedings of the Moscow Symposium*. Pergamon Press, Great Britain.

Sun, X., & Waters, K. E. (2014). Development of Industrial Extractants into Functional Ionic Liquids for Environmentally Friendly Rare Earth Separation. *ACS Sustainable Chemistry & Engineering*, *2*(7), 1910–1917. http://doi.org/10.1021/sc500255n

Suresh Gandhi, M., & Raja, M. (2014). Heavy mineral distribution and geochemical studies of coastal sediments between Besant Nagar and Marakkanam, Tamil Nadu, India. *Journal of Radiation Research and Applied Sciences*, *7*(3), 256–268. http://doi.org/10.1016/j.jrras.2014.06.002

Taylor SR, and McLennan SM. (1985). *The continental crust: its composition and evolution*. pp. 312. T Blackwell Scientific Publication, Carlton.

Traversa, G., Gomes, C. B., Brotzu, P., Buraglini, N., Morbidelli, L., Principato, M. S., Ruberti, E. (2001). Petrography and mineral chemistry of carbonatites and mica-rich rocks from the Araxá complex (Alto Paranaíba Province, Brazil). *Anais Da Academia Brasileira de Ciências*, *73*(1), 71–98. http://doi.org/10.1590/S0001-37652001000100008

Trindade, M. J., Prudêncio, M. I., Burbidge, C. I., Dias, M. I., Cardoso, G., Marques, R., & Rocha, F. (2013). Distribution of Naturally Occurring Radionuclides (K, Th & U) in Weathered Rocks of Various Lithological Types from the Uranium Bearing Region of Fornos de Algodres, Portugal. *Mediterranean Archaeology and Archaeometry*, *13*(3), 71–79.

UMD, (2016). GEOL212 - Planetary Geology. Retrieved December 27, 2016, from https://www.geol.umd.edu/~jmerck/geol212/lectures/09.html

UNSCEAR. (2000). *Sources and Effects of Ionizing Radiation*. *UNSCEAR 2000 Report* (1): 1-659.

Uosif, M. A. M., El-Taher, A., & Abbady, A. G. E. (2008). Radiological significance of beach sand used for climatotherapy from Safaga, Egypt. *Radiation Protection Dosimetry*, *131*(3), 331–339. http://doi.org/10.1093/rpd/ncn175

USGS. (2010). The Principal Rare Earth Elements Deposits of the United States — A Summary of Domestic Deposits and a Global Perspective Gd Pr Sm Nd La Ce. *US Geological Survey Scientific Investigations*, *89*(5220), 96. http://doi.org/10.1007/978-90-481-8679-2_7

USGS, (2017)a. U.S. Geological Survey, Mineral Commodity Summaries, Retrieved July 31, 2017, from https://minerals.usgs.gov/minerals/pubs/commodity/

USGS. (2017)b. Olympic Dam (Record #273) rare-earth element deposit in South Australia, Australia. Retrieved May 31, 2017, from https://mrdata.usgs.gov

USGS. (2015). Shuttle Radar Topography Mission (SRTM) 1 Arc-Second Global data. Retrieved: June 20, 2017, from the online Data Pool, courtesy of the NASA Land Processes Distributed Active Archive Center (LP DAAC), USGS/Earth Resources Observation and Science (EROS) Center, ttps://earthexplorer.usgs.gov/

USGS, (2014a). Rare earth element deposits containing calcite. *United States Geological Survey Document.* Retrieved June 10, 2017, from https://mrdata.usgs.gov/ree/ree.php?mineral=calcite

USGS, (2014b). Rare Earths Statistics and Information. *United States Geological Survey Document.* Retrieved June 17, 2017, from https://minerals.usgs.gov/minerals/pubs/commodity/rare_earths/

Van Straaten, P. (2002). *Rocks for Crops -151traaten, Peter van*. Retrieved from http://www.uoguelph.ca/~geology/rocks_for_crops/28ghana.PDF

Varnavas, S. P. (1990). Formation of placer mineral deposits in high energy environments: The Cyprus continental shelf. *Geo-Marine Letters*, *10*(1), 51–58. http://doi.org/10.1007/BF02431022

Vasconcelos, D. C., Reis, P. A. L., Pereira, C., Oliveira, A. H., Santos, T. O., & Rocha, Z. (2013). Modelling Natural Radioactivity in Sand Beaches of Guarapari, Espírito Santo State, Brazil. *World Journal of Nuclear Science and Technology*, *3*, 65–71. http://doi.org/10.4236/wjnst.2013.32011

Venugopal.R, Sham .T., Saxena . V.K., Mandre N.R. (2005). *Mineral Processing Technology Mpt-2005*. Tata McGraw-Hill Education. International Seminar on Mineral Processing Technology January 6-8. New Delhi, India.

Vértes Attila, Sándor Nagy, Zoltán Klencsár, Rezso György Lovas, Frank Rösch (2011). *Handbook of Nuclear Chemistry*. (2nd Ed.) Springer, London, New York.

Wang Lijun & Wu Haoqing (2003). Carbon film and $LiFePO_4$ composite nm conductive material and its synthesis method. Retrieved from Google Patent CN1442917A

Wang, Y., Zhou, H., Wang, Y., Li, F., & Sun, X. (2017). Separation of high-purity yttrium from ion-absorbed rare earth concentrate using (2,6-dimethylheptyl)

phenoxy acetic/propanoic acid. *Separation and Purification Technology*, *184*, 280–287. http://doi.org/10.1016/j.seppur.2017.04.049

Weng, Z. H., Jowitt, S. M., Mudd, G. M., & Haque, N. (2013). Assessing rare earth element mineral deposit types and links to environmental impacts. *Applied Earth Science*, *122*(2), 83–96. http://doi.org/10.1179/1743275813Y.0000000036

Wenk, H.-R., & Bulakh, A. (2003). *Minerals: Their Constitution and Origin*. *Cambridge*. http://doi.org/10.1086/430509

William M. Nelson. (2002). *Ionic Liquids*. (R. D. Rogers & K. R. Seddon, Eds.) (Vol. 818). Washington, DC: American Chemical Society. http://doi.org/10.1021/bk-2002-0818

Williams, A. (2001). *Handbook of Analytical Techniques*. (H. Gnzler & A. Williams, Eds.). Weinheim, Germany: Wiley-VCH Verlag GmbH. http://doi.org/10.1002/9783527618323

Williams, N. (2008). *Australia's identified mineral resources 2008*. Canberra. Retrieved from http://www.ga.gov.au/metadata-gateway/metadata/record/78988/

Woolley, A. R. (1987). Kipawa Lake (Record #203) rare-earth element deposit in Ontario, Canada. Retrieved June 10, 2017, from https://mrdata.usgs.gov/ree/show-ree.php?rec_id=203

Workman, R. K., & Hart, S. R. (2005). Major and trace element composition of the depleted MORB mantle (DMM). *Earth and Planetry Science Letters 235, 53-72*.

Wyllie, P. J. (1988). Magma Genesis, Plate Tectonics, and Chemical Differentiation of the Earth. *Reviews of Geophysics*, *26*(3), 370–404.

Xie, F., Zhang, T. A., Dreisinger, D., & Doyle, F. (2014). A critical review on solvent extraction of rare earths from aqueous solutions. *Minerals Engineering*, *56*, 10–28. http://doi.org/10.1016/j.mineng.2013.10.021

Yamada, E., & Freiser, H. (1981). Mixed ligand chelate extraction of lanthanide ions in systems involving 7-(1-vinyl-3,3,6,6-tetramethylhexyl)-8-quinolinol, 8-quinolinol, and 1,10-phenanthroline. *Analytical Chemistry*, *53*(13), 2115–2117. http://doi.org/10.1021/ac00236a039

Yendaw, J. (2004). Geology of Ghana. Retrieved from http://www.academia.edu/10359116/Geology_of_Ghana

Yiming, Z., Ge, B., & Daxin, L. (2005). REE-Nb (Fe, U, Th)-bearing alkaline skarns of China. In *Mineral Deposit Research: Meeting the Global Challenge* (pp. 507–509). Berlin, Heidelberg: Springer Berlin Heidelberg. http://doi.org/10.1007/3-540-27946-6_131

Zhang, S., Sun, N., He, X., Lu, X., & Zhang, X. (2006). Physical properties of ionic liquids: Database and evaluation. *Journal of Physical and Chemical Reference Data*, *35*(4), 1475–1517. http://doi.org/10.1063/1.2204959

APPENDICES

APPENDIX A: Calibration curve for γ-ray spectrometry

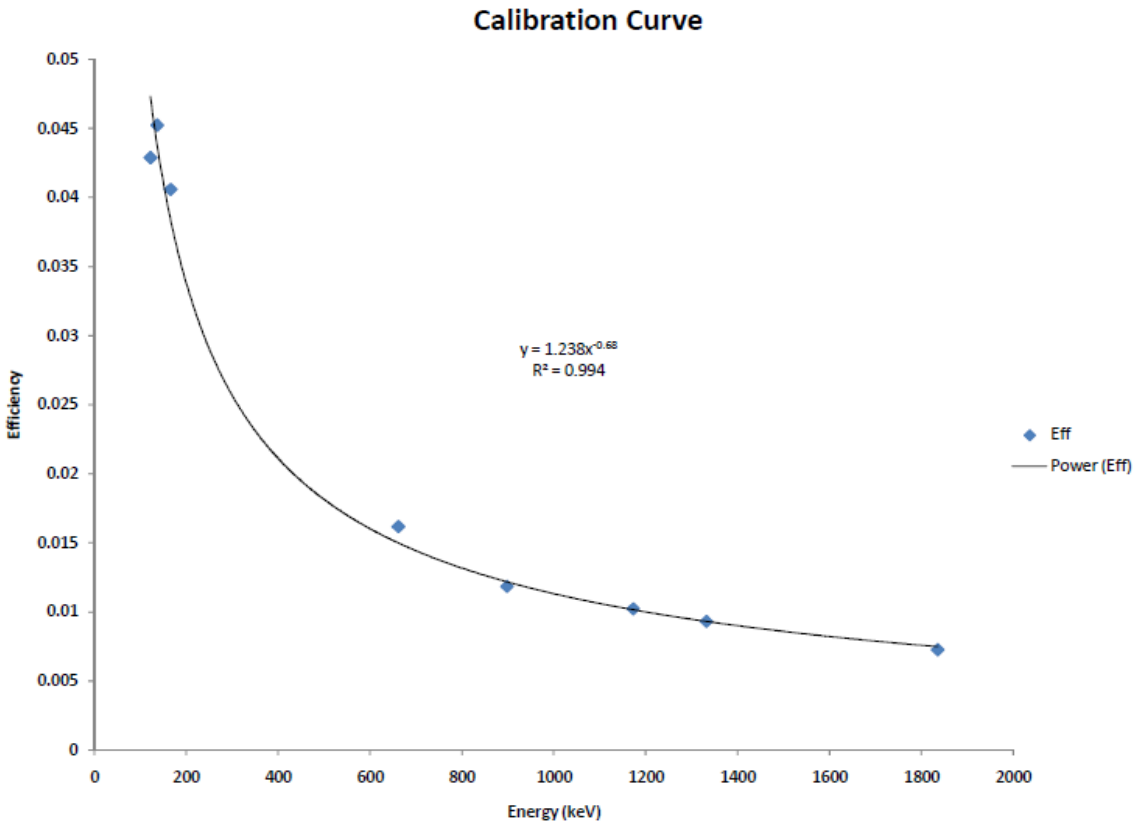

APPENDIX B: Particle size data statistics

CR1 (Fetteh)

	METHOD OF MOMENTS			FOLK & WARD METHOD		
	Arithmetic μm	Geometric μm	Logarithmic ϕ	Geometric μm	Logarithmic ϕ	Description
MEAN ($\bar{x}$)	272.8	254.1	1.977	245.0	2.029	Fine Sand
SORTING (σ)	90.42	1.411	0.497	1.398	0.484	Well Sorted
SKEWNESS (*Sk*)	2.014	-0.660	0.660	-0.553	0.553	Very Fine Skewed
KURTOSIS (*K*)	29.50	3.834	3.834	0.690	0.690	Platykurtic

	MODE 1	MODE 2	MODE 3	D_{10}	MEDIANorD$_{50}$	D_{90}	(D_{90}/D_{10})	(D_{90}-D_{10})	(D_{75}/D_{25})	(D_{75}-D_{25})
μm	302.5	152.5	-	143.4	282.0	342.7	2.390	199.3	1.779	1.503
ϕ	1.747	2.737	-	1.545	1.826	2.802	1.814	1.257	1.503	0.831

CR2 (Senya)

	METHOD OF MOMENTS			FOLK & WARD METHOD		
	Arithmetic μm	Geometric μm	Logarithmic ϕ	Geometric μm	Logarithmic ϕ	Description
MEAN ($\bar{x}$)	317.0	297.8	1.748	297.9	1.747	Medium Sand
SORTING (σ)	109.0	1.355	0.438	1.315	0.395	Well Sorted
SKEWNESS (*Sk*)	3.076	-0.110	0.110	0.002	-0.002	Symmetrical
KURTOSIS (*K*)	24.42	7.686	7.686	2.582	2.582	Very Leptokurtic

	MODE 1	MODE 2	MODE 3	D_{10}	MEDIANorD$_{50}$	D_{90}	(D_{90}/D_{10})	(D_{90}-D_{10})	(D_{75}/D_{25})	(D_{75}-D_{25})
μm	302.5	-	-	251.6	297.9	352.8	1.402	101.2	1.235	63.1
ϕ	1.747	-	-	1.503	1.747	1.991	1.325	0.488	1.191	0.305

CR3 (Winneba)

	METHOD OF MOMENTS			FOLK & WARD METHOD		
	Arithmetic μm	Geometric μm	Logarithmic ϕ	Geometric μm	Logarithmic ϕ	Description
MEAN ($\bar{x}$)	349.6	295.5	1.759	297.6	1.749	Medium Sand
SORTING (σ)	194.0	1.755	0.811	1.802	0.849	Moderately Sorted
SKEWNESS (*Sk*)	1.116	-0.112	0.112	-0.001	0.001	Symmetrical
KURTOSIS (*K*)	5.683	2.507	2.507	0.596	0.596	Very Platykurtic

	MODE 1	MODE 2	MODE 3	D_{10}	MEDIANorD$_{50}$	D_{90}	(D_{90}/D_{10})	(D_{90}-D_{10})	(D_{75}/D_{25})	(D_{75}-D_{25})
μm	302.5	605.0	152.5	139.4	297.3	633.2	4.543	493.8	3.091	355.2
ϕ	1.747	0.747	2.737	0.659	1.750	2.843	4.312	2.184	2.752	1.628

CR4 (Mankwadze)

	METHOD OF MOMENTS			FOLK & WARD METHOD		
	Arithmetic μm	Geometric μm	Logarithmic ϕ	Geometric μm	Logarithmic ϕ	Description
MEAN ($\bar{x}$)	287.6	244.2	2.034	236.1	2.083	Fine Sand
SORTING (σ)	186.0	1.686	0.753	1.591	0.670	Moderately Well Sorted
SKEWNESS (*Sk*)	2.804	0.431	-0.431	-0.172	0.172	Fine Skewed
KURTOSIS (*K*)	15.58	3.690	3.690	0.896	0.896	Platykurtic

	MODE 1	MODE 2	MODE 3	D_{10}	MEDIANorD$_{50}$	D_{90}	(D_{90}/D_{10})	(D_{90}-D_{10})	(D_{75}/D_{25})	(D_{75}-D_{25})
μm	302.5	152.5	605.0	134.4	267.8	539.7	4.014	405.2	2.083	167.8
ϕ	1.747	2.737	0.747	0.890	1.901	2.895	3.253	2.005	1.649	1.059

CR5 (Apam)

	METHOD OF MOMENTS			FOLK & WARD METHOD		
	Arithmetic μm	Geometric μm	Logarithmic ϕ	Geometric μm	Logarithmic ϕ	Description
MEAN ($\bar{x}$)	356.3	272.7	1.875	283.9	1.817	Medium Sand
SORTING (σ)	297.4	1.976	0.982	1.986	0.990	Moderately Sorted
SKEWNESS (*Sk*)	2.339	0.443	-0.443	0.170	-0.170	Coarse Skewed
KURTOSIS (*K*)	10.45	2.995	2.995	1.085	1.085	Mesokurtic

	MODE 1	MODE 2	MODE 3	D_{10}	MEDIANorD_{50}	D_{90}	(D_{90}/D_{10})	(D_{90}-D_{10})	(D_{75}/D_{25})	(D_{75}-D_{25})
μm	302.5	152.5	605.0	132.6	275.7	666.7	5.028	534.1	2.270	196.4
ϕ	1.747	2.737	0.747	0.585	1.859	2.915	4.984	2.330	1.783	1.183

CR6 (Mumford)

	METHOD OF MOMENTS			FOLK & WARD METHOD		
	Arithmetic μm	Geometric μm	Logarithmic ϕ	Geometric μm	Logarithmic ϕ	Description
MEAN ($\bar{x}$)	333.9	287.4	1.799	254.5	1.974	Medium Sand
SORTING (σ)	223.3	1.619	0.695	1.549	0.631	Moderately Well Sorted
SKEWNESS (*Sk*)	3.655	0.758	-0.758	-0.235	0.235	Fine Skewed
KURTOSIS (*K*)	222.91	4.783	4.783	2.408	2.408	Very Leptokurtic

	MODE 1	MODE 2	MODE 3	D_{10}	MEDIANorD_{50}	D_{90}	(D_{90}/D_{10})	(D_{90}-D_{10})	(D_{75}/D_{25})	(D_{75}-D_{25})
μm	302.5	152.5	605.0	146.5	290.8	568.4	3.880	421.9	1.316	80.08
ϕ	1.747	2.737	0.747	0.815	1.782	2.771	3.400	1.956	1.250	0.396

CR7 (Dago)

	METHOD OF MOMENTS			FOLK & WARD METHOD		
	Arithmetic µm	Geometric µm	Logarithmic ϕ	Geometric µm	Logarithmic ϕ	Description
MEAN ($\bar{x}$)	441.1	349.9	1.515	363.9	1.458	Medium Sand
SORTING (σ)	395.1	1.817	0.862	1.726	0.788	Moderately Sorted
SKEWNESS (*Sk*)	3.459	0.874	-0.874	0.383	-0.383	Very Coarse Skewed
KURTOSIS (*K*)	16.62	4.496	4.496	1.246	1.246	Leptokurtic

	MODE 1	MODE 2	MODE 3	D_{10}	MEDIANorD_{50}	D_{90}	(D_{90}/D_{10})	(D_{90}-D_{10})	(D_{75}/D_{25})	(D_{75}-D_{25})
µm	302.5	605.0	152.5	158.1	311.4	677.3	4.285	519.2	2.011	268.7
ϕ	1.747	0.747	2.737	0.562	1.683	2.661	4.734	2.099	2.115	1.008

CR8 (Akra)

	METHOD OF MOMENTS			FOLK & WARD METHOD		
	Arithmetic µm	Geometric µm	Logarithmic ϕ	Geometric µm	Logarithmic ϕ	Description
MEAN ($\bar{x}$)	418.8	353.3	1.501	367.4	1.444	Medium Sand
SORTING (σ)	303.0	1.687	0.754	1.575	0.656	Moderately Well Sorted
SKEWNESS (*Sk*)	3.917	0.536	-0.536	0.263	-0.263	Coarse Skewed
KURTOSIS (*K*)	24.14	4.639	4.639	0.938	0.938	Mesokurtic

	MODE 1	MODE 2	MODE 3	D_{10}	MEDIANorD_{50}	D_{90}	(D_{90}/D_{10})	(D_{90}-D_{10})	(D_{75}/D_{25})	(D_{75}-D_{25})
µm	302.5	605.0	152.5	172.4	316.6	657.9	3.816	485.5	1.993	270.1
ϕ	1.747	0.747	2.737	0.604	1.659	2.536	4.198	1.932	2.126	0.995

CR9 (Ekumpoano)

	METHOD OF MOMENTS			FOLK & WARD METHOD		
	Arithmetic µm	Geometric µm	Logarithmic ϕ	Geometric µm	Logarithmic ϕ	Description
MEAN ($\bar{x}$)	368.1	322.2	1.634	349.8	1.516	Medium Sand
SORTING (σ)	232.2	1.578	0.658	1.534	0.617	Moderately Well Sorted
SKEWNESS (*Sk*)	4.451	0.548	-0.548	0.281	-0.281	Coarse Skewed
KURTOSIS (*K*)	34.17	5.891	5.891	2.393	2.393	Very Leptokurtic

	MODE 1	MODE 2	MODE 3	D_{10}	MEDIANorD_{50}	D_{90}	(D_{90}/D_{10})	$(D_{90}-D_{10})$	(D_{75}/D_{25})	$(D_{75}-D_{25})$
µm	302.5	605.0	152.5	166.6	304.8	616.4	3.700	449.8	1.304	81.10
ϕ	1.747	0.747	2.737	0.698	1.714	2.586	3.703	1.887	1.251	0.383

CR10 (Edumafa)

	METHOD OF MOMENTS			FOLK & WARD METHOD		
	Arithmetic µm	Geometric µm	Logarithmic ϕ	Geometric µm	Logarithmic ϕ	Description
MEAN ($\bar{x}$)	300.7	268.6	1.896	248.2	2.0101	Fine Sand
SORTING (σ)	151.3	1.541	0.624	1.541	0.624	Moderately Well Sorted
SKEWNESS (*Sk*)	3.214	0.165	-0.165	-0.257	0.257	Fine Skewed
KURTOSIS (*K*)	28.54	4.124	4.124	1.000	1.000	Mesokurtic

	MODE 1	MODE 2	MODE 3	D_{10}	MEDIANorD_{50}	D_{90}	(D_{90}/D_{10})	$(D_{90}-D_{10})$	(D_{75}/D_{25})	$(D_{75}-D_{25})$
µm	302.5	152.5	605.0	142.8	285.1	522.7	3.662	380.0	1.87	153.0
ϕ	1.747	2.737	0.747	0.936	1.810	2.808	3.001	1.872	1.563	0.904

CR11 (Anomabu)

	METHOD OF MOMENTS			FOLK & WARD METHOD		
	Arithmetic µm	Geometric µm	Logarithmic ϕ	Geometric µm	Logarithmic ϕ	Description
MEAN ($\bar{x}$)	455.1	389.8	1.359	381.6	1.390	Medium Sand
SORTING (σ)	303.1	1.638	0.711	1.634	0.708	Moderately Sorted
SKEWNESS (*Sk*)	3.340	0.769	-0.769	0.418	-0.418	Very Coarse Skewed
KURTOSIS (*K*)	19.11	4.188	4.188	1.045	1.045	Mesokurtic

	MODE 1	MODE 2	MODE 3	D_{10}	MEDIANorD_{50}	D_{90}	(D_{90}/D_{10})	(D_{90}-D_{10})	(D_{75}/D_{25})	(D_{75}-D_{25})
µm	302.5	605.0	-	257.2	328.1	679.4	2.641	422.2	2.034	291.4
ϕ	1.747	0.747	-	0.558	1.608	1.959	3.513	1.401	2.276	1.024

CR12 (Cape Coast)

	METHOD OF MOMENTS			FOLK & WARD METHOD		
	Arithmetic µm	Geometric µm	Logarithmic ϕ	Geometric µm	Logarithmic ϕ	Description
MEAN ($\bar{x}$)	375.0	327.8	1.609	318.3	1.652	Medium Sand
SORTING (σ)	191.8	1.635	0.710	1.729	0.790	Moderately Sorted
SKEWNESS (*Sk*)	1.914	-0.063	-0.063	0.016	-0.016	Symmetrical
KURTOSIS (*K*)	14.52	2.737	2.737	0.923	0.923	Mesokurtic

	MODE 1	MODE 2	MODE 3	D_{10}	MEDIANorD_{50}	D_{90}	(D_{90}/D_{10})	(D_{90}-D_{10})	(D_{75}/D_{25})	(D_{75}-D_{25})
µm	302.5	605.0	152.5	153.4	311.2	637.8	4.157	484.4	2.028	270.4
ϕ	1.747	0.747	2.737	0.649	1.684	2.704	4.168	2.056	2.125	1.020

CR13 (Elmina)

	METHOD OF MOMENTS			FOLK & WARD METHOD		
	Arithmetic µm	Geometric µm	Logarithmic ϕ	Geometric µm	Logarithmic ϕ	Description
MEAN ($\bar{x}$)	401.8	343.9	1.540	362.3	1.465	Medium Sand
SORTING (σ)	273.9	1.641	0.714	1.566	0.647	Moderately Well Sorted
SKEWNESS (*Sk*)	3.869	0.685	-0.685	-0.287	-0.278	Coarse Skewed
KURTOSIS (*K*)	25.22	4.427	4.427	0.975	0.975	Mesokurtic

	MODE 1	MODE 2	MODE 3	D_{10}	MEDIANorD_{50}	D_{90}	(D_{90}/D_{10})	(D_{90}-D_{10})	(D_{75}/D_{25})	(D_{75}-D_{25})
µm	302.5	605.0	152.5	169.8	312.2	649.3	3.823	479.5	1.934	251.9
ϕ	1.747	0.747	2.737	0.623	1.680	2.558	4.106	1.935	2.014	0.951

CR14 (Dutch Komenda)

	METHOD OF MOMENTS			FOLK & WARD METHOD		
	Arithmetic µm	Geometric µm	Logarithmic ϕ	Geometric µm	Logarithmic ϕ	Description
MEAN ($\bar{x}$)	429.0	333.3	1.585	314.1	1.671	Medium Sand
SORTING (σ)	414.6	1.833	0.874	1.873	0.905	Moderately Sorted
SKEWNESS (*Sk*)	3.286	1.231	-1.231	0.201	-0.201	Coarse Skewed
KURTOSIS (*K*)	14.67	4.926	4.926	3.228	3.228	Extremely Leptokurtic

	MODE 1	MODE 2	MODE 3	D_{10}	MEDIANorD_{50}	D_{90}	(D_{90}/D_{10})	(D_{90}-D_{10})	(D_{75}/D_{25})	(D_{75}-D_{25})
µm	302.5	152.5	605.0	155.6	301.3	699.6	4.496	544.0	1.321	84.26
ϕ	1.747	2.737	0.747	0.515	1.731	2.864	5.208	2.169	1.263	0.402

CR15 (Kafodzizi)

	METHOD OF MOMENTS			FOLK & WARD METHOD		
	Arithmetic µm	Geometric µm	Logarithmic ϕ	Geometric µm	Logarithmic ϕ	Description
MEAN ($\bar{x}$)	439.7	394.6	1.342	384.3	1.380	Medium Sand
SORTING (σ)	220.3	1.512	0.596	1.436	0.522	Moderately Well Sorted
SKEWNESS (*Sk*)	2.921	0.589	-0.589	0.487	-0.487	Very Coarse Skewed
KURTOSIS (*K*)	20.49	3.572	3.572	0.594	0.594	Very Platykurtic

	MODE 1	MODE 2	MODE 3	D_{10}	MEDIANorD_{50}	D_{90}	(D_{90}/D_{10})	(D_{90}-D_{10})	(D_{75}/D_{25})	(D_{75}-D_{25})
µm	302.5	605.0	-	262.1	333.4	663.8	2.5333	401.7	2.004	288.0
ϕ	1.747	0.747	-	0.591	1.585	1.932	3.268	1.341	2.256	1.003

WR1 (Shama)

	METHOD OF MOMENTS			FOLK & WARD METHOD		
	Arithmetic µm	Geometric µm	Logarithmic ϕ	Geometric µm	Logarithmic ϕ	Description
MEAN ($\bar{x}$)	556.6	477.1	1.068	469.6	1.090	Medium Sand
SORTING (σ)	331.9	1.685	0.753	1.585	0.665	Moderately Well Sorted
SKEWNESS (*Sk*)	2.505	0.029	-0.029	-0.214	0.214	Fine Skewed
KURTOSIS (*K*)	12.98	4.028	4.028	0.880	0.880	Platykurtic

	MODE 1	MODE 2	MODE 3	D_{10}	MEDIANorD_{50}	D_{90}	(D_{90}/D_{10})	(D_{90}-D_{10})	(D_{75}/D_{25})	(D_{75}-D_{25})
µm	605.0	302.5	1200.0	265.0	538.8	1018.1	3.842	753.1	2.084	333.8
ϕ	0.747	1.747	-0.243	-0.026	0.892	1.916	-74.149	1.942	2.655	1.060

WR2 (Abuesi)

	METHOD OF MOMENTS			FOLK & WARD METHOD		
	Arithmetic µm	Geometric µm	Logarithmic ϕ	Geometric µm	Logarithmic ϕ	Description
MEAN ($\bar{x}$)	261.7	239.0	2.065	236.8	2.078	Fine Sand
SORTING (σ)	107.4	1.483	0.568	1.425	0.511	Moderately Well Sorted
SKEWNESS (*Sk*)	3.200	-0.301	0.301	-0.511	0.511	Very Fine Skewed
KURTOSIS (*K*)	43.61	3.490	3.490	0.619	0.619	Very Platykurtic

	MODE 1	MODE 2	MODE 3	D_{10}	MEDIANorD_{50}	D_{90}	(D_{90}/D_{10})	(D_{90}-D_{10})	(D_{75}/D_{25})	(D_{75}-D_{25})
µm	302.5	152.5	-	137.3	273.3	342.2	2.493	205.0	1.936	152.1
ϕ	1.747	2.737	-	1.547	1.871	2.865	1.852	1.318	1.571	0.953

WR3 (Sekondi)

	METHOD OF MOMENTS			FOLK & WARD METHOD		
	Arithmetic µm	Geometric µm	Logarithmic ϕ	Geometric µm	Logarithmic ϕ	Description
MEAN ($\bar{x}$)	123.4	104.7	3.255	98.97	3.337	Very Fine Sand
SORTING (σ)	132.7	1.594	0.673	1.436	0.522	Moderately Well Sorted
SKEWNESS (*Sk*)	12.08	0.908	-0.908	0.455	-0.455	Very Coarse Skewed
KURTOSIS (*K*)	186.8	11.73	11.73	0.591	0.591	Very Platykurtic

	MODE 1	MODE 2	MODE 3	D_{10}	MEDIANorD$_{50}$	D_{90}	(D_{90}/D_{10})	(D_{90}-D_{10})	(D_{75}/D_{25})	(D_{75}-D_{25})
µm	76.5	152.5	-	67.00	86.54	169.9	2.536	102.9	2.011	74.56
ϕ	3.731	2.737	-	2.557	3.530	3.900	1.525	1.342	1.366	1.008

WR4 (Takoradi)

	METHOD OF MOMENTS			FOLK & WARD METHOD		
	Arithmetic µm	Geometric µm	Logarithmic ϕ	Geometric µm	Logarithmic ϕ	Description
MEAN ($\bar{x}$)	235.0	215.6	2.231	225.5	2.149	Fine Sand
SORTING (σ)	90.11	1.458	0.544	1.428	0.514	Moderately Well Sorted
SKEWNESS (*Sk*)	1.407	-0.068	0.068	-0.403	0.403	Very Fine Skewed
KURTOSIS (*K*)	11.39	3.013	3.013	0.583	0.583	Very Platykurtic

	MODE 1	MODE 2	MODE 3	D_{10}	MEDIANorD$_{50}$	D_{90}	(D_{90}/D_{10})	(D_{90}-D_{10})	(D_{75}/D_{25})	(D_{75}-D_{25})
µm	302.5	152.5	-	134.2	254.1	334.7	2.494	200.5	2.001	151.0
ϕ	1.747	2.737	-	1.579	1.977	2.898	1.835	1.319	1.579	1.001

WR5 (Cape Three Point)

	METHOD OF MOMENTS			FOLK & WARD METHOD		
	Arithmetic μm	Geometric μm	Logarithmic ϕ	Geometric μm	Logarithmic ϕ	Description
MEAN ($\bar{x}$)	421.9	322.7	1.632	307.5	1.701	Medium Sand
SORTING (σ)	358.5	1.973	0.981	2.003	1.002	Poorly Sorted
SKEWNESS (*Sk*)	2.576	0.460	-0.460	0.153	-0.153	Coarse Skewed
KURTOSIS (*K*)	12.08	3.135	3.135	0.764	0.764	Platykurtic

	MODE 1	MODE 2	MODE 3	D_{10}	MEDIANorD$_{50}$	D_{90}	(D_{90}/D_{10})	(D_{90}-D_{10})	(D_{75}/D_{25})	(D_{75}-D_{25})
μm	302.5	152.5	605.0	140.4	300.0	704.7	5.018	564.3	3.266	384.2
ϕ	1.747	2.737	0.747	0.505	1.737	2.832	5.609	2.327	3.002	1.708

WR6 (Egyembra)

	METHOD OF MOMENTS			FOLK & WARD METHOD		
	Arithmetic μm	Geometric μm	Logarithmic ϕ	Geometric μm	Logarithmic ϕ	Description
MEAN ($\bar{x}$)	374.7	323.7	1.627	314.1	1.671	Medium Sand
SORTING (σ)	210.0	1.657	0.729	1.740	0.799	Moderately Sorted
SKEWNESS (*Sk*)	2.096	0.173	-0.173	0.024	-0.024	Symmetrical
KURTOSIS (*K*)	12.07	2.880	2.880	0.946	0.946	Mesokurtic

	MODE 1	MODE 2	MODE 3	D_{10}	MEDIANorD$_{50}$	D_{90}	(D_{90}/D_{10})	(D_{90}-D_{10})	(D_{75}/D_{25})	(D_{75}-D_{25})
μm	302.5	605.0	152.5	151.6	307.5	640.2	4.222	488.6	2.006	262.3
ϕ	1.747	0.747	2.737	0.643	1.701	2.721	4.229	2.078	2.074	1.004

WR7 (Axim)

	METHOD OF MOMENTS			FOLK & WARD METHOD		
	Arithmetic µm	Geometric µm	Logarithmic ϕ	Geometric µm	Logarithmic ϕ	Description
MEAN ($\bar{x}$)	796.7	487.6	1.036	564.5	0.825	Coarse Sand
SORTING (σ)	844.6	2.526	1.337	2.641	1.401	Poorly Sorted
SKEWNESS (*Sk*)	1.255	0.708	-0.708	0.599	-0.599	Very Coarse Skewed
KURTOSIS (*K*)	2.773	2.186	2.186	0.898	0.898	Platykurtic

	MODE 1	MODE 2	MODE 3	D_{10}	MEDIANorD_{50}	D_{90}	(D_{90}/D_{10})	(D_{90}-D_{10})	(D_{75}/D_{25})	(D_{75}-D_{25})
µm	302.5	2400.0	605.0	165.1	326.9	2377.2	14.40	2212.1	3.741	747.4
ϕ	1.747	-1.243	0.747	-1.249	1.613	2.599	-2.080	3.848	-65.557	1.904

WR8 (Esiama)

	METHOD OF MOMENTS			FOLK & WARD METHOD		
	Arithmetic µm	Geometric µm	Logarithmic ϕ	Geometric µm	Logarithmic ϕ	Description
MEAN ($\bar{x}$)	560.1	405.9	1.301	388.7	1.363	Medium Sand
SORTING (σ)	515.2	2.145	1.101	2.209	1.143	Poorly Sorted
SKEWNESS (*Sk*)	2.256	0.205	-0.205	-0.235	-0.235	Coarse Skewed
KURTOSIS (*K*)	8.157	3.516	3.516	1.114	1.114	Leptokurtic

	MODE 1	MODE 2	MODE 3	D_{10}	MEDIANorD_{50}	D_{90}	(D_{90}/D_{10})	(D_{90}-D_{10})	(D_{75}/D_{25})	(D_{75}-D_{25})
µm	302.5	605.0	152.5	150.9	335.0	1199.9	7.952	1049.1	2.367	366.1
ϕ	1.747	0.747	2.737	-0.263	1.578	2.728	-10.376	2.991	2.890	1.243

WR9 (Sanzule)

	METHOD OF MOMENTS			FOLK & WARD METHOD		
	Arithmetic µm	Geometric µm	Logarithmic ϕ	Geometric µm	Logarithmic ϕ	Description
MEAN ($\bar{x}$)	558.6	398.8	1.326	384.2	1.380	Medium Sand
SORTING (σ)	493.3	2.231	1.158	2.297	1.200	Poorly Sorted
SKEWNESS (*Sk*)	1.990	0.095	-0.095	0.184	-0.184	Coarse Skewed
KURTOSIS (*K*)	7.458	2.736	2.736	1.004	1.004	Mesokurtic

	MODE 1	MODE 2	MODE 3	D_{10}	MEDIANorD$_{50}$	D_{90}	(D_{90}/D_{10})	(D_{90}-D_{10})	(D_{75}/D_{25})	(D_{75}-D_{25})
µm	302.5	605.0	152.5	142.1	341.1	1211.7	8.529	1069.6	2.598	403.1
ϕ	1.747	0.747	2.737	-0.277	1.552	2.815	-10.164	3.092	3.259	1.377

WR10 (Atuabo)

	METHOD OF MOMENTS			FOLK & WARD METHOD		
	Arithmetic µm	Geometric µm	Logarithmic ϕ	Geometric µm	Logarithmic ϕ	Description
MEAN ($\bar{x}$)	391.4	336.1	1.573	361.1	1.470	Medium Sand
SORTING (σ)	239.9	1.674	0.744	1.581	0.661	Moderately Well Sorted
SKEWNESS (*Sk*)	3.347	-0.025	0.025	0.246	-0.246	Coarse Skewed
KURTOSIS (*K*)	23.87	5.235	5.235	0.946	0.946	Mesokurtic

	MODE 1	MODE 2	MODE 3	D_{10}	MEDIANorD$_{50}$	D_{90}	(D_{90}/D_{10})	(D_{90}-D_{10})	(D_{75}/D_{25})	(D_{75}-D_{25})
µm	302.5	605.0	152.5	158.8	312.5	646.4	4.070	487.6	1.997	266.0
ϕ	1.747	0.747	2.737	0.629	1.678	2.654	4.217	2.025	2.098	0.998

APPENDIX C: Pearson correlation data of LREE and HREE in beach sands

Region	Fraction	LREE Vs HREE
Central	Coarse	0.877 High positive correlation
	Medium	0.975 High positive correlation
	Fine	0.999 High positive correlation
Western	Coarse	0.957 High positive correlation
	Medium	0.948 High positive correlation
	Fine	0.558 positive correlation

CORREL FUNCTION = CORREL (array1, array2)

APPENDIX D: Range of REE distribution in central and western region summary data

Region	Fraction	REE	Range	Location
Central	Coarse	TREE	6.35 – 13.3	Anomabu, Akra(CR11, 8) – Dago (CR7)
		LREE	5.56 – 11.7	Anomabu (CR11) – Dago (CR7)
		HREE	0.64 – 1.53	Akra(CR8) – Dago (CR7)
		LREE/HREE	5.81 – 9.89	Ekumpoano(CR9) – Senya (CR2)
	Medium	TREE	8.56 – 53.15	Anomabu (CR11) – Dago (CR7)
		LREE	7.72 – 48.13	Anomabu (CR11) – Dago (CR7)
		HREE	0.84 – 5.02	Anomabu (CR11) – Dago (CR7)
		LREE/HREE	5.83 – 9.95	Ekumpoano(CR9) – Elmina (CR13)
	Fine	TREE	16.67 – 795.01	Edumafa(CR10) – Dago (CR7)
		LREE	14.98 – 727	Edumafa(CR10) – Dago (CR7)
		HREE	1.69 – 74.53	Edumafa(CR10) – Ekumpoano (CR9)
		LREE/HREE	4.43 – 10.79	Elmina (CR13) – Dago (CR7)
Western				
	Coarse	TREE	5.69 – 29.78	Egyembra (WR6) – Axim (WR7)
		LREE	5.07 – 26.08	Egyembra (WR6) – Axim (WR7)
		HREE	0.62 – 3.70	Egyembra (WR6) – Axim (WR7)
		LREE/HREE	6.67 – 10.11	Shama (WR1) – Takoradi (WR4)
	Medium	TREE	9.51- 85.58	Atuabo(WR10) – Sekondi (WR3)
		LREE	8.47 – 76.8	Atuabo(WR10) – Sekondi (WR3)
		HREE	1.04 – 8.78	Sanzule, Atuabo(WR9,1)–Sekondi (WR3)
		LREE/HREE	3.97 – 9.56	Shama(WR1) – Esiama (WR8)
	Fine	TREE	24.3 – 86.28	Takoradi(WR4) – Sekondi (WR3)
		LREE	21.76 – 77.46	Takoradi(WR4) – Sekondi (WR3)
		HREE	2.70 – 17.66	Esiama (WR8) - Takoradi(WR4)
		LREE/HREE	2.76 – 8.78	Esiama (WR8) - Sekondi (WR3)

APPENDIX E: Comparison of activity concentration in beach sands in the central and western region with others around the world

S/N	Locations	238U (Bq/Kg)	232Th (Bq/Kg)	40K (Bq/Kg)	References
1	World	35	30	400	UNSCEAR, (2000)
2	India	28.67	63.83	327.6	UNSCEAR, (2000)
3	Beach sand Egypt	-	177	815	Uosif et al, (2008)
4	Beach sand Red Sea Coast, Egypt	23.1	7.2	338	Harb, (2008)
5	Hungary	28.67	27.96	302.4	UNSCEAR, (2000)
6	Kuwait	36	6	227	Saad & Al-Azmi, (2002)
7	Aden coast on Gulf of Aden, South Yemen	46.3	48.7	646.8	(Harb et al, 2012)
8	Western Coast of Suez Gulf, Egypt	-	6.6	172.15	Salama et al, (2015)
9	Kalpakkam in Tamilnadu, India	112	1455.8	351	Kannan et al, (2002)
10	Ullal in Karnataka, India	374	158	158	Radhakrishna et. al. (1993)
11	North East coast Tamilnadu, India	35.12	713.6	349.6	Ramasamy et al, (2014)
12	Rhizao, China	12	15.2	1079.2	(Lu, Zhang, & Wang, 2008)
13	South Bahia, Brazil	910	2,220	352	(Pereira et al., 2011)
14	Guarapari, Brazil	-	57,000	3000	(Vasconcelos et al., (2013)
15	Northwest Libya	-	4.2	27.5	El-Kameesy et. al, (2008)
16	Coastal belt, Ghana	1.87-27	2.5-26.9	47.8-276	Lawluvi, (2016)
17	**Central region, Ghana**	**5.18**	**6**	**206.36**	**Present study**
18	**Western region, Ghana**	**2.5**	**1.4**	**107**	**Present study**

APPENDIX F: Pie chart representation of YREE in the beach sands of the Western region of Ghana

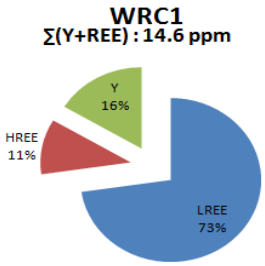

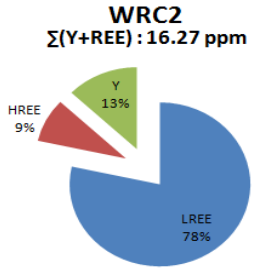

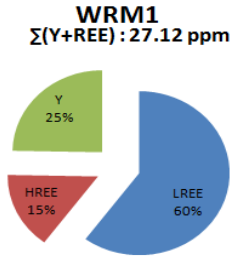

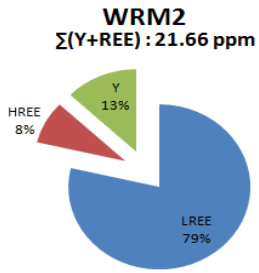

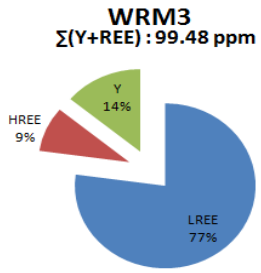

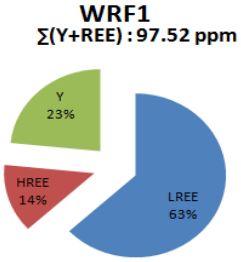

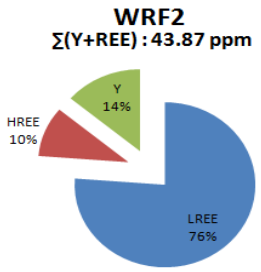

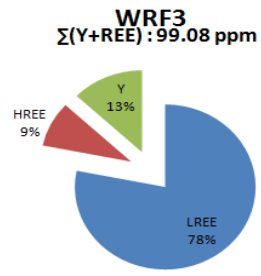

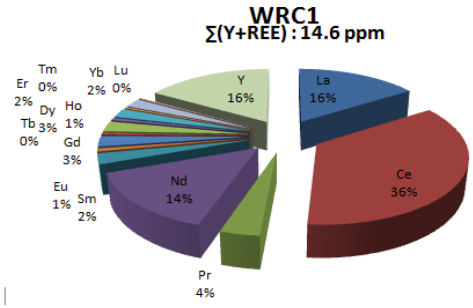

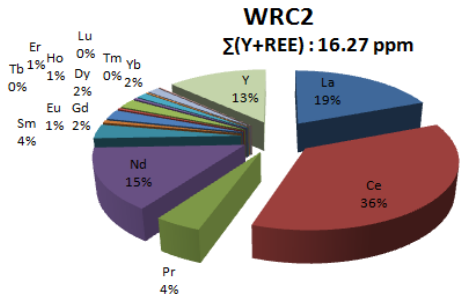

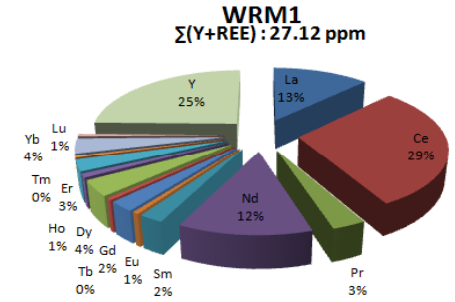

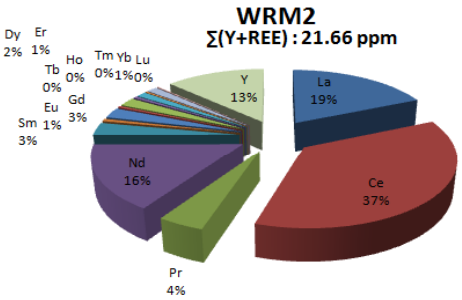

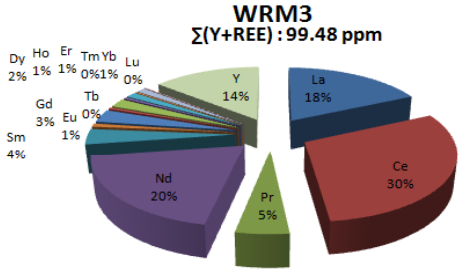

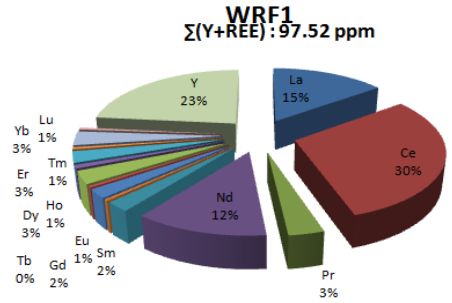

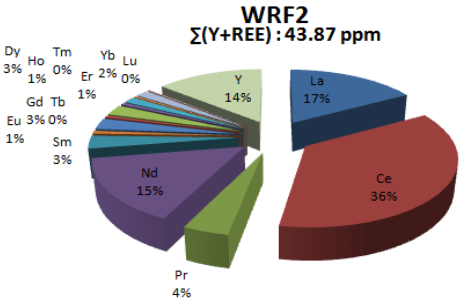

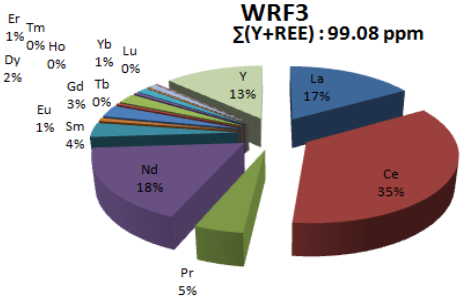

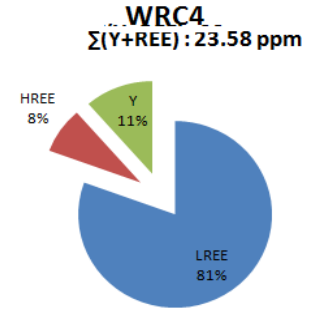

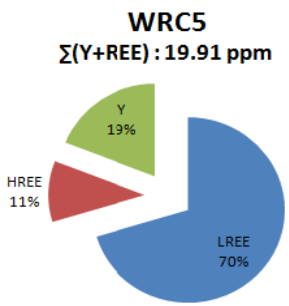

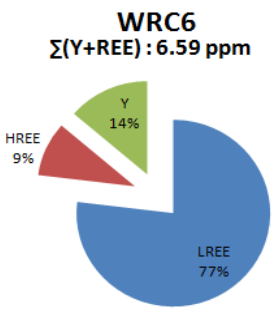

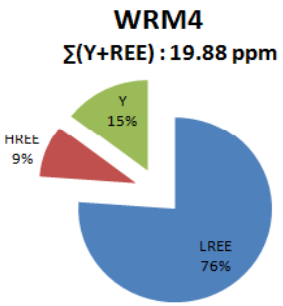

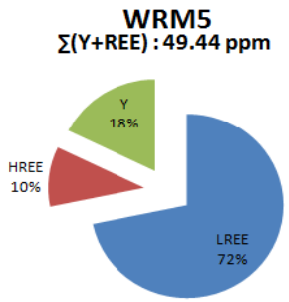

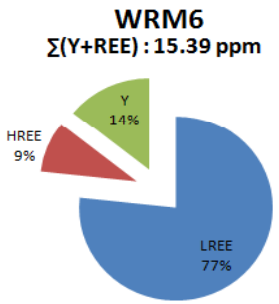

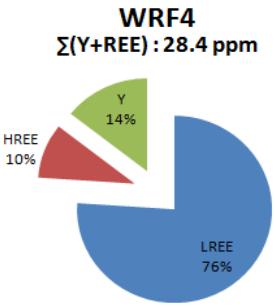

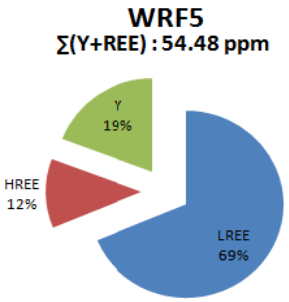

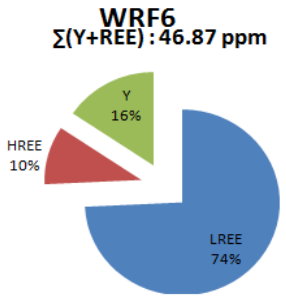

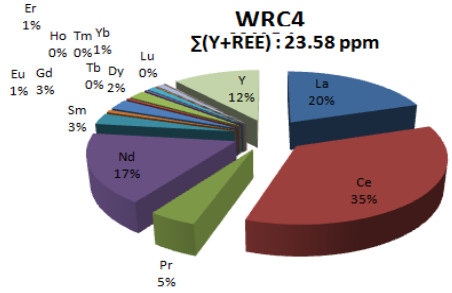

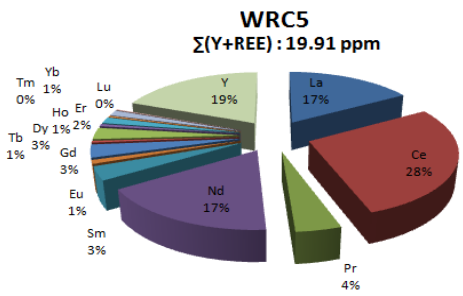

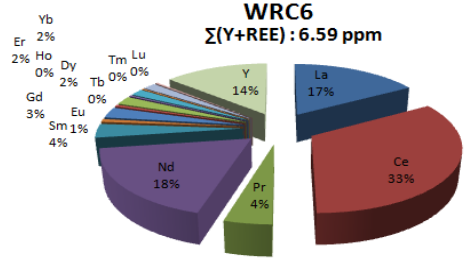

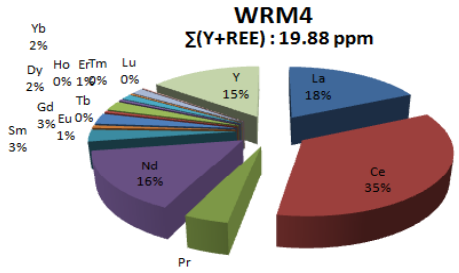

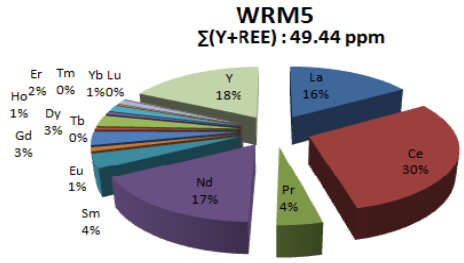

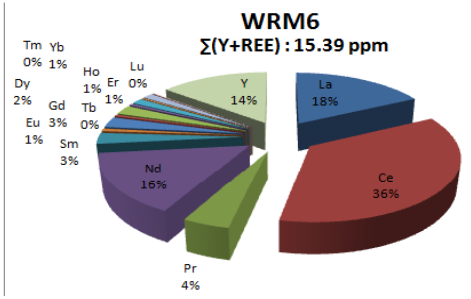

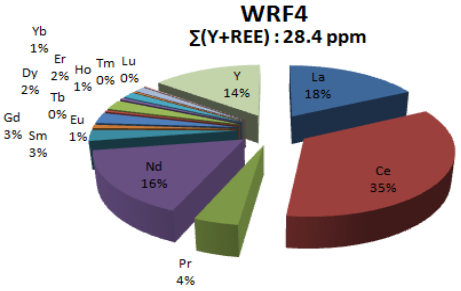

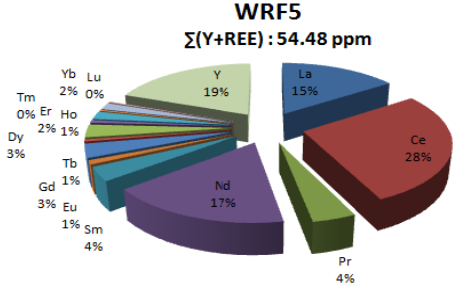

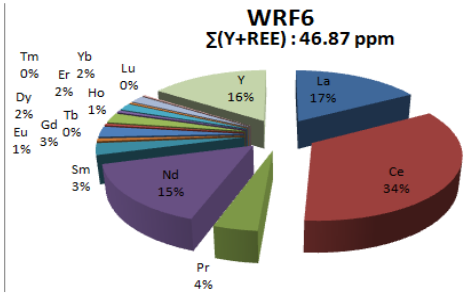

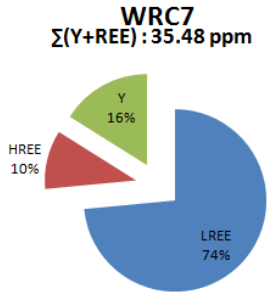

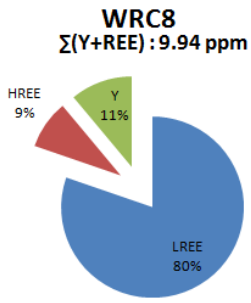

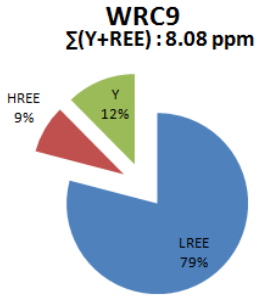

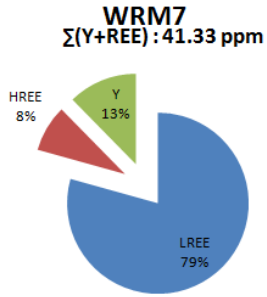

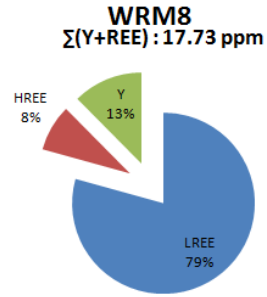

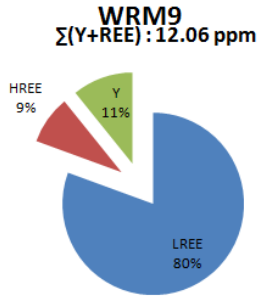

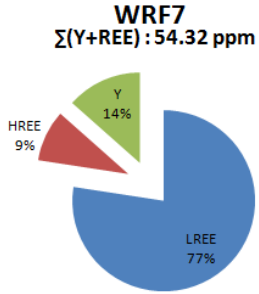

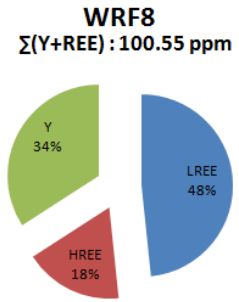

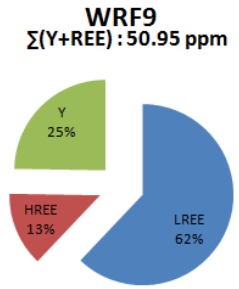

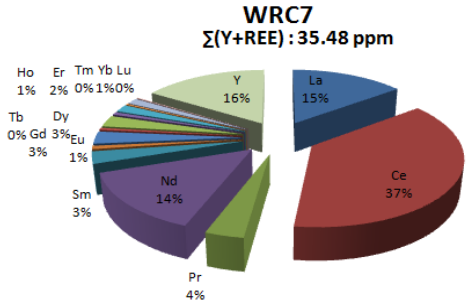

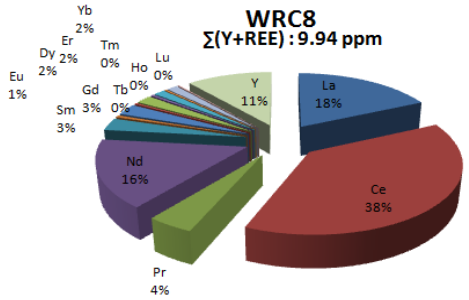

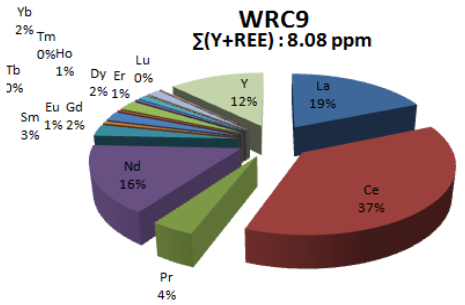

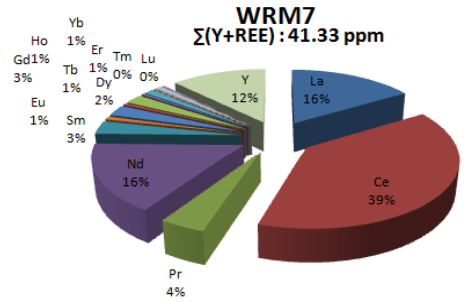

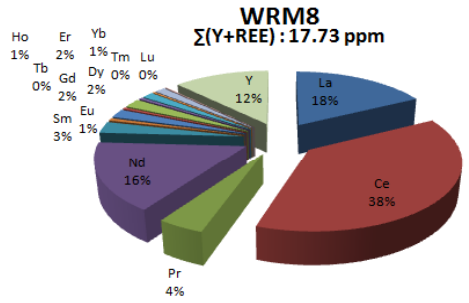

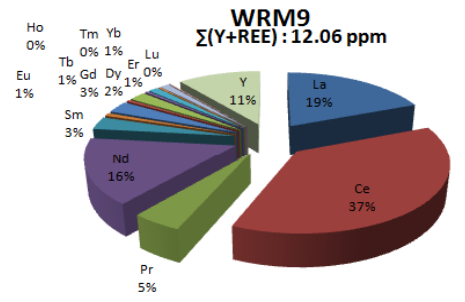

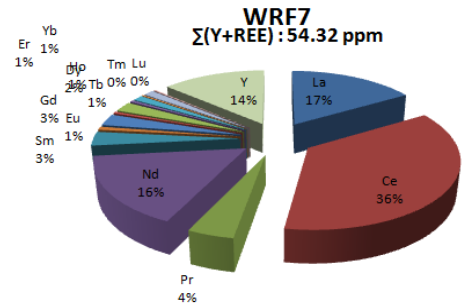

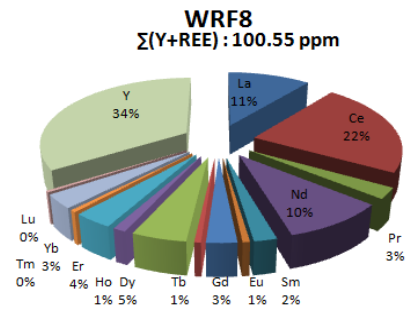

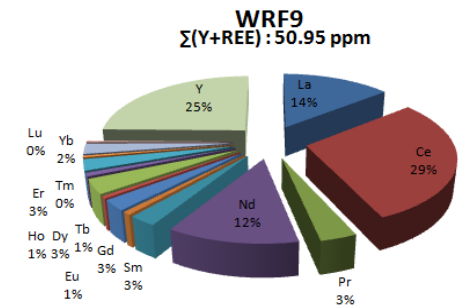

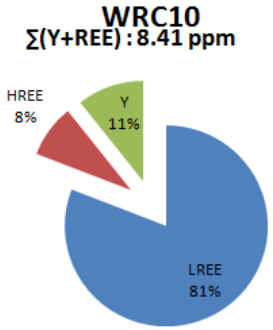

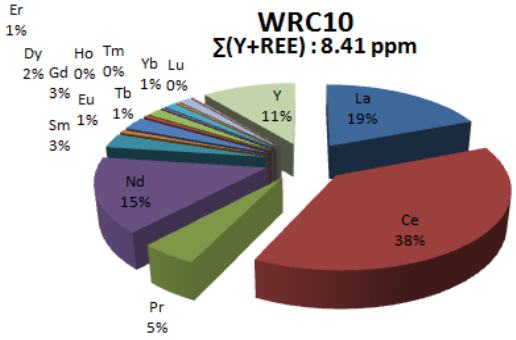

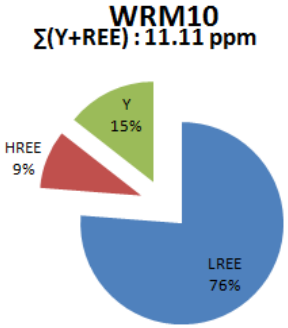

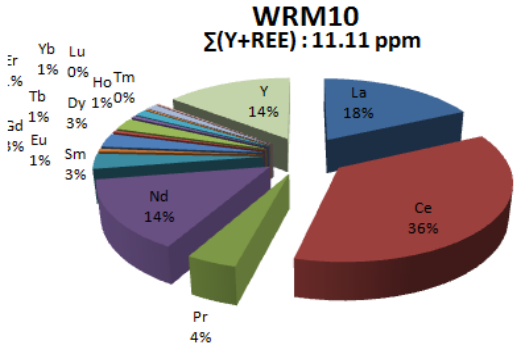

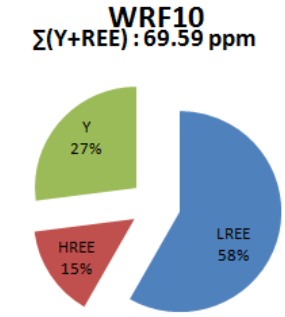

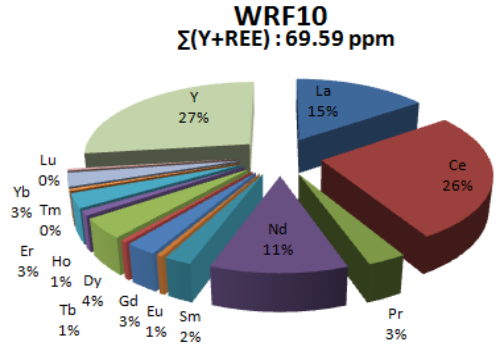

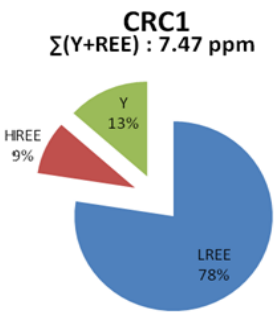

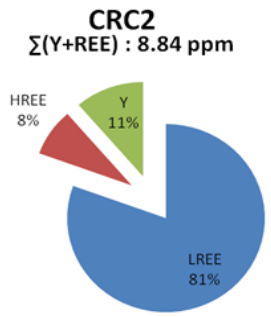

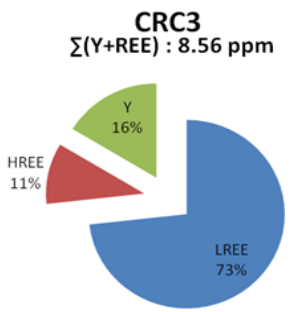

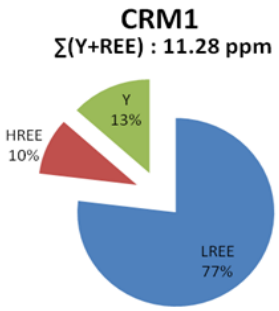

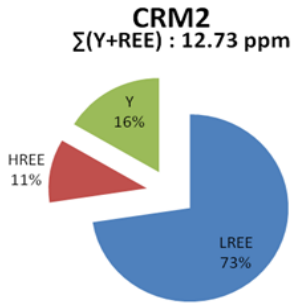

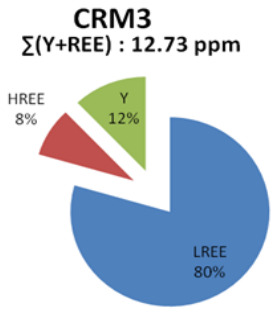

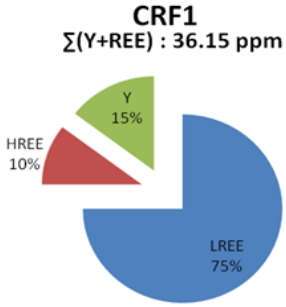

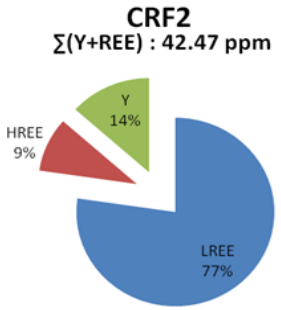

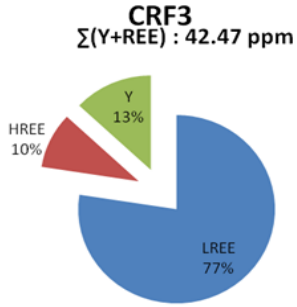

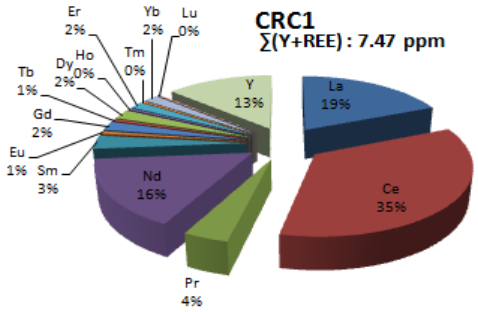

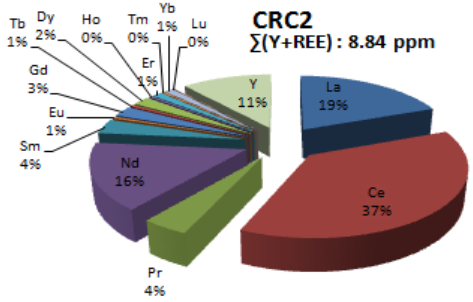

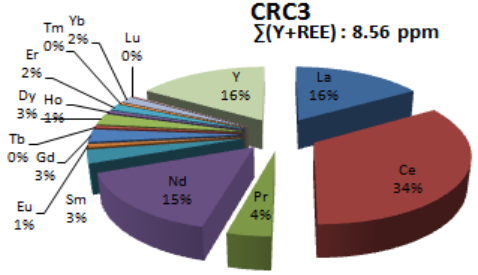

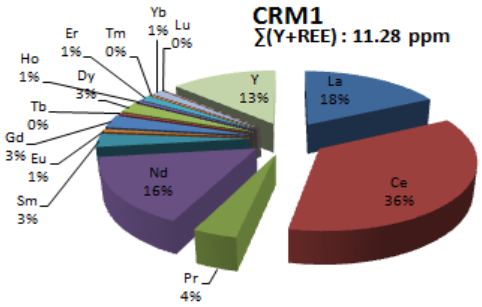

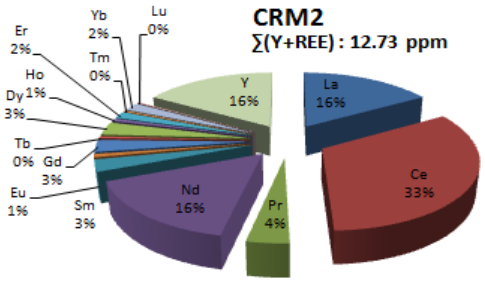

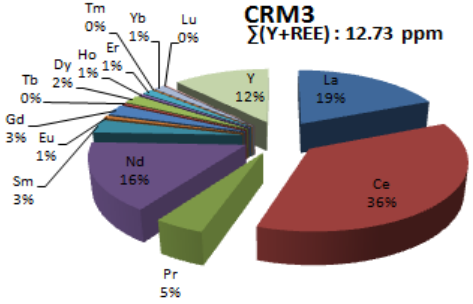

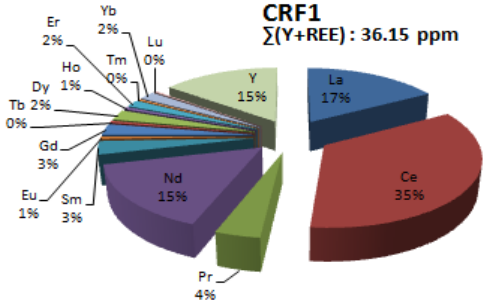

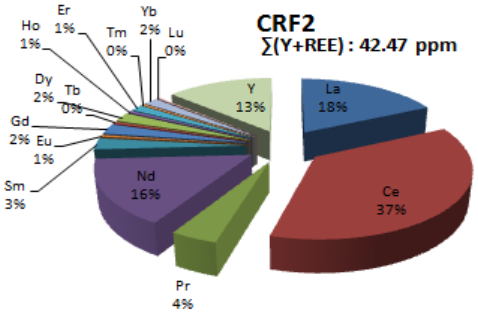

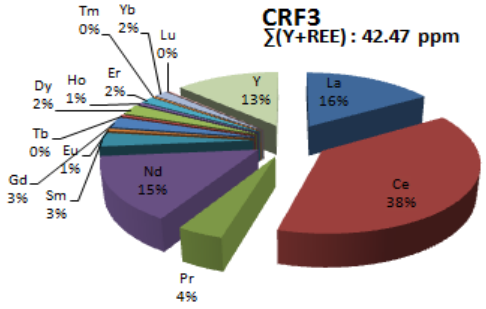

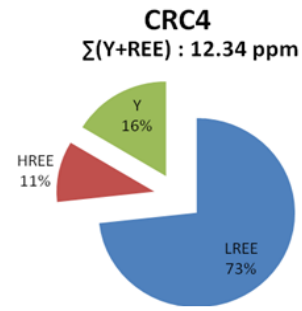

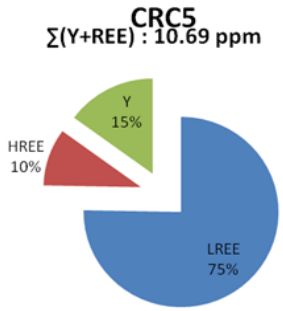

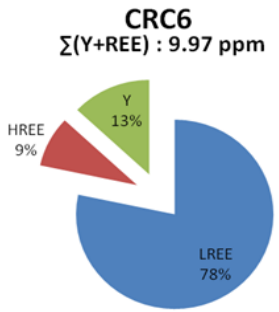

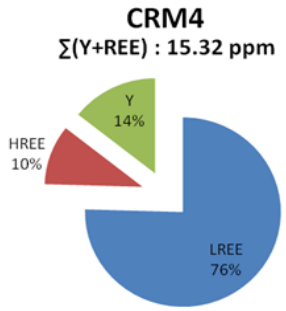

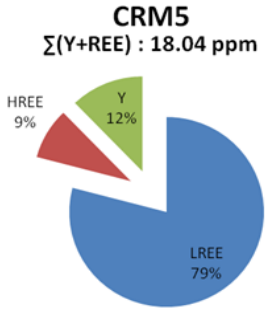

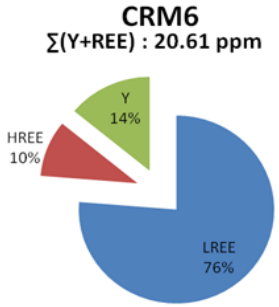

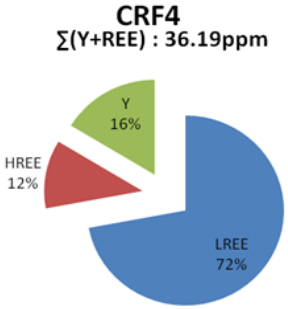

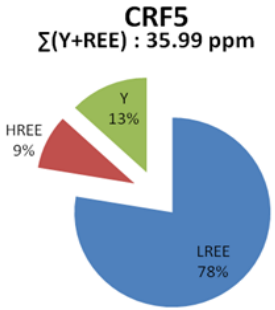

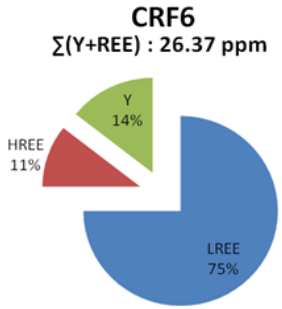

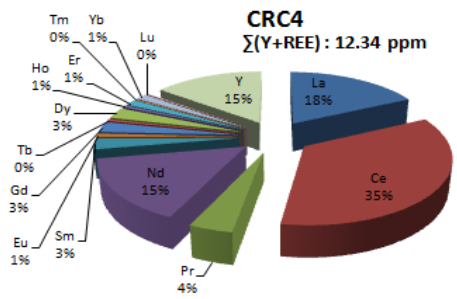

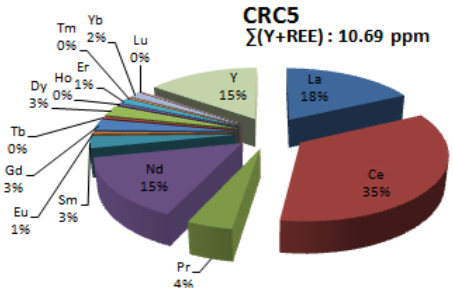

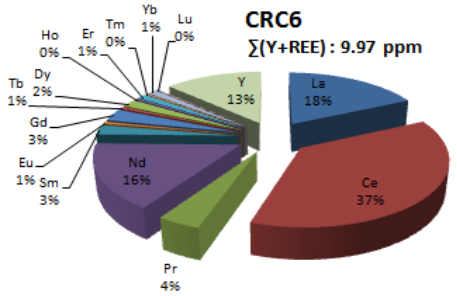

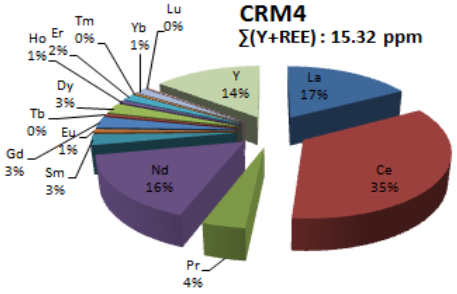

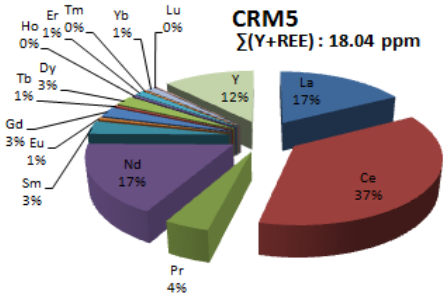

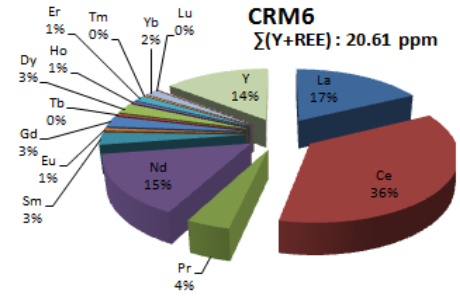

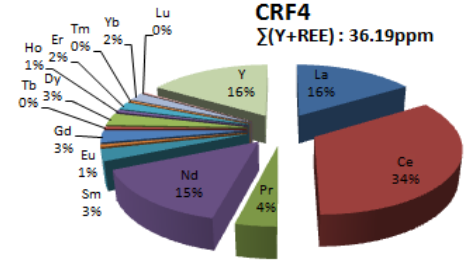

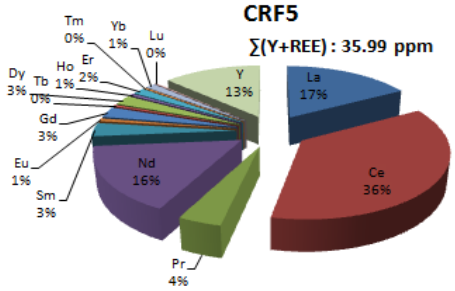

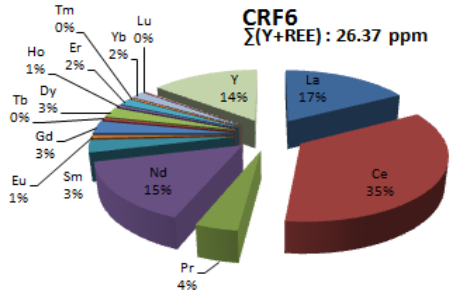

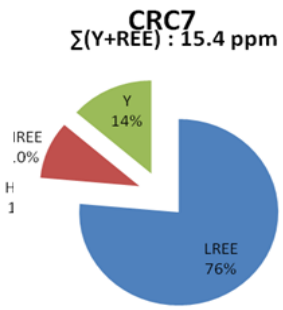

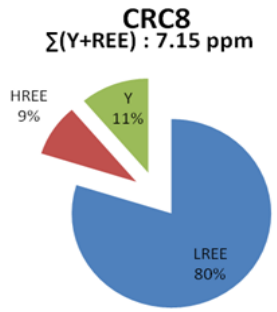

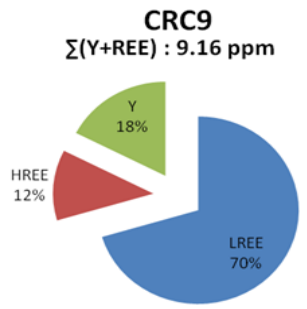

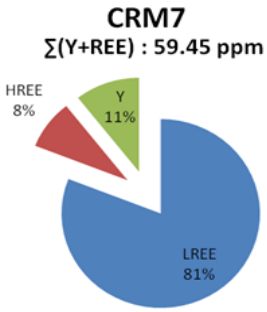

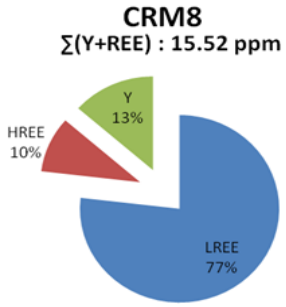

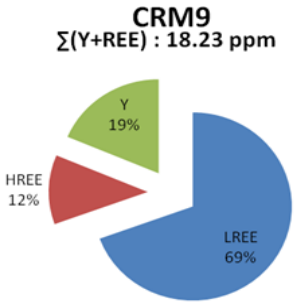

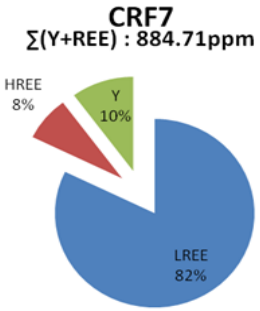

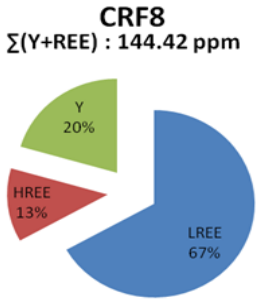

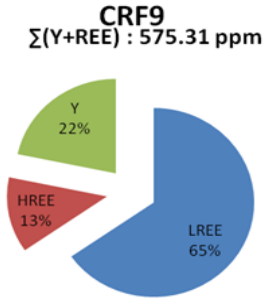

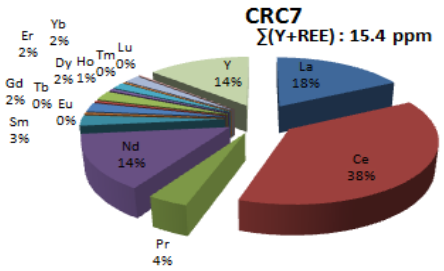

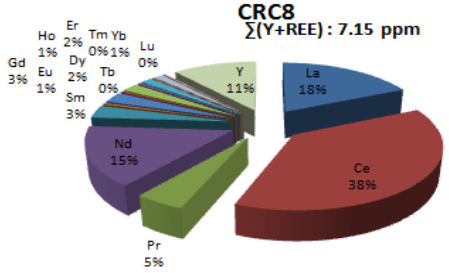

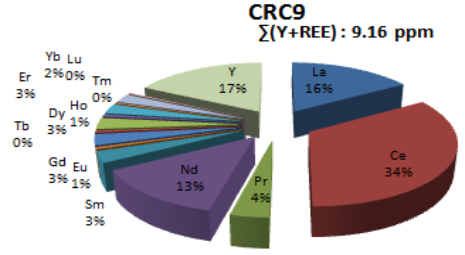

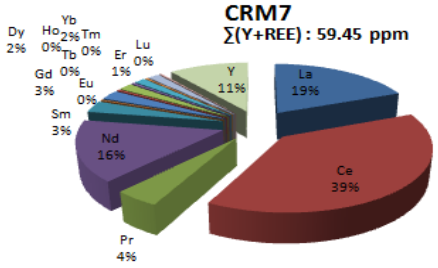

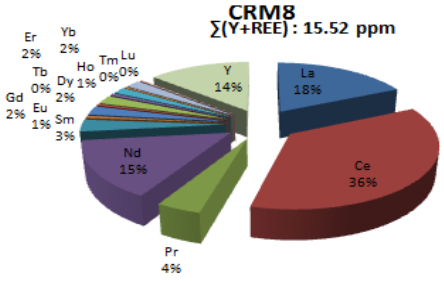

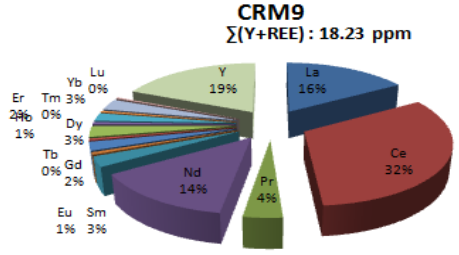

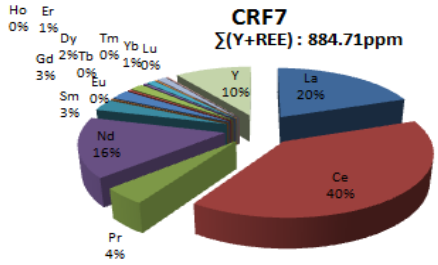

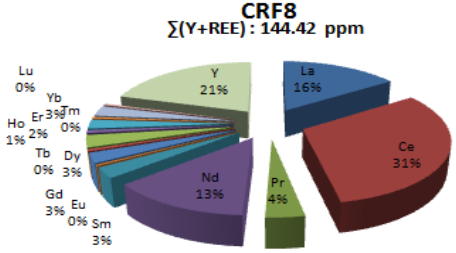

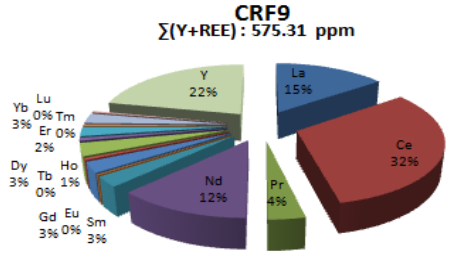

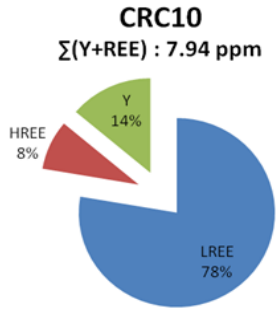

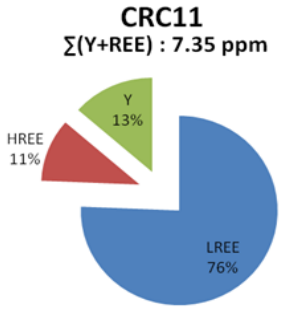

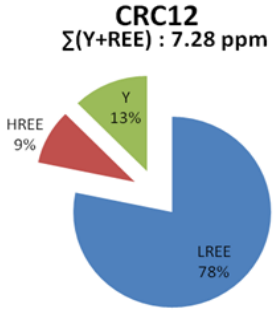

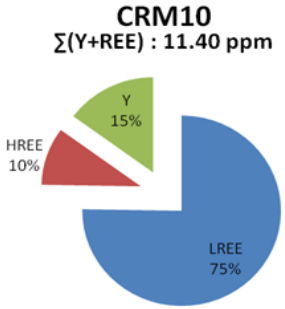

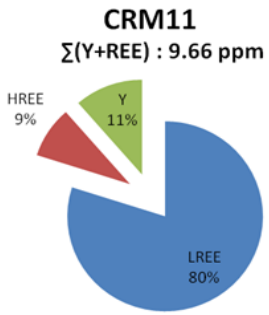

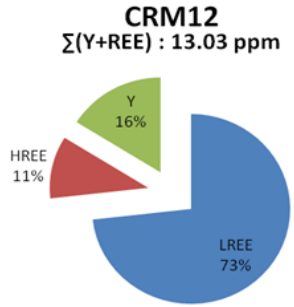

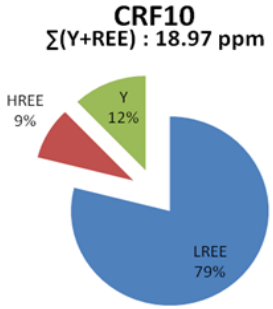

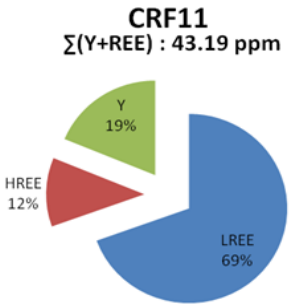

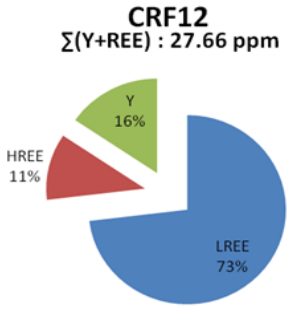

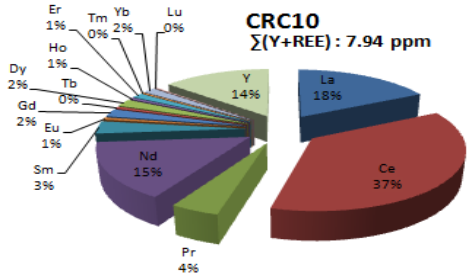

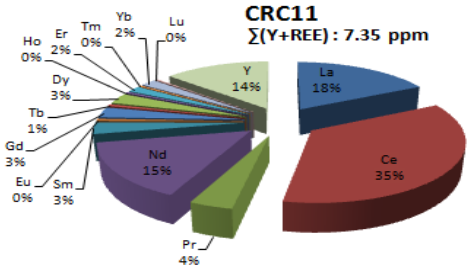

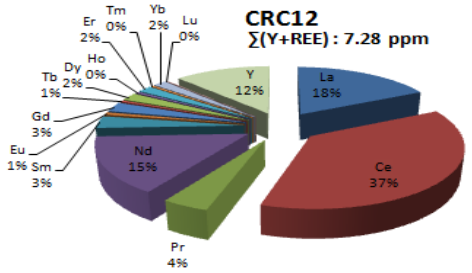

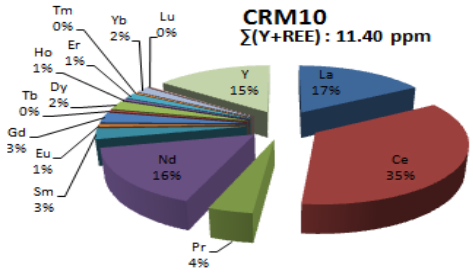

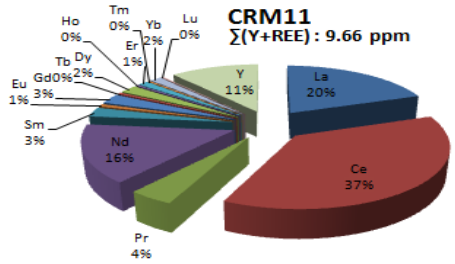

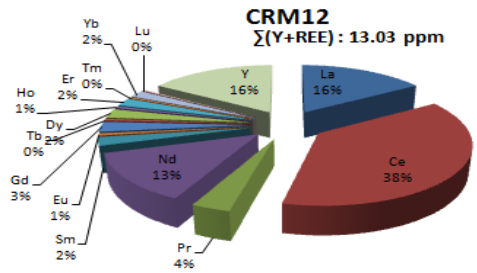

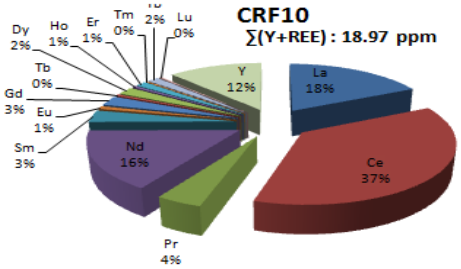

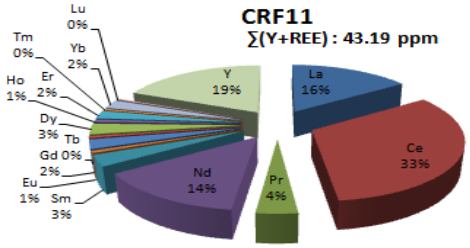

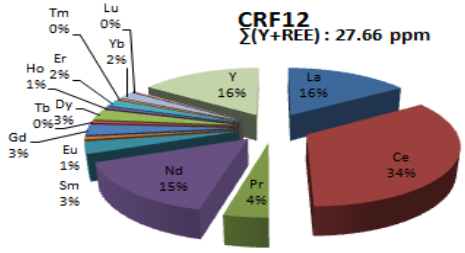

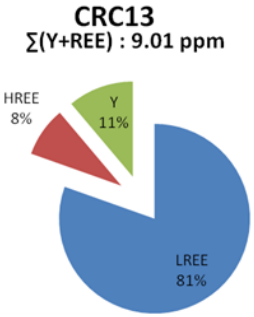

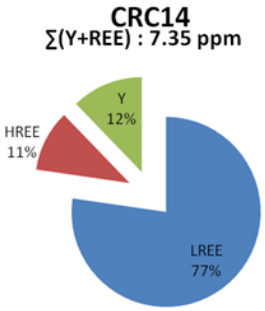

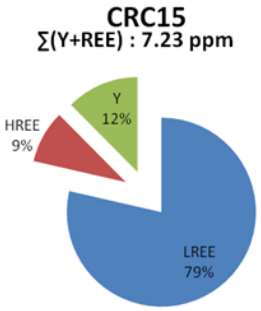

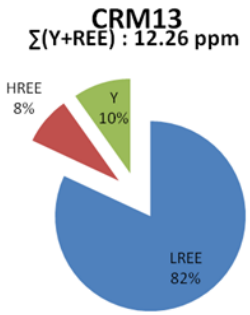

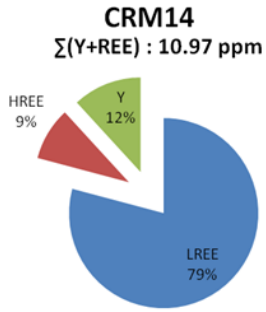

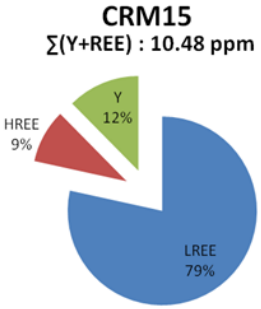

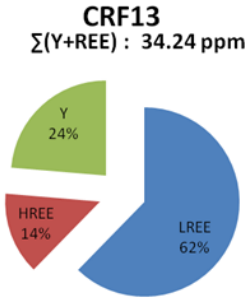

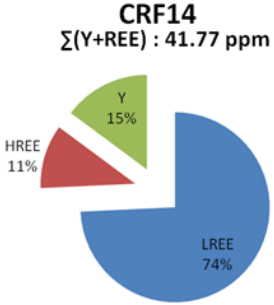

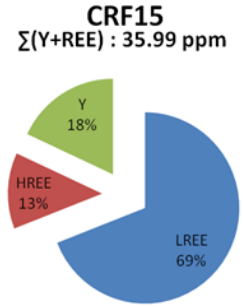

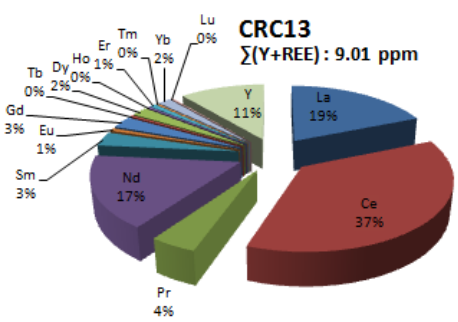

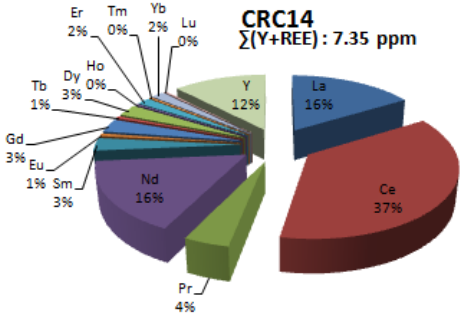

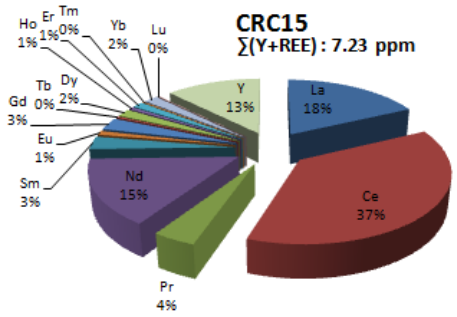

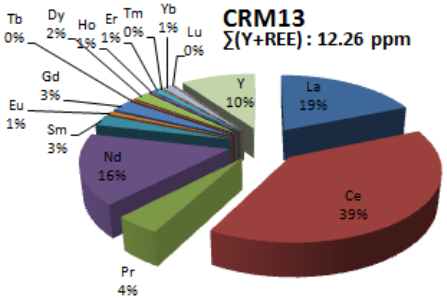

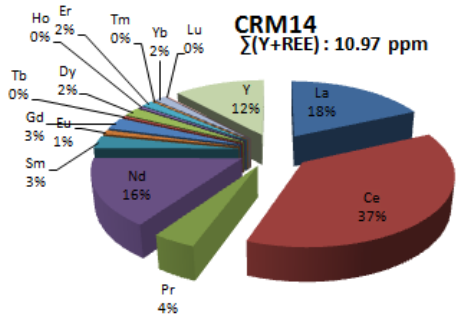

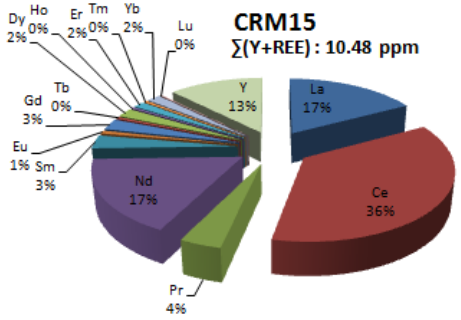

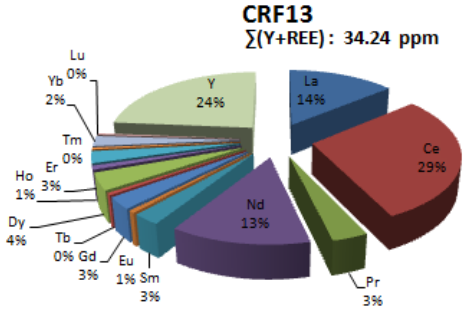

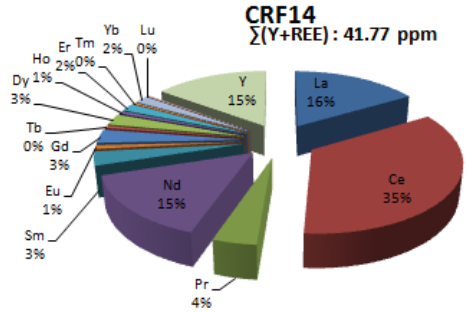

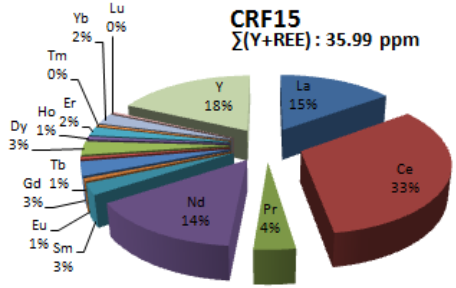

APPENDIX G: Photomicrograph of selected minerals in the beach sands along the coastline of the Central and Western regions.

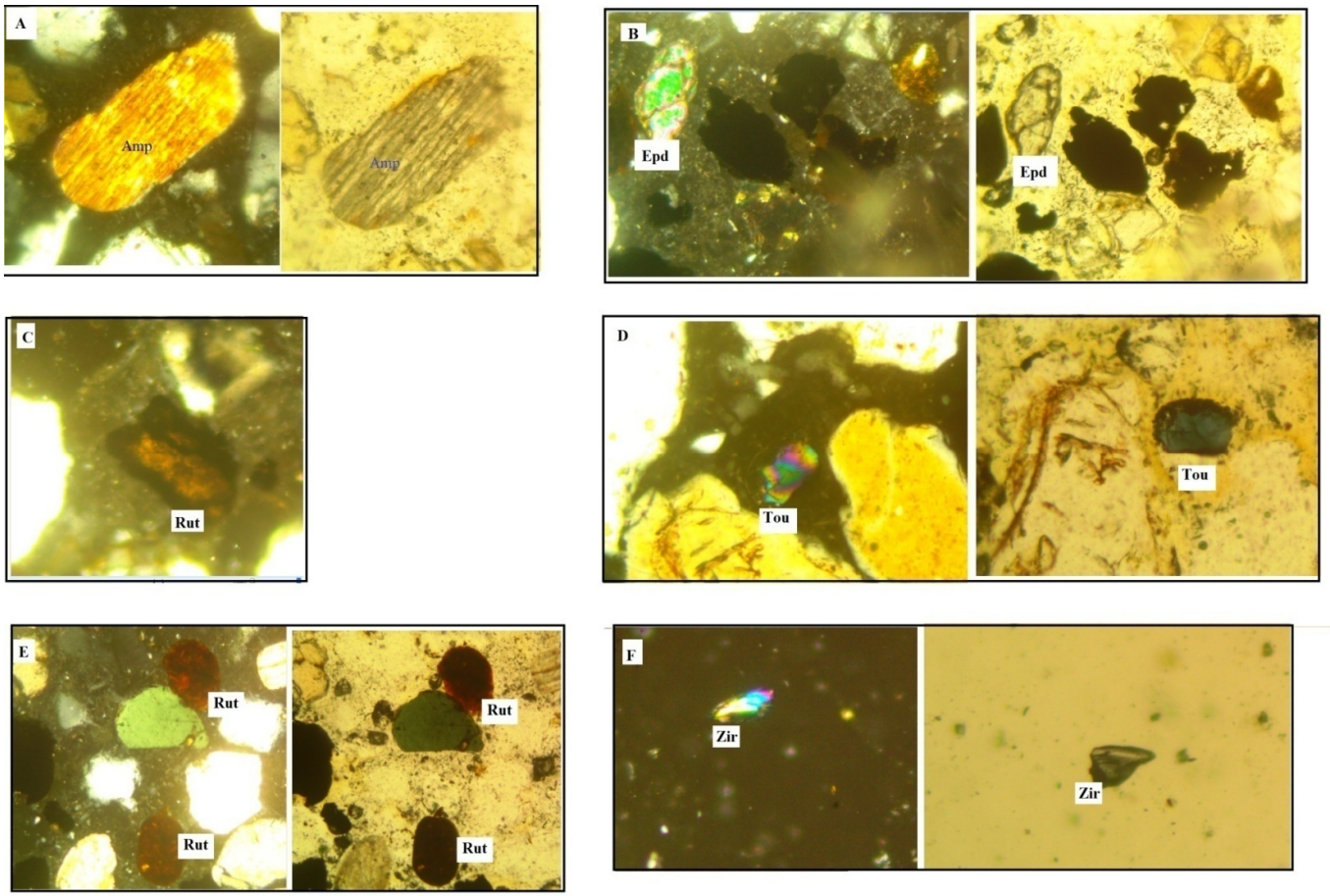

Photomicrograph of selected minerals in the beach sands of Dago; A) Amphibole (B) Epidote (C) Rutile (D) Tourmaline (E)Rutile (F) Zircon

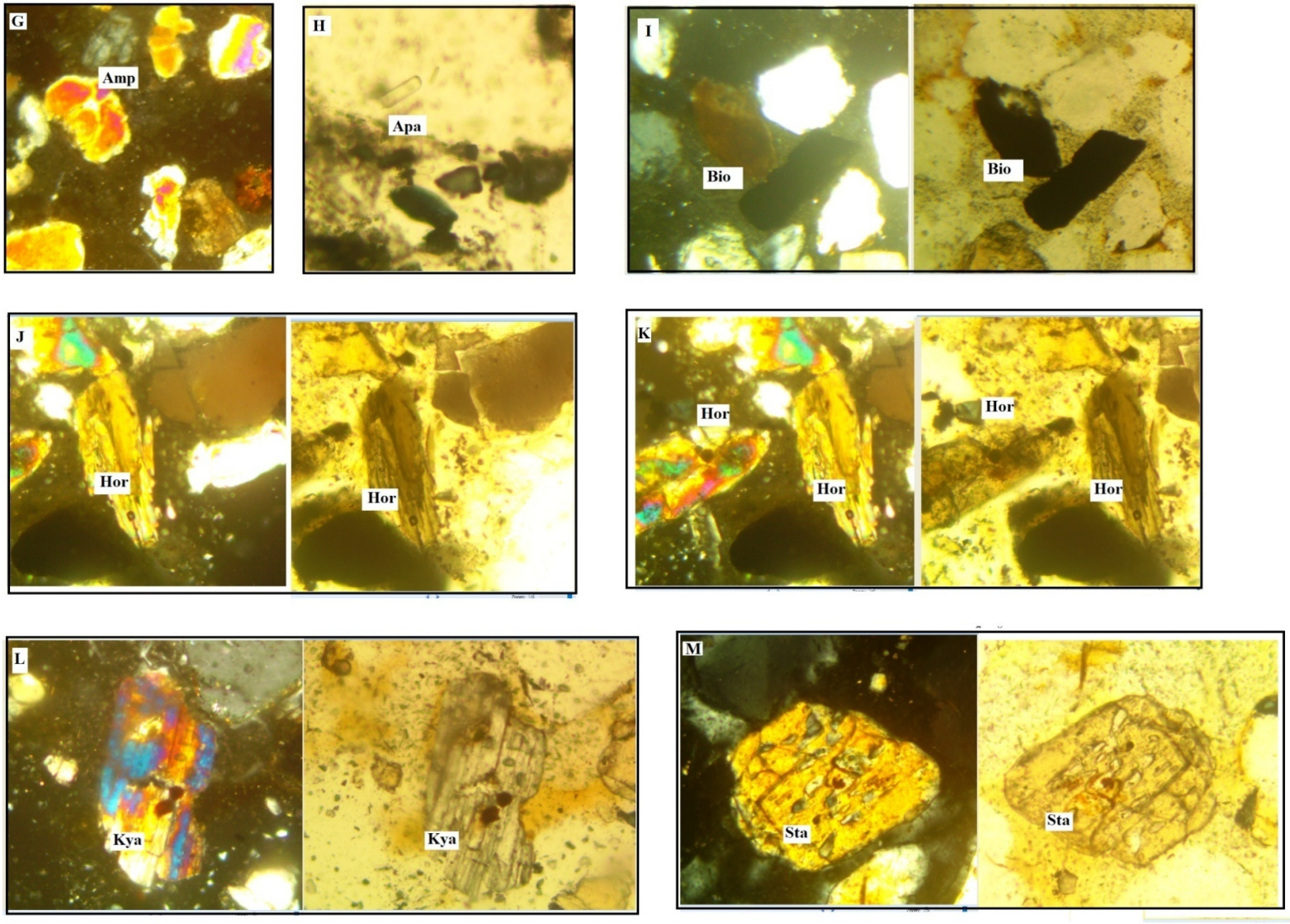

Photomicrograph of Selected minerals in the beach sands of Edumafa and Ekumpoano; (G) Amphiboles (H) Apatite (I) Biotite (J) Hornblende (K) Hornblende and Tourmaline (L) Kyanite (M) Staurolite (N) Zircon

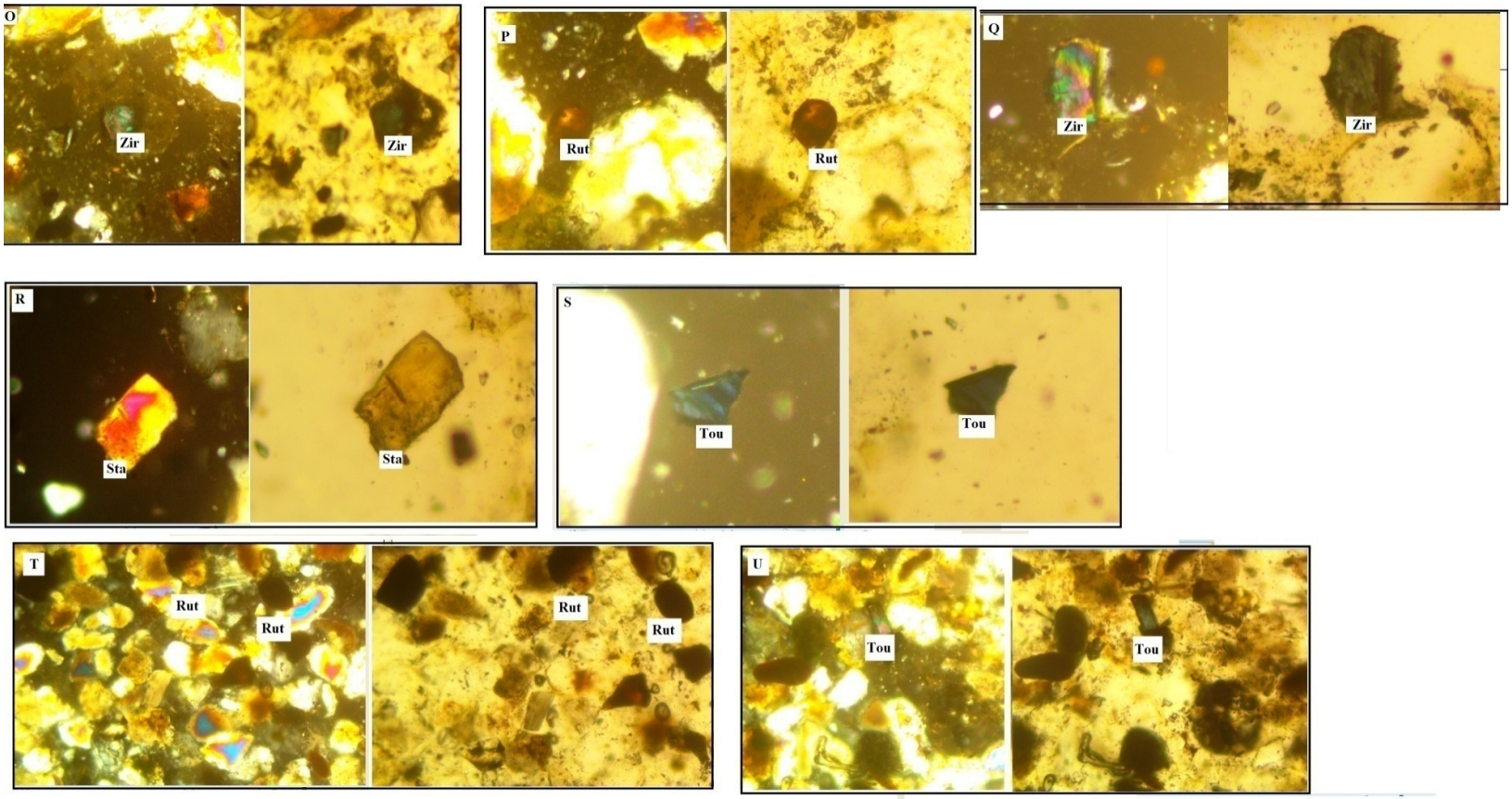

Photomicrograph of selected minerals in the beach sands of Sekondi; (O) Zircon, (P) Rutile, (Q) Zircon, (R) Staurolite, (S) Tourmaline, (T) Rutile, (U) Tourmaline

APPENDIX H: Suggested complex structure of HDEHP, TBP and CMPO with lanthanide in nitric acidic medium